KANSAS GEOLOGICAL SURVEY
OPEN-FILE REPORT 86-23

Depositional Environment, Diagenesis and Petrophysical Properties of the Upper Bluejacket Sandstone (Desmoinesian), KB Field, Allen County, Kansas

by

Douglas H. Rofheart

KANSAS GEOLOGICAL SURVEY
1930 Constant Avenue
University of Kansas
Lawrence, KS 66047

DEPOSITIONAL ENVIRONMENT, DIAGENESIS AND PETROPHYSICAL PROPERTIES OF THE UPPER BLUEJACKET SANDSTONE (DESMOINESIAN), KB FIELD, ALLEN COUNTY, KANSAS

by

Douglas H. Rofheart
B.S., University of Kansas, 1980

Submitted to the Department of Geology and the Faculty of the Graduate School of the University of Kansas in partial fulfillment of the requirements of the degree of Master of Science

Professor in charge

Committee Members

For the Department

TABLE OF CONTENTS

TABLE OF CONTENTS (CONTINUED)

TABLE OF CONTENTS (CONTINUED)

LIST OF FIGURES

LIST OF FIGURES (CONTINUED)

LIST OF FIGURES (CONTINUED)

Page

LIST OF FIGURES (CONTINUED)

Page

LIST OF FIGURES (CONTINUED)

LIST OF FIGURES (CONTINUED)

Page

LIST OF PLATES
(in pocket in back)

LIST OF TABLES

Page

ABSTRACT

The Upper Bluejacket Sandstone in the KB Field, Allen County, Kansas was deposited by low gradient, meandering streams associated with a Middle Pennsylvanian fluvio-deltaic system. The sandstone reservoir is composed of four multilateral and multistory sand bodies. Each sand body shows an erosional base, a basal sandstone containing coal and shale clasts, and vertical decrease in mean grain size and scale of the sedimentary structures.

The sequence of diagenetic changes in the Upper Bluejacket Sandstone was: 1) precipitation of spherulitic and poikilotopic siderite; 2) formation of pyrite; 3) compaction of the reservoir; 4) development of authigenic chlorite; 5) formation of silica overgrowths; 6) dissolution of siderite; 7) precipitation of Ca-Mg-Fe carbonate; 8) dissolution of feldspar and argillaceous rock fragments; and 9) precipitation of kaolinite. Hydrocarbon migrated into the reservoir subsequent to these diagenetic changes.

The permeability of the sandstones in the KB Field is controlled by the pore type. Highly permeable samples (>150 md.) exhibit few micropores (<10%), abundant intergranular pores (>50%), and moderate dissolution pores (<40%). These samples also contained at least four unoccluded intergranular pores for each kaolinite-filled pore. Abundant allogenic and authigenic clays greatly reduce the permeability.

ACKNOWLEDGEMENTS

This research was funded by the Tertiary Oil Recovery Project of the University of Kansas, Lawrence. The Kansas Geological Survey also provided support and facilities for the thin-sections used for petrographic analysis.

I would like to thank Dr. Anthony W. Walton, Chairman of the Advisory Committee, for his invaluable assistance in facilitating the completion of this research. Dr. Walton critically examined this thesis several times and provided numerous poignant and pragmatic suggestions for improvement. I will forever be indebted to Dr. Walton for his help and direction and, particularly, for his patience.

I would also like to thank the other committee members, Dr. Ernest E. Angino and Dr. Donald Green, for critically reviewing this manuscript and for their helpful suggestions.

Finally, I would like to thank Mr. Mack C. Colt of M. C. Colt, Inc. for graciously providing the materials used in this study. Mr. Colt's support of geological and engineering studies at the University of Kansas is greatly appreciated.

INTRODUCTION

PURPOSE OF INVESTIGATION

As the price of petroleum rose rapidly during the 1970's, great emphasis was placed on the search for alternative sources of energy. One such area of interest is enhanced oil recovery (EOR). Enhanced oil recovery is the attempt to extract additional hydrocarbon from reservoirs by modifying the properties of residual oil or by injecting driving fluids into the reservoir. Efficient, economical production of hydrocarbons through enhanced oil recovery requires a three-dimensional understanding of the reservoir, including a synthesis of engineering and geological properties. This research emphasizes the geological and petrophysical properties of the reservoir that are significant to the development of an enhanced oil recovery project.

The purpose of this research is to:

1) Determine the effect of environment of deposition on reservoir properties important in enhanced oil recovery.
2) Determine the sequence of diagenetic changes in the sandstone reservoir.
3) Determine the geological factors affecting petrophysical properties, especially permeability.

LOCATION OF STUDY AREA

The Bronson-Xenia Field in Allen County, Kansas (Figure 1) produces from the Upper Bluejacket Sandstone of the Middle Pennsylvanian (Demoinesian) Cherokee Group (Figure 2). The study area is found in section 33 of Township 24 south, Range 21 east in southeastern Kansas and constitutes only a small portion of the Bronson-Xenia Field. The study area is informally called the "KB Field" by the operator, Mack C. Colt, Inc. In the KB Field, the Upper Bluejacket Sandstone reservoir is located only 750 feet below the surface (350 feet above sea-level) and produces from over 150 wells (Plate 1).

PETROLEUM GEOLOGY OF THE CHEROKEE GROUP

Surface oil seeps along creek beds in southeastern Kansas and southwestern Missouri prompted early prospectors to search for hydrocarbons in this region (Weirich, 1968). In 1860, wells that were drilled into the Cherokee Group near Paola, Kansas discovered abundant gas. The abundance of shallow gas reserves provided energy for extensive local industry and fueled the growth of many small towns in southeastern Kansas, such as Iola, Chanute and Coffeyville.

The Mills well, drilled near Neodesha, Wilson County, Kansas in November, 1892, was the first

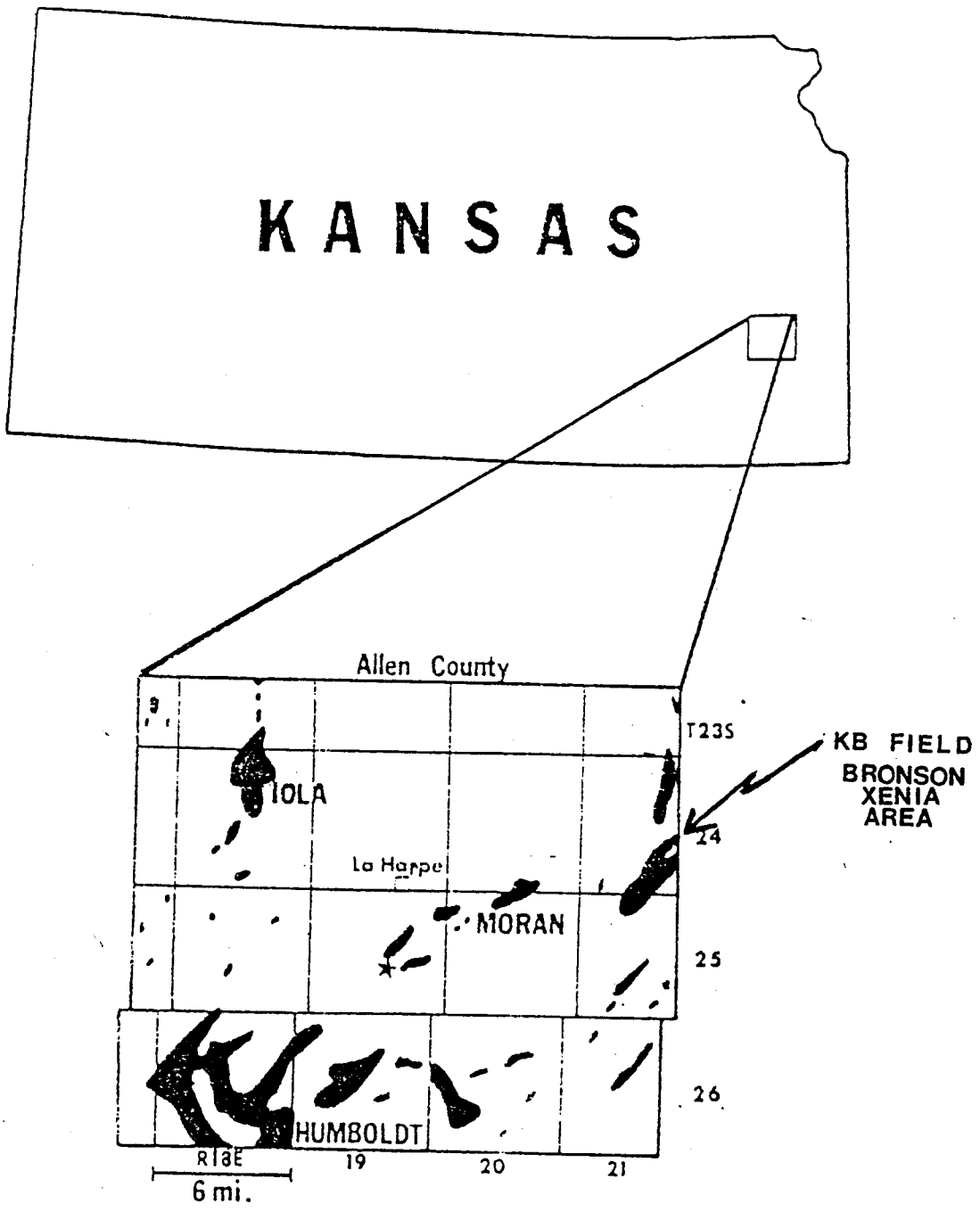

Figure 1. Location of the KB Field in Allen County, Kansas (After Schumacher, 1976)

COMPOSITE SECTION OF THE CHEROKEE GROUP, SOUTHEASTERN KANSAS

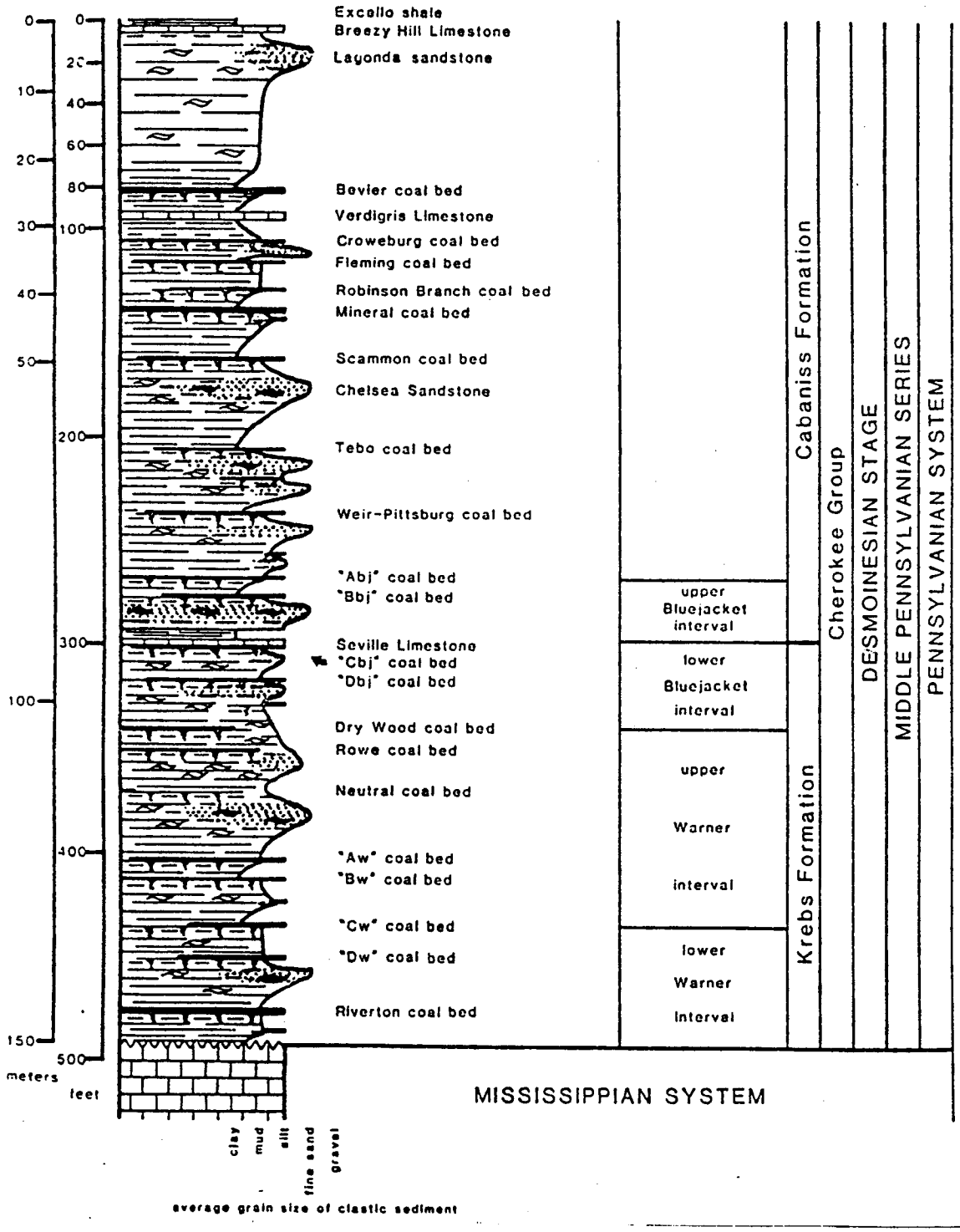

Figure 2. Composite section of the Cherokee Group in Cherokee and Crawford Counties, Southeast Kansas (Harris, 1985).

economically significant discovery in the Bluejacket Sandstone (Weirich, 1968). The well encountered 22 feet of oil-saturated sand at a total depth of 832 feet.

The cumulative resources remaining in the Cherokee, Marmaton and Pleasanton Groups total 879 million barrels of the original 1.4 billion barrels of oil-in-place (Ebanks, 1975). The Cherokee Group contains most of this hydrocarbon in numerous, single-pay reservoirs. The hydrocarbons produced from the Cherokee Group are found predominately in relatively thin, lenticular sandstone bodies. The sandstones are interbedded with carbonaceous siltstone and shale units, which are believed to be the source for the hydrocarbons in the Cherokee Group (Baker, 1962).

The mechanism that traps the oil and gas in the Cherokee Group is a combination of structure and stratigraphy (Busch, 1959). The oil and gas accumulated on the up-dip portions of sand bodies draped over pre-Pennsylvanian topographic and structural features (Cole, 1969; Hudson, 1969). The shales that encase the sandstones form an impermeable barrier, or stratigraphic trap, to hydrocarbon migration. Hulse (1978) proposed that the entire region dips slightly northwestward due to Permian tectonic movement associated with the Ozark Uplift.

Dissolved gas in the liquid hydrocarbon is the mechanism that drives the primary production in the Cherokee Group reservoirs. This type of drive mechanism depletes rapidly, causing precipitous decline in production. The loss of energy is commonly compensated by injecting water into the reservoir to displace oil and gas. Many of the Cherokee Group reservoirs are currently showing declining production in spite of water injection. Ebanks (1975) stated that 40 to 70 percent of the original hydrocarbon will remain in place after the completion of water flooding. Ebanks (1975) also suggested that successful enhanced oil recovery programs could possibly recover an additional 35 percent of this residual oil.

GEOLOGY OF THE CHEROKEE GROUP

NOMENCLATURE

The Cherokee Group was first described from surface exposures by Haworth and Kirk in 1894 (Jordan, 1957). The Cherokee occupies the interval between the base of the Fort Scott Limestone and the unconformable pre-Pennsylvanian surface (Zeller, 1968). The Cherokee Group is defined as the basal unit of the Desmoinesian Stage of the Middle Pennsylvanian Series. This group was subdivided into two formations by Jewett (1959) based on the occurrence of the thin and discontinuous Seville (?) Limestone (Fig. 2). The Cabaniss and Krebs Formations are predominantly composed of shale with sandstone, limestone, coal and underclay. The Upper Bluejacket Sandstone of the Cabaniss Formation overlies the informal Bluejacket "B" Coal ("Bbj" coal bed, Fig. 2; Harris, 1985) and underlies the Weir-Pittsburg Coal in the KB Field.

STRATIGRAPHY

The authors of The Kansas Rock Column (Moore, et al., 1951) subdivided the Cherokee into cyclothems or units that represent deposition during cyclical transgressive and regressive periods. Howe (1956) raised the Cabaniss and Krebs to subgroups and

recognized a total of 18 different formations. The formations were defined as the intervals between successive coal beds. The subgroups were later changed to the Cabaniss and Krebs Formations because of the difficulty in mapping the units outlined by Howe (1956). Zeller (1968) states that the Cherokee is not readily divisible into mapable units either in the surface or subsurface. Ebanks (1979) emphasized the difficulty in correlating the Cherokee Group because of the discontinuous nature of the deposits. Based on the continuous coal beds mined in the Cherokee Group in the past, it was assumed by early stratigraphers that all of the sandstones, shales and thin coals were also continuous (Ebanks, 1979). This assumption created a great deal of confusion when attempts to correlate sandstone units in the Cherokee Group were made. Recently Harris (1985) recognized several informal coal beds (Fig. 2) that serve as excellent correlation horizons in southeastern Kansas and adjacent Missouri and Oklahoma.

STRUCTURAL SETTING

The Cherokee Basin (Fig. 3) lies between the Ozark Uplift on the east, and the Nemaha Uplift on the west. The Cherokee Basin is the northern shallow shelf of the Arkoma Basin of Oklahoma and Arkansas. The Bourbon Arch, a low-relief topographic feature on the pre-Pennsylvanian surface, separates this basin from

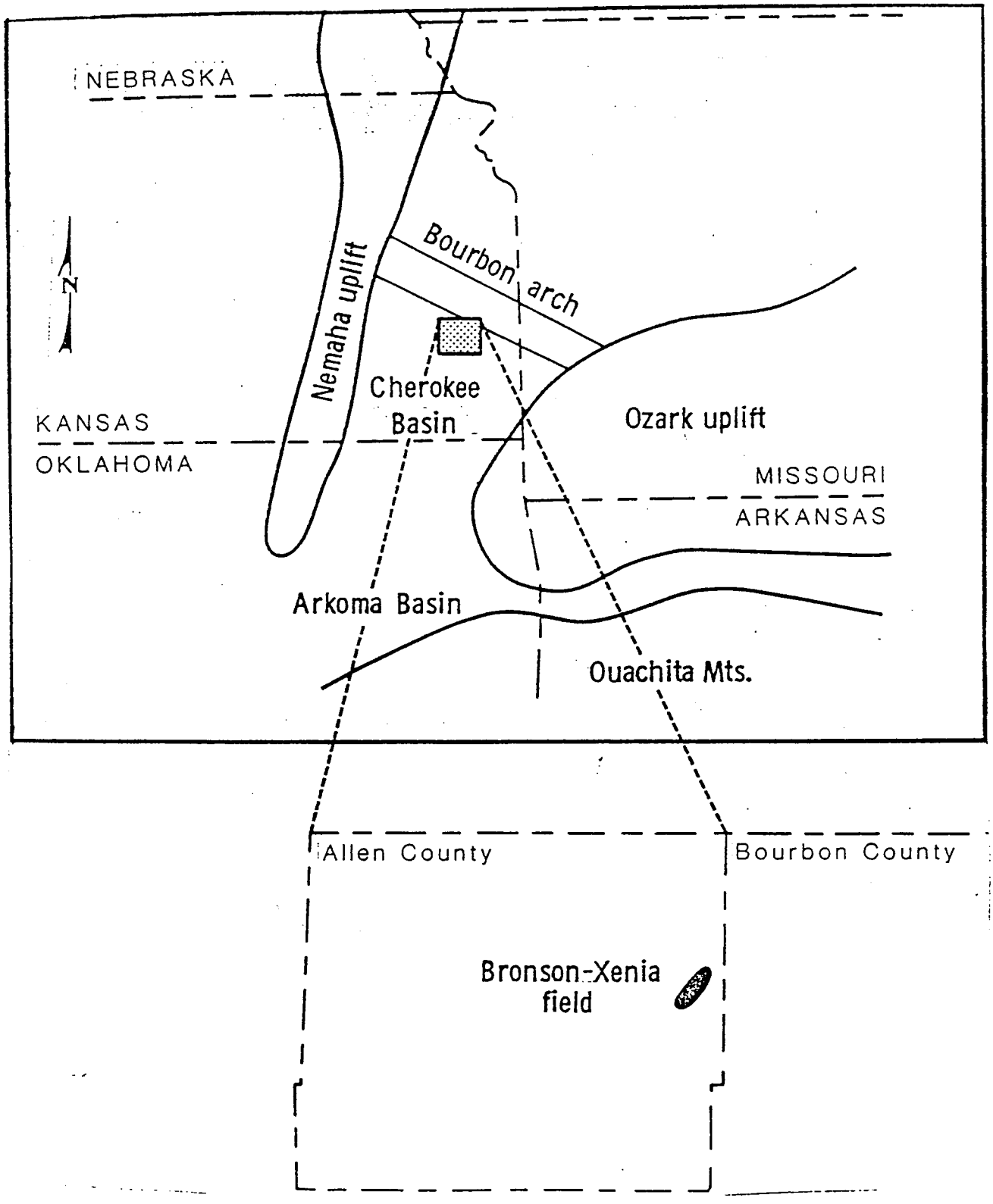

Figure 3. Structural setting of Southeastern Kansas and location of the study area in Allen County.

the Forest City Basin to the north. Note that the Bourbon Arch is located just to the north of the Bronson-Xenia Field in Allen County (Fig. 3). The thickness of the Desmoinesian stratigraphic section ranges from 110 m (360 ft.) to 275 m (900 ft.) in the Cherokee Basin (Ebanks and James, 1974). The outcrop thickness of the Desmoinesian section ranges from 180 m (600 ft.) to 230 m (750 ft.) (Zeller, 1968).

→ The Cherokee Basin developed through slow and gradual southward subsidence after the emergence of the Nemaha Uplift (Ebanks and James, 1974). Erosion of the pre-Pennsylvanian surface resulted in highly irregular topography with considerable relief (Hulse, 1978). The irregularity of the surface was also a function of pre-Pennsylvanian folding and faulting (Cole, 1969; Hudson, 1969). Periodic tectonic movement occurred during Desmoinesian deposition, which facilitated the encroachment of the seas from the south (Weirich, 1953).

Middle Pennsylvanian sediments accumulated during a major transgression as evidenced by the change from predominantly clastics in the Cherokee Group to carbonates in the Marmaton Group (Weirich, 1953; Visher, et al., 1971; Ebanks and James, 1974). This transgression was interrupted by several regressive periods, which resulted in the deposition of lenticular "shoestring" sandstones, shale, coal and underclay.

GEOLOGY, DEPOSITIONAL ENVIRONMENT AND DEPOSITIONAL HISTORY OF THE KB FIELD

INTRODUCTION

The environment of deposition of the Cherokee Group sandstones in northeastern Oklahoma and southeastern Kansas has been a subject of controversy since late in the nineteenth century. Nearly the gamut of possible clastic depositional environments has been proposed, including marine offshore barrier bars and marine beaches (Cheyney, 1929; Bass, 1934, 1936; Bass et al., 1937; and Leatherock, 1937.), tidal channels (Phares, 1969; and Hayes, 1962), fluvial channels (Woody, 1983; Hulse,1978; and MacKenzie, 1972.) and strike-valley sandstones deposited in low lying areas between cuestas during marine transgression (Busch, 1959). Current opinion has settled upon a fluvial-deltaic depositional environment with modest marine influence for the Cherokee Group (Ebanks, 1979). Desmoinesian deposition in the Mid-Continent was characterized by cyclical changes in sea level resulting in deposits that are variable both areally and vertically (Ebanks, 1979). Considering the cyclical nature of the transgressive and regressive episodes, it is conceivable that all of the aforementioned depositional environments were present

in southeastern Kansas and northeastern Oklahoma. The multiplicity of depositional environments of the Cherokee sediments was first proposed by Rich (1923) and later supported by research conducted by Visher, Saitta and Phares (1971) in northern Oklahoma.

Weirich (1953) described a fluvial system extending from northeastern Kansas to a deltaic plain in central Oklahoma (Fig. 4). This fluvial-deltaic system was responsible for the deposition of the Desmoinesian sandstones in Kansas and Oklahoma, including most of the Bluejacket Sandstones.

WELL DATA

The study of the KB Field was based on information gathered from 167 wells (Plate 1). The data incorporated in the study are from wells drilled in a symmetrical grid pattern as part of a water flood project. For each of the wells, a full diameter core was taken from the Upper Bluejacket Sandstone reservoir and subsequently the well was logged with a gamma-ray tool. One hundred simple core descriptions (Fig. 5) conducted by Dr. Daniel A. Busch, the consulting geologist for Mack C. Colt, Inc., were also available. Dr. Busch's descriptions are helpful in determining grain-size and facies changes in cores that subsequently have been discarded. For this study, nine

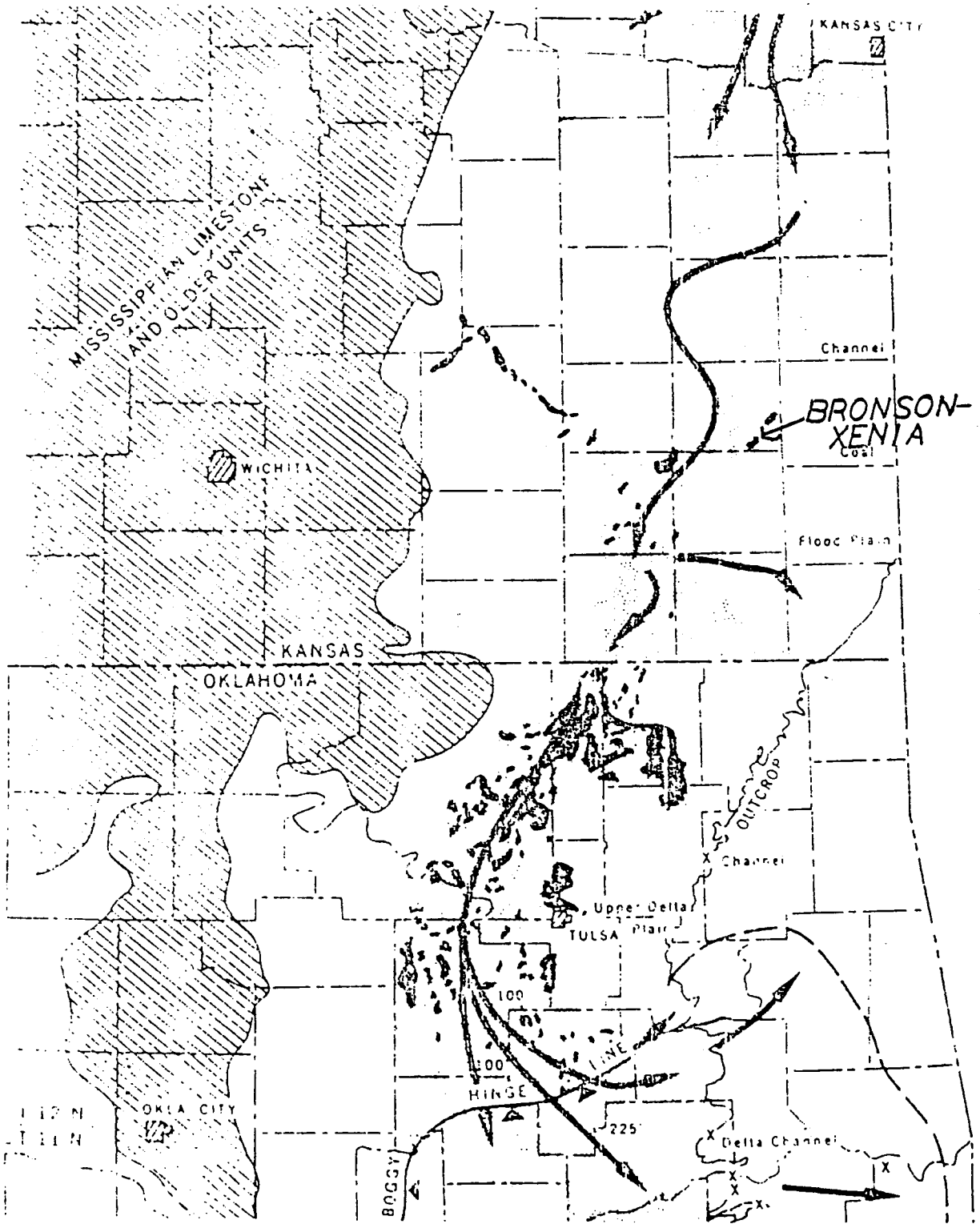

Figure 4. Drainage pattern of the Desmoinesian (Cherokee) fluvio-deltaic system (after Weirich, 1953).

full diameter drill cores from the Kansas Geological Survey Core Repository were slabbed, measured and described in detail (Appendix A).

GENERAL RESERVOIR CHARACTERISTICS

Examination of the cores revealed general characteristics of sandstones previously described from the Kansas-Oklahoma-Missouri tri-state area (Hulse, 1978; Ebanks, 1979; Woody, 1983). A generalized lithologic column of the Upper Bluejacket Sandstone from the KB Field is shown in Figure 6. All of the wells studied from the KB Field reached total depth in dark gray siltstone or mudstone. This lithologic unit is featureless in terms of sedimentary structure and fissility, but does exhibit common root marks. Directly overlying this unit is the thin Bluejacket B Coal (Fig. 7). This friable bituminous coal reaches a maximum thickness of 30.5 cm (1 ft.) but generally averages 10 cm (4 in.). The Upper Bluejacket Sandstone overlies the Bluejacket B Coal and commonly includes coal and clay-ironstone clasts directly above the sharp bottom contact (Fig. 8). The sandstone reaches a maximum thickness of 15.25 m (50 ft.) but averages 9.1 to 10.7 m (30 to 35 ft.). The lower portion of the sandstone exhibits high angle planar-tabular cross-stratification that grades vertically upward into

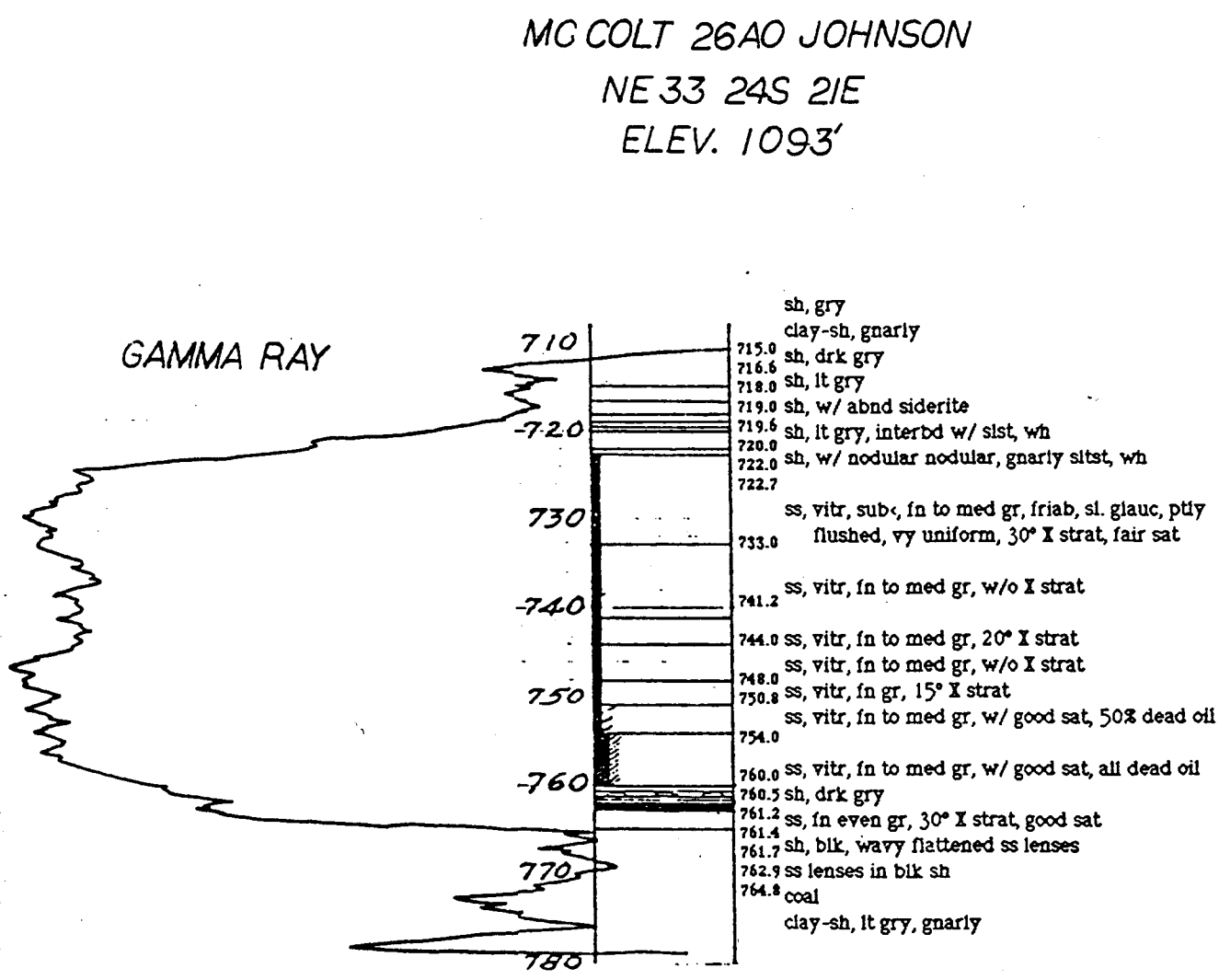

Figure 5. Example of core description conducted by Dr. D.A. Busch for M.C. Colt, Inc. (Colt 26AO Johnson).

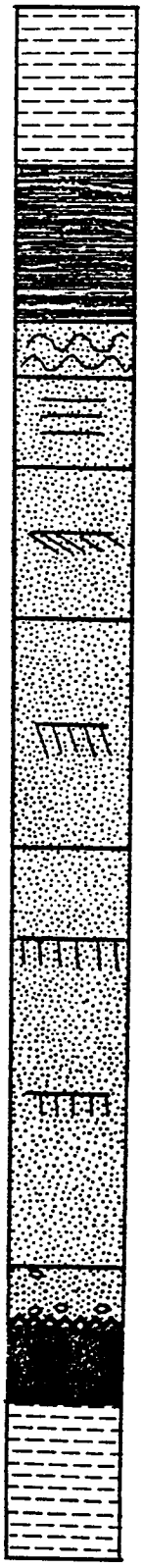

Dark gray mudstone with common sideritic concretions.

SUBFACIES 7 Burrowed, interbedded or linsen-bedded sandstone, siltstone and black shale. Probably sound or bay deposits.

SUBFACIES 6 Current-ripple bedded very-fine-grained sandstone.

SUBFACIES 5 Horizontally bedded very-fine- to fine-grained sandstone.

SUBFACIES 4 Low angle (<10°) planar-tabular cross-stratified very-fine- to fine-grained sandstone.

SUBFACIES 3 Moderate angle (10°-30°) planar-tabular cross-stratified fine-grained sandstone.

SUBFACIES 2 High angle (>30°) planar-tabular cross-stratified fine- to medium-grained sandstone.

SUBFACIES 1 Structureless medium-grained sandstone with common coal and shale clasts, and erosional base.

BLUEJACKET B COAL

Dark gray siltstone or mudstone.

Figure 6. Generalized lithologic column from the KB Field, Allen Co., Kansas.

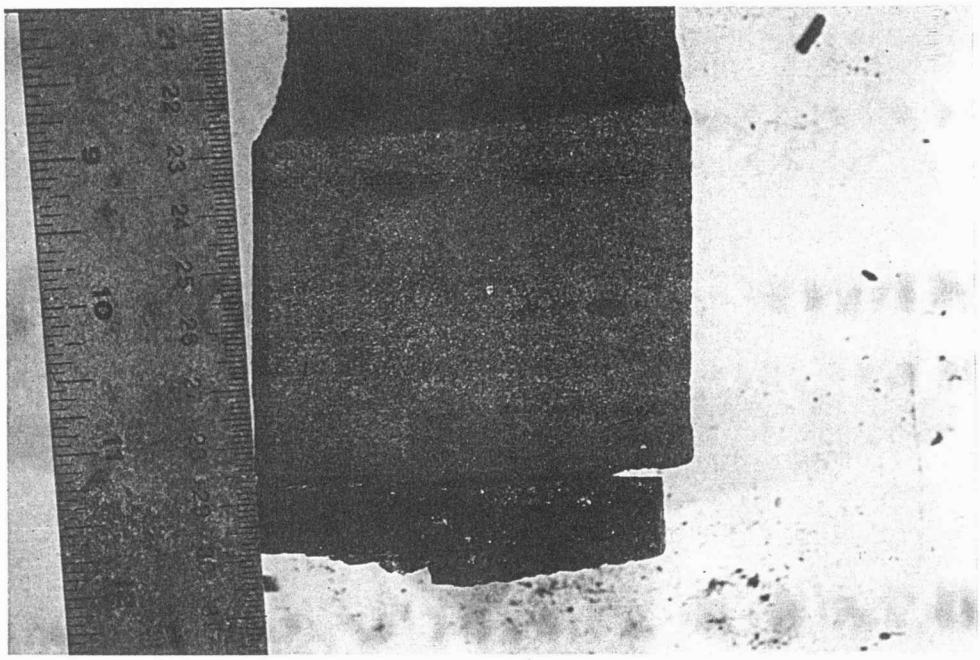

Figure 7. Colt 50AO Johnson, 779.5 ft. (Scale is in./cm.) Sharp basal contact of Upper Bluejacket Sandstone and Bluejacket B Coal (Entire thickness of coal not shown). Note shale clasts in basal sand.

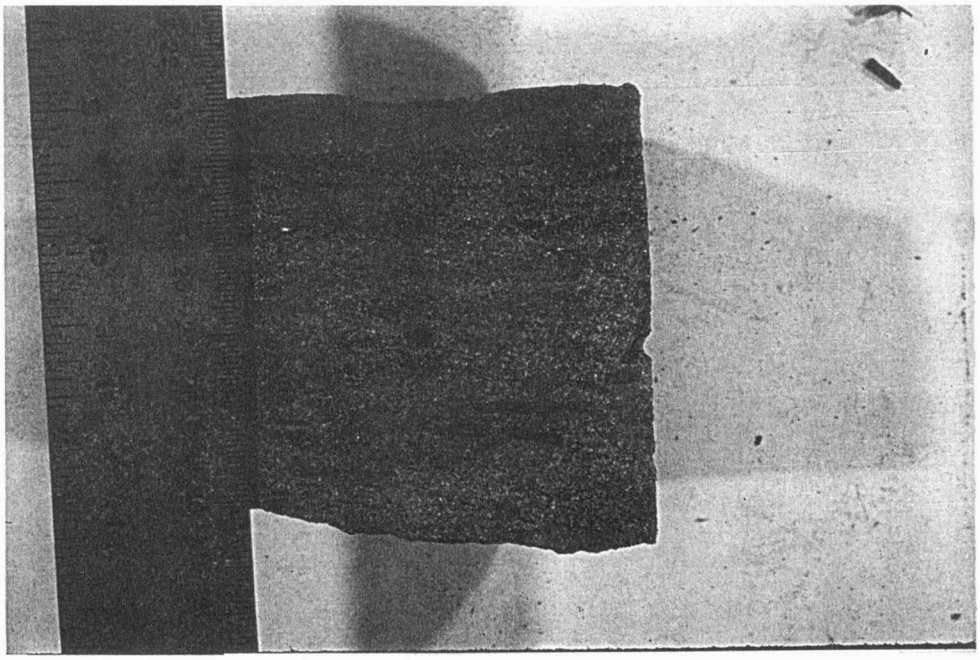

Figure 8. Colt 28A Smith, 782 ft. (Scale is in. and cm.). Basal Upper Bluejacket Sandstone showing common clay-ironstone and shale clasts.

moderate and low angle planar-tabular and ripple crossbedded sands. The average grain-size of the sand decreases vertically throughout the field. The vertical decrease of the grain-size is rarely gradational, but is characterized by two or more fining-upward sand sequences. The main body of the Upper Bluejacket Sandstone is overlain by linsen-bedded or interbedded sandstone and shale. The thickness and number of sand lenses gradually decrease upward into an overlying dark gray mudstone. The mudstone commonly shows large sideritic concretions or fracture fills (Fig. 9). Stratigraphically the youngest lithology observed is the Weir-Pittsburg coal. This coal was not observed in the cores of the Kansas Geological Survey Collection but was encountered in other cores (Core descriptions provided by M.C. Colt, Inc.).

Wells that were drilled beyond the areal limits of the sandstone reservoir provide details of the laterally equivalent facies. In the Mack C. Colt 3AO Harvey well (Appendix A) for example, the Bluejacket A Coal underlies 3.1 m (10 ft.) of linsen-bedded sandstone and shale (Fig. 2). The maximum sand thickness is 75 cm (2.5 ft.) and is found directly above the coal bed. This well reached total depth 1 m (3 ft.) above the Bluejacket B Coal horizon. The well lies only 61 m (200 ft.) from wells that encountered

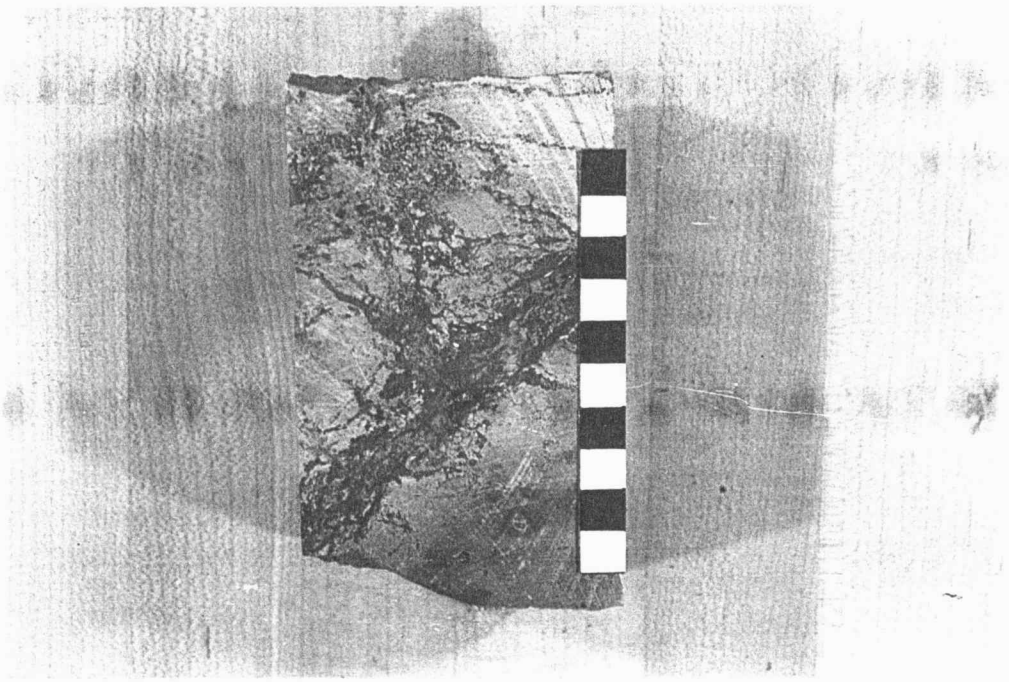

Figure 9. Colt 26AO Johnson, 720 ft. (Scale=10 cm) Large siderite fracture fill associated with soil development in gray shale superjacent to the Upper Bluejacket Sandstone.

sand thicknesses averaging 11.5 m (33 ft.). The absence of sand in this well provides evidence of the abrupt lateral termination of the sandstones in this area. The interbedded sandstones and shales were obviously deposited under a regime considerably different from the main body of the sand.

Other wells that were drilled beyond the limits of the reservoir also encountered the Bluejacket A Coal (Fig. 2). The Bluejacket A Coal is located 2.4 m (8 ft.) above the Bluejacket B Coal. The interval between these two coals is composed of dark gray shale with carbonized plant fragments. The interval between the Bluejacket A Coal and the Weir-Pittsburg Coal is composed of 3.6 m (12 ft.) of linsen-bedded sandstone and shale, similar to the deposits in the Colt 3AO Harvey core, and 3 m (10 ft.) of dark gray shale (core descriptions provided by M.C. Colt, Inc.).

As previously stated, the Upper Bluejacket Sandstone has an abrupt basal contact with the subjacent Bluejacket B Coal. This contact appears to be erosional, but this relationship is equivocal. The bottom 15 cm (6 in.) of the Upper Bluejacket Sandstone commonly shows rare pebble-sized shale or coal clasts, which compose approximately 5 percent of the sediment of this lowermost unit. These clasts are believed to be of local derivation and indicate scouring of older deposits.

SANDSTONE SUBFACIES

The Upper Bluejacket Sandstone has been subdivided into seven genetically related subfacies based on sedimentary structure and grain-size. These subfacies are: 1) structureless medium grained sandstone with minor pebble-sized coal and shale clasts; 2) fine to medium grained sandstone with high angle (>30 degrees) planar-tabular cross-stratification; 3) fine sandstone with moderate angle (10-30 degrees) planar-tabular cross-stratification; 4) fine sandstone with low angle (<10 degrees) planar-tabular cross-stratification; 5) very fine to fine grained sandstone with horizontal bedding; 6) very fine grained sandstone with current-ripple bedding; and 7) very fine sandstone interbedded with mudstone. These subfacies are depicted graphically as an idealized stratigraphic column in Figure 6. The distribution of the subfacies in the cores commonly shows one or more of the units absent, but the progression from Subfacies 1 to Subfacies 7 is preserved (Appendix A).

Subfacies 1 is a poorly sorted, medium grained sandstone that commonly contains minor pebble-sized shale and coal clasts (Fig. 10). This subfacies ranges in thickness from 5 cm (2.0 in.) to 20 cm (8.0 in.) and is not present in all the cores examined. The subfacies is devoid of sedimentary structure and is

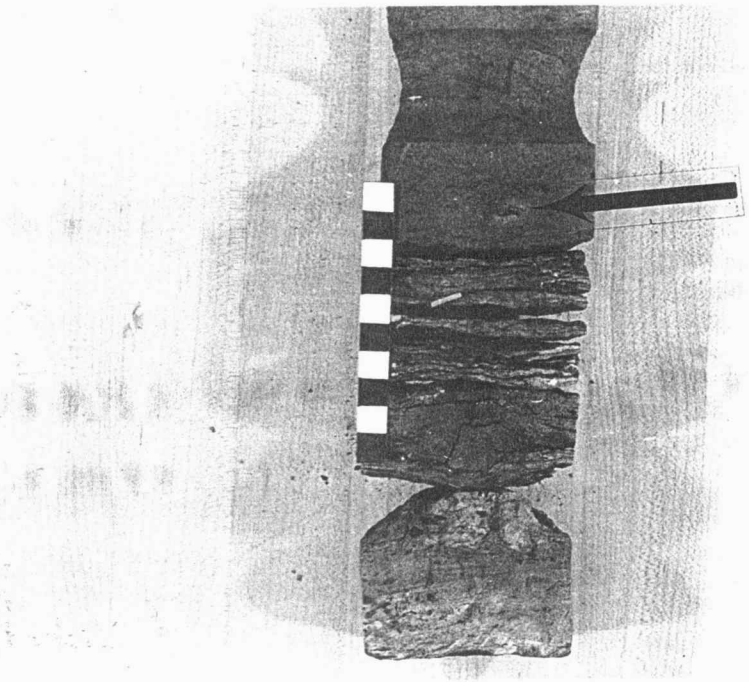

Figure 10. Colt 28A Smith, 776 ft. (Scale=10 cm). Subfacies 1. Poorly sorted, medium-grained basal sandstone (located at top of photo above coal). Note carbonaceous material in the sand (arrow). Sand/Coal contact is located 2.4 cm. below top of scale.

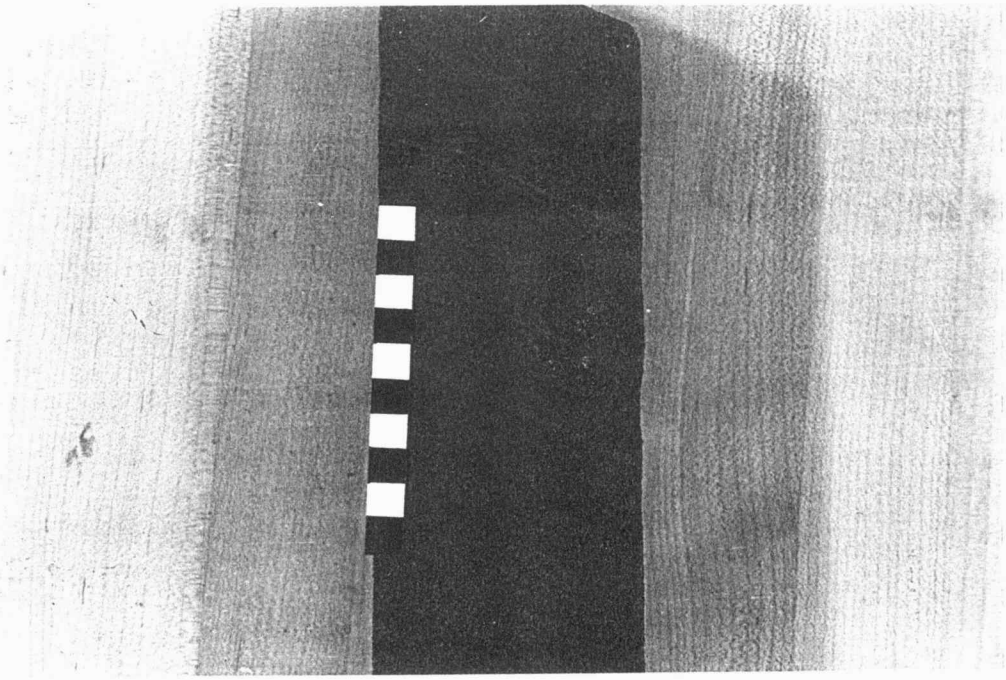

Figure 11. Colt 26AO Johnson, 744 ft. (Scale=10 cm). Subfacies 2. High angle, planar-tabular crossbedded sandstone showing preferential cementation along crossbed faces.

usually found directly overlying the surface scoured basal coal. This subfacies contains minor amounts of authigenic pyrite along the contact with the coal. Subfacies 1 constitutes a total of only 1.1 m (3.5 ft.) of the entire 92.4 m (303 ft.) of sand measured in the nine cores described.

Subfacies 2 is composed of moderately sorted fine to medium sand that exhibits high angle planar-tabular crossbedding. High angle cross-stratification, as defined by this study, exceeds 30 degrees dip from the horizontal. The maximum angle of dip observed in the cores examined was 40 degrees. Individual crossbeds range in thickness from 0.5 cm (0.2 in.) to 4 cm (1.6 in.) and commonly show preferential carbonate cementation along crossbed faces (Fig. 11). Individual crossbed sets range in thickness from 10 cm (3.9 in.) to 2 m (6.6 ft.) and are bounded on both top and bottom by subtle scour surfaces. Each crossbed set represents one continuous and undisturbed period of deposition. The subfacies reaches a maximum thickness of 4.9 m (16 ft.). This subfacies constitutes 33.5 m (110 ft.) or 36% of the total sand measured and described.

Individual crossbeds commonly show a marked increase in grain size from the bottom crossbed face to the upper crossbed face. This phenomenon is a function of the greater dispersive pressure exerted on the large

grains relative to the small grains during transport. The gravity induced movement of the sand grains down the avalanche face creates a dispersive pressure that tends to separate the grains by size and this results in the vertically upward coarsening grain size distribution observed within each crossbed.

The large scale sedimentary structures observed in Subfacies 2 are likely the result of deposition by migrating sandwaves and, possibly, large dunes (Harms et al., 1982). Crossbeds resulting from dune migration commonly show curvilinear and tangential crossbed faces in cross-section as opposed to the linear faces observed in the cores. Examples of curvilinear faces were rarely observed but it is difficult to recognize large scale sedimentary structures in a 9 cm (3.5 in.) diameter core.

Subfacies 3 is similar to Subfacies 2 except it shows planar-tabular crossbeds that dip less steeply (10-30 degrees) and is commonly finer grained (Fig. 12). Crossbeds range from 0.3 cm (0.2 in.) to 2 cm (0.8 in.) in thickness and rarely exhibit the graded bedding that is prevalent in Subfacies 2. Crossbed sets range in thickness from 4 cm (1.6 in.) to 50 cm (19.7 in.). This subfacies reaches a maximum thickness of 3.7 m (12 ft.). The total thickness of Subfacies 3 described was 17.4 m (57 ft.) or 19% of the sand

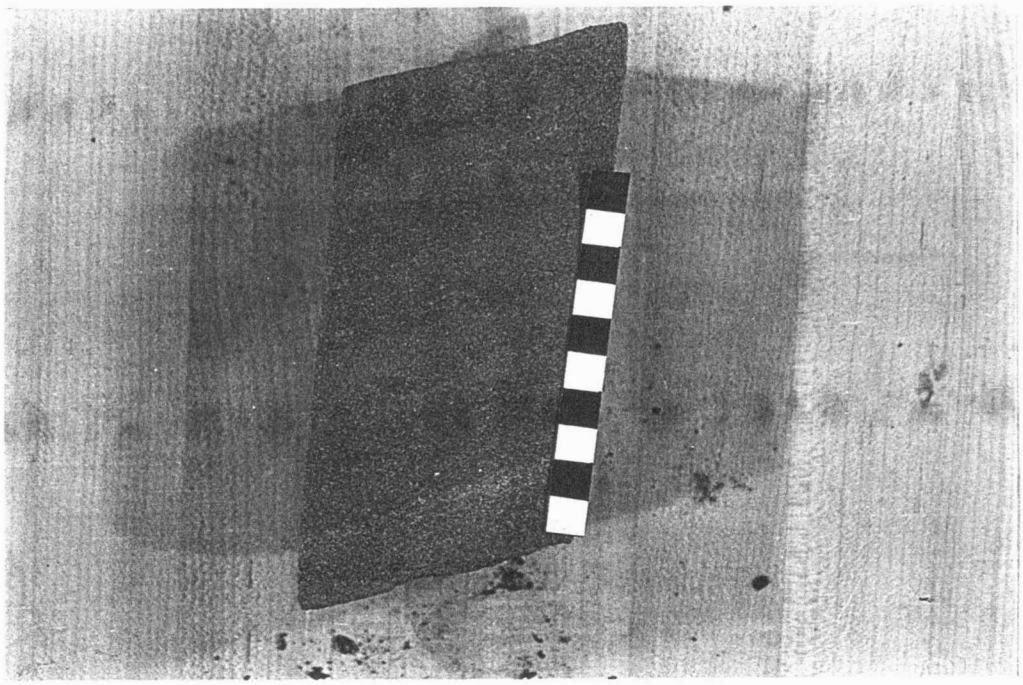

Figure 12. Colt 26AO Johnson, 726 ft. (Scale=10 cm). Subfacies 3. Fine sandstone with moderate angle, planar-tabular crossbedding Similar to Subfacies 2 but crossbeds dip less steeply and the sand is finer grained.

observed in the cores. Subfacies 3 also shows abundant preferential cementation along crossbed faces.

The sedimentary structures observed in Subfacies 2 and 3 appear to have been the result of sands deposited by a unidirectional current (Reineck and Singh, 1980). All crossbeds of a given set dip in approximately the same direction. This indicates the sands were deposited by similarly oriented currents during successive periods of deposition.

Subfacies 4 is composed of moderately sorted very fine to fine grained sand that exhibits low angle (<10 degrees) planar-tabular cross-stratification (Fig. 13). Crossbeds range in thickness from 0.3 cm (0.2 in.) to 2 cm (0.8 in.). This subfacies reaches a maximum thickness of 1.2 m (4 ft.). The subfacies constitutes 15.2 m (50 ft.) or 17% of the total sand thickness measured.

Crossbed faces commonly exhibit abundant carbonate cement, similar to Subfacies 2 and 3. This selective distribution of the cement is easily observed in Subfacies 2, 3, and 4 because of the strong contrast between the lightly colored carbonate cement and the darker, oil-stained zones (Fig. 11). Subfacies 4 also contains entire individual crossbeds that show less residual oil saturation because of the high degree of cementation (Fig. 13).

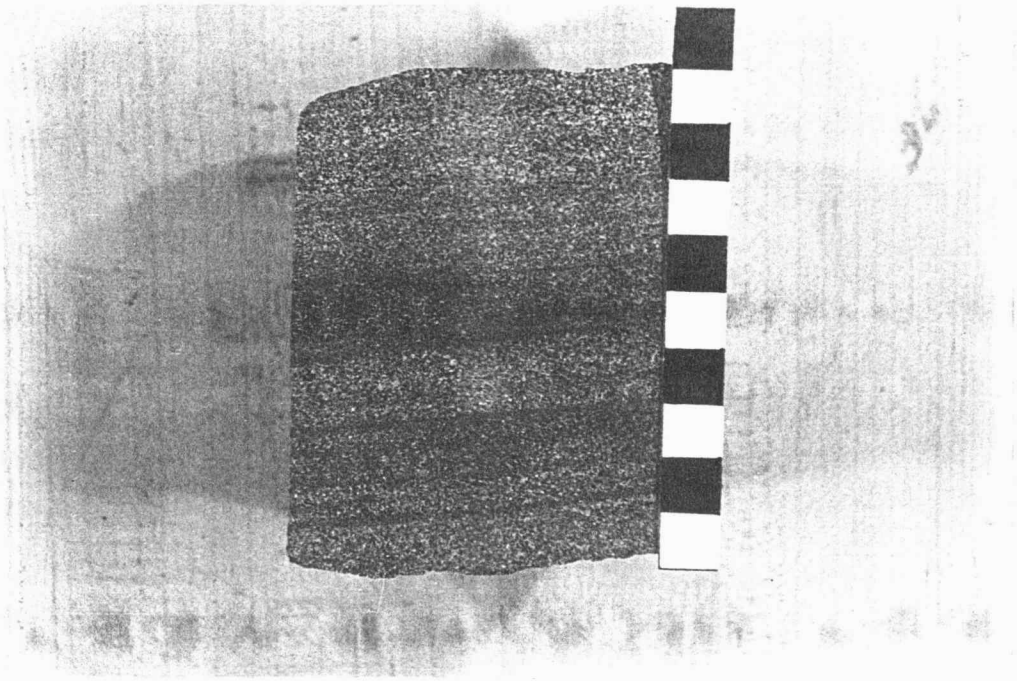

Figure 13. Colt 26AO Johnson, 759 ft. (Scale=10 cm). Subfacies 4. Very fine to fine grained, low angle planar-tabular crossbedded sandstone.

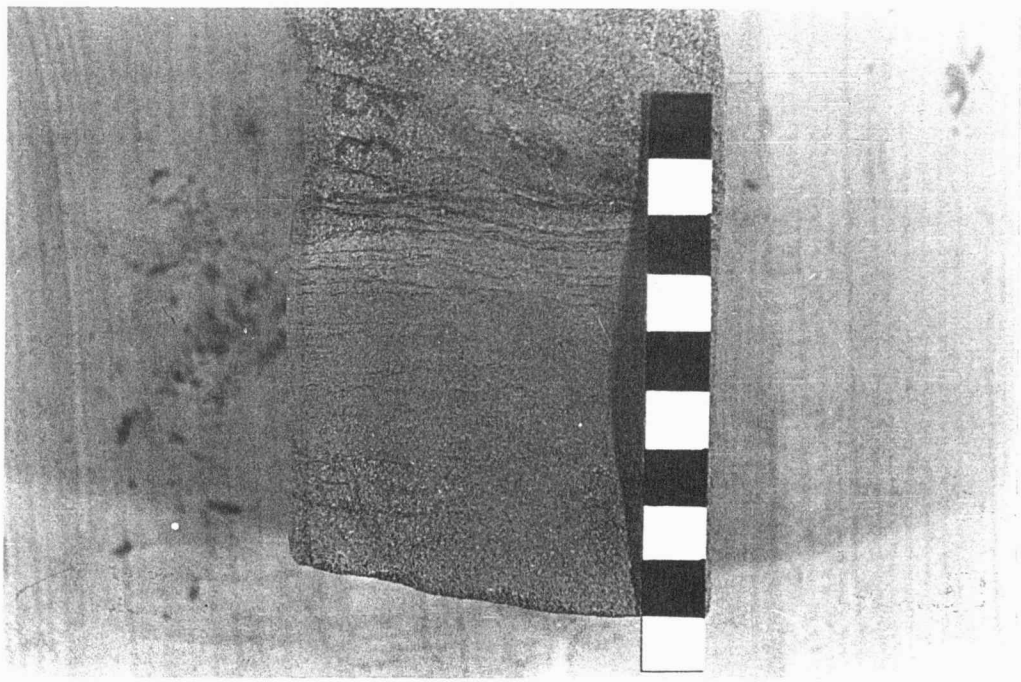

Figure 14. Colt 5A Harvey, 756.5 ft. (Scale=10 cm). Subfacies 5. Very fine to fine grained, horizontally bedded sandstone.

Unlike Subfacies 2 and 3, Subfacies 4 may contain minor shale laminae or rippled mud drapes deposited on the lee face of the migrating small dunes and sand waves. During periods of reduced current velocity, fine sediment may accumulate in protected areas between crests of adjacent bed-forms. The fine sediment is covered and preserved by fine-grained sand deposited by later dune migration. Subfacies 4 also contains moderate (>5%) amounts of syndepositional matrix relative to Subfacies 2 and 3.

Subfacies 5 is horizontally laminated very fine to fine grained, moderately sorted sandstone (Fig. 14). Laminae range in thickness from 0.2 cm (0.08 in.) to 0.5 cm (0.2 in.). The subfacies reaches a maximum thickness of 0.6 m (2 ft.). Subfacies 5 composes 15.5 m (51 ft.) or 17% of the total 92.3 m (303 ft.) of sand measured. This subfacies is characterized by common thin (5 mm) drapes of rippled shale that demarcate the horizontal beds.

Subfacies 6 consists of current-ripple laminated very fine grained sandstone (Fig. 15). These sands were deposited by the migration of small scale ripples driven by a relatively low energy unidirectional current (Reineck and Singh, 1980). This subfacies exhibits abundant thin shale drapes, micaceous partings and minor carbonized plant fragments. The lamina

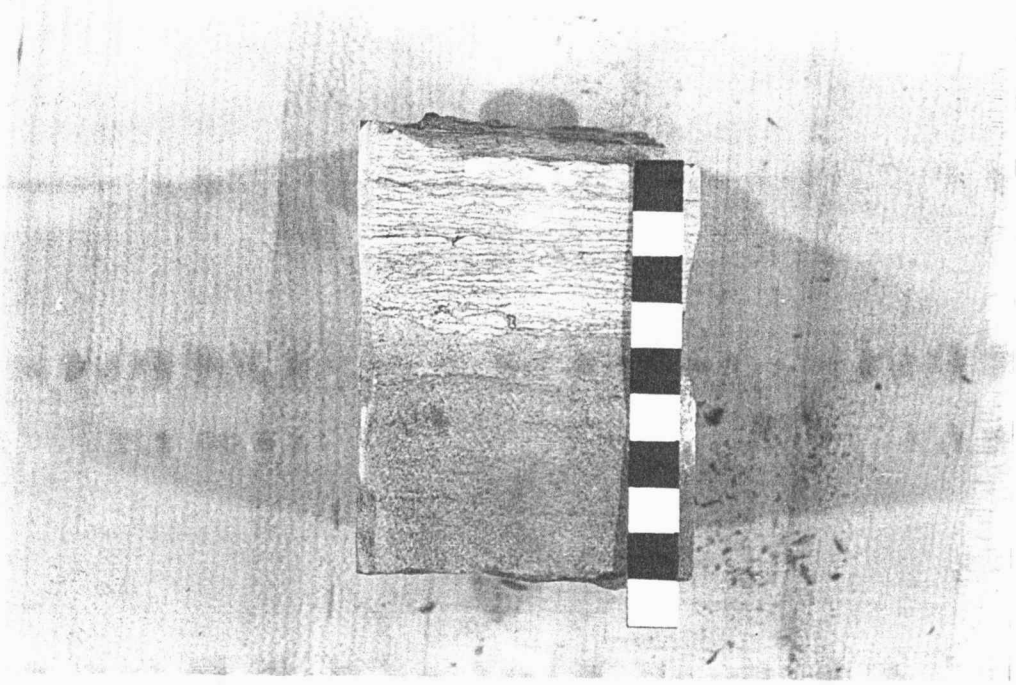

Figure 15. Colt 5A Johnson, 710 ft. (Scale=10cm). Subfacies 6. Very fine grained, current ripple bedded sandstone (upper 4 cm of core in photograph).

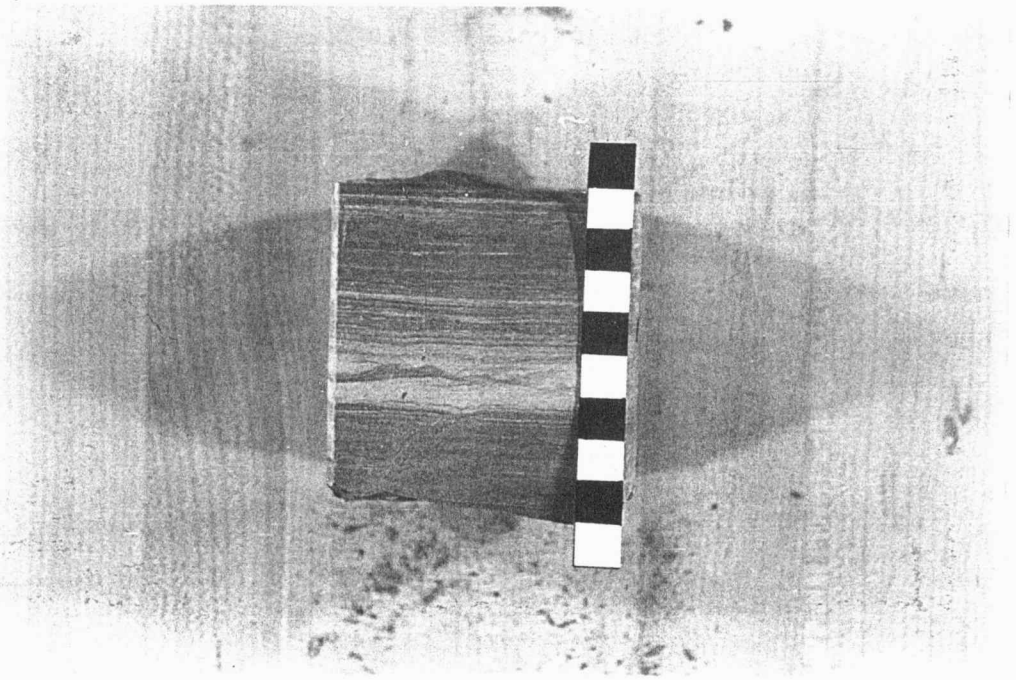

Figure 16. Colt 5A Harvey, 741.5 ft. (Scale=10 cm). Subfacies 7. Interbedded very fine sandstone, siltstone and shale.

reaches a maximum thickness of 0.5 cm (0.2 in.) and shows rare bioturbation. This subfacies reaches a maximum thickness of 61 cm (2 ft.). The cumulative thickness of Subfacies 6 described was 3% of the total sand measured in the cores. This subfacies shows very little oil saturation because of extensive cementation.

Subfacies 7 is composed of interbedded or linsen-bedded very fine sandstone and shale (Fig. 16). This subfacies rarely shows disrupted bedding, which results from horizontal or vertical burrowing. This subfacies contains numerous micaceous partings and authigenic carbonate nodules. Subfacies 7 reaches a maximum thickness of 3 m (10 ft.) and is usually found overlying the other subfacies previously described. The subfacies composes 7% of the total sand measured. Thin intervals (15 cm.) of this subfacies are also found directly overlying or near the Bluejacket B Coal.

The core from Colt 3AO Harvey (Appendix A), the well studied that did not penetrate the main body of the sand, is composed almost entirely of linsen-bedded sandstone and shale (Subfacies 7) overlying the Bluejacket A Coal. Unlike the interbedded sandstone and shale seen in Figure 16, this well exhibits predominately shale with minor sand lenses that reach a maximum thickness of 0.3 cm (0.2 in; Figs. 17 and 18).

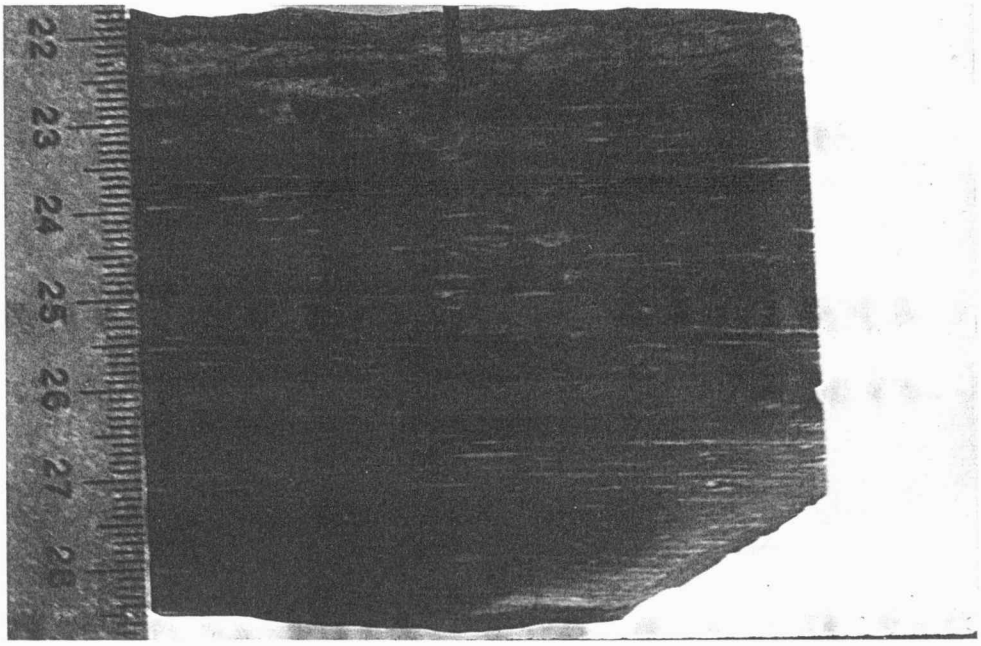

Figure 17. Colt 3AO Harvey, 764 ft. (Scale=cm). Linsen-bedded very fine sandstone, siltstone and shale. Note horizontal burrows (arrows).

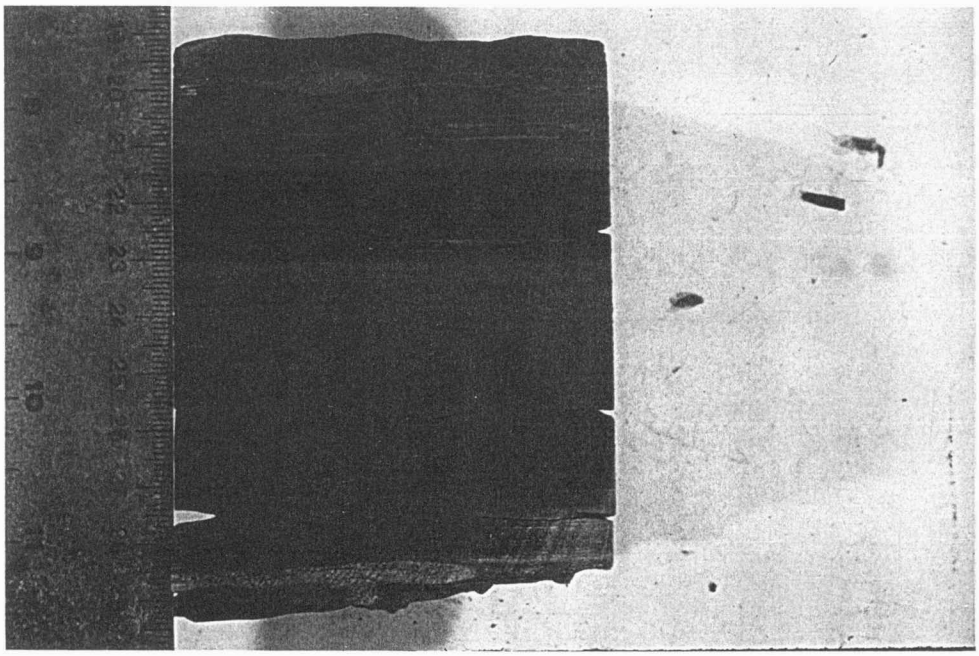

Figure 18. Colt 3AO Harvey, 759 ft. (Scale=cm). Streaked shale (De Raaf, et al., 1977) interbedded with very fine sandstone and siltstone. Note the burrows and paucity of sand lenses relative to Figure 17.

Subfacies 7 is interpreted to have been deposited in a low energy environment that lacked sufficient sand input, such as a bay with minor marine influence. The minor amount of sand tends to arrange or organize into sand ripples on the cohesive mud substrate. The depositional environment of this subfacies is discussed in the following section.

DEPOSITIONAL ENVIRONMENT

The sandstones of the KB Field exhibit features that are indicative of deposition by a meandering fluvial system. These features are: 1) An overall decrease in average sand grain-size from the basal contact to the upper contact of the sand body; 2) A decrease in the scale of the sedimentary structures from the basal contact to the upper contact; 3) Sedimentary features associated with deposition by a unidirectional current; 4) Complete absence of fossil evidence such as shell debris; 5) A paucity of bioturbation; and 6) sandstones that are texturally and mineralogically immature (Jackson, 1978).

The features observed in the Upper Bluejacket Sandstone can be compared to the salient features of sands from other clastic depositional environments. Marine depositional environments, such as offshore bars and barrier islands, are characterized by an upward increase in mean grain-size and are composed of very well sorted sands (Reineck and Singh, 1980). Deposits of this type also contain abundant biotic constituents and glauconite. Tidal channels are similar to fluvial deposits in that they show a fining-upward grain-size sequence (Johnson, 1978). Unlike fluvial deposits, tidal sands contain abundant shell fragments,

glauconite and bidirectional cross-stratification. Delta distributary channel deposits commonly show either an upward increase in mean grain-size or no change in grain-size throughout the sand body (Elliott, 1978). Braided stream deposits are generally not characterized by an orderly vertical succession of sedimentary structures and grain size changes (Miall, 1978).

The study of sediments deposited by modern and ancient meandering fluvial systems resulted in the development of an idealized point bar model (Fig. 19) (Allen, 1963, 1964, 1965, 1970; Visher, 1965; Jackson, 1975; Reineck and Singh, 1980; Harms et al., 1982). Point bars of a meandering fluvial system show a vertical decrease in mean grain-size and scale of sedimentary structures. The succession of grain-sizes and sedimentary structures is a function of declining velocity of the depositional current. The coarsest sands and largest scale sedimentary structures are found in the thalweg of the channel where the current velocity and shear stress are greatest (Fig. 20). The sediment in the thalweg is commonly conglomeratic and composed of material eroded from the cut-bank during channel migration. Finer sediments showing smaller scale sedimentary structures are deposited on the shallow, upper reaches of the point bar where the

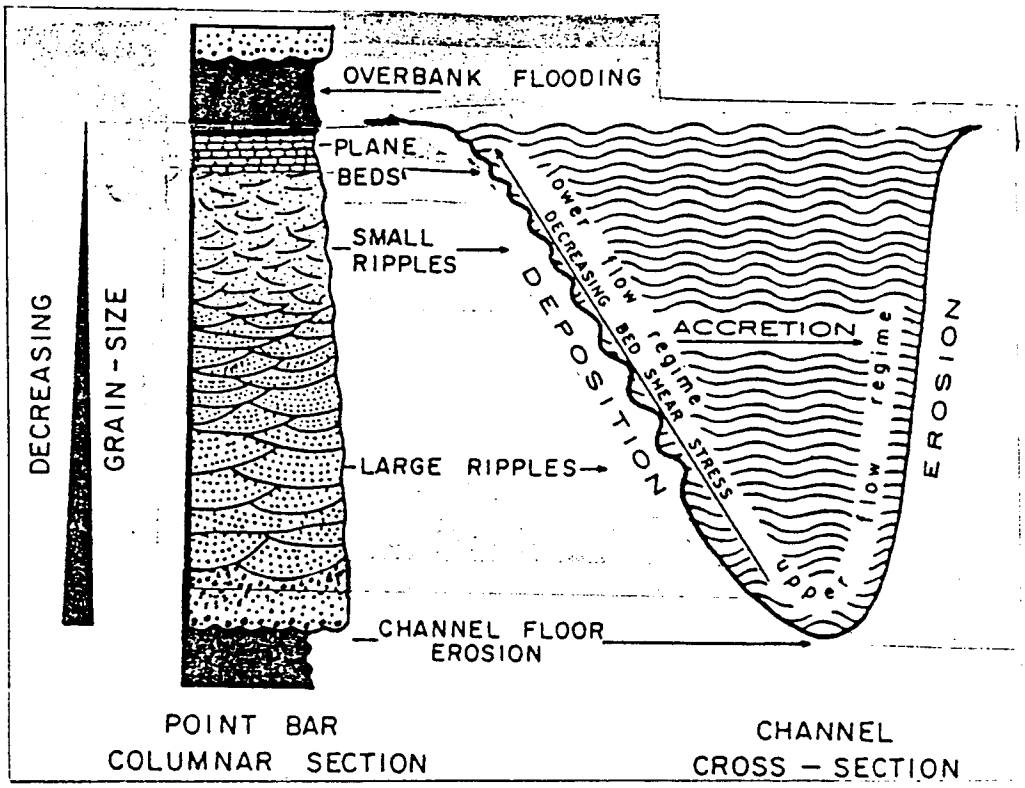

Figure 19. Idealized columnar section and channel cross-section of fluvial point bar deposits (modified from Allen, 1963).

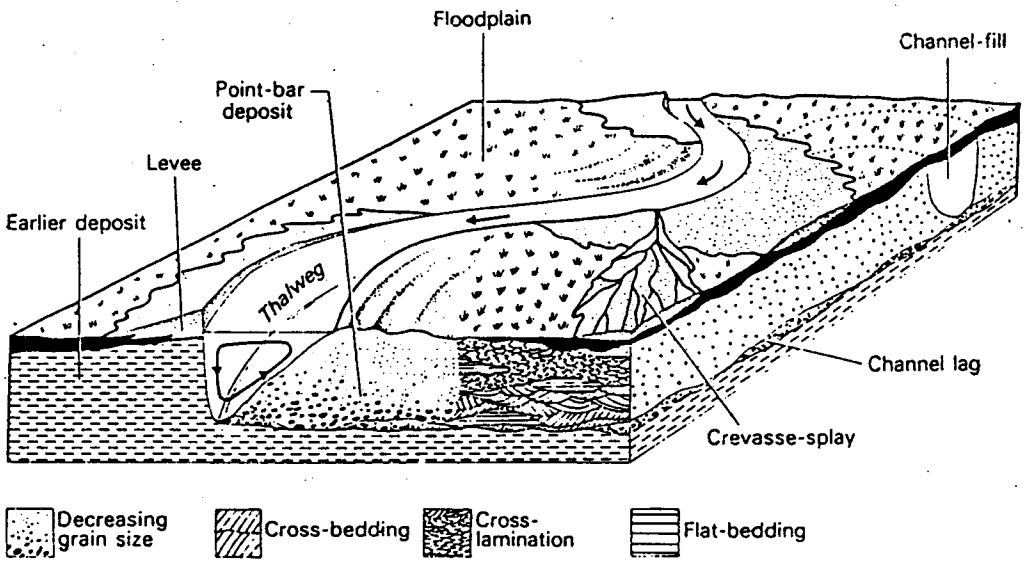

Figure 20. Facies model of meandering river alluvial plain (after Allen, 1964, 1970).

current velocity and shear stress decrease. Lateral channel migration results in entire sand bodies that display a vertical decrease in grain-size and scale of sedimentary structure (Fig. 20). A vertical sandstone sequence represents a continuum of progressively lower energy deposits, each deposited successively higher on the point bar.

The idealized model of the point bar demonstrates a predictable succession of sedimentary structures (Fig. 19). The vertical sequence of sedimentary structures is: 1) structureless, conglomeratic basal sandstone above the channel-floor erosional surface; 2) large-scale crossbedding; 3) small-scale crossbedding; 4) plane beds and 5) fine sediment deposited on the floodplain during flooding. One or more of these sedimentary structures is commonly absent from point bar deposits, but the transition from large scale to small scale sedimentary structures is retained. The actual distribution of bedforms depends upon the available grain size, the current velocity and depth of the channel (Collinson, 1978).

In all of the cores described, including the descriptions conducted by Dr. Busch, a vertical decrease in mean grain-size from the sand directly above the basal contact to the contact with the superjacent shale was observed (Appendix A). As stated

previously, the basal sands (Subfacies 1) are composed of medium- to fine-sand with common pebble-sized clasts, while the upper portion of the sequence contains rippled very-fine sand (Subfacies 6). This indicates that the vertical sandstone sequence observed in the Upper Bluejacket Sandstone was the result of deposition by progressively lower velocity currents.

The vertical decrease of the mean grain-size in the Upper Bluejacket Sandstone was not gradual and progressive as depicted in the point-bar model. The upward decrease in the grain-size from the base to the top of the reservoir sandstone consisted of a series of punctuated fining-upward sequences. All of the cores described for this study showed one or more erosional surfaces above which the mean grain-size increased. The erosional surfaces and the subsequent deposition of coarser sands are the result of a sudden increase in the velocity of the depositional current. The greater velocity enabled the current to erode and transport the finer sands that were previously deposited. An abrupt increase in the current velocity can result from either the rejuvenation of the previously active, lower energy current during flooding or the migration of a second and discrete fluvial channel eroding into the older deposits. This topic will be discussed in the section dealing with reservoir geometry.

The range of grain sizes observed in the Upper Bluejacket Sandstone in the KB Field is small compared to most modern fluvial point-bar deposits (e.g. Wabash River, Jackson, 1975, 1976). The average grain-size observed in the Upper Bluejacket Sandstone ranged from medium sand (0.27 mm., 1.8 phi) at the base to very-fine sand (0.10 mm., 3.3 phi) at the top. Modern fluvial systems commonly exhibit grain-sizes that range from granules (2.5 mm., -1.3 phi) to very-fine sand (0.10 mm., 3.3 phi) (Jackson, 1978). The overall fine grain-sizes observed in the Upper Bluejacket Sandstone suggests that the velocity of the depositional current was low and that coarse sand was unavailable.

The depositional system that deposited the Upper Bluejacket Sandstone in the KB Field was likely a small, low velocity, low gradient meandering stream as indicated by the fine grain-size (Appendix A). These streams should not be confused with the coarse-grained, relatively high energy fluvial systems that have been extensively studied by modern sedimentologists (e.g. Brazos, Colorado and Wabash Rivers). The stream that deposited the reservoir sandstone was likely a small tributary of the major depositional system outlined by Weirich (1953; see Fig. 4).

Subfacies 1, the basal sandstone member, is analogous to the coarse channel lag deposits commonly

seen in fluvially derived sands. During channel incision and migration in modern fluvial environments, lag deposits develop from the erosion of adjoining floodplain shales. Large blocks of shale slough into the channel along the cut-bank and are partially disaggregated by the current in the thalweg (Fig. 20). Residual concentrations of coarse material remain because the velocity of the depositional current is insufficient to transport this coarse material (Reineck and Singh, 1980). The pebble-sized shale and coal clasts observed in Subfacies 1 were probably eroded from the Bluejacket A and B peats and shales during channel development (Fig. 2; Plate 6a). The dearth of coarse material in Subfacies 1 relative to most channel lag deposits probably is a function of the lack of cohesiveness of vegetal matter. As the peat deposits eroded, the plant debris likely broke into easily transportable fragments.

The streams that deposited the Upper Bluejacket Sandstone in the KB Field eroded into the thick (>10 ft.) peat deposits of the Bluejacket A and B Coals (Plate 6a). Peat, the precursor to coal, commonly contains more than 80% water and can compact to a tenth of the original thickness (Brown and Dey, 1975). Large quantities of peat were eroded and transported during the incision and subsequent migration of the channel.

The lack of cohesiveness of the peat precluded the formation of the well developed basal conglomerates observed elsewhere in the Cherokee Basin (Woody, 1983; Hulse, 1978; Ebanks and James, 1974).

The Upper Bluejacket Sandstone exhibits a decrease in the scale of the sedimentary structures from the basal contact to the upper contact. The idealized stratigraphic column (Fig. 6) shows the vertical sequence of sedimentary structures observed in the cores. The sandstone shows an incremental sequence from Subfacies 1, the basal sandstone to Subfacies 7, the interbedded sandstone and shale. This sequence is interpreted to be the result of deposition by progressively slower velocity currents for each subfacies. This conclusion is supported by the finer grain-size observed in each successive subfacies.

The sedimentary structures of the Upper Bluejacket Sandstone in the KB Field indicate deposition by a unidirectional current. Planar-tabular cross-stratification is the product of downstream migration of large bedforms driven by a dip-fed fluvial system (Harms et al., 1982). A less intense unidirectional current also produced the current-ripple bedding in the fine to very fine sand (Subfacies 6). The rippled sand and the linsen-bedded sand and mud subfacies do not show any evidence of bidirectional flow such as

herring-bone cross-stratification. The lack of evidence of frequent shifts in current direction or strength in the linsen-bedded subfacies supports the interpretation that these sediments were deposited in a fluvial overbank environment as opposed to a tidal flat (Dickinson, 1975). This is significant because Reineck and Singh (1980) believe interbedded sandstones and shales are associated with tidal flat deposition.

The lack of fossils and bioturbation further supports the interpretation of a fluvial depositional environment. No fossil shell fragments indicative of marine, estuarine or lacustrine environments were observed in any of the cores examined for this study, or in the cores described by Dr. Busch. A conodont observed in the Colt 28A Smith core is not indicative of any specific depositional environment and was probably transported from outside the study area. Other studies found Cherokee Group sandstones to be completely devoid of any invertebrate fossil remains (Hulse, 1978; Woody, 1983). Unlike numerous other clastic depositional environments, relatively few invertebrates with resistant skeletal parts are found in the fluvial environment. Bioturbation is rarely as abundant in the fluvial environment as the marine environment. Horizontal burrowing was observed in the interbedded sandstone and shale (Subfacies 7), but is

relatively rare. Minor burrowing was observed in the overbank deposits in this study (Figs. 17 and 18) and other studies of Cherokee Group sandstones (Hulse, 1978; Woody, 1983).

SUMMARY-DEPOSITIONAL ENVIRONMENT

The fluvial system that deposited the Upper Bluejacket Sandstone in the KB Field is envisioned to have been a small, meandering stream that eroded into the Bluejacket A and B peats and shales during channel incision (Plate 6a, Fig. 2). Lateral channel migration resulted in extensive erosion, fragmentation and transportation of the vegetal matter and shale. The lack of cohesiveness of the peat precluded the formation of well developed basal conglomerates. The lateral migration of the channel also resulted in the development of point-bars with characteristic vertical decrease in mean grain-size and scale of the sedimentary structures.

RESERVOIR GEOMETRY

Previous studies of Cherokee Group sandstones revealed sand bodies that are elongate in plan-view and lenticular in cross-section (Ebanks, 1979; Hulse, 1978; Schumacher, 1976). It is significant to note that the interpreted depositional environment of these sandstones and the proposed environment of deposition of the Upper Bluejacket Sandstone in this study are identical. Maps of the reservoir in the KB Field were constructed to determine the reservoir geometry and to compare with the geometries of other locations in the Cherokee Basin. Descriptions of the maps constructed, and their significance, are presented in the following section.

Plate 2 is a net sand isolith map of the Upper Bluejacket Sandstone that was constructed from over 150 gamma-ray logs. The geometry of the reservoir in the study area is not elongate and is not a lenticular, simple lens in cross-section. The overall reservoir geometry is blanket-like in plan view and irregular in cross-section. The sandstone reservoir shows an irregular distribution of sand thicknesses, particularly when compared to other parts of the Bronson-Xenia Field and other Upper Bluejacket Sandstone reservoirs (Fig. 21). Moreover, the width of the reservoir in the KB Field is great compared to

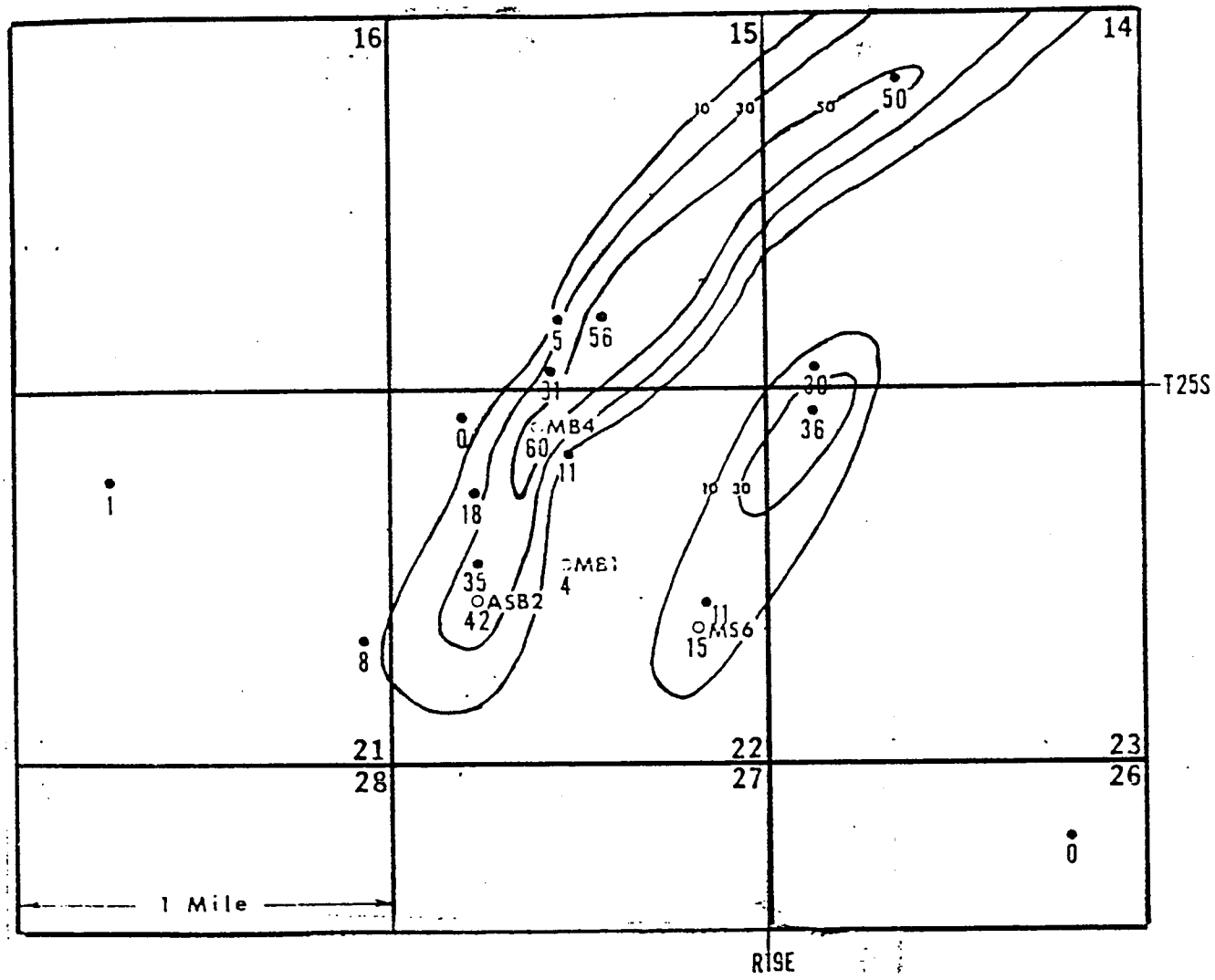

Figure 21. Net sand isolith map of the Upper Bluejacket Sandstone, La Harpe Field, Allen County, Kansas (Schumacher, 1976). Contour interval=20 ft.

these other reservoirs. The KB Field reservoir is 1280 m (4200 ft.) wide, while many Upper Bluejacket reservoirs are commonly less than 760 m (2500 ft.) wide (Fig. 21). The KB Field area of the Bronson-Xenia Field appears to be locally broadened.

Cross-sections of the reservoir (Plate 6b) demonstrate that the geometry in the KB Field is not lenticular, but composed of laterally alternating thick- and thin-sand zones. The reservoir is bisected by an elongate region of thin sand that trends northeast-southwest (Plate 2). Colt 37A Johnson, a dry hole, is situated in roughly the center of the "central thin-sand zone" of the reservoir and contains only 0.6 m (2 ft.) of sand. The trend of thinner sand divides the reservoir into two quasi-lenticular parts (Plate 6b). Neither of these sandstone bodies approaches the degree of lenticularity observed elsewhere in the Cherokee Basin (Figs. 21 and 22). The reservoir southeast of this trend is more lenticular than the northwestern portion. The northwestern segment of the reservoir is highly irregular showing a number of loci of thick and thin sands.

An abrupt lateral termination of the sandstone body is characteristic of fluvial deposits in the Cherokee Basin (Schumacher, 1976; Hulse, 1978). The net sand isolith map shows the lateral termination of

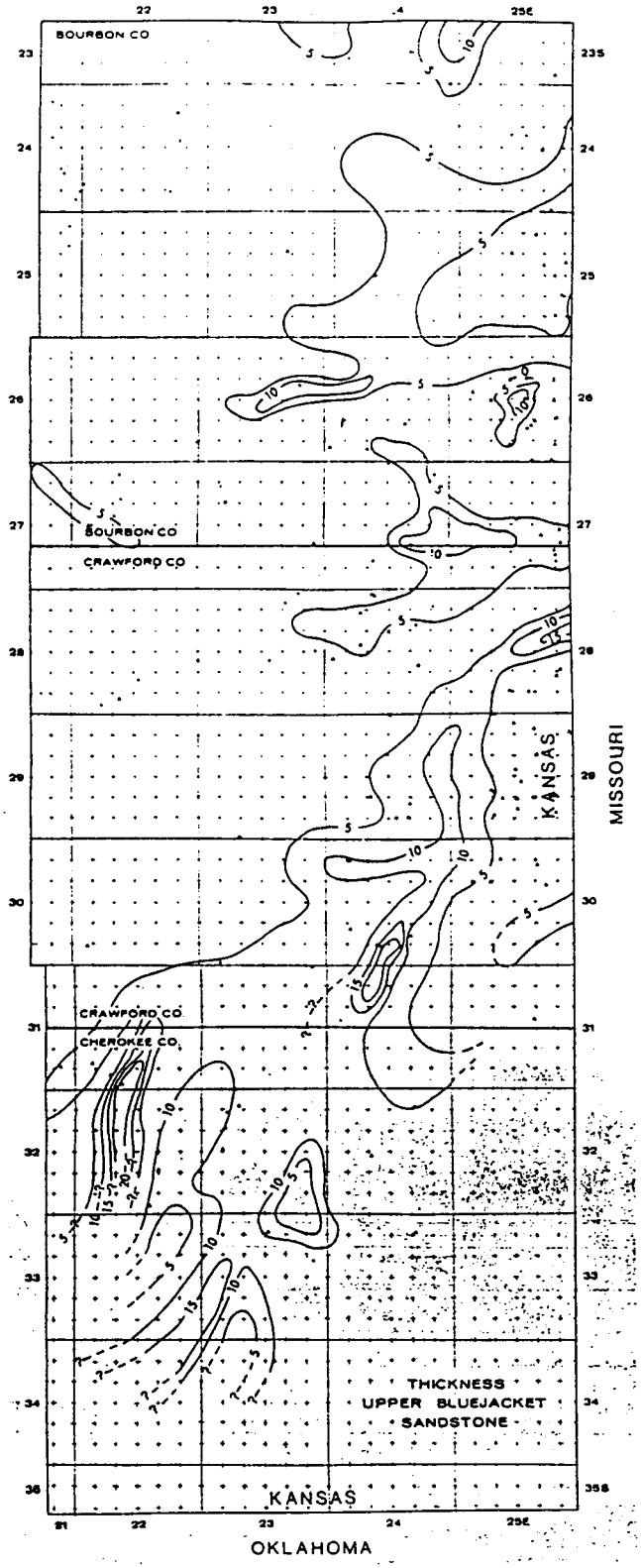

Figure 22. Map of thickness of Upper Bluejacket Sandstone in Southernmost Kansas (Ebanks, 1979).

the sand to the northwest and to the central thin-sand zone. Colt 37A Johnson shows virtually no sand while over 7.6 m (25 ft.) of sand is observed 137 m (450 ft.) away in Colt 36A Johnson. As noted earlier, Colt 3AO Harvey contains less than 0.9 m (3 ft.) of sand and is located only 61 m (200 ft.) from wells containing an average sand thickness of 11.6 m (38 ft.). The lateral terminations are interpreted to be cut-banks of the meandering stream that deposited these sandstones.

Though not readily apparent on the net sand isolith map, the sand body continues both to the northeast and to the southwest (Plate 2). The northeastern portion of the reservoir contains a gas cap and considerably less oil. This section of the reservoir has not been exploited due to unfavorable economic conditions. The southwestern region of the reservoir contains abundant water and, therefore, was not drilled. Well information from the wells to the northeast and southwest was not available for this study (Plate 1).

A series of structure and isopach maps was constructed from log data to understand the configuration of the KB Field (Plates 3, 4 & 5). Plate 3 is a structure map (Datum=sea level) of the top of the Bluejacket B Coal located just below the Upper Bluejacket Sandstone. On average, the base of the

sandstone lies at 100 m (330 ft.) above sea level and the sand body dips to the south-southwest. The structure of the top of the coal bed forms a symmetrical basin with the center located in the south-central portion of the Johnson lease. The elevation of the coal bed increases to the northwest, which is interpreted to be a function of the lateral thinning of the sand. The amount of compaction of the underlying coal and shale is greatest under the main body of sandstone.

In order to minimize the effect of post-depositional tectonism on the structure of the KB Field, two isopach maps were constructed using easily correlated and recognizable stratigraphic horizons. The gamma-ray logs exhibit two highly radioactive black shales in the stratigraphic column above the Upper Bluejacket Sandstone (Fig. 23). It is assumed that the black shales were deposited as thin horizontal beds and, therefore, make excellent horizons upon which to base paleo-reconstructions. The contours on Plate 4 represent the thickness between the upper black shale (informally called the V-shale; BlkSh-1, Fig. 23) and the top of the Bluejacket B Coal. The contours on Plate 5 represent the thickness between the lower black shale (associated with the Tebo Coal; BlkSh-2, Fig. 23) and the top of the Bluejacket B Coal. The construction

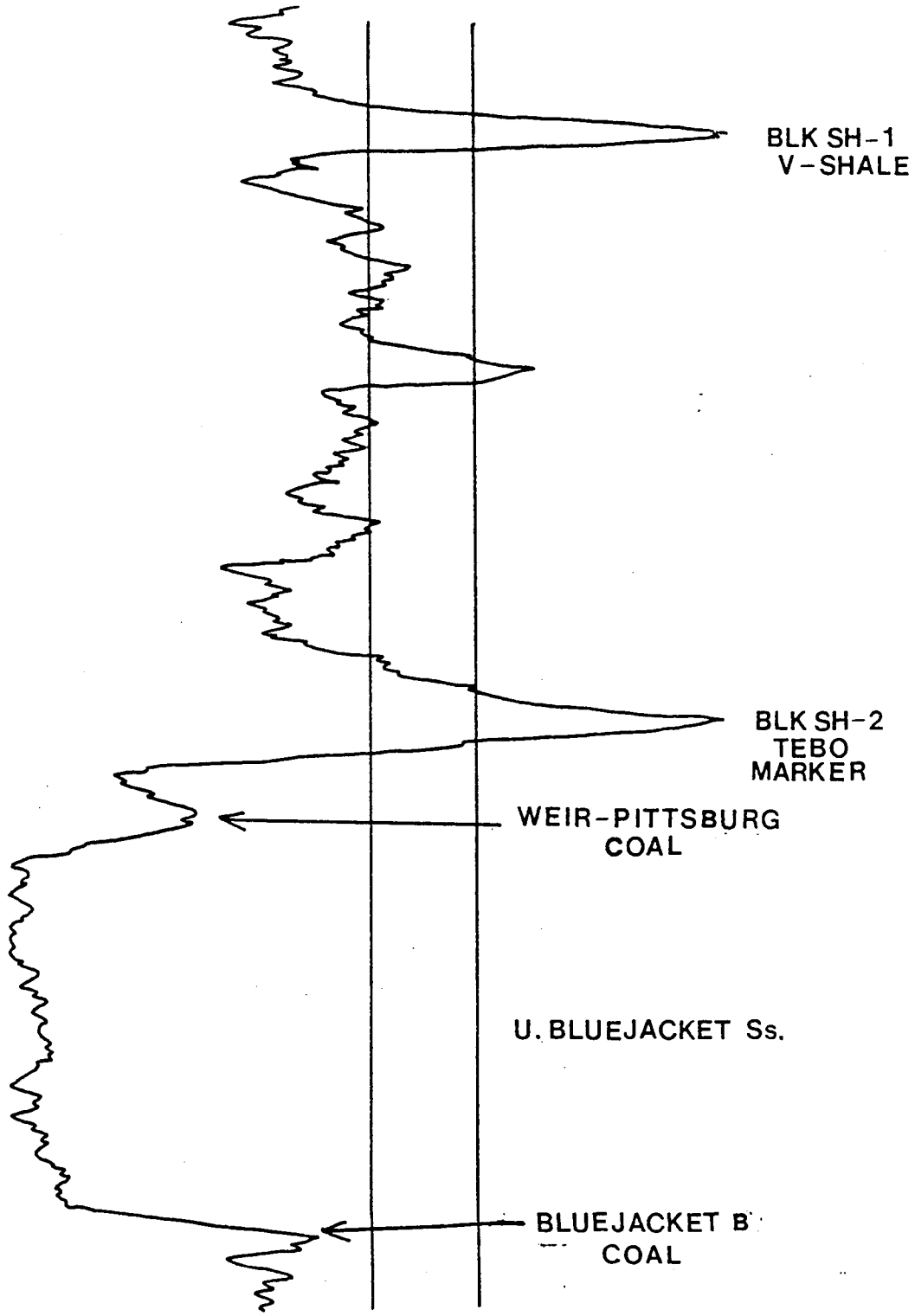

Figure 23. Gamma ray log from Colt 21A Johnson. Note Upper Bluejacket Sandstone and highly radioactive shales.

of these maps was intended to show the structural configuration of the coal at the time of upper and lower black shale deposition.

The isopach map drawn from the upper black shale to the Bluejacket B Coal (Plate 4) shows that the thickest section lies in the central and south-central portion of the Johnson Lease, where the sandstone is thickest. If the assumption that the black shale was deposited as a thin horizontal bed is correct, the contours demonstrate that the degree of compaction of the Bluejacket B peat and the underlying shale is related to the thickness of the sand. The central thin-sand zone appears as a vague trend. In this area, compaction of the peat was less extensive. The thickness of the section between the upper black shale and the Bluejacket B Coal is also a function of erosion that occurred at the time of deposition.

The isopach map of the interval from the lower black shale to the Bluejacket B Coal (Plate 5) is the most useful in delineating the configuration of the coal bed subsequent to sand deposition. The lower black shale is situated directly above the top of the sand body and, therefore, does not reflect compaction of the section between the two black shales. This map clearly shows the central thin-sand zone as a high relief trend. The isopach map also shows the thickest

stratigraphic interval coincides with the greatest accumulation of sand. This pattern is believed to the result of not only differential compaction, but erosion of the Bluejacket B peat bed during channel incision.

As stated earlier, previous studies of fluvial Upper Bluejacket Sandstones reported sand-body geometries that were lenticular in cross-section and elongate in plan view. Considering the similarity of the depositional environments of the sandstones in the KB Field and other reservoirs in the Cherokee Basin, the dissimilarity of the reservoir geometries is curious. The possibility that the sandstones in the study area reflect a more highly complex geometry than other Cherokee reservoirs was investigated. As noted earlier, the cores from the Upper Bluejacket Sandstone exhibited erosional surfaces above which a marked increase in mean grain-size was observed (Figs. 24 and 25). The sands directly above the scour surfaces commonly contained carbonized plant fragments and shale clasts (Appendix A). Generally, surfaces of this type are interpreted to be the result of an increase or rejuvenation of the depositional current during flooding (Collinson, 1978). The possibility exists that these surfaces are not merely reactivation surfaces but the boundry between two distinct and different multistoried sand bodies. If indeed the

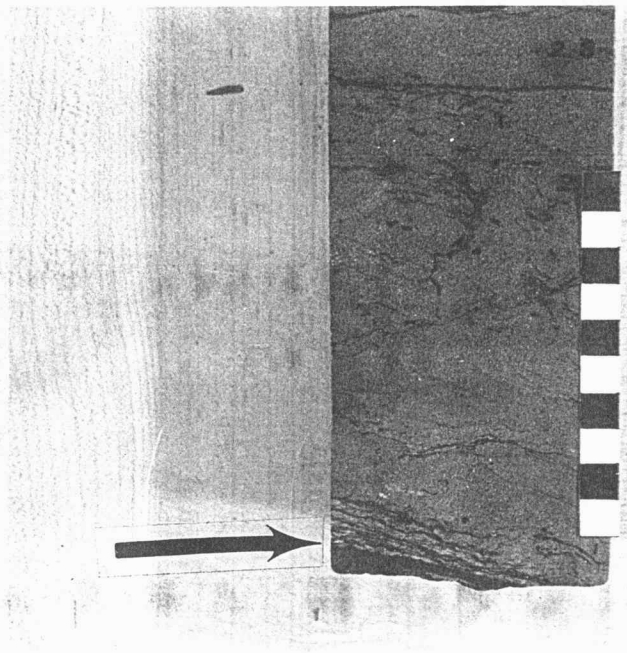

Figure 24. Colt 28A Smith, 775 ft. (Scale=10 cm.)
The core section shows abundant carbonaceous matter (plant fragments) directly above erosional surface (arrow). Erosional surfaces in the Upper Bluejacket Sandstone are commonly found in association with coal clasts.

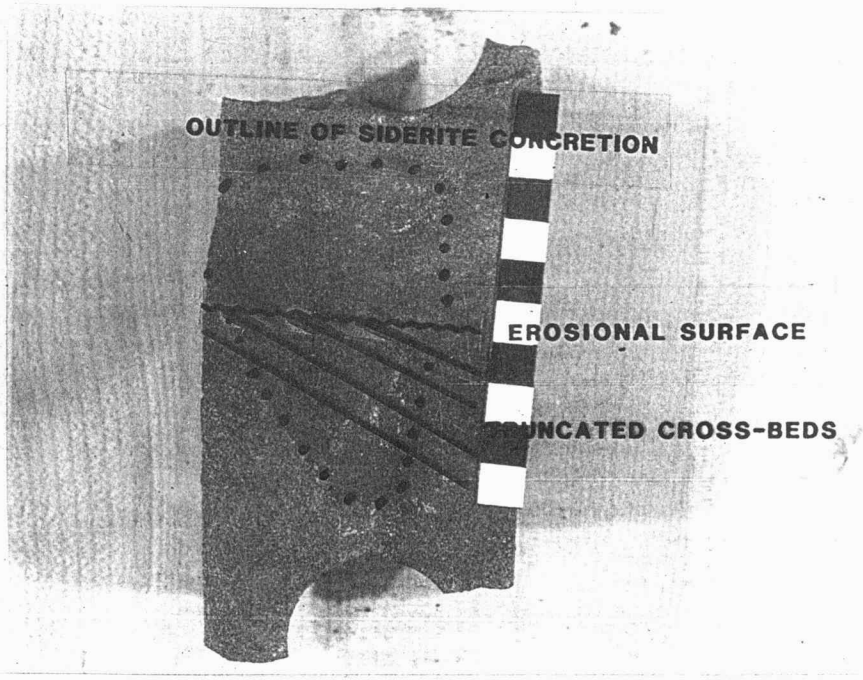

Figure 25. Colt 26AO Johnson, 742.5 ft. (Scale=10 cm)
The core exhibits truncated crossbeds associated with erosional surface (see diagram). Note large siderite concretion surrounding the scour surface.

reservoir is composed of a number of multistory or multilateral sand bodies, the task of differentiating the individual channel sandstones in the subsurface is onerous.

Comparison of the cores and the gamma-ray logs from individual wells revealed strong deflections in the gamma-ray curve at the depths corresponding to the erosional surfaces (Fig. 26). The deflection of the gamma-ray curve is indicative of a zone of greater radioactivity relative to the surrounding sand. The gamma-ray tool measures the level of natural radioactivity emitted by the lithologies that line the borehole (Schlumberger, 1972). The principal radioactive elements are those of the thorium and the uranium series and especially, potassium-40 (^{40}K). Relatively high levels of ^{40}K are commonly encountered in shales and shaly sandstones. The high radioactivity zones in the sandstone reservoir are believed to be a function of the shale clasts commonly observed overlying the erosional surfaces. Nearly all of the gamma-ray logs from the KB Field show at least one strong gamma-ray deflection within the sandstone column (Fig. 27).

Cross-sections of the reservoir that trend northwest-southeast exhibit gamma-ray deflections at different depth intervals (Plate 6c). The depth of the

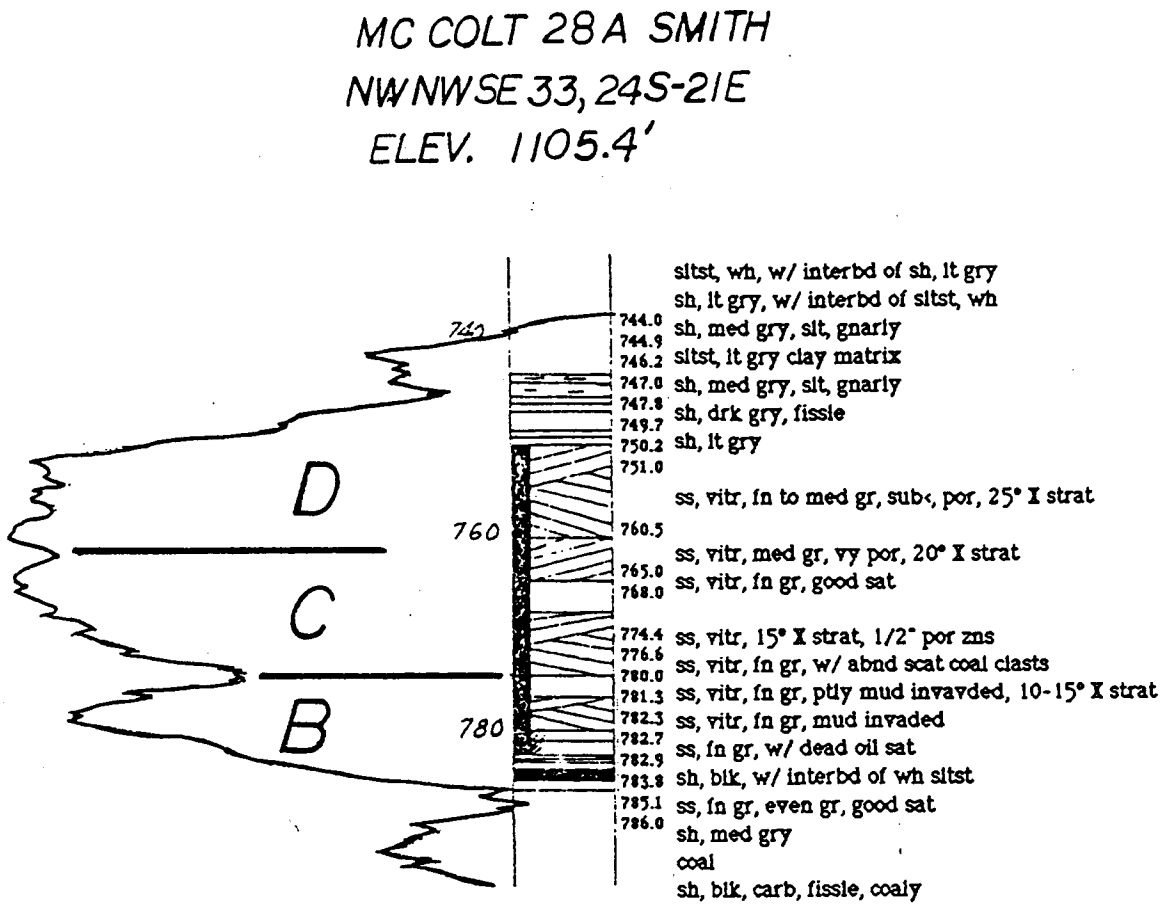

Figure 26. Gamma ray log and Dr. Busch's core description for Colt 28A Smith (with sand body subdivisions superimposed). Note gamma ray deflections at depths corresponding to erosional surfaces such as the one at 775 ft. shown in Figure 24.

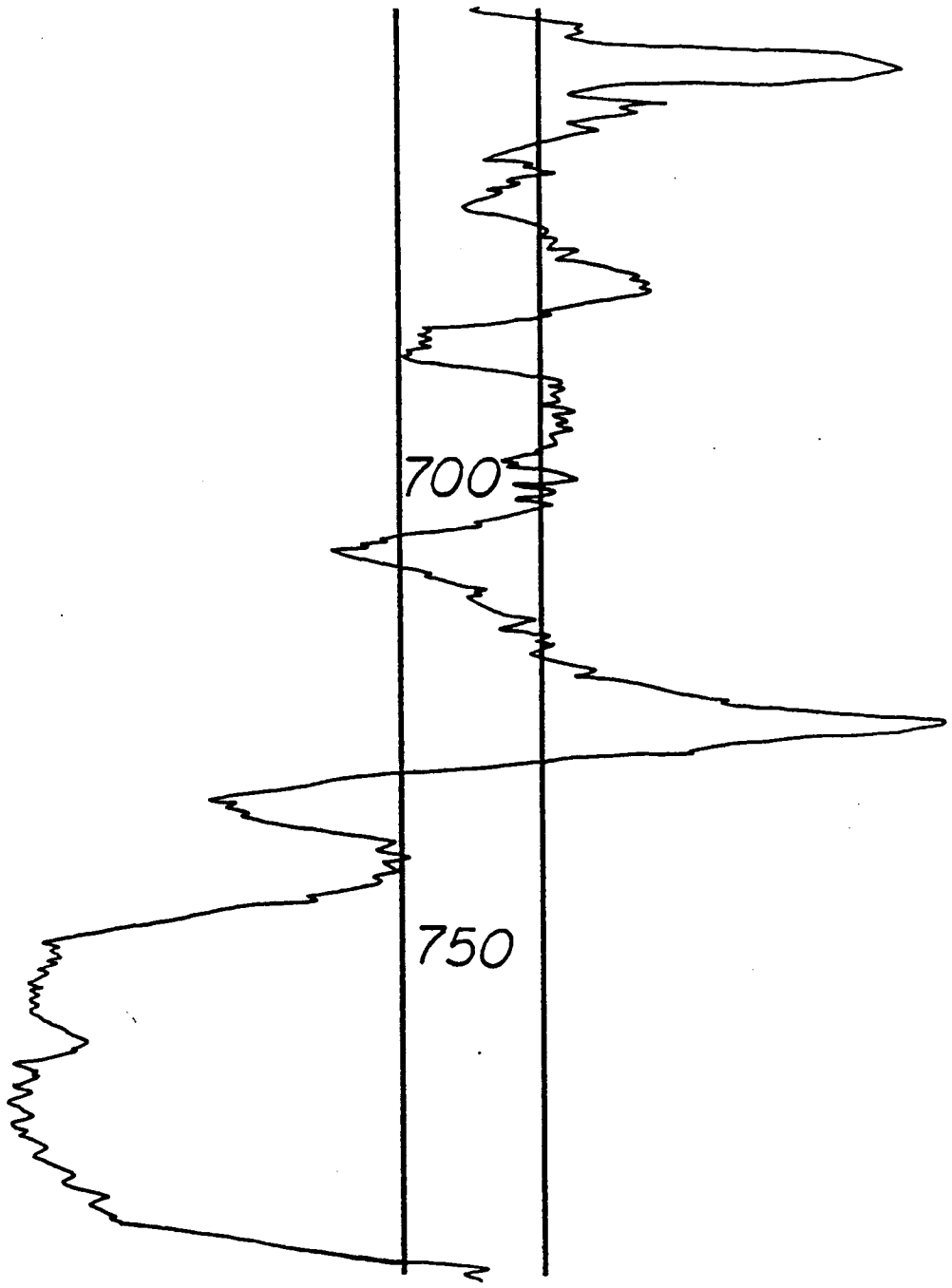

Figure 27. Gamma ray log from Colt 40A Johnson. Note gamma ray deflection at mid-sand interval.

deflection, relative to the top of the sandstone, predictably increases or decreases laterally from one well to the next. Correlation of the deflections across the reservoir revealed sand bodies that were lenticular in cross-section (Plate 6d). The deflections are associated with the erosional surfaces found at the base of each individual sand body. The changes in the depth of the deflections are interpreted to be a function of the lateral thinning or "pinching-out" of parts of the sand body. Well logs that contained more than one strong deflection were interpreted to define the superposition of the individual sands.

A fence-diagram of the KB Field was constructed from gamma-ray logs in order to gain a clearer understanding of the reservoir geometry (Plate 7). Three-dimensional correlation of the individual sand bodies demonstrated that the reservoir in the KB Field is composed of four multilateral, multistoried channel sandstones. These four sands bodies will be designated by the letters A, B, C and D. Superposition of the sand bodies shows that Sand A is the oldest and Sand D is the youngest.

Sands A, B, C, and D were each deposited by a meandering stream that eroded into the older deposits. Each sand body shows a vertical reduction in average grain size and scale of sedimentary structure above an

erosional base (Appendix A). It is emphasized that each sand body is of scale similar to that of other Upper Bluejacket reservoirs (Fig. 21). The mechanism by which each sand was deposited will be discussed in detail in the section dealing with depositional history of the KB Field.

Sand A (Plate 8) is located in the extreme southern portion of the study area and reaches a maximum thickness of 6.4 m (21 ft.). The thickest section of this sand was observed in the southeastern corner of the study area. From this trend of southward thickening, it is concluded that the main body of Sand A lies outside the study area in the C. Jones and southeastern Smith leases. The edge of the Sand A unit observed in the study area thins gradually to the northwest in the Smith lease. Sand A was easily recognizable in logs but was observed in only one core from the KB Field (Colt 31A Smith; Appendix A). The gamma-ray log from this well showed a definite break in the middle of the sand column (Fig. 28, Plate 6d). The core from Colt 31A Smith showed Sand A to consist of 2.1 m (7 ft.) of fine and very fine sand and 61 cm (2 ft.) of interbedded siltstone and shale. The interbedded deposits were located at the depth corresponding to the strong deflection on the gamma-ray log.

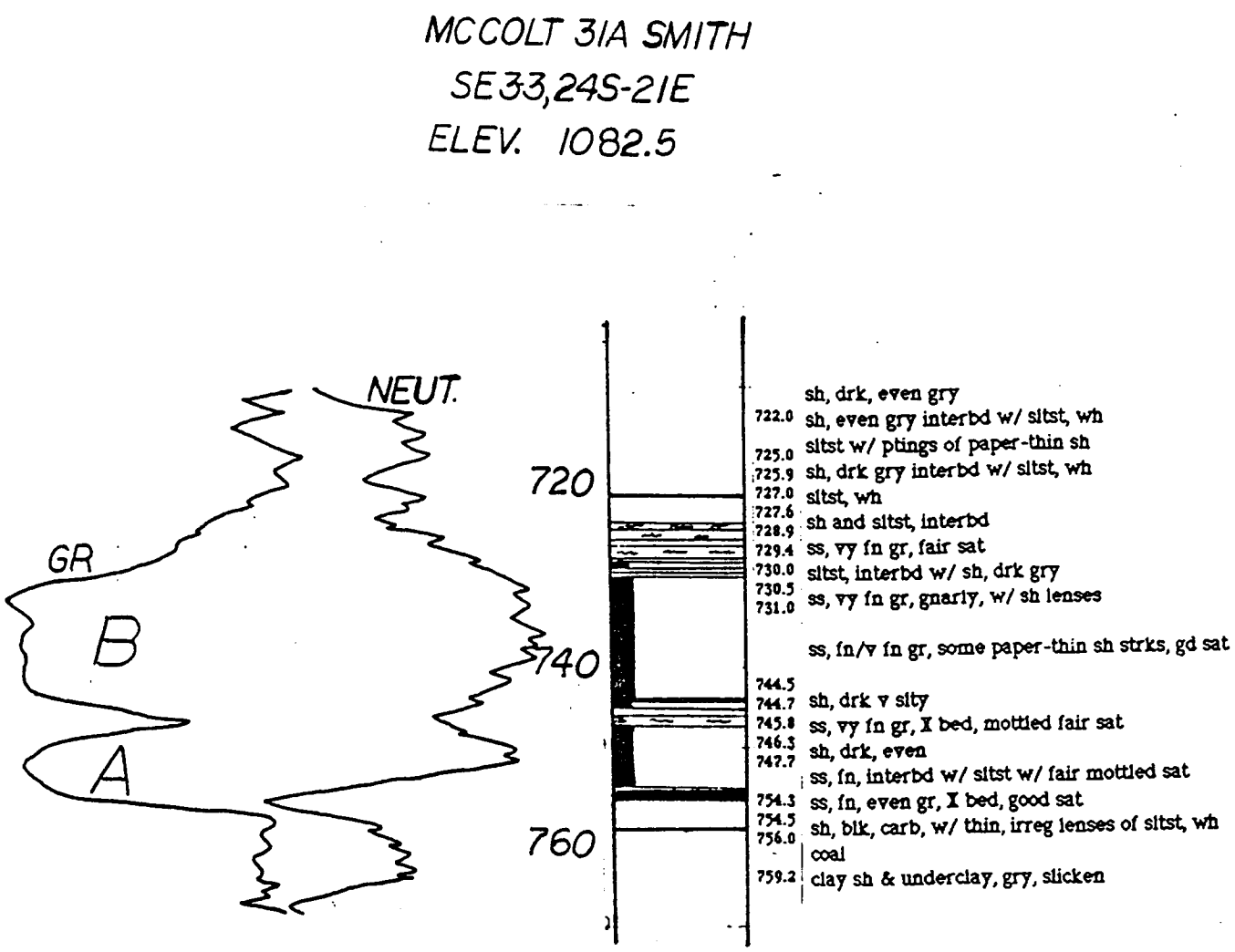

Figure 28. Gamma ray/ Neutron log and Dr. Busch's description from Colt 31A Smith. Note shale that separates Sand A and Sand B.

Sand B is an elongate, slightly sinuous sand body trending northeast-southwest that partially overlaps and lies northwest of Sand A (Plate 9). Sand B reaches a maximum thickness of 9.7 m (32 ft.) and is lenticular in cross-section. This sand body is observed in three cores (Colt 50AO Johnson, Colt 28A Smith and Colt 31A Smith) with the thickest section seen in the upper portion of Colt 31A Smith (Fig. 28; Appendix A). The overall geometry of this individual sand body is very similar to the shape reported for other Upper Bluejacket Sandstone reservoirs (Fig. 21) (Schumacher, 1976; Ebanks, 1979). Sand B differs from other reservoirs in that it is slightly sinuous as opposed to the nearly straight sand bodies observed elsewhere in the Cherokee Basin.

Sand C (Plate 10) is the most irregularly shaped of the four sand bodies in the KB Field. The irregularity of the sand-body geometry is interpreted to be a function of post-depositional erosion (See below). Sand C reaches a maximum thickness of 12.5 m (41 ft.) and is observed in all cores except for Colt 31A Smith (Appendix A). Figures 26 and 29 exhibit gamma-ray logs that show the interpreted contact between Sand C and Sand B. The core from Colt 28A Smith shows common shale clasts and abundant plant fragments at the interface between these two sands.

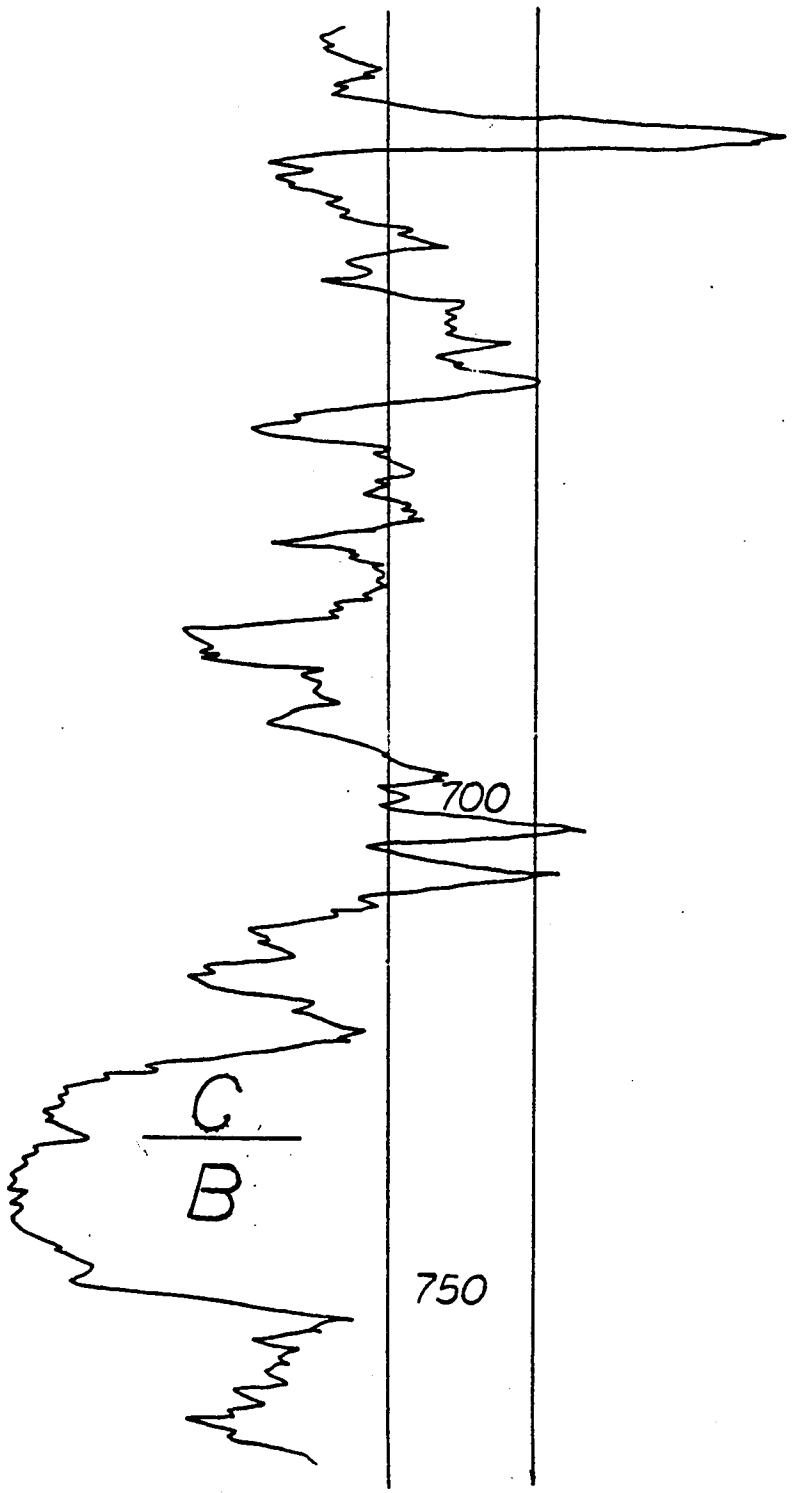

Figure 29. Gamma ray log from Colt 29AO Johnson. Log shows interpreted contact of Sand C and Sand B.

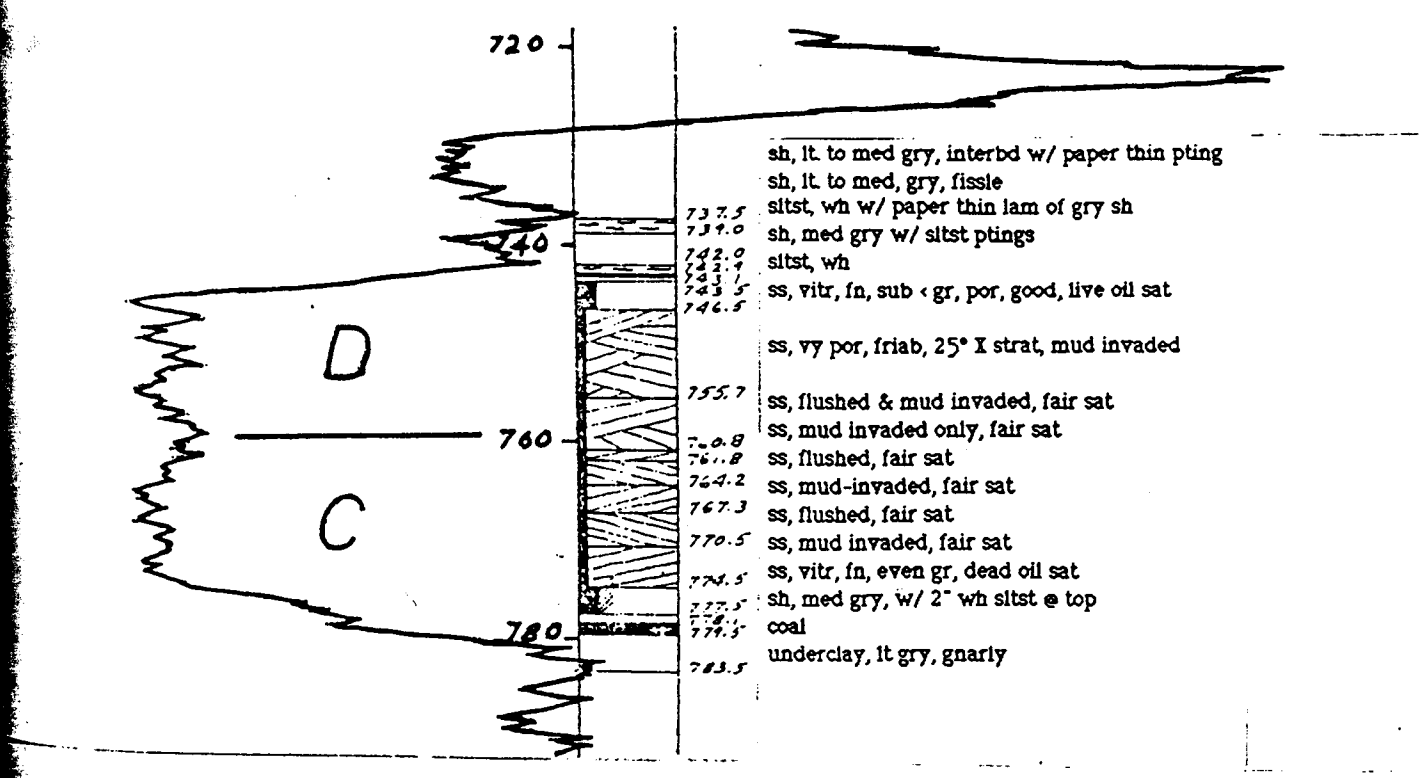

Figure 30. Gamma ray log and Dr. Busch's description from Colt 39A Johnson. Note interpreted contact of Sand C and Sand D.

Unlike Sands A, B, and C, which are multilateral sand bodies showing only partial vertical stacking, Sand D (Plate 11) is a multistory sand body that is superjacent to the older channel deposits. The stream that deposited Sand D eroded into the underlying deposits of Sand C, removing a large portion of the sand body. This period of erosion resulted in the irregular sand body geometry of Sand C. It is assumed that the original shape of Sand C was elongate and sinuous like the other sands that comprise the reservoir.

Sand D is an elongate and highly sinuous sand body that reaches a maximum thickness of 7.6 m (25 ft.). The sand body is deeply incised into the underlying deposits, shows a concave base, and is lenticular in cross-section. The contact between Sands D and C is marked by abundant coal clasts in the core from Colt 28A Smith (Appendix A). The core from Colt 13AO Johnson exhibits 1.2 m (4 ft.) of Sand D overlying 30 cm (1 ft.) of interbedded sand and shale. Figures 26 and 30 show examples of the interpreted gamma-ray contact between the two sands.

DEVELOPMENT OF THE RESERVOIR GEOMETRY

A generalized discussion of the factors that lead to the development of a multistory and multilateral sand body geometry is given below. The discussion is presented to describe factors that probably controlled deposition in the KB Field but cannot be determined from either core or gamma-ray log data. This discussion will be based on theoretical simulations of the distributions of channel sands presented by Allen (1978), Leeder (1978), and Bridge and Leeder (1979).

Allen (1978) asserts that the development of multistory and multilateral sand bodies is a function of the interaction between the rate of avulsion and the subsidence rate of the floodplain. Avulsion is defined as the rapid abandonment of the stream channel during periods of flood to a position of lower elevation on the alluvial plain. In a computer model, Allen attempted to simulate the spacial arrangements of individual sand bodies by varying the rate of subsidence while the rate of avulsion remained constant (one channel avulsion every 2000 yrs). From this simulation, he proposed that the degree of interconnection between sand bodies will decrease with increasing rate of tectonic subsidence. He assumes that a rapid subsidence rate results in the deposition of approximately equal thicknesses of fine-grained

floodplain sediments and coarse-grained meander belt alluvium. Deposition during periods of rapid subsidence will result in the formation of discrete sand bodies in a "matrix" of fine-grained overbank deposits.

Bridge and Leeder (1979) state that the orientation of different sand bodies depends upon the rate of avulsion and the relative rate of vertical aggradation of the sandy channel belt and adjoining overbank deposits. They propose a rapid rate of channel-belt aggradation will tend to increase the rate of avulsion. The greater avulsion rates are a function of the normal increase in channel elevation relative to the floodplain that results from the high rate of vertical aggradation of the sandy channel deposits as contrasted to that of the fine-grained sediments on the floodplain. During floods, levees that constrain the stream can be breached and the channels abruptly shift to a lower elevation on the alluvial plain.

Leeder (1978) and Allen (1978) point out that previously deposited sand bodies remain as barriers to further channel migration. Subsequent to avulsion, the older channel-belt sand body is located at a higher elevation and, therefore, partitions the alluvial plain until it subsides or the younger deposits aggrade to a similar elevation. The gradual subsidence of the sand

body occurs because of differential compaction of the underlying deposits from the weight of the sand.

The studies of Allen (1978), Leeder (1978), and Bridge and Leeder (1979) are useful in understanding factors that probably controlled deposition in the KB Field. It is very difficult to determine the actual factors that controlled deposition based on the information available for this study. For example, the difference in elevation between the floodplain and the meander belt is impossible to determine because of post-depositional compaction of the overbank sediments. The effect of subsidence rate of the floodplain on reservoir geometry is also difficult to determine because of the interaction of rapid changes in sea level and the subsidence rate of the Cherokee Basin.

DEPOSITIONAL HISTORY OF THE KB FIELD

A multicolor sand isolith map (Plate 12) shows the intricate intertwining nature of the four sand bodies in the KB Field. Using this map as a guide, the depositional history of the individual sand components of the reservoir can be described.

Plate 12 shows that Sands A, B, and C are predominately multilateral with only partial vertical stacking. The history of these three sand bodies was marked by progressively thicker sand deposition followed by relocation of the channel to the northwest through avulsion. As noted earlier, the thickest portion of Sand A lies outside of the study area to the southeast. Moreover, the maximum thickness of this sand body is unknown but assumed to be on the order of 9 m (30 ft.) or similar to that of the other sand bodies. Little further can be said regarding Sand A, but it may have been controlled by factors similar to those of Sands B, C, and D.

Sand A was deposited by a fluvial channel that likely avulsed upstream, to the northeast, shifting the region of channel influence to lower elevations on the alluvial plain. It is strongly emphasized that only the relative age of each sand body is known, not the duration of time between events. Sand B is younger than Sand A as determined by superposition, but this

does not preclude deposition outside the study area on the floodplain after the accumulation of Sand A but before Sand B. The period of time that elapsed between the deposition of Sand A and Sand B is manifest by the two feet of interbedded siltstone and shale exhibited in the core from Colt 31A Smith (Appendix A). It is impossible to determine the length of time these deposits represent but it is probably appreciable. It is also probable that some of the siltstone and shale was eroded and removed by the stream that deposited Sand B.

When the channel returned to the area of the KB Field, Sand B was deposited northwest of the residual high elevation of Sand A. Sand B was deposited by a meandering stream that eroded in to the underlying peat and mud, resulting in the shale clasts and wood fragments observed in the basal sands (ie. Colt 28A Smith, Appendix A). Much of the underlying sediment was lifted by the turbulence and carried down stream (Harms, et al., 1982). The fluvial system that deposited this sand meandered across a slightly sinuous channel-belt roughly the width of the sand body (Allen, 1978). Through the processes of lateral migration and vertical aggradation, Sand B reached a maximum thickness of 9.8 m (32 ft.) and overlapped the northwestern portion of Sand A. The vertical stacking

of the sand bodies was facilitated by the slow subsidence of Sand A into the subjacent peat.

Sand B continued to accumulate until the stream channel avulsed, shifting the site of active deposition to the northwest (Plate 12). The period of time that elapsed between the deposition of Sand B and Sand C is believed to have been slight. This belief is supported by the absence of overbank deposits between the sand bodies (see Colt 50AO Johnson and Colt 28A Smith, Appendix A).

Sand C is the thickest of the sand bodies, but it has undergone extensive erosion indicated by its highly irregular geometry. Prior to erosion, this sand body was slightly sinuous with an average thickness of 10.7 m (35 ft.). Note that the maximum thickness of this sand is 2.4 m (8 ft.) greater than the maximum thickness of Sand B. The greater thickness of this sand and the eventual stacking of Sand D is believed to be a function of floodplain constriction. Plate 1 shows that an elongate sand body lies just outside the study area to the north in sections 27 and 28 of Township 24 south, Range 21 east. Although the relative age of this sand body is unknown, it is believed this sand was already deposited and, therefore, would have acted as a barrier (Allen, 1978). Sand B also would have been located at a higher

elevation and partitioned the alluvial plain to the south. With the completion of Sand C deposition, there were no longer any low-lying areas remaining in the KB Field area. This forced deposition to occur at either a totally different location or for multistory sand deposition to commence.

The constriction of the floodplain due to previous sand deposition resulted in the vertical stacking of Sand D above Sand C. Unlike the other sand bodies that compose the reservoir, Sand D eroded into the underlying sands during channel incision. The erosion removed parts of Sand C and Sand B (Plate 12). The stream that deposited Sand D probably eroded into older channel deposits because sand was more easily eroded than peat.

The high sinuosity observed in the meander belt of Sand D is interpreted to be a function of the stream adjusting to local base level. Differential compaction of the peat or residual high relief areas may have resulted in the observed sinuosity. The streams that deposited Sand D probably avoided the areas of high relief and meandered to lower elevation. The movement of the stream resulted in the channel eroding into the thickest portion of Sand C (Plate 12).

SANDSTONE PETROGRAPHY

INTRODUCTION

The mineralogy, petrology and diagenesis of the Upper Bluejacket Sandstone in the KB Field was studied in 122 thin-sections and 11 scanning electron microscope (S.E.M.) samples. The cores were sampled at 0.75 m (2.5 ft.) intervals in order to eliminate sampling bias. The thin-sections were impregnated with blue-dyed epoxy to facilitate identification of pore space. All thin-sections were point-counted for pore type (100 points). Pore types recognized include dissolution and intergranular pores, micropores and intercrystalline pores among kaolinite crystals (Schmidt and MacDonald, 1979).

As stated in the "Purpose of Investigation" section, this study emphasizes the relationship between diagenesis and petrophysics. Forty-four samples were selected for measurement of porosity and permeability, and thin-sectioned to point-count mineralogy in addition to pore type. The samples were selected to provide adequate representation of each subfacies from Sands A, B, C, and D. The results of the point-counts and the petrophysical measurements are shown in Tables 1a through 1h (pages 85-92). The point-counts were conducted to not only gain an understanding of the

mineralogy but also to attempt to demonstrate the factors controlling fluid transmissibility through the sandstone reservoir. Some of these factors were pore type, mean grain-size, the type and degree of cementation, and the effects of pore-filling authigenic clays.

SANDSTONE FRAMEWORK MINERALOGY

Quartz

Quartz is the most abundant of the framework grains constituting 45 to 75 percent. Monocrystalline quartz is the most common detrital constituent of the sandstones, comprising 40 to 70 percent (Fig. 31). Individual monocrystalline quartz grains range in size from very fine to medium, and are subangular and subequant in shape. These quartz grains commonly exhibit trains of fluid-filled vacuoles and mineral inclusions such as apatite, vermicular chlorite, rutile and zircon. Syntaxial overgrowths are common on quartz grains (Fig. 32). The monocrystalline quartz grains usually show straight to slightly undulose extinction between crossed nicols. Also observed, but less abundant, were grains that showed strongly undulose extinction.

Polycrystalline quartz grains compose between 2 and 8 percent of the Upper Bluejacket Sandstone. As the name implies, these grains comprise two or more

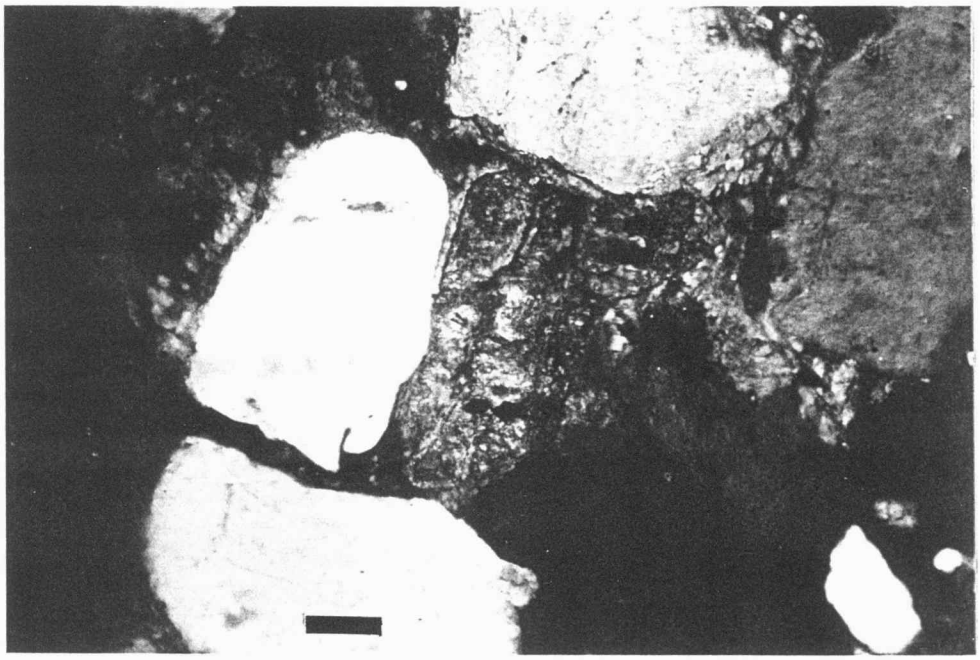

Figure 31. Colt 14AO Johnson, 729 ft. (X-nicols, 100x). Examples of large, monocrystalline quartz grains (Q) with unit extinction. (Scale=0.1 mm.)

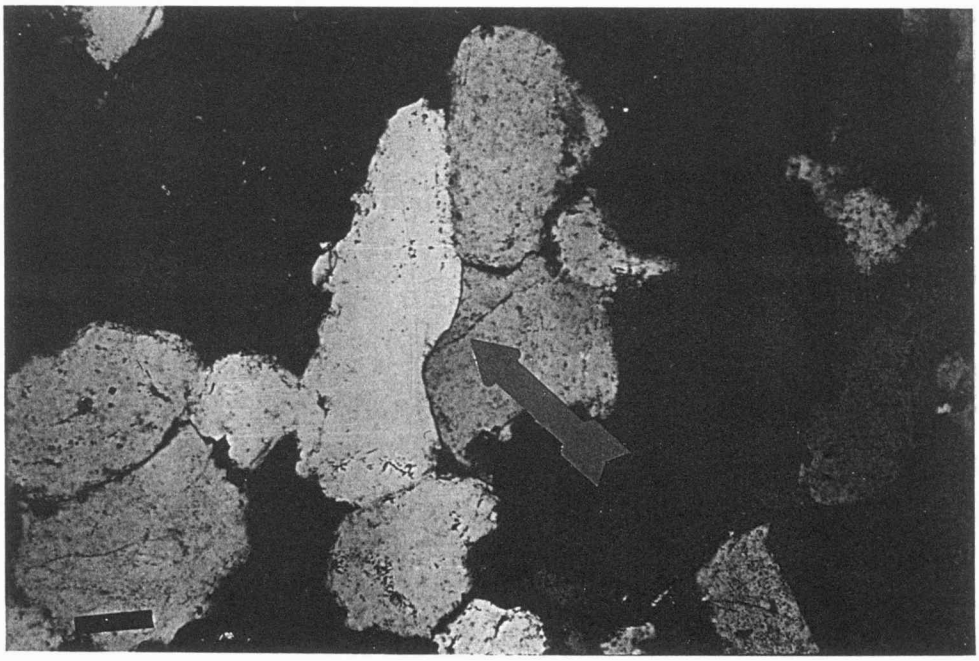

Figure 32. Colt 28A Smith, 782.8 ft. (X-nicols, 100X) Abundant well developed silica overgrowths on detrital quartz grains. Note dust rims marking the interface between grain and overgrowth (arrow). (Scale=0.1 mm)

quartz crystals forming one detrital grain, commonly they show sutured internal contacts (Fig. 33). Individual polycrystalline quartz grains range in size from fine to medium and are subangular. Chert was not counted in the category of polycrystalline quartz but as a sedimentary rock fragment.

FELDSPAR

Feldspars constitute up to 15 percent of the sand grains counted. Plagioclase feldspars were identified by the presence of albite twinning and constitute the most abundant feldspar observed (Fig. 34). Untwinned feldspars were counted as orthoclase. Microcline was very rare but marked by its cross-hatched twinning. The feldspars were subequant and subangular to subround in shape, rarely exhibited any overgrowth, and commonly were etched by carbonate cement.

The ratio of plagioclase to potassium feldspar ranged from 1:1 to 10:1 with plagioclase constituting as much as 14 percent of the total points counted. Plagioclase ranged in size from very fine to medium sand and was observed both as altered and unaltered grains. Plagioclase commonly has undergone chemical alteration, such as sericitization, kaolinitization and vacuolization (Figs. 35 and 36). The plagioclase also shows common partial replacement by authigenic

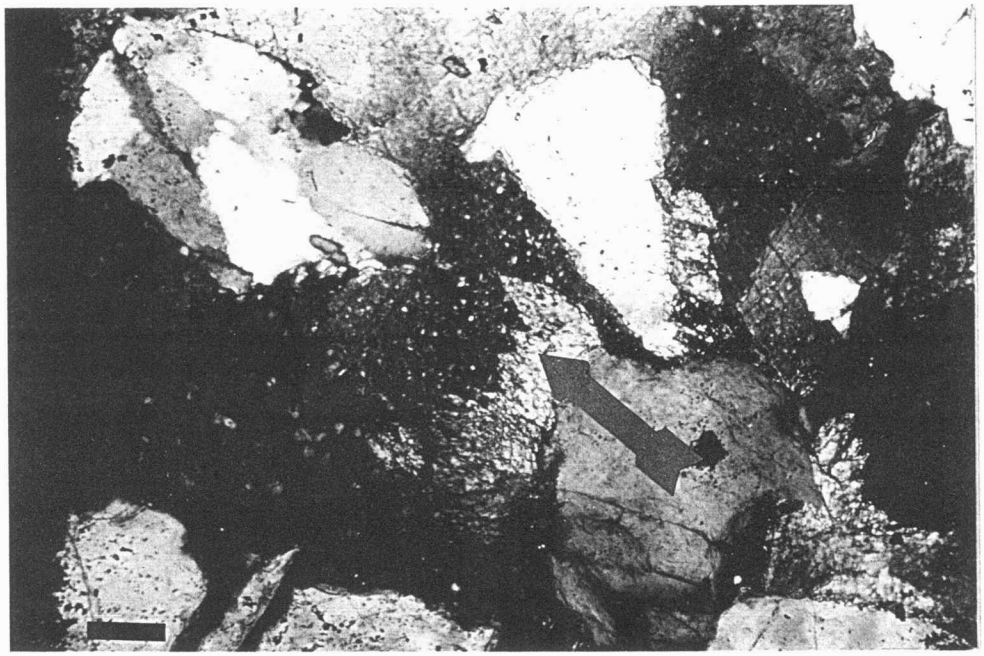

Figure 33. Colt 28A Smith, 759.5 ft. (X-nicols, 100x) Polycrystalline quartz grain (Q) in upper-left corner of photomicrograph. Also note the two different types of carbonate cement. Siderite (S) appears as the cox-comb cement in center of photo (arrow). (Scale=0.1 mm.)

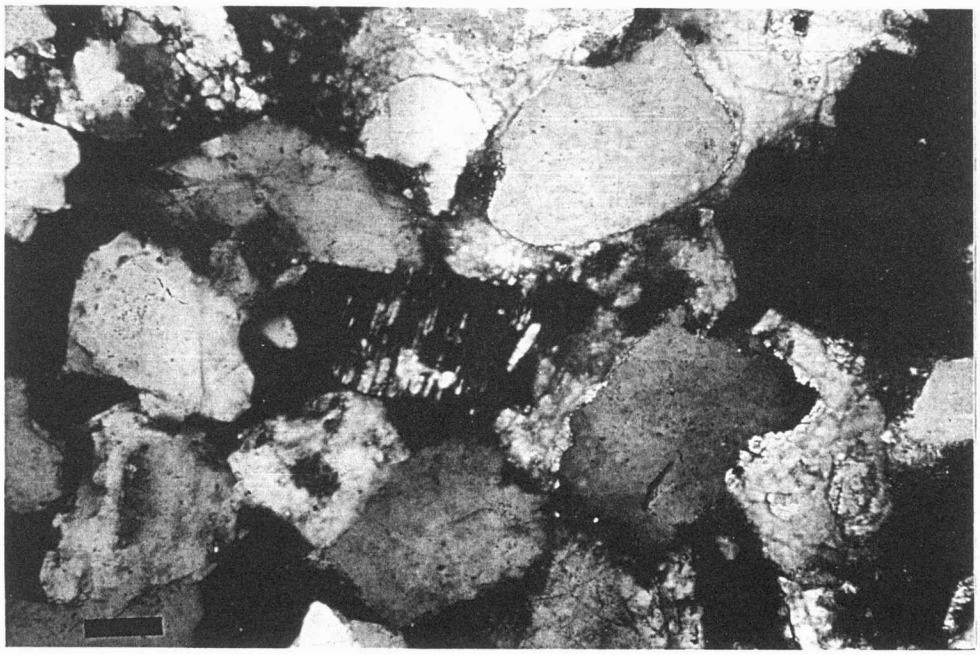

Figure 34. Colt 28A Smith, 752 ft. (X-nicols, 100X) Plagioclase feldspar (P) in center of photomicrograph. Note the albite twinning characteristic of plagioclase. (Scale=0.1 mm.)

carbonate cement (Figs. 37 and 38). Dissolution of the plagioclase is very common and greatly contributes to the porosity of these reservoir sandstones (Figs. 39 and 40). Partial dissolution was the most common form of plagioclase alteration observed in the samples.

Potassium feldspar is untwinned, but is recognizable by the low-relief and birefringence, and generally well developed cleavage (Fig. 41). Potassium feldspars compose up to 3 percent of the points counted and show relatively abundant alteration. Few unaltered potassium feldspars were noted. The chemical alteration observed in the potassium feldspars was identical to the alteration of the plagioclase.

SEDIMENTARY ROCK FRAGMENTS

Sedimentary rock fragments compose up to 30 percent of the points counted; most are argillaceous rock fragments. Chert composes less than 1 percent of the framework grains. The argillaceous rock fragments were likely eroded from penecontemporaneous muds during channel incision and migration. The argillaceous rock fragments were nonfoliated, well rounded, and equant to elongate when deposited (Fig. 42). However, they retain this shape only when early carbonate cement prevented deformation of the soft argillaceous grains that normally occurs through compaction of the

Figure 35. Colt 13AO Johnson, 754.5 ft. (X-nicols, 100X) Feldspar framework grain showing alteration by sericite and kaolinite. Sericite is highly birefringent while kaolinite shows 'salt and pepper' low birefringence. (Scale=0.1 mm.)

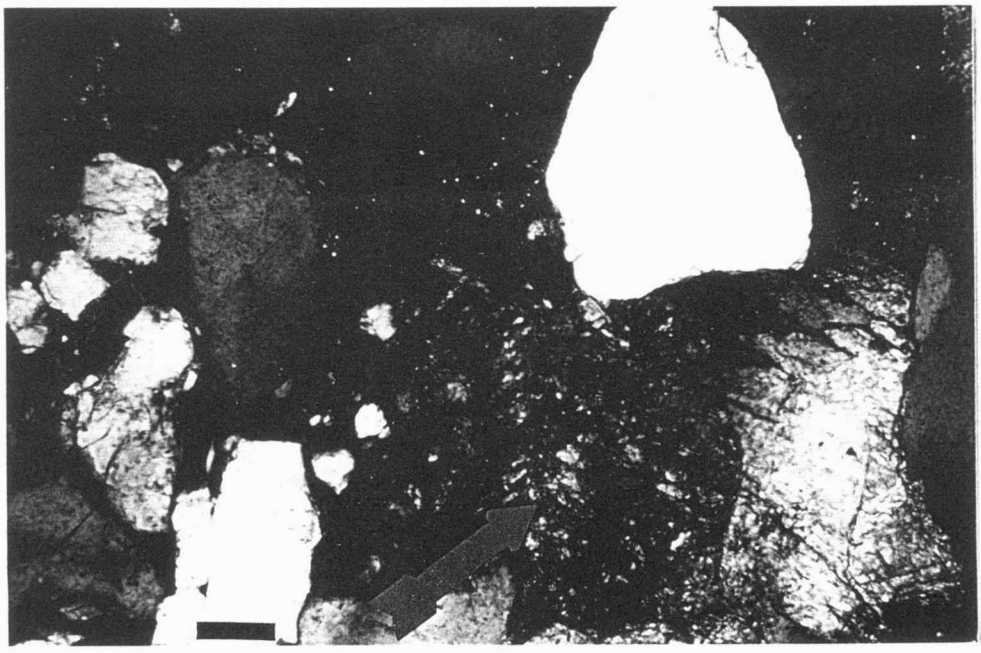

Figure 36. Colt 5A Harvey, 762 ft. (X-nicols, 100X) Feldspar partially altered by siderite and kaolinite in lower-center of photomicrograph. Siderite appears as 'rusty' patches on the feldspar (arrow). (Scale= 0.1 mm.)

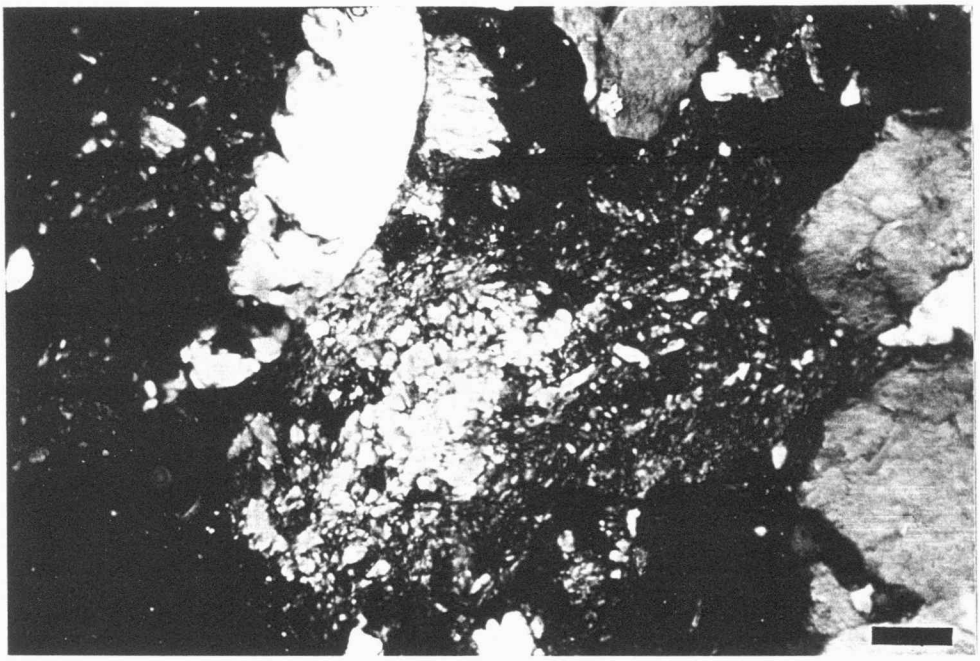

Figure 37. Colt 14AO Johnson, 711.5 ft. (X-nicols, 100X) Feldspar showing replacement by sericite and carbonate in center of photo. (Scale=0.1 mm.)

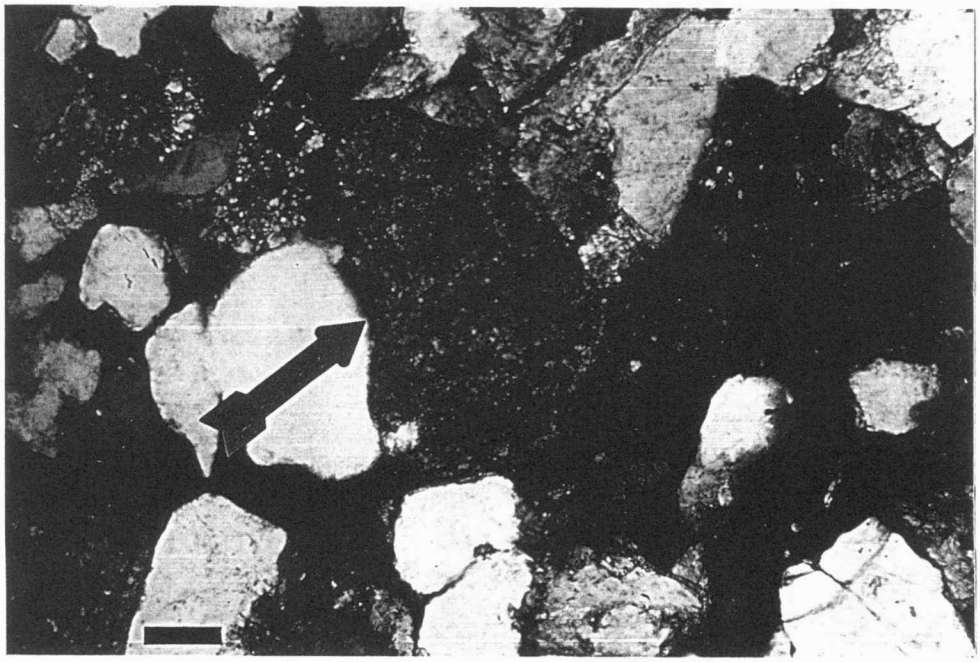

Figure 38. Colt 13AO Johnson, 737 ft. (X-nicols, 100X) Feldspar almost completely replaced by cryptocrystalline siderite (arrow). (Scale=0.1 mm.)

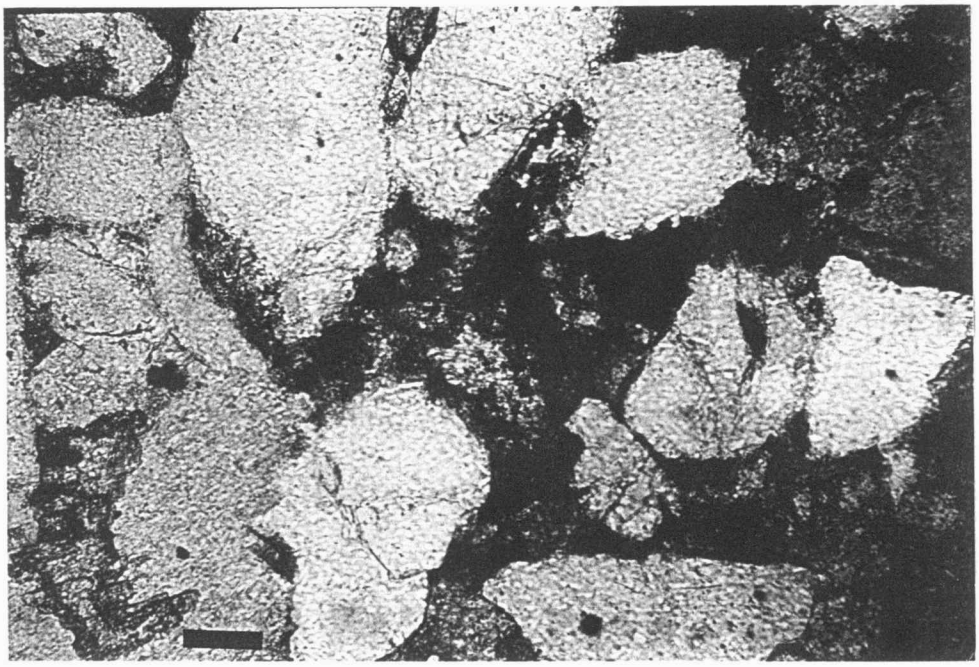

Figure 39. Colt 28A Smith, 752 ft. (Pl-light, 100X) Feldspar (F) showing partial dissolution photo). The blue epoxy fills both the primary porosity between framework grains and the feldspar dissolution porosity. (Scale=0.1 mm.)

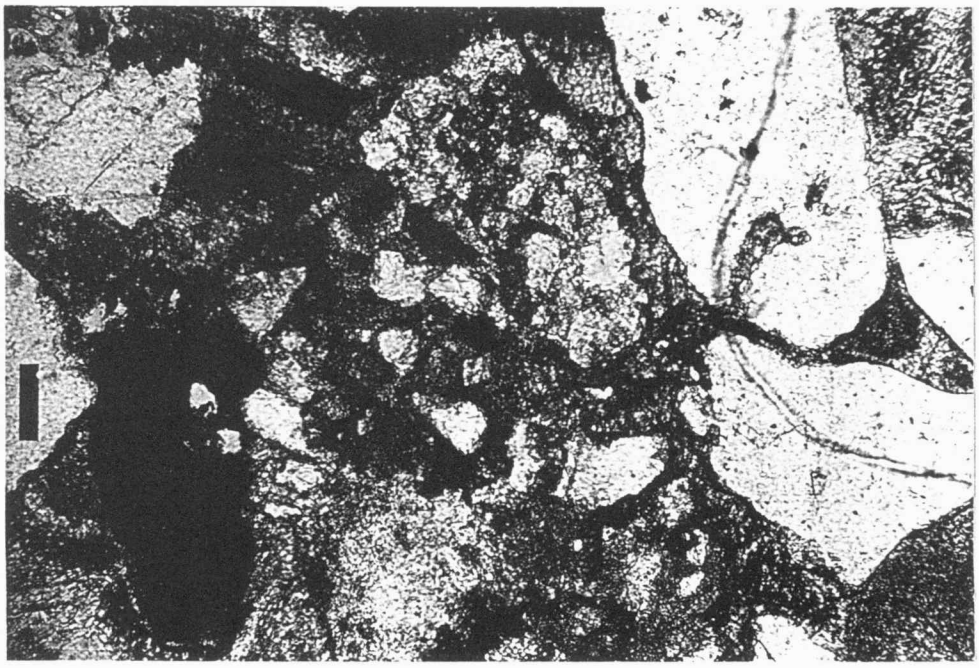

Figure 40. Colt 28A Smith, 757 ft. (Pl-light, 100X) Dissolution pores resulting from the partial removal of feldspar in solution. (Scale=0.1 mm.)

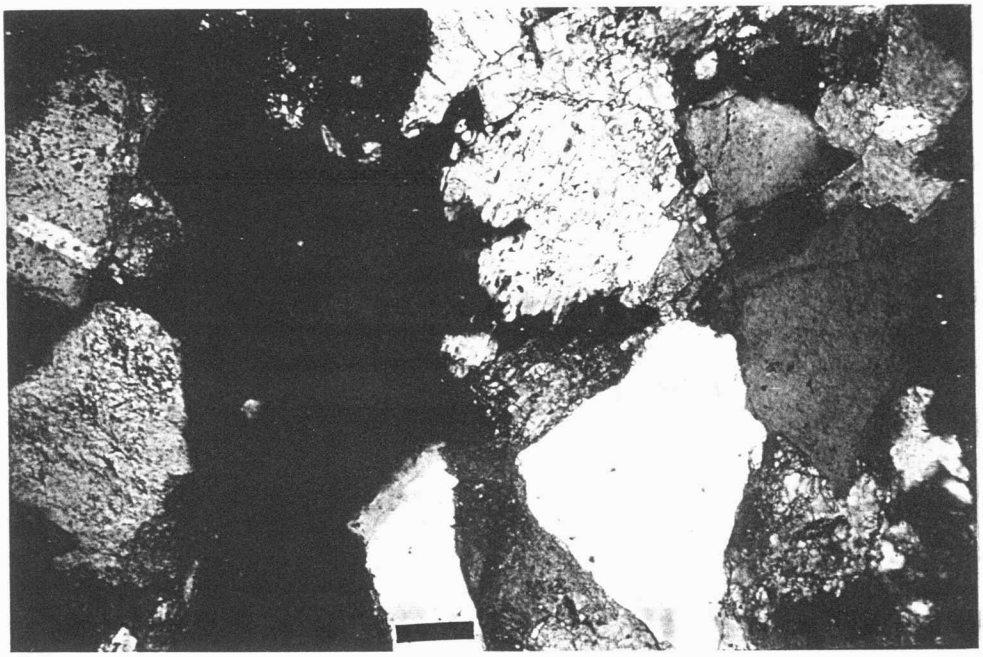

Figure 41. Colt 28A Smith, 752 ft. (X-nicols, 100X) Potassium feldspar (F) showing well developed cleavage. Cleavage and lack of twinning were used to differentiate K-feldspar and plagioclase. (Scale=0.1 mm)

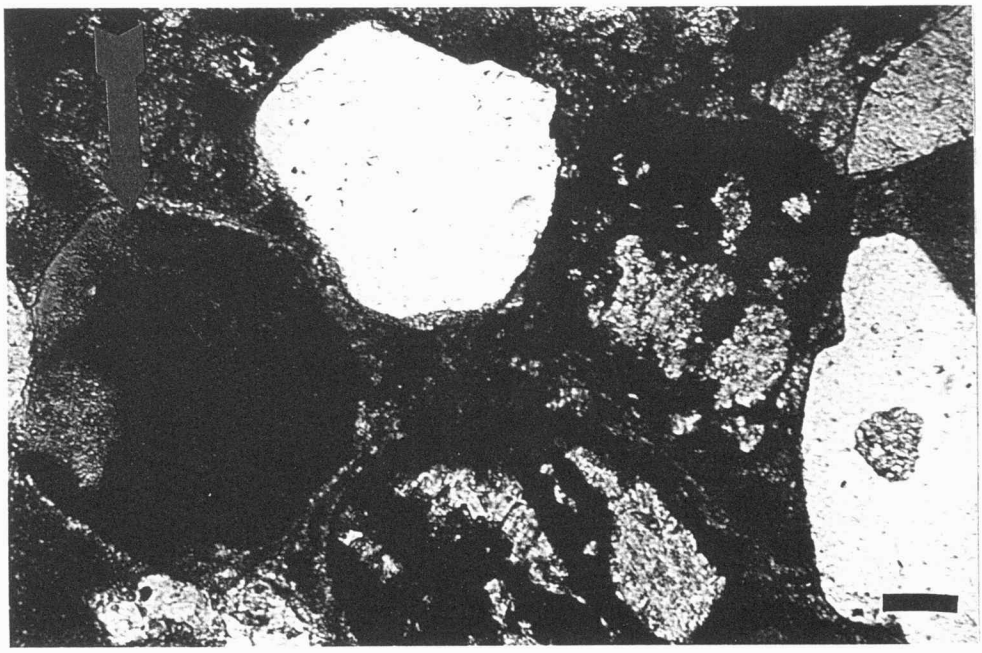

Figure 42. Colt 5A Harvey, 769.5 ft. (Pl-light, 100X) This sample exhibits poikilotopic carbonate cement that formed early in the diagenetic history. This cement prevents compaction of SRF's (arrow). (Scale=0.1 mm.)

sediment. Argillaceous rock fragments that were not cemented by early poikilotopic carbonate showed deformation at the point of contact with adjacent framework grains (Fig. 43). These rock fragments are composed of mainly low birefringent clay minerals but some of the grains contain silt-sized quartz (Fig. 44). The argillaceous rock fragments commonly show partial to complete dissolution and greatly contribute to the porosity of the samples (Fig. 45). In most samples that exhibit pervasive early carbonate cement, dissolved rock fragments are the only pores.

ACCESSORY MINERALS

MICAS

Muscovite and biotite compose less than 3 percent of the individual samples studied. Muscovite is the more common mineral, but was not observed in all the thin-sections examined. This mineral is generally more abundant in the finer grained lithofacies located at the top of the sandstone section (ie. Colt 5A Johnson, 710.5 ft., Table 1d). Muscovite was particularly abundant in shale partings observed mesoscopically in the cores.

Greenish-brown to dark brown, strongly pleochroic biotite was observed and point-counted in only a few samples, and rarely exceeded 0.5 percent of the grains

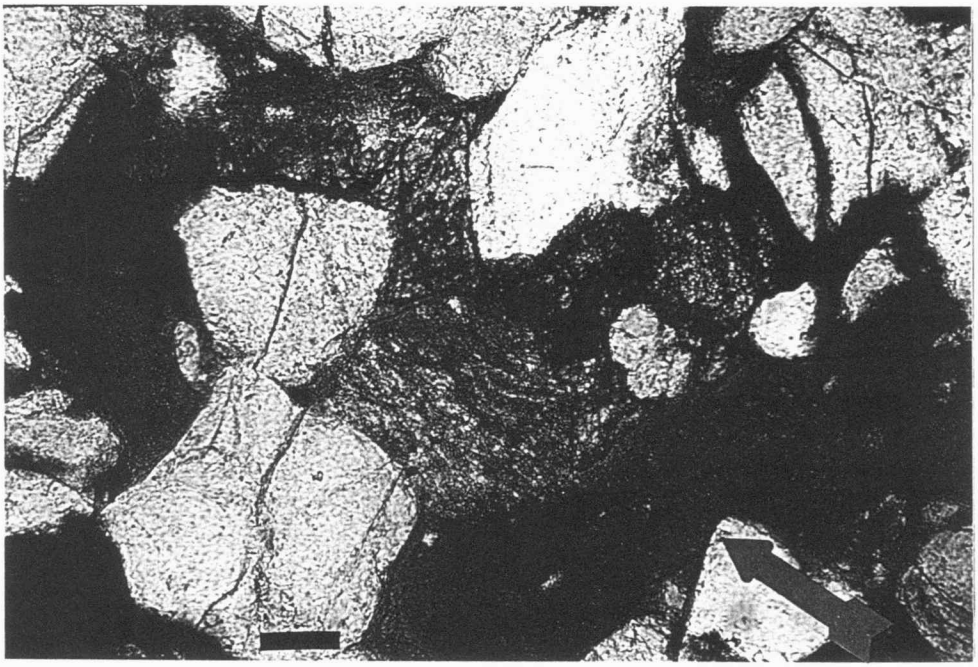

Figure 43. Colt 5A Harvey, 749.5 ft. (Pl-light, 100X) Samples without early carbonate cement show compaction of sedimentary rock fragments at grain contacts (arrow). (Scale=0.1 mm.)

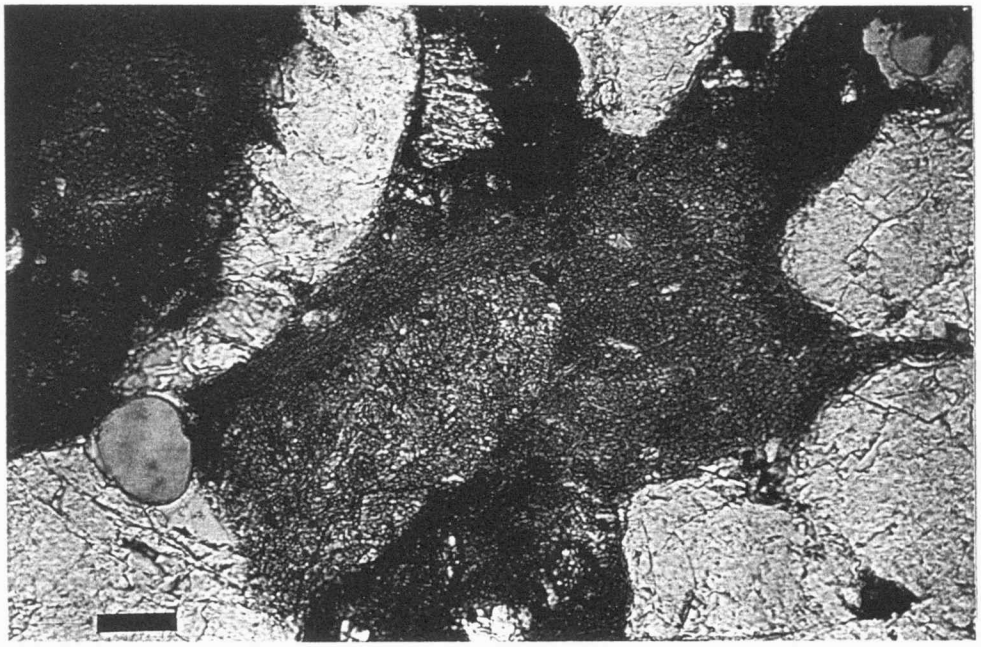

Figure 44. Colt 13AO Johnson, 729.5 ft. (Pl-light, 100X) Shale fragments (SRF) showing minor silt-sized quartz. Note abundant syndepositional matrix and SRF's in this sample. (Scale=0.1 mm.)

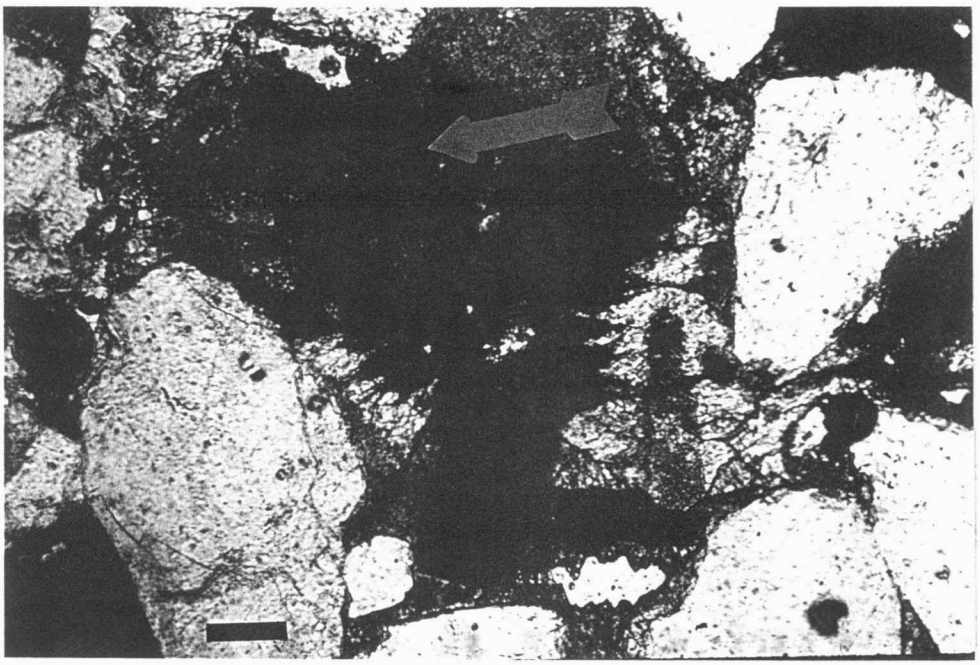

Figure 45. Colt 28A Smith, 759.5 ft. (Pl-light, 100X) Large dissolution pore resulting from partial dissolution of sedimentary rock fragment (arrow) and carbonate cement. (Scale=0.1 mm.)

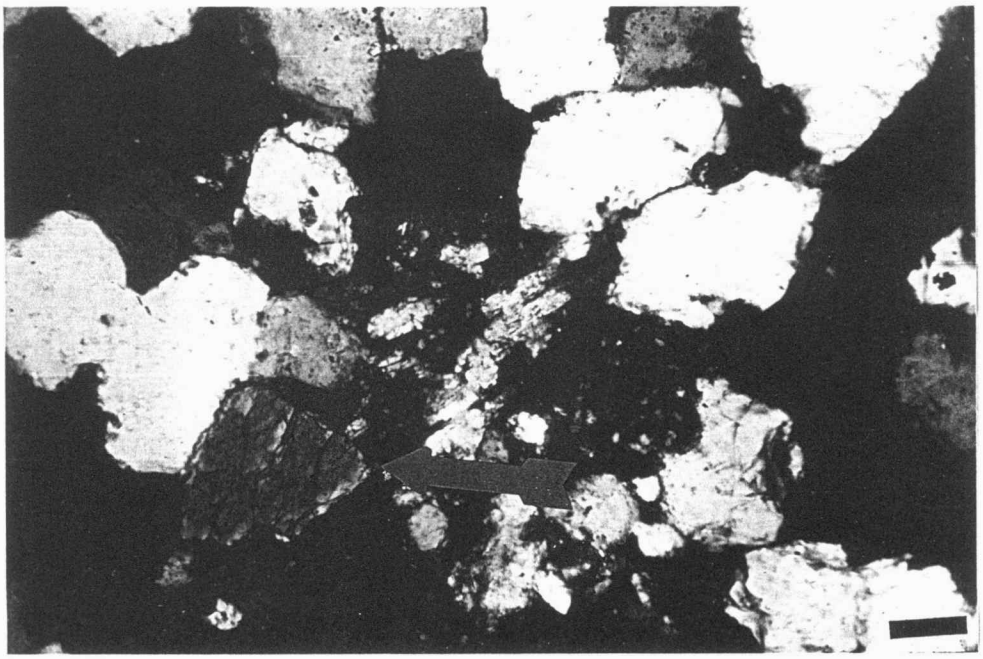

Figure 46. Colt 28A Smith, 782.8 ft. (X-nicols, 100X) This sample contains tourmaline (arrow), one of the very rare heavy minerals observed in the Upper Bluejacket Sandstone. (Scale=0.1 mm.)

counted. This mica commonly shows chemical alteration, such as oxidation of iron and replacement of chlorite.

HEAVY MINERALS

Heavy minerals are very rare and constitute an insignificant portion of the sandstones in the KB Field. Some of the heavy minerals noted were zircon, rutile and tourmaline (Fig. 46). Pyrite was observed and will be discussed in the portion of this section dealing with authigenic minerals.

SYNDEPOSITIONAL MATRIX

Few of the samples that were point-counted for mineralogy contain mud that was deposited contemporaneously with the framework grains. Some of the thin-sections that were examined solely for pore type showed substantial syndepositional matrix (Fig. 47 and 48). The samples that did contain matrix commonly also contain abundant authigenic chlorite.

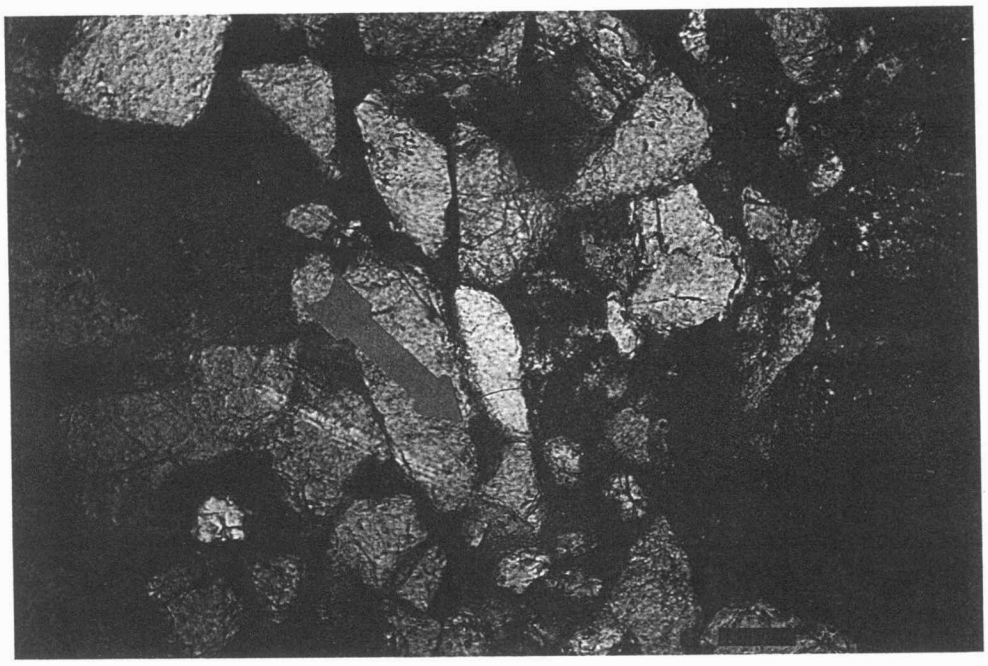

Figure 47. Colt 13AO Johnson, 752 ft. (Pl-light, 100X) Sample shows abundant syndepositional matrix (arrow) and authigenic clay cement. (Scale=0.1 mm.)

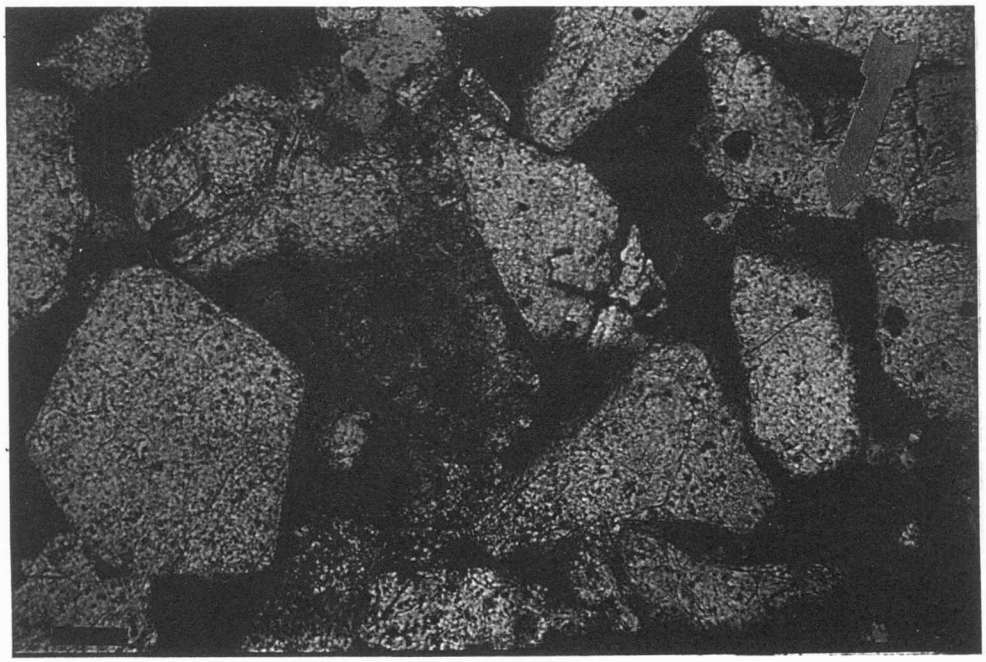

Figure 48. Colt 5A Harvey, 747 ft. (Pl-light, 100X) Sample shows abundant syndepositional matrix (arrow) and common authigenic clay cement. (Scale=0.1 mm.)

WELL NAME	M.C. COLT 28A SMITH					
DEPTH (FEET)	780	775.5	772.5	767	764.5	754.5
DETRITAL (PERCENT)						
QUARTZ						
MONOCRYSTALLINE	71.5	61.1	73.1	67.4	57.5	51.4
POLYCRYSTALLINE	5.6	7.2	4.3	3.0	8.0	4.3
FELDSPAR						
POTASSIUM	3.3	1.3	1.3	1.7	0	0
PLAGIOCLASE	3.0	4.6	3.3	5.3	0	0
SEDIMENTARY ROCK FRAGMENTS	4.3	4.9	5.6	7.0	9.0	4.0
MICAS						
MUSCOVITE	0	0.3	0.3	0.7	0	0.3
BIOTITE	0	0	0	0	0	0
AUTHIGENIC (PERCENT)						
SILICA	1.0	4.2	0.7	1.0	1.0	1.2
SIDERITE						
SPHERULITIC	0	0	0	0	0	0
IRON-CARBONATE	1.0	2.4	0.3	1.7	8.6	20.7
CLAY						
KAOLINITE	10.5	14.1	11.5	12.3	15.6	18.0
CHLORITE	0	0	0	0	0	0
TOTAL (PERCENT)	100	100	100	100	100	100
AVERAGE GRAIN-SIZE (mm)	.22	.19	.18	.18	.24	.26
POROSITY (%)	19.9	17.6	23.3	21.8	21.8	22.1
PERMEABILITY (md)	180	13.4	261.3	137.7	145.2	162.2
PORE TYPE (%)						
INTERGRANULAR	65	22	74	72	37	25
KAOLINITE (INTERCRYSTALLINE)	15	29	15	14	18	22
MICROPORES	4	38	3	4	6	4
DISSOLUTION PORES	16	11	8	10	39	49
TOTAL (PERCENT)	100	100	100	100	100	100

TABLE 1a. RESULTS OF POINT-COUNTS: COLT 28A SMITH

WELL NAME	M.C. COLT		31A		SMITH
DEPTH (FEET)	753.5	751	743.8	738.5	733.5
DETRITAL (PERCENT)					
QUARTZ					
MONOCRYSTALLINE	64.9	52.4	67.4	57.6	70.3
POLYCRYSTALLINE	5.4	4.4	3.3	4.6	3.0
FELDSPAR					
POTASSIUM	2.3	1.7	3.0	1.3	1.0
PLAGIOCLASE	14.0	5.1	10.0	13.6	7.0
SEDIMENTARY ROCK FRAGMENTS	4.3	5.4	4.7	10.3	4.3
MICAS					
MUSCOVITE	0.7	0	1.3	1.1	0.7
BIOTITE	0	0	0	0.6	0
AUTHIGENIC (PERCENT)					
SILICA	0.3	1.3	1.3	2.3	0.3
SIDERITE					
SPHERULITIC	0	13.3	0	0	0
IRON-CARBONATE	1.3	4.2	0.7	1.3	5.3
CLAY					
KAOLINITE	6.7	12.2	8.3	7.3	8.0
CHLORITE	0	0	0	0	0
TOTAL (PERCENT)	100	100	100	100	100
AVERAGE GRAIN-SIZE	.16mm	.25mm	.18mm	.17mm	.16mm
POROSITY (%)	17.9	19.0	19.8	22.7	21.0
PERMEABILITY (md)	169.5	62.1	159.3	151.4	158.0
PORE TYPE (%)					
INTERGRANULAR	68	56	58	49	68
KAOLINITE (INTERCRYSTALLINE)	6	22	14	7	8
MICROPORES	10	7	8	5	4
DISSOLUTION PORES	16	15	20	39	20
TOTAL (PERCENT)	100	100	100	100	100

TABLE 1b. RESULTS OF POINT-COUNTS: COLT 31A SMITH

WELL NAME	M.C. COLT		5A		HARVEY
DEPTH (FEET)	775.5	759.5	752	749.5	742
DETRITAL (PERCENT)					
QUARTZ					
MONOCRYSTALLINE	56.7	57.7	36.7	43.3	50.0
POLYCRYSTALLINE	4.7	2.0	3.0	3.7	2.0
FELDSPAR					
POTASSIUM	0	0.7	0.3	0	0
PLAGIOCLASE	6.7	2.3	5.0	3.0	0
SEDIMENTARY ROCK FRAGMENTS	19.3	24.0	30.0	28.0	16.0
MICAS					
MUSCOVITE	1.3	0.3	0	0	0
BIOTITE	0	0	0	0	0
AUTHIGENIC (PERCENT)					
SILICA	5.3	6.7	4.0	4.3	12.0
SIDERITE					
SPHERULITIC	0	0	0	0	0
IRON-CARBONATE	4.7	6.3	20.3	17.7	14.0
CLAY					
KAOLINITE	1.3	0	0.7	0	1.0
CHLORITE	0	0	0	0	2.0
TOTAL (PERCENT)	100	100	100	100	100
AVERAGE GRAIN-SIZE	.27mm	.22mm	.29mm	.24mm	.14mm
POROSITY (%)	25.6	28.0	26.1	26.3	7.0
PERMEABILITY (md.)	160.5	<1.0	<1.0	2.57	<1.0
PORE TYPE (%)					
INTERGRANULAR	10	25	14	17	16
KAOLINITE (INTERCRYSTALLINE)	8	1	0	0	0
MICROPORES	58	64	56	68	53
DISSOLUTION PORES	24	10	30	25	31
TOTAL (PERCENT)	100	100	100	100	100

TABLE 1c. RESULTS OF POINT-COUNTS: COLT 5A HARVEY

WELL NAME	M.C. COLT			5A		JOHNSON		
DEPTH (FEET)	740.5	738	733	730.5	728	721.5	713	710.5
DETRITAL (PERCENT)								
QUARTZ								
MONOCRYSTALLINE	55.4	68.9	52.9	65.5	41.3	46.7	50.8	74.4
POLYCRYSTALLINE	3.6	7.0	3.2	7.0	6.1	6.9	5.9	4.3
FELDSPAR								
POTASSIUM	0	0	0	1.1	0.3	0	0.8	0
PLAGIOCLASE	0	1.3	0.3	0	0	0.3	0	4.0
SEDIMENTARY ROCK FRAGMENTS	1.6	1.3	4.5	8.1	1.0	2.3	1.2	0
MICAS								
MUSCOVITE	0.3	0.3	0	0	0.3	0	0	2.3
BIOTITE	0	0	0	0	0	0	0	0.3
AUTHIGENIC (PERCENT)								
SILICA	1.6	1.3	3.6	0	1.7	1.0	0	0
SIDERITE								
SPHERULITIC	0	0	0	0	0	0	0	0
IRON-CARBONATE	19.7	5.0	11.4	1.1	39.7	29.4	23.8	7.3
CLAY								
KAOLINITE	17.7	14.5	24.0	17.1	9.0	13.4	17.6	7.3
CHLORITE	0	0	0	0	0.6	0	0	0
TOTAL(PERCENT)	100	100	100	100	100	100	100	100
AVERAGE GRAIN-SIZE (mm)	.16	.20	.24	.19	.22	.20	.21	.05
POROSITY (%)	24.1	19.2	20.7	20.6	22.0	23.4	25.1	13.9
PERMEABILITY (md)	116	114	125	51.6	131	126	131	8.1
PORE TYPE (%)								
INTERGRANULAR	21	37	26	21	8	38	22	48
KAOLINITE (INTERCRYSTALLINE)	14	36	20	33	13	31	38	7
MICROPORES	2	4	7	41	4	7	10	33
DISSOLUTION PORES	63	23	47	5	75	24	30	12
TOTAL (PERCENT)	100	100	100	100	100	100	100	100

TABLE 1d. RESULTS OF POINT-COUNTS: COLT 5A JOHNSON

WELL NAME	M.C. COLT			13AO		JOHNSON	
DEPTH (FEET)	757	749.5	744.5	734.5	727	724.5	714.5
DETRITAL (PERCENT)							
QUARTZ							
MONOCRYSTALLINE	74.0	40.7	63.0	59.6	48.0	48.3	57.4
POLYCRYSTALLINE	3.3	3.0	4.7	4.0	4.7	5.7	6.8
FELDSPAR							
POTASSIUM	3.3	0.3	0	0	0	1.0	0
PLAGIOCLASE	6.3	6.0	3.0	5.0	2.3	8.0	9.0
SEDIMENTARY ROCK FRAGMENTS	9.7	4.0	14.0	24.2	21.0	16.0	18.1
MICAS							
MUSCOVITE	0	0	0	0.7	0	0	0.3
BIOTITE	0	0	0	0.3	0.3	0	0
AUTHIGENIC (%)							
SILICA	1.0	0	2.0	3.6	2.0	11.3	0.3
SIDERITE							
SPHERULITIC	0	0	0	0	0	0	1.2
IRON-CARBONATE	1.3	45.0	4.7	2.6	19.7	1.3	5.9
CLAY							
KAOLINITE	1.0	1.0	0.3	0	0.7	1.0	1.0
CHLORITE	0	0	8.3	0	1.3	7.3	0
TOTAL (PERCENT)	100	100	100	100	100	100	100
AVERAGE GRAIN-SIZE (mm)	.21	.25	.17	.21	.25	.22	.26
POROSITY (%)	10.2	16.7	29.0	26.1	28.0	24.4	24.4
PERMEABILITY (md)	19.7	<1.0	60.0	N/A	153.2	<1.0	31.6
PORE TYPE (%)							
INTERGRANULAR	-	12	20	15	29	13	30
KAOLINITE (INTERCRYSTALLINE)	-	2	0	0	1	2	6
MICROPORES	-	8	57	40	24	46	33
DISSOLUTION PORES	-	78	23	45	46	39	29
TOTAL (PERCENT)	-	100	100	100	100	100	100

TABLE 1e. RESULTS OF POINT-COUNTS: COLT 13AO JOHNSON

WELL NAME	M.C. COLT	14AO	JOHNSON	
DEPTH (FEET)	751.5	744	724	714
DETRITAL (PERCENT)				
QUARTZ				
MONOCRYSTALLINE	59.8	55.7	54.2	54.7
POLYCRYSTALLINE	2.3	3.0	3.7	4.0
FELDSPAR				
POTASSIUM	0	0.3	0.3	0
PLAGIOCLASE	3.6	1.7	0.7	6.7
SEDIMENTARY ROCK FRAGMENTS	28.5	16.4	18.4	22.0
MICAS				
MUSCOVITE	0	0.3	0.3	0.3
BIOTITE	0.3	0	0	0.3
AUTHIGENIC (PERCENT)				
SILICA	1.0	1.7	1.7	3.3
SIDERITE				
SPHERULITIC	0	0	0	0
IRON-CARBONATE	0	15.4	17.1	1.7
CLAY				
KAOLINITE	0.6	5.4	3.7	0.7
CHLORITE	3.9	0	0	6.3
TOTAL (PERCENT)	100	100	100	100
AVERAGE GRAIN-SIZE	.05mm	.23mm	.24mm	.18mm
POROSITY (%)	23.2	26.0	26.0	23.9
PERMEABILITY (md)	N/A	140.5	<1.0	116.4
PORE TYPE (%)				
INTERGRANULAR	-	65	26	56
KAOLINITE (INTERCRYSTALLINE)	-	3	2	2
MICROPORES	-	25	54	34
DISSOLUTION PORES	-	7	18	8
TOTAL (PERCENT)	100	100	100	100

TABLE 1f. RESULTS OF POINT-COUNTS: COLT 14AO JOHNSON

WELL NAME	M.C. COLT		26AO	JOHNSON	
DEPTH (FEET)	757.5	752.5	745	743	735
DETRITAL (PERCENT)					
QUARTZ					
MONOCRYSTALLINE	58.7	68.8	58.5	63.1	63.2
POLYCRYSTALLINE	2.6	3.7	3.7	3.6	4.3
FELDSPAR					
POTASSIUM	0.3	2.3	0.3	0	0.3
PLAGIOCLASE	4.9	2.3	0.3	1.0	0.7
SEDIMENTARY ROCK FRAGMENTS	7.5	4.7	2.7	3.6	11.9
MICAS					
MUSCOVITE	0.3	0.7	0.3	0.7	0.7
BIOTITE	0	0	0	0	0.3
AUTHIGENIC (PERCENT)					
SILICA	0.3	0.3	0	2.0	2.0
SIDERITE					
SPHERULITIC	0	0	0	0	0
IRON-CARBONATE	15.1	4.3	23.9	17.6	13.2
CLAY					
KAOLINITE	8.5	13.0	10.3	8.5	2.3
CHLORITE	1.6	0	0	0	1.0
TOTAL (PERCENT)	100	100	100	100	100
AVERAGE GRAIN-SIZE	.27mm	.22mm	.24mm	.24mm	.22mm
POROSITY (%)	20.3	19.7	23.9	22.4	24.3
PERMEABILITY (md)	16.3	95.1	214.7	96.4	18.4
PORE TYPE (%)					
INTERGRANULAR	32	60	55	47	49
KAOLINITE (INTERCRYSTALLINE)	4	13	13	8	7
MICROPORES	34	9	2	14	4
DISSOLUTION PORES	30	18	30	31	3
TOTAL (PERCENT)	100	100	100	100	100

TABLE 1g. RESULTS OF POINT-COUNTS: COLT 26AO JOHNSON

WELL NAME	M.C. COLT	50AO	JOHNSON	
DEPTH (FEET)	780	764	757	752
DETRITAL (PERCENT)				
QUARTZ				
MONOCRYSTALLINE	57.0	59.6	68.8	66.3
POLYCRYSTALLINE	5.6	3.3	3.0	3.0
FELDSPAR				
POTASSIUM	0.3	0.3	0	0
PLAGIOCLASE	5.0	1.7	1.3	0
SEDIMENTARY ROCK FRAGMENTS	4.6	3.0	4.3	3.0
MICAS				
MUSCOVITE	0	0	0	0.3
BIOTITE	0	0	0.3	0
AUTHIGENIC (PERCENT)				
SILICA	6.0	1.0	0.3	2.0
SIDERITE				
SPHERULITIC	0	0	0	0
IRON-CARBONATE	4.3	23.2	11.0	11.7
CLAY				
KAOLINITE	6.0	7.3	11.0	13.7
CHLORITE	11.3	0.7	0	0
TOTAL (PERCENT)	100	100	100	100
AVERAGE GRAIN-SIZE	.24mm	.20mm	.24mm	.20mm
POROSITY (%)	17.1	22.1	18.5	19.8
PERMEABILITY (md)	45.9	211.5	43.5	116.5
PORE TYPE (%)				
INTERGRANULAR	41	53	40	46
KAOLINITE (INTERCRYSTALLINE)	9	9	22	26
MICROPORES	36	7	10	8
DISSOLUTION PORES	14	31	28	20
TOTAL (PERCENT)	100	100	100	100

TABLE 1h. RESULTS OF POINT-COUNTS: COLT 50AO JOHNSON

AUTHIGENIC CEMENT AND CLAY

SILICA CEMENTS

Silica cement occurs as euhedral, syntaxial overgrowths on quartz grains (Figs. 49 and 50). Quartz overgrowths compose 0 to 12 percent of the points counted and were observed in all but a few thin-sections. The samples that did not exhibit any silica overgrowth were pervasively cemented with carbonate or thick clay coatings early in the diagenetic history (Fig. 51 and 52). Abundant early cementation also reduces or eliminates the permeability of the sandstone and precludes the introduction of numerous pore volumes of silica-rich waters needed to produce abundant overgrowths (Blatt, 1979).

Thin clay coatings on the quartz grains also tend to inhibit the formation of silica overgrowths, but are less effective than thick coatings. Commonly, small crystals nucleate on many different sites on the quartz grains that are sparsely coated with clay. These numerous small crystals eventually grow and coalesce to form a single, large crystal (Fig. 53). As the quartz crystals coalesce, the clay coatings are replaced by the overgrowth. The only evidence of the clay coating observed was insoluble material that remains as a

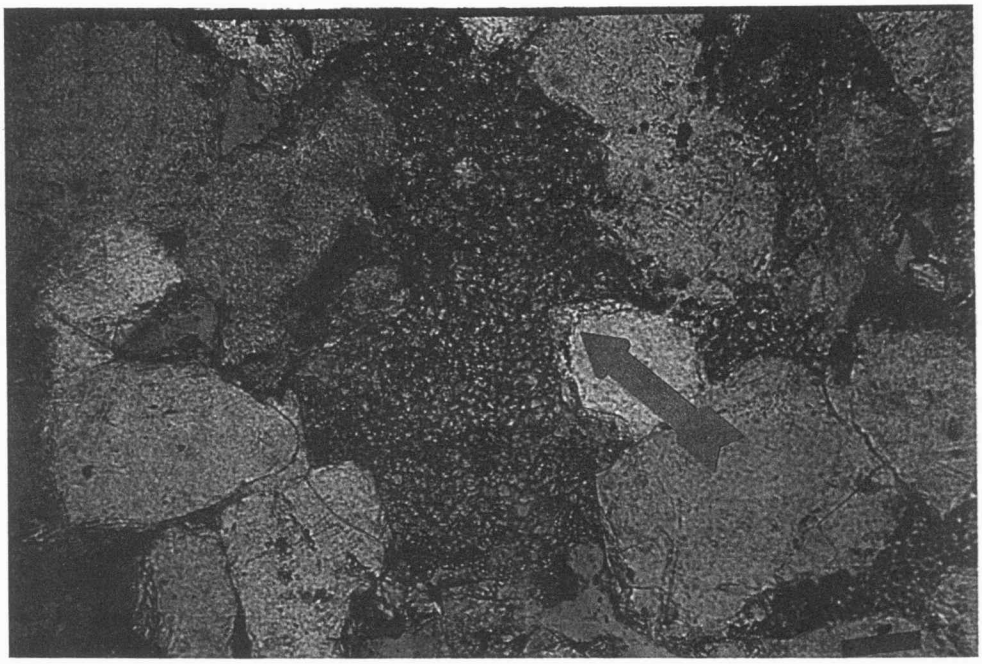

Figure 49. Colt 28A Smith, 782.8 ft. (Pl-light, 100X) This sample exhibits quartz grains with euhedral, syntaxial silica overgrowths (arrow). Note the "dust rims" at the contact between grain and overgrowth. Also note the large pore filled with kaolinite (K). (Scale=0.1 mm.)

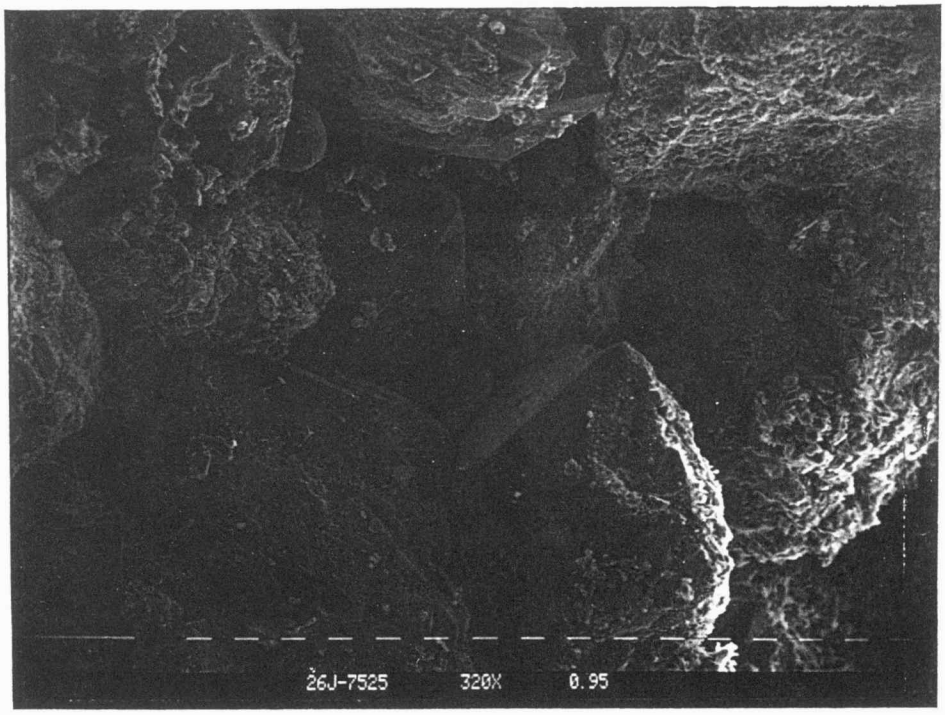

Figure 50. Colt 26AO Johnson, 752.5 ft. (320 X) Scanning electron photomicrograph of detrital quartz grains with euhedral silica overgrowths. (Divisions on scale=0.01 mm.)

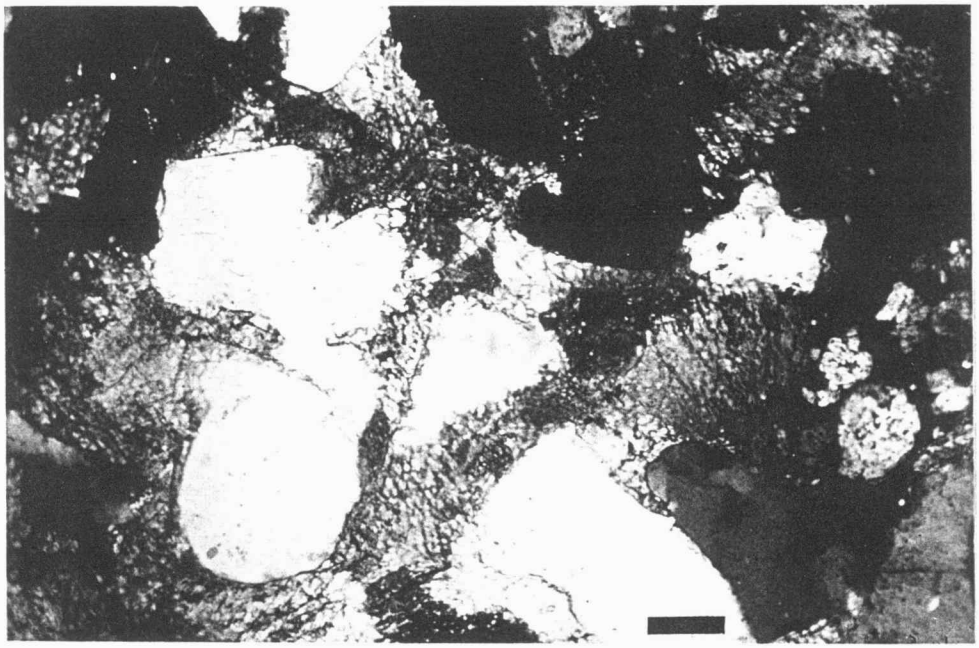

Figure 51. Colt 28A Smith, 759.5 ft. (X-nicols, 100X) This sample shows abundant early carbonate cement that has prevented the development of quartz overgrowths. (Scale=0.1 mm.)

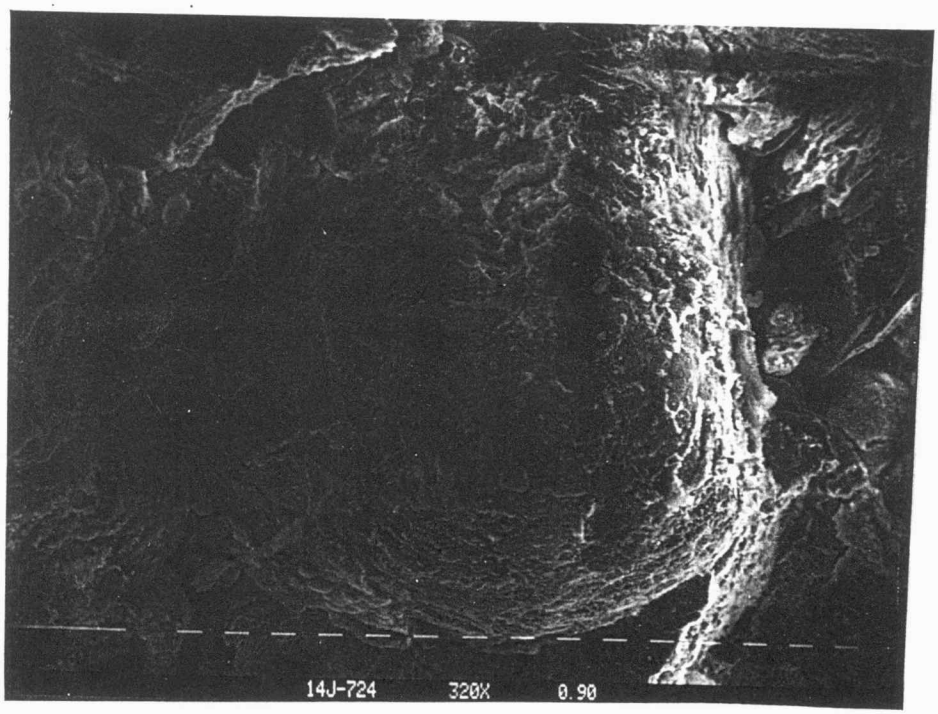

Figure 52. Colt 14AO Johnson, 724 ft. (320X) S.E.M. photomicrograph of rounded quartz grain with chlorite coatings. Clay coatings inhibit the development of silica overgrowths. See Fig. 67 for high-power view of this quartz grain. (Divisions on scale=0.01 mm.)

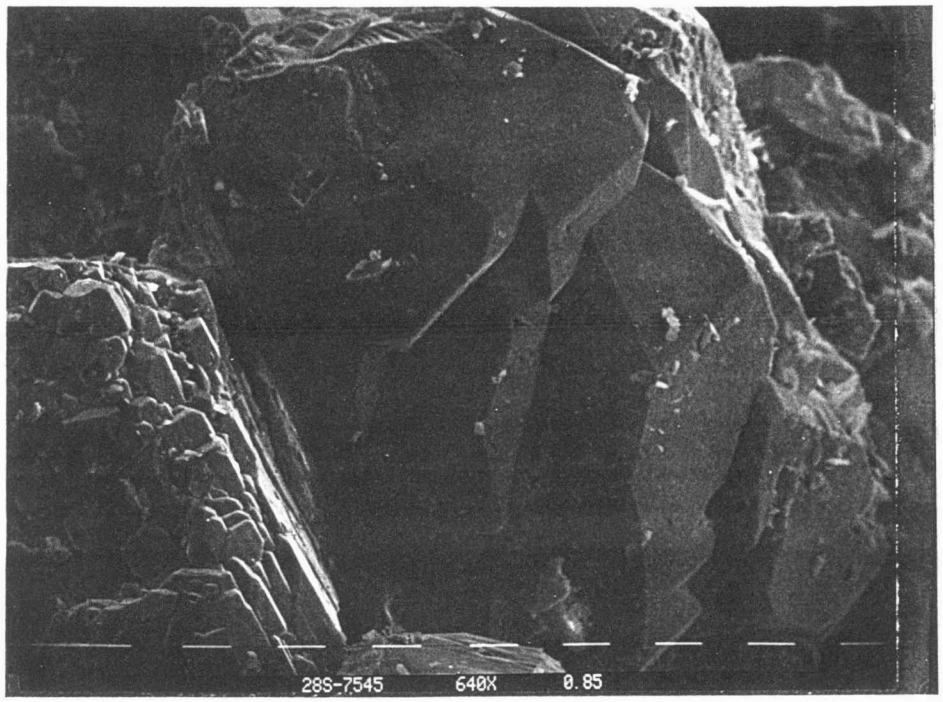

Figure 53. Colt 28A Smith, 754.5 ft. (640X)
Both quartz grains in this photomicrograph show multiple overgrowths in different stages of coalescence. The overgrowths would have eventually coalesced to form one single overgrowth (see below). (Scale divisions=0.01 mm.)

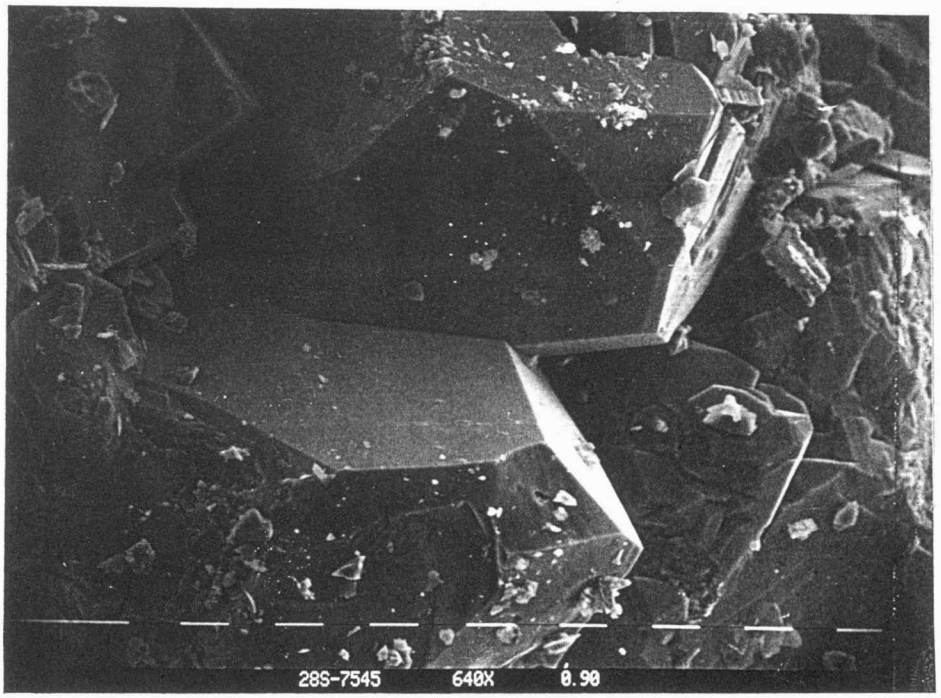

Figure 54. Colt 28A Smith, 754.5 ft. (640X)
Abundant silica overgrowths completely clogging the pore space. The overgrowths from adjacent grains have interlocked to indurate the sample. (Scale divisions=0.01 mm.)

residue or dust rim (Fig. 32). This rim is useful in differentiating detrital cores and overgrowths for point counting.

Extensive silica overgrowth can effectively eliminate pores and destroy the permeability of some samples (Fig. 54). Fine-grained samples commonly exhibited extensive silica cement while coarse-grained sediments did not. Woody (1983) reported a similar relationship between grain-size and degree of silica cementation.

CARBONATE CEMENTS

Three distinct carbonate cements were observed in the samples from the KB Field: spherulitic siderite, pore-filling or poikilotopic siderite and Ca-Mg-Fe carbonate. Spherulitic or "buckshot" siderite was identified in few of the thin sections and appears as small, dark red, high-relief spheres in hand specimen (Figs. 55 and 56). In one sample, spherulitic siderite was the predominant cement accounting for 13 percent of the points counted (Colt 31A Smith, 751 ft., Table 1b).

Siderite is also a pore-filling or, less commonly, a poikilotopic cement. It appears as a subhedral, turbid, and high relief mineral with moderately undulose extinction (Fig. 57). This cement changes in

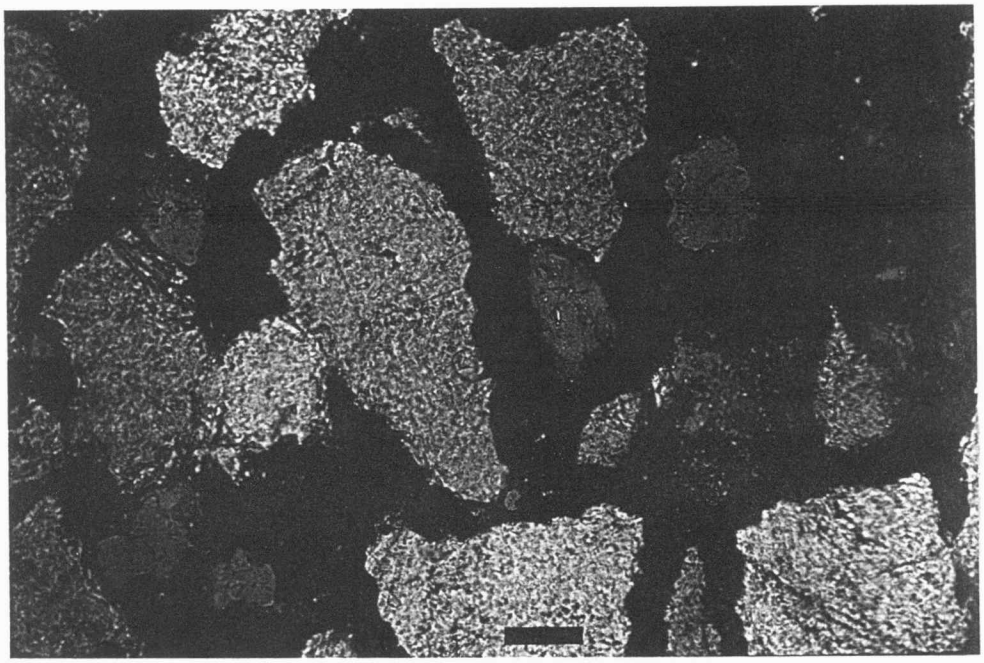

Figure 55. Colt 31A Smith, 751 ft. (Pl-light, 100X) Though difficult to photograph, the cement in this sample is composed of spherulitic or "buckshot" siderite. This dark-red, granular cement was the first carbonate phase to precipitate. (Scale=0.1 mm.)

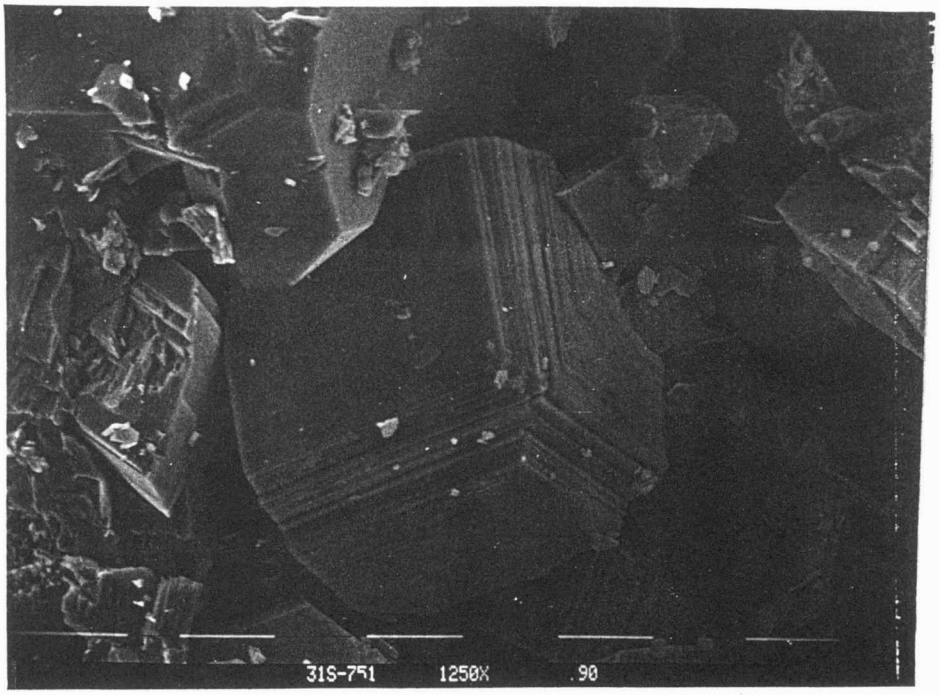

Figure 56. Colt 31A Smith, 751 ft. (1250X) S.E.M. photomicrograph of the same sample as above. The spherulitic siderite appears isometric at first glance, but is actually slightly rhombic. (Scale divisions=0.01 mm.)

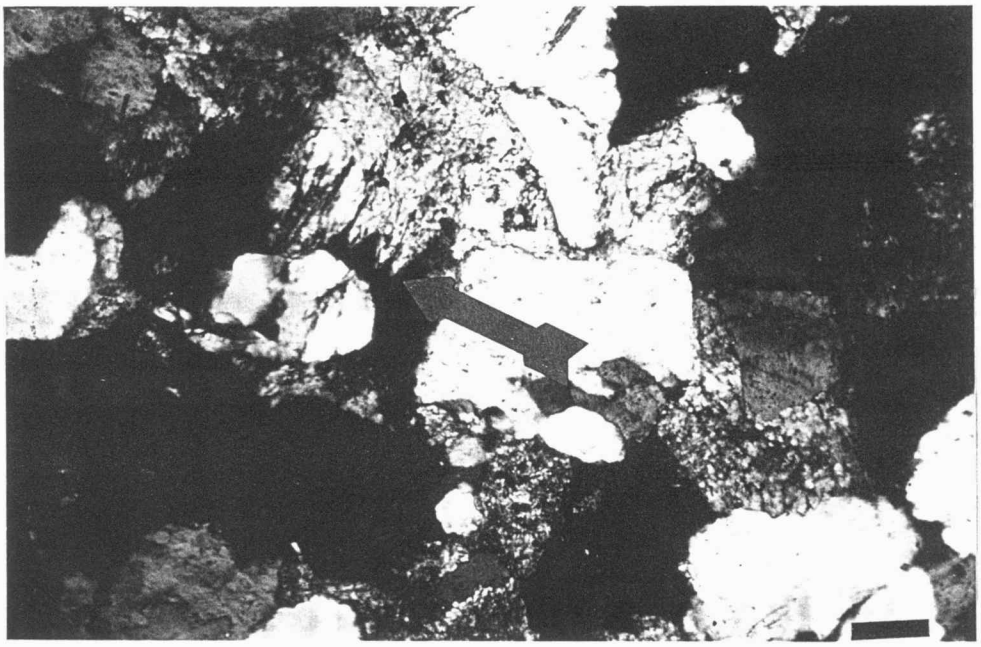

Figure 57. Colt 28A Smith, 759.5 ft. (Pl-light, 100X) This sample shows early pore-filling siderite cement. Note the partial dissolution of the siderite as evidenced by the "cox-comb" structure (arrow). (Scale=0.1 mm.)

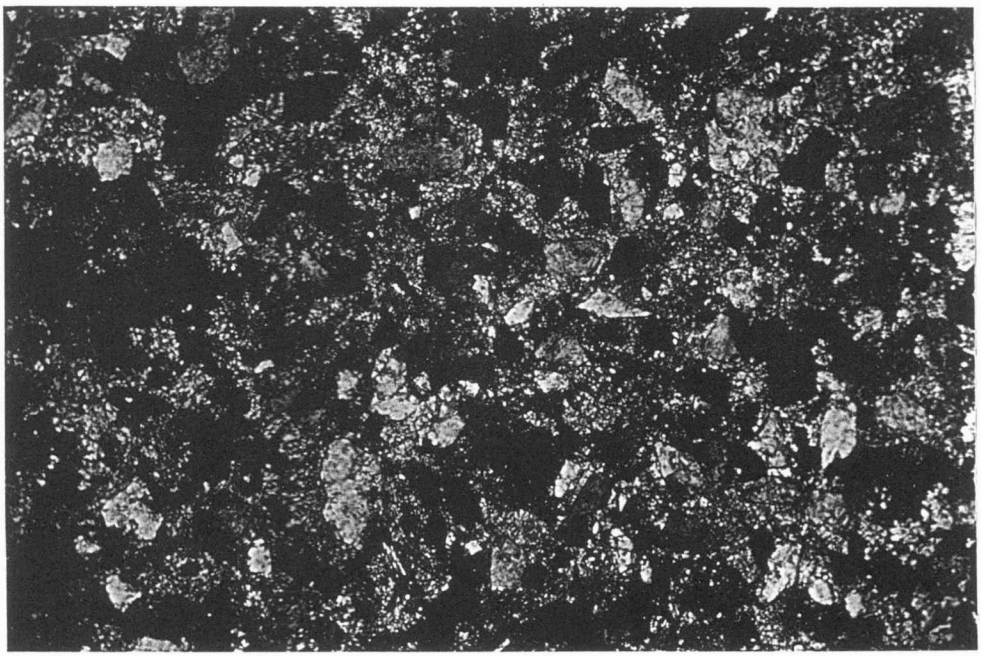

Figure 58. Colt 5A Johnson, 728.5 ft. (X-nicols, 100X) Poikilotopic siderite nodule containing coarse silt. (Scale=0.1 mm.)

relief with rotation of the microscope stage because of the large birefringence, but its extraordinary ray index is always above that of quartz, unlike calcite or Ca-Mg-Fe carbonate.

Poikilotopic cements are concretions that encase several detrital grains and were one of the first authigenic phases to form. Poikilotopic cements precipitate prior to compaction of the sediment and, therefore, the detrital grains appear to "float" in a carbonate matrix (Fig. 58).

Siderite also was observed as a patchy, pore-filling cement (Fig. 59). The pore-filling siderite cement was noted in many of the samples and commonly completely occluded the pore throats. The amount of cementation differed greatly in each of the samples ranging from minor amounts in the interstices between framework grains to complete filling of the primary pores.

Ca-Mg-Fe carbonate is the third carbonate cement in the samples studied. This cement is limpid, euhedral, and shows strongly undulose extinction (Figs. 60 and 61). Bouquet (1984) gives the composition of similar cements from the Strauss Field in Crawford, Labette and Neosho Counties as Ca-Mg-Fe carbonate, based on electron probe analyses. This carbonate was observed in two habits; as a pore-filling cement and as

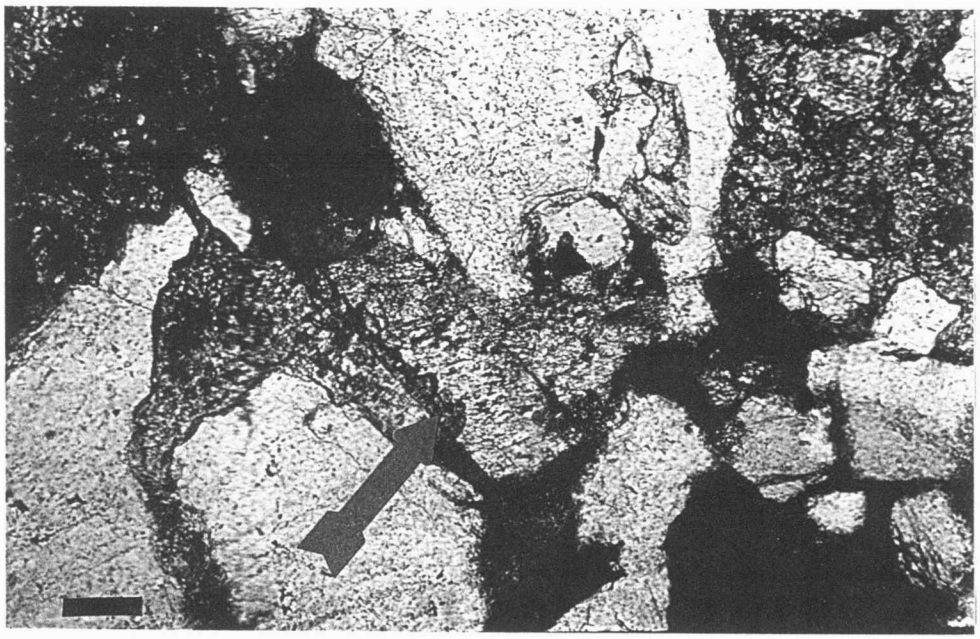

Figure 59. Colt 28A Smith, 752 ft. (Pl-light, 100X) Patchy pore-filling siderite cement. Note the partially dissolved feldspar (F) etched by the carbonate (arrow). (Scale=0.1 mm.)

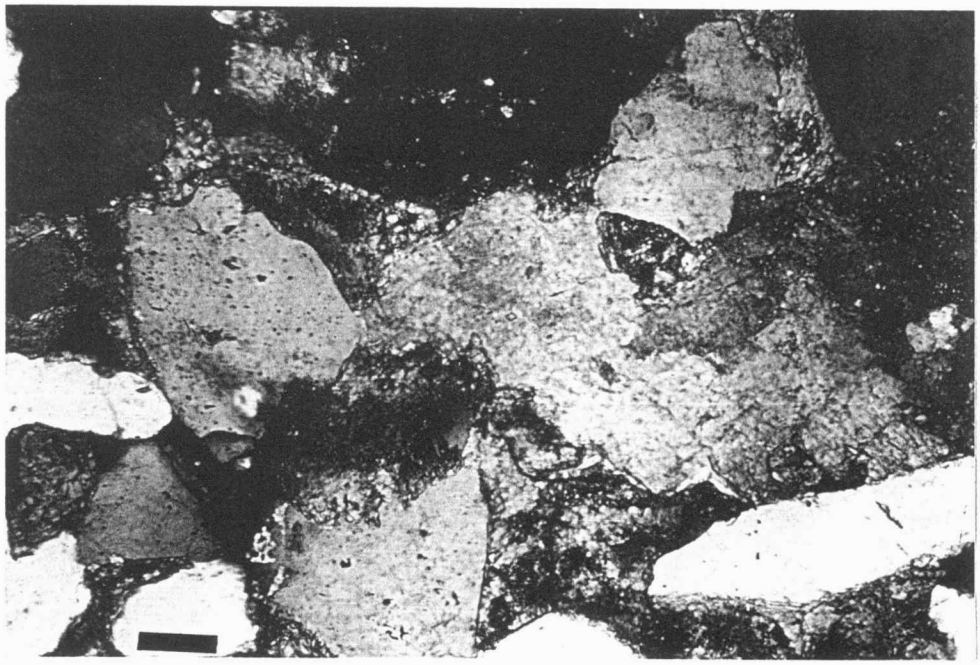

Figure 60. Colt 28A Smith, 759.5 ft. (X-nicols, 100X) Limpid, euhedral Ca-Mg-Fe carbonate (C) is observed in the center of the photomicrograph. Note the turbid siderite (S) also in this sample. (Scale=0.1 mm.)

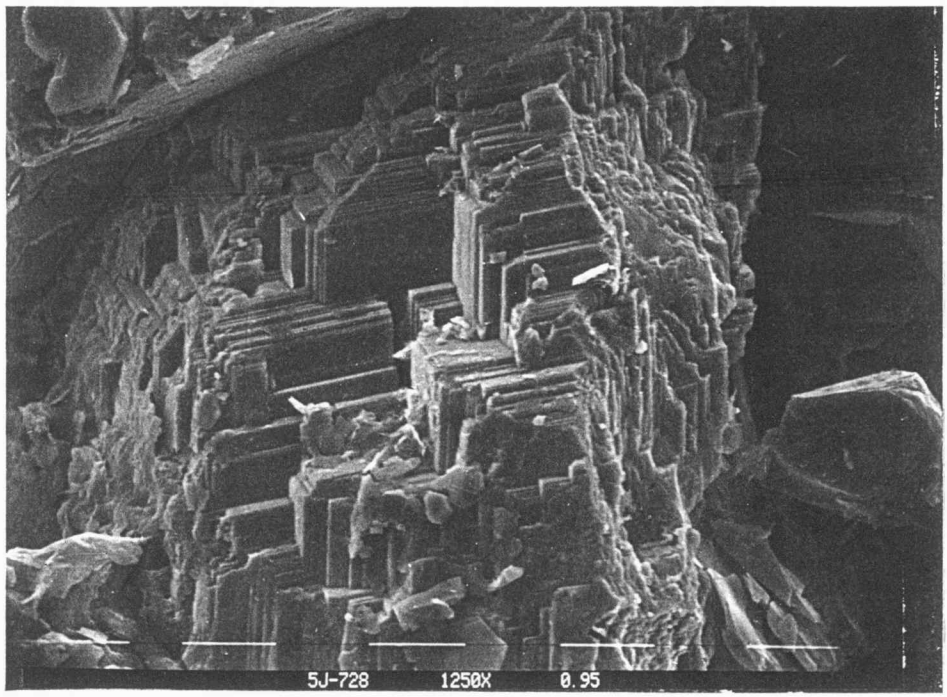

Figure 61. Colt 5A Johnson, 728 ft. (1250X) S.E.M. photomicrograph of euhedral Ca-Mg-Fe carbonate cement. (Scale divisions=0.01 mm.)

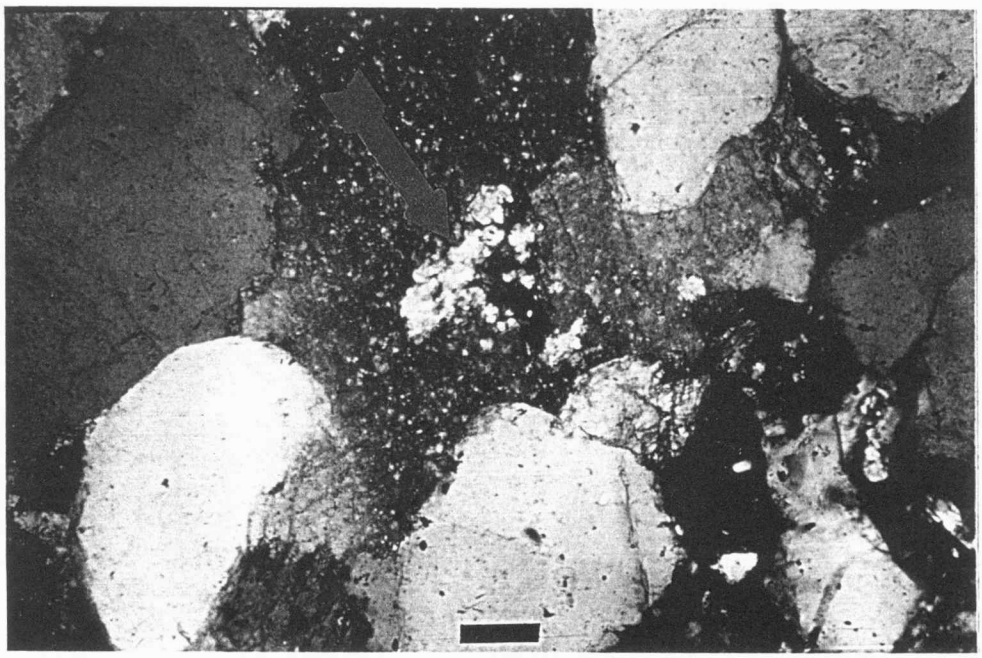

Figure 62. Colt 28A Smith, 752 ft. (X-nicols, 100X) This sample shows pore filling Ca-Mg-Fe carbonate (C) that partially replaced feldspar (arrow). (Scale=0.1 mm.)

a grain replacement. The pore-filling Ca-Mg-Fe carbonate cement was the most common of the three cements recognized and was noted in nearly all the samples from the KB Field. Ca-Mg-Fe carbonate was observed as discrete patches that partially or completely plug the pore throats (Fig. 62). This cement was observed to fill the void space that remained after dissolution of both feldspar and siderite. Ca-Mg-Fe carbonate commonly replaces both quartz (Fig. 63) and feldspar. Numerous examples of feldspars that were almost completely replaced by carbonate were noted (Fig. 64).

Pore-filling siderite and Ca-Mg-Fe carbonate were incorrectly identified as the same mineral during initial point-counting. It was assumed initially that the turbid or dusty siderite was actually Ca-Mg-Fe carbonate that contained abundant insoluble residue. The siderite and Ca-Mg-Fe carbonate are in optical continuity in some samples and initially appeared to have precipitated contemporaneously. Subsequent investigation and staining of the thin-section proved this observation to be false. The Ca-Mg-Fe carbonate precipitated much later in the diagenetic sequence than the pore-filling siderite (Figs. 33 and 60). This topic will be discussed in detail in the section dealing with "Paragenesis".

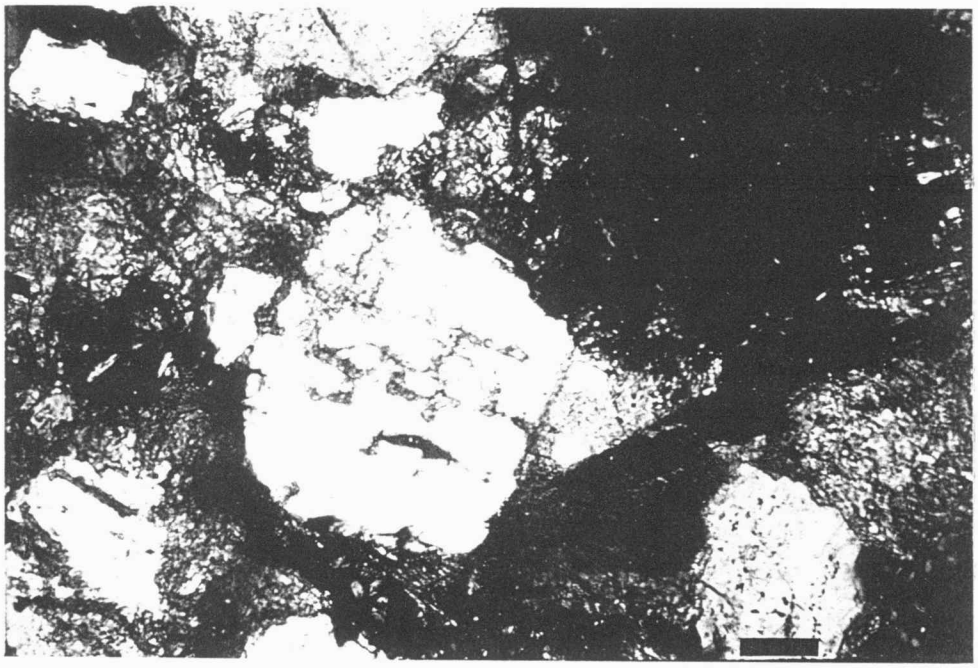

Figure 63. Colt 28A Smith, 762 ft. (X-nicols, 100X) Example of Ca-Mg-Fe carbonate partially replacing quartz (Q). (Scale=0.1 mm.)

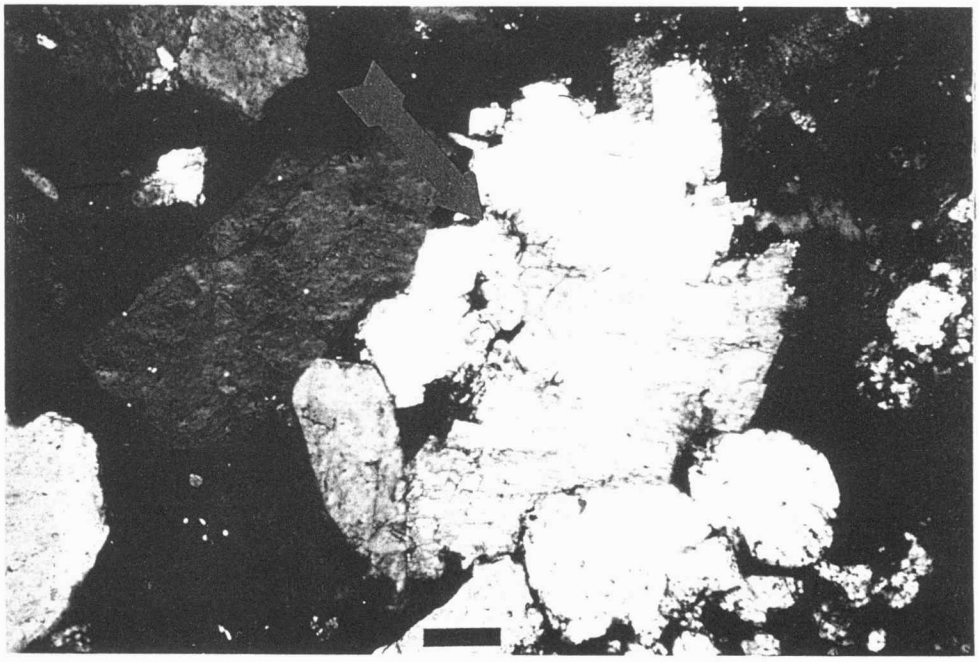

Figure 64. Colt 13AO Johnson, 752 ft. (X-nicols, 100X) This sample exhibits Ca-Mg-Fe carbonate (C) partially replacing feldspar (arrow). (Scale=0.1 mm)

The patchy siderite and the Ca-Mg-Fe carbonate are classified collectively as "IRON-CARBONATE" on Tables 1a through 1h. Cumulatively these cements range in abundance from <1 to >40 percent of the points counted. Most samples that contained greater than 20 percent carbonate are cemented by poikilotopic siderite.

KAOLINITE

Kaolinite is the most abundant of the authigenic clay minerals in the KB Field and composes up to 24 percent of the samples studied. Kaolinite forms long, curving, vermicular crystals that are hexagonal in cross section, shows low birefringence, and commonly fills both primary pores between framework grains and secondary dissolution pores (Figs. 65 and 66). Many samples exhibit extensive authigenic kaolinite that completely occludes the pores. Kaolinite appears to be particularly abundant in samples that contain partially dissolved feldspars or large dissolution pores. These large dissolution pores are interpreted to be the void space remaining after complete dissolution of feldspar. A direct proportion between the degree of feldspar dissolution and the amount of kaolinite was noted in many samples, supporting the notion that feldspar contributes components that are necessary for the formation of authigenic kaolinite (Boles, 1978; Milliken et al., 1981).

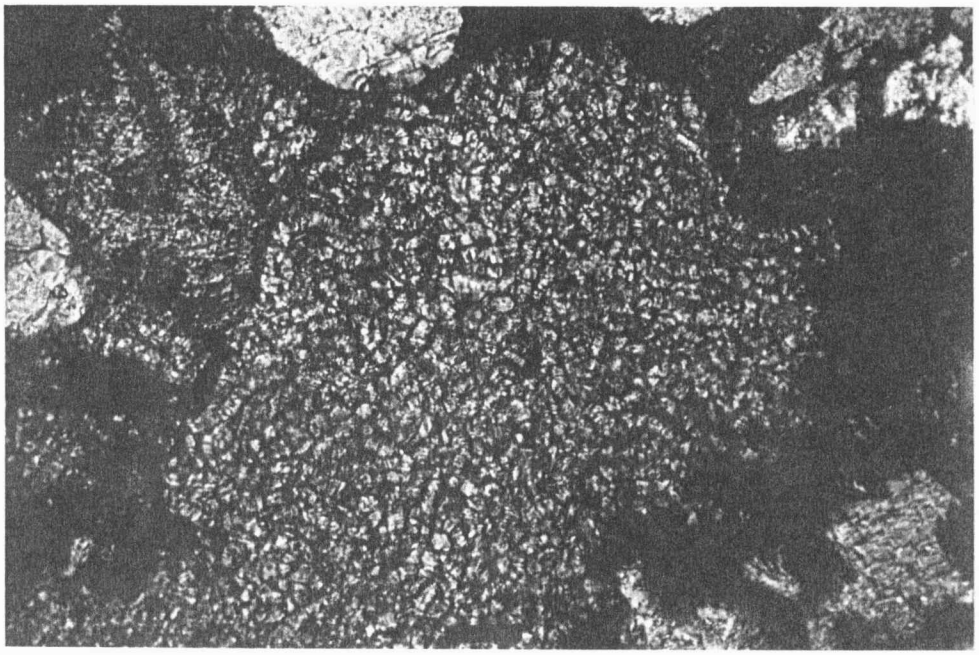

Figure 65. Colt 28A Smith, 762 ft. (Pl-light, 100X) Large dissolution pore filled with kaolinite. Note the porosity between kaolinite crystals is filled with blue-dyed epoxy. (Scale=0.1 mm)

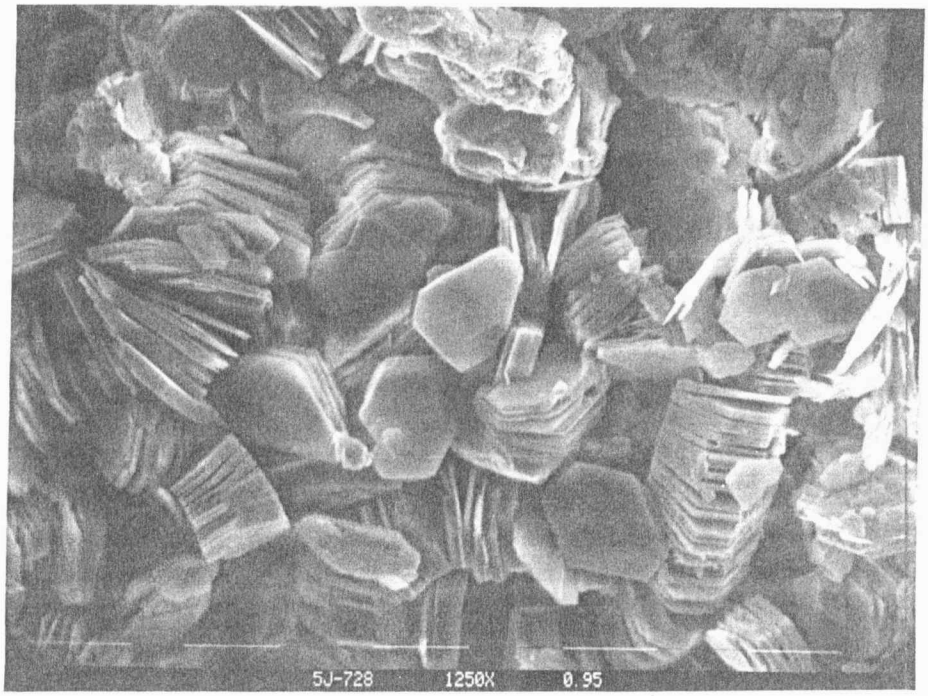

Figure 66. Colt 5A Johnson, 728 ft. (1250X) S.E.M. photomicrograph of euhedral "booklets" of kaolinite. Note porosity between individual crystals. (Scale divisions=0.01 mm.)

CHLORITE

Chlorite is a light green, slightly pleochroic authigenic clay that coats the surface of detrital grains. The clay is oriented radially on the surface of the grain and lines the surface of the pore throats (Fig. 67). Most chlorite forms a thin coating but may appear as a thick isopachous cement (Fig. 68). Most of the thin-sections that exhibited the thick grain coatings contained numerous sedimentary rock fragments that were partially dissolved. As stated earlier, thin chlorite coatings commonly were replaced by authigenic silica.

PYRITE

Authigenic pyrite was observed in the Upper Bluejacket Sandstone, but this sulfide is relatively rare and is not evenly distributed throughout the sand body. Pyrite was only observed in the sands directly in contact with the Bluejacket B Coal (Fig. 69). Pyrite formed from the sulfur present in the Bluejacket B Coal. The cored samples of this coal exhibit yellow- and white-colored iron sulfate that has formed since the cores were exhumed (Fig. 69).

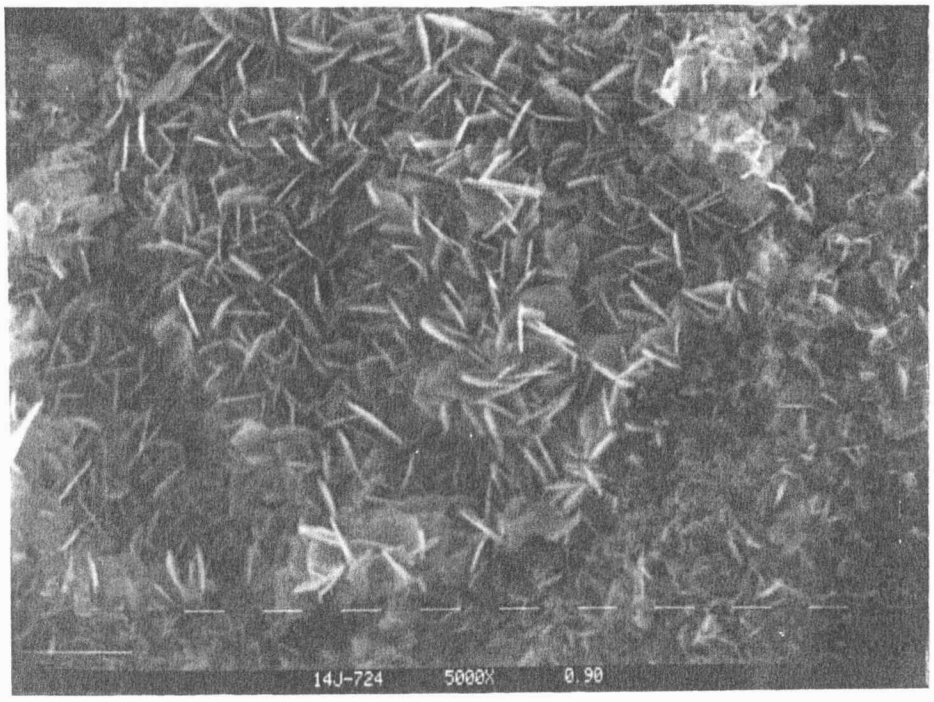

Figure 67. Colt 14AO Johnson, 724 ft. (5000X)
Chlorite clay coatings on quartz framework grain.
(Scale divisions=0.001 mm.)

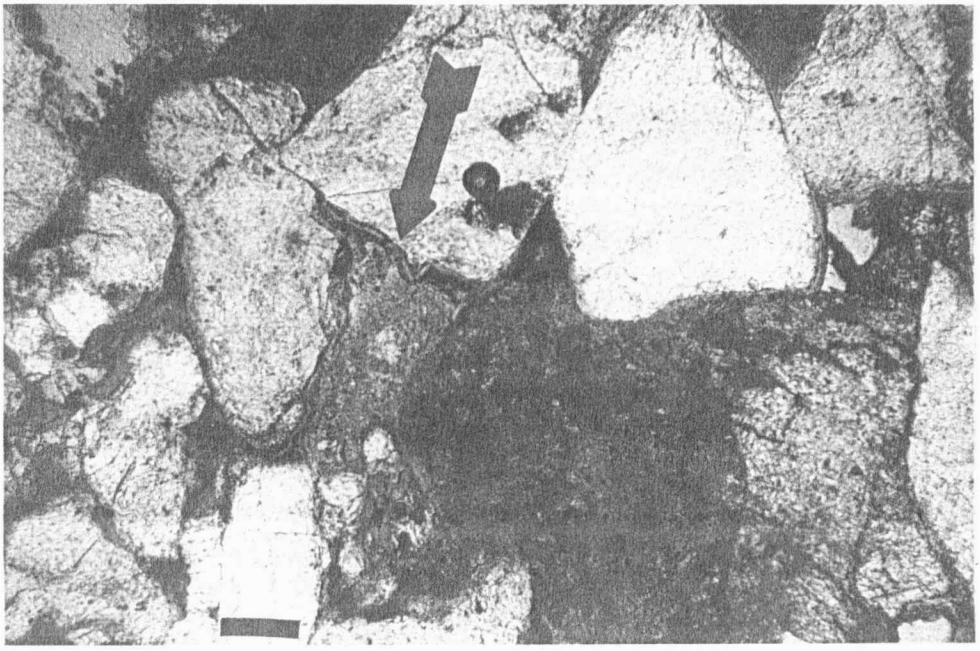

Figure 68. Colt 5A Harvey, 752 ft. (Pl-light, 100X)
This sample shows thick isopachous authigenic chlorite cement (arrow). Note the SRF in the center of the photo partially replaced by siderite. (Scale=0.1 mm.)

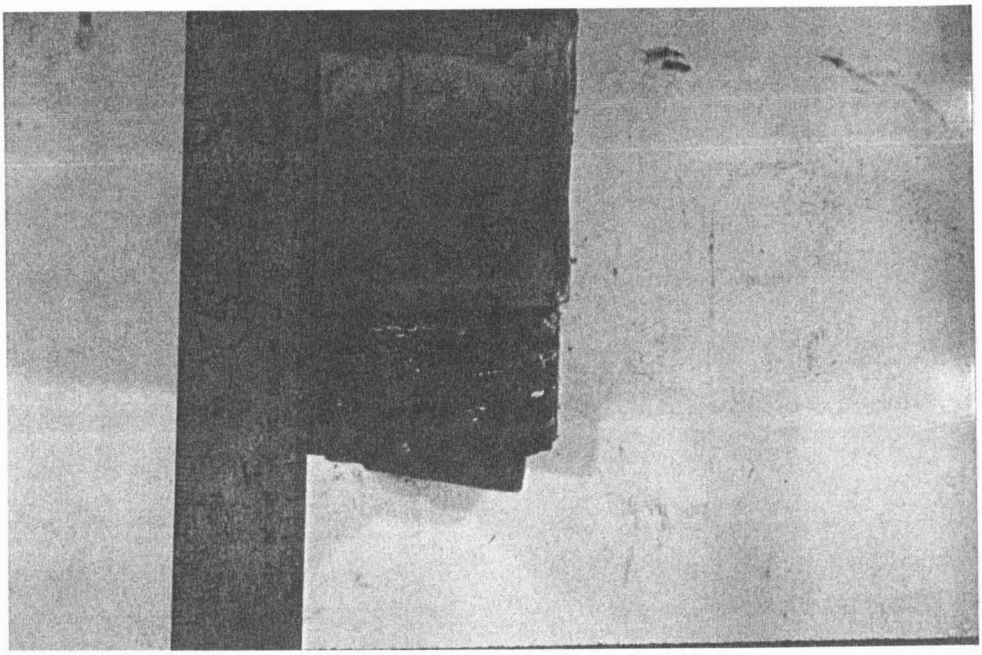

Figure 69. Colt 5A Johnson, 780.2 ft. (Scale=cm/in.) Pyrite appears along the contact with the Bluejacket B Coal. The pyrite is found in the dark region of the sand at the sand/coal contact.

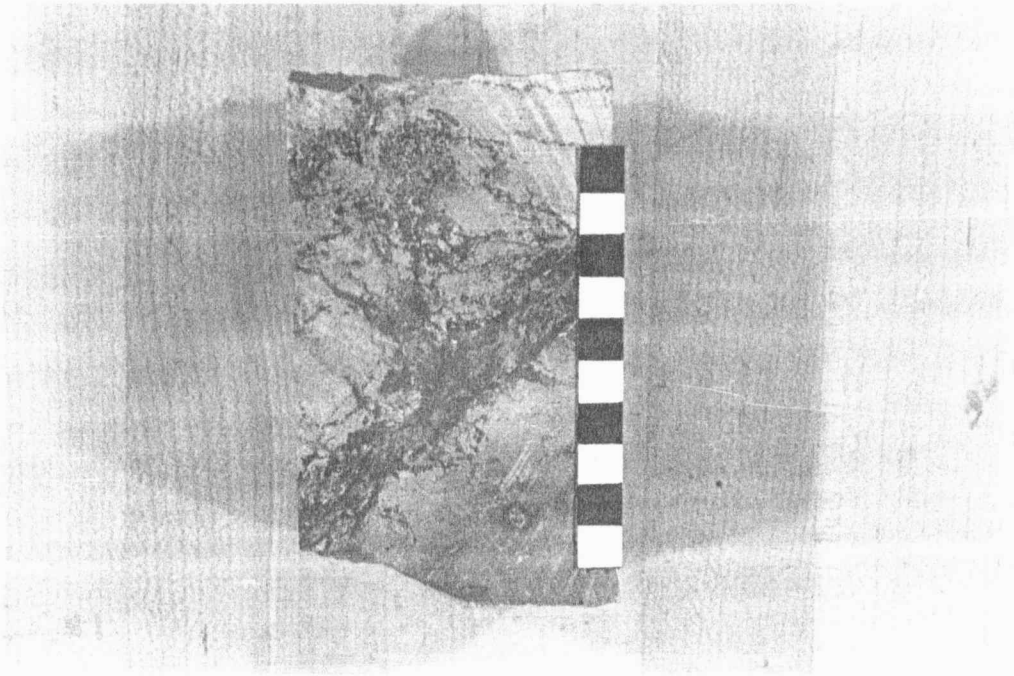

Figure 70. Colt 26AO Johnson, 720 ft. (Scale=10cm) This sample shows siderite vein in the gray shales superjacent to the Upper Bluejacket Sandstone.

DIAGENESIS AND PARAGENESIS OF THE UPPER BLUEJACKET SANDSTONE

The paragenesis, or the sequential order, of diagenetic changes in the reservoir sandstones of the KB Field was determined from relationships observable in thin-section. The diagenetic sequence was: 1) formation of poikilotopic, spherulitic and pore-filling siderite; 2) precipitation of pyrite; 3) compaction of the reservoir sand; 4) formation of chlorite grain coatings; 5) development of quartz overgrowths; 6) partial dissolution of pore-filling siderite; 7) precipitation of Ca-Mg-Fe carbonate; 8) dissolution of feldspar and argillaceous rock fragments; 9) formation of kaolinite; and 10) migration of hydrocarbons into the reservoir. It is emphasized that this sequence simply outlines the beginning of each diagenetic phase relative to the other phases. The onset of a new phase did not necessarily mark the end of the previous phase.

The diagenetic sequence observed in the KB Field is remarkably similar to the sequences determined in other studies (Woody, 1983; Land and Dutton, 1978.). Woody's (1983) study of Cherokee Group Sandstones outlined a virtually identical sequence to that found in the study area. Some of Woody's samples contained poikilotopic calcite, which was not observed in the KB

Field. Land and Dutton (1978) recognized a similar diagenetic sequence in Desmoinesian sandstones from north-central Texas, but did not observe poikilotopic carbonate as the first phase to precipitate. Unlike the KB Field, Land and Dutton (1978) also observed calcite precipitation following the development of quartz overgrowths.

Siderite was likely the first authigenic mineral to form, although the sequential order with respect to pyrite was impossible to determine. These two authigenic minerals were never observed in the same sample and, therefore, their paragenesis cannot be determined. Pyrite was only observed in a thin zone along the contact with the Bluejacket B Coal. Pyrite formation requires slightly acidic, reducing conditions with abundant dissolved sulfur, while siderite precipitates in acidic, reducing environments with low dissolved sulfur concentrations (Garrels and Christ, 1965). Berner (1980) believes bacterial decomposition of organic matter is instrumental in producing the sulfur-rich formation waters needed for pyrite precipitation. Berner's interpretation is supported by the observed distribution of the pyrite in the Upper Bluejacket Sandstone. Sulfur concentrations sufficient for the precipitation of pyrite only existed in contact with the coal.

Spherulitic and poikilotopic siderite were the first authigenic phases to form in the sands not affected by pyrite precipitation. Poikilotopic siderite cement precluded further diagenesis of some samples by completely filling the pores. Samples containing abundant siderite spherules also lack other authigenic phases, such as quartz overgrowths and clay coatings.

Large concretions of siderite were common in the gray shales above the Upper Bluejacket Sandstone (Fig. 70). These concretions appear as large veins and may be soil structures associated with plant roots. Sideritic concretions in the shale units also appear as large (1 cm) spheres that exhibit concentric zonation.

Cross-stratified sandstones commonly show preferential siderite cementation along crossbed faces (Fig. 11). This phenomenon was clearly observed in several of the thin-sections, but the factors controlling carbonate distribution are enigmatic (Fig. 71). Thin-sections revealed no evidence, such as finer grain-size or increased matrix content, to explain the sharp contact between the cemented and uncemented zones.

Authigenic chlorite coatings were the next stage of the diagenetic sequence. Clay coatings are not evenly distributed throughout the reservoir and appear to be associated with argillaceous rock fragments.

Samples that exhibited thick, isopachous chlorite coatings commonly contained abundant shale clasts (Fig. 72). Chlorite is interpreted to precede quartz overgrowths because grains that were thickly coated showed no evidence of authigenic silica. Clay coatings on quartz grains may preserve the porosity and permeability because they actually inhibit silica overgrowth (Pittman, et al., 1968).

The sequencial order of the formation of quartz overgrowths relative to siderite dissolution is equivocal. Many quartz grains without overgrowths were observed close to definite siderite dissolution pores (Fig. 73). From the lack of silica overgrowths it is inferred that the precipitation of authigenic silica preceded the dissolution of siderite.

Quartz overgrowths were noted in all samples except those pervasively cemented with siderite or authigenic chlorite. Many individual quartz grains exhibited large overgrowths that interlocked with adjacent grains (Figs. 74 and 54). Grains commonly show partial silica overgrowths that probably would have coalesced with continued growth (Fig. 75).

Dissolution of siderite cement was the next diagenetic change to occur in the Upper Bluejacket Sandstone. The degree of siderite dissolution ranged from extensive to minor. Partial dissolution of

Figure 71. Colt 31A Smith, 741 ft. (X-nicols, 50X) Sample exhibits the abrupt termination of carbonate cement along crossbed face (face is vertical in photomicrograph). (Scale=0.1 mm.)

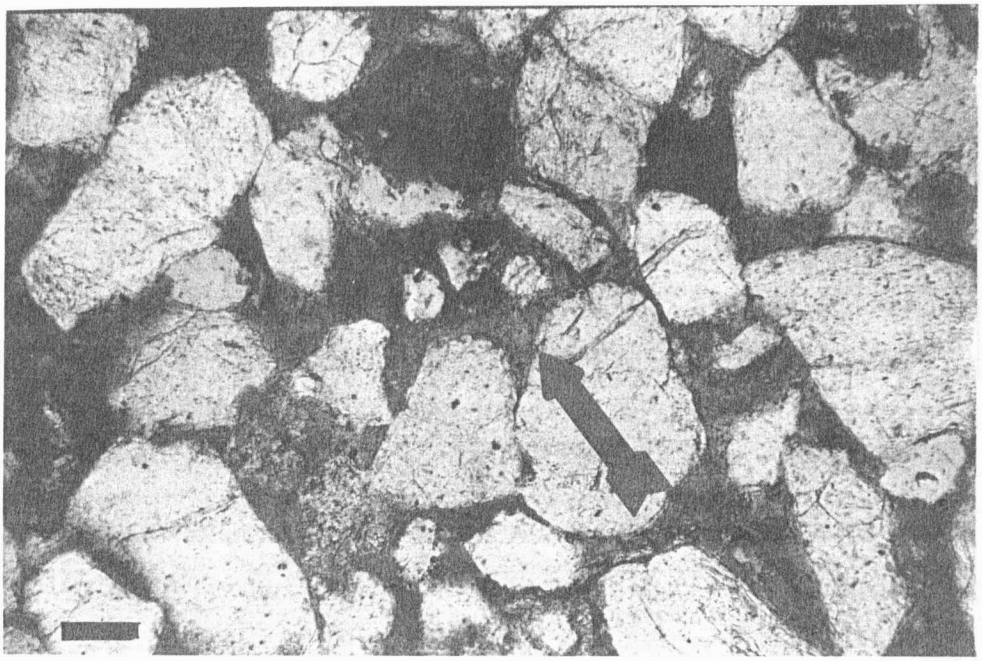

Figure 72. Colt 13AO Johnson, 737 ft. (Pl-light, 100X) Sample shows abundant, thick authigenic chlorite cement (arrow). Development of authigenic clay predates quartz overgrowth. (Scale=0.1 mm.)

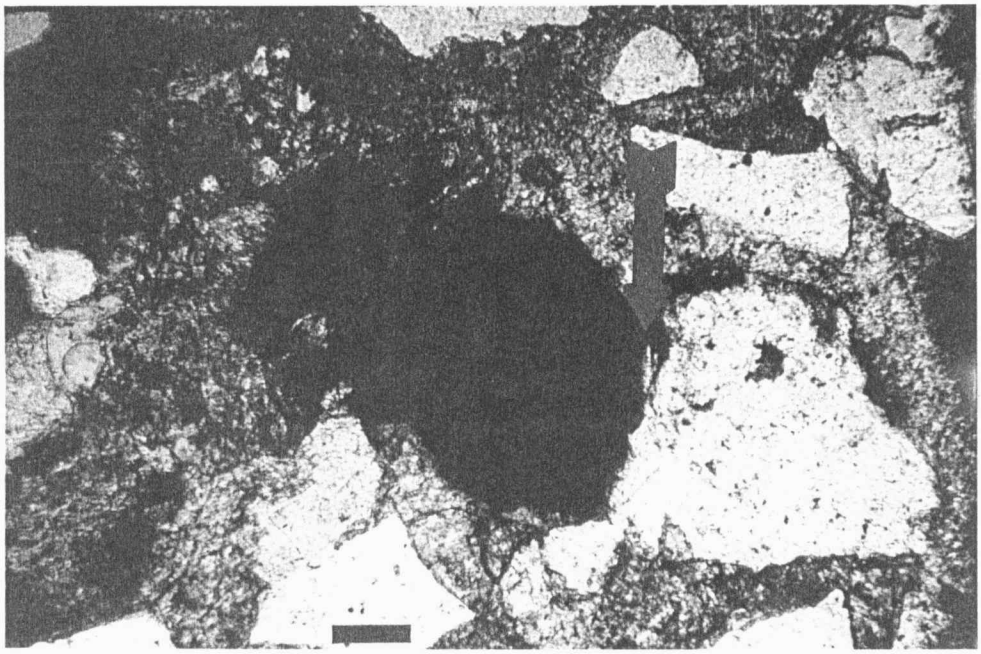

Figure 73. Colt 28A Smith, 762 (Pl-light, 100X) Quartz grains adjacent to carbonate dissolution pores do not exhibit silica overgrowth (arrow). It is inferred from this observation that carbonate dissolution post-dates quartz overgrowth. (Scale=0.1 mm.)

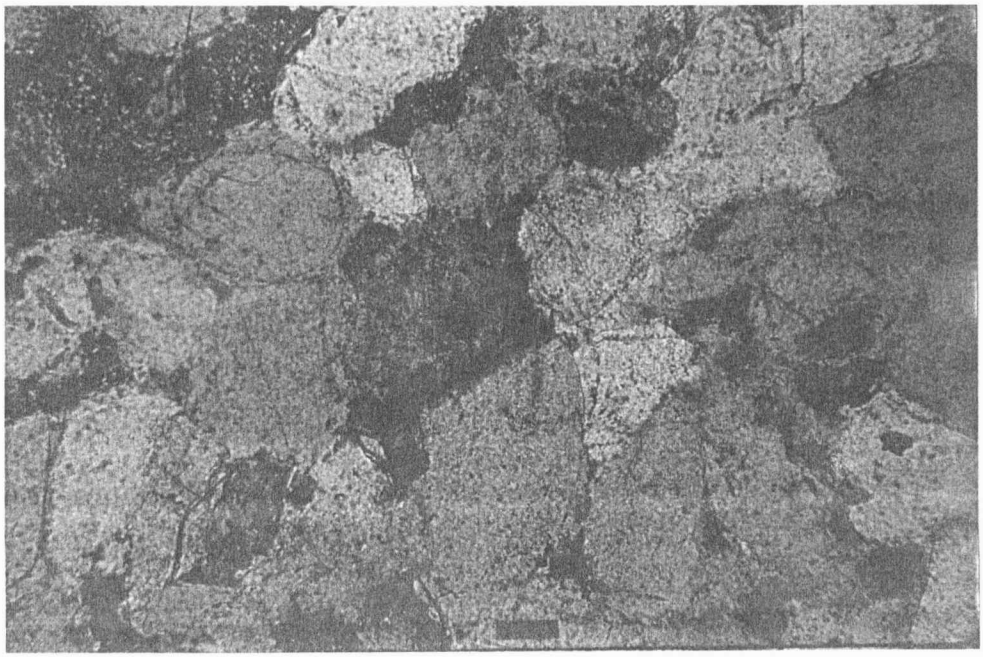

Figure 74. Colt 5A Johnson, 728ft. (Pl-light, 75X) Sample shows abundant silica overgrowths that greatly reduce the porosity. (Scale=0.1 mm.)

siderite cement is easily recognized because it takes place along cleavage faces (Fig. 76). Extensive dissolution commonly results in large vuggy porosity with the siderite exhibiting a serrated or "cox-comb" appearance (Figs. 77 and 78). Dissolution of siderite was also inferred from the presence of quartz grains that showed serrated edges that are adjacent to pores. These quartz grains were probably etched by carbonate that subsequently dissolved.

Precipitation of Ca-Mg-Fe carbonate followed the dissolution of siderite and the development of quartz overgrowths. Numerous examples of Ca-Mg-Fe carbonate filling siderite dissolution pores were noted (Figs. 79 and 33). Most Ca-Mg-Fe carbonate was in optical continuity with the older siderite. Ca-Mg-Fe carbonate was observed replacing various grain types, such as quartz, feldspar and rock fragments (Figs. 80 and 81). The mineral does not exhibit any evidence of partial dissolution, such as cox-comb crystal fringes. Ca-Mg-Fe carbonate definitely followed the precipitation of silica as evidenced by the well developed quartz overgrowths contiguous with carbonate (Fig. 82).

Widespread feldspar dissolution was the next stage of diagenesis. Many examples of partially dissolved feldspars were observed throughout the Upper Bluejacket Sandstone (Figs. 39 and 83). Dissolution greatly

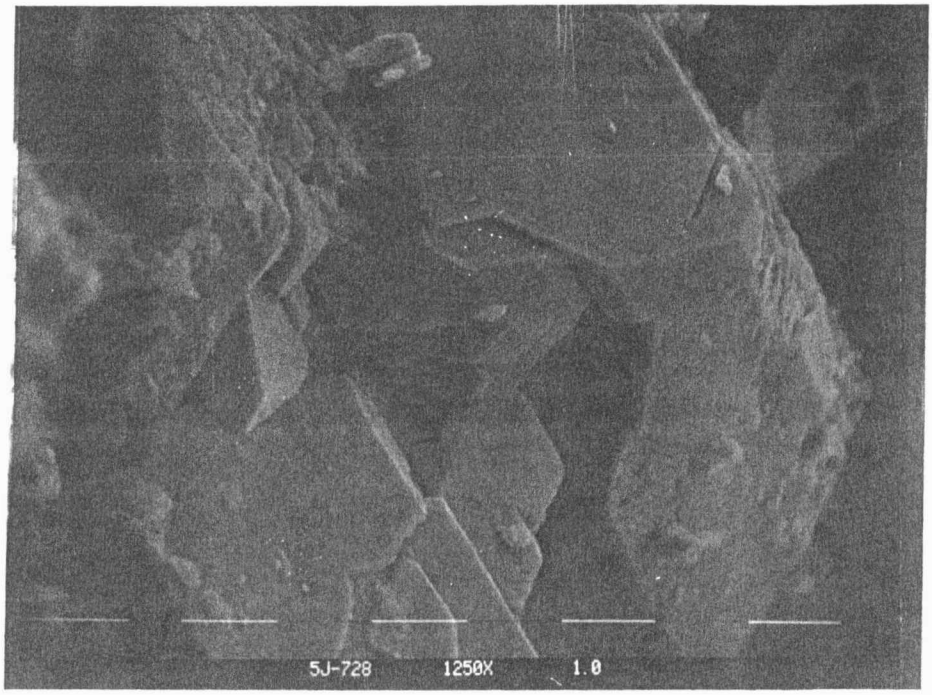

Figure 75. Colt 5A Johnson, 728 ft. (1250X) S.E.M. photomicrograph of euhedral silica overgrowths from same sample as Figure 74. (Scale divisions=0.01 mm.)

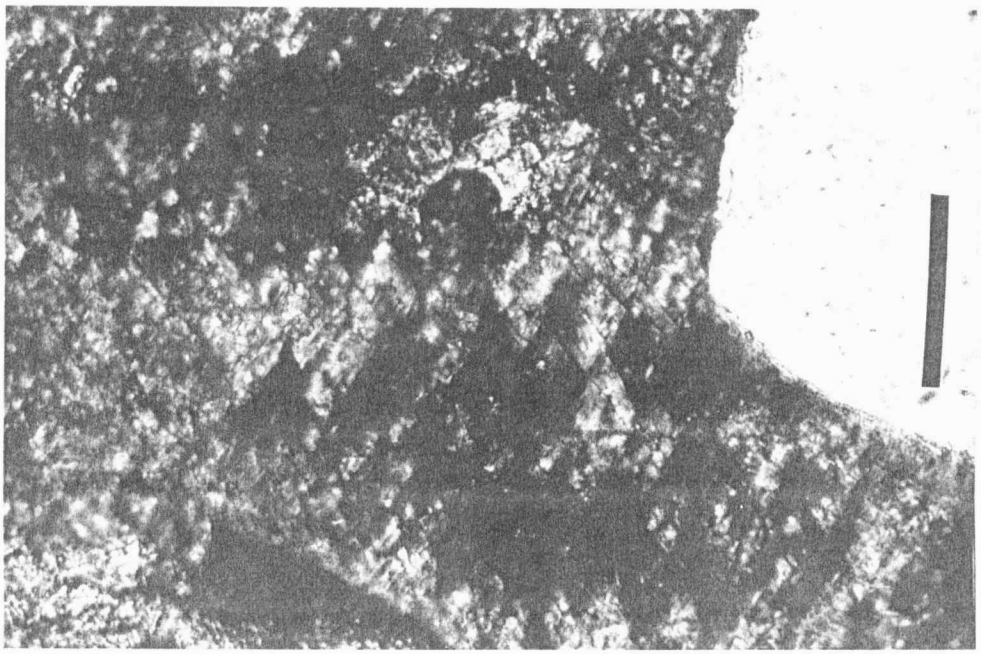

Figure 76. Colt 5A Harvey, 767 ft. (Pl-light, 250X) Partial dissolution of siderite along cleavage faces. Note blue epoxy in dissolution pores. (Scale=0.1 mm.)

Figure 77. Colt 28A Smith, 752 ft. (Pl-light, 100X) "Cox-comb" structures in siderite (arrow) are indicative of partial dissolution (also see Figure 46). (Scale=0.1 mm.)

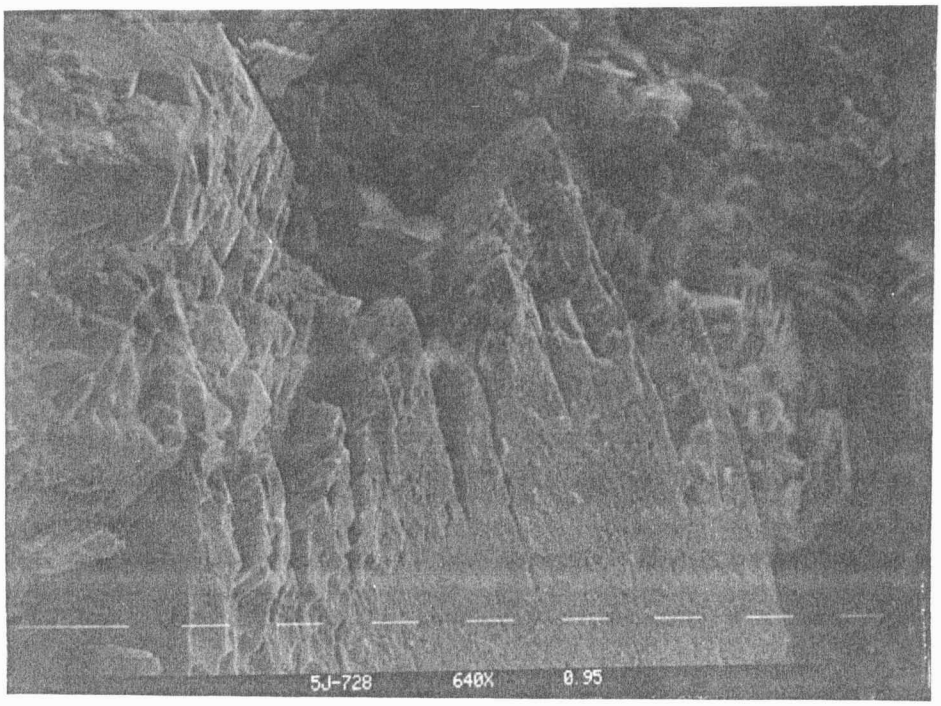

Figure 78. Colt 5A Johnson, 728 ft. (640X) Sample shows carbonate cement that is partially dissolved forming "cox-comb" structure. (Scale divisions=0.01 mm.)

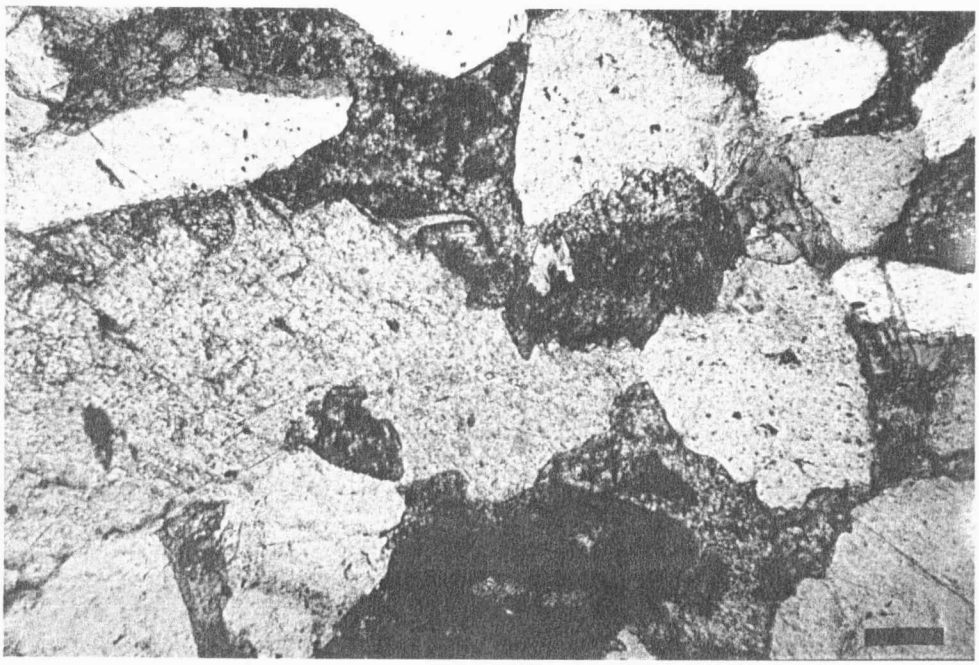

Figure 79. Colt 28A Smith, 759.5 (Pl-light, 100X) Example of Ca-Mg-Fe carbonate (limpid cement; Q) filling siderite (turbid cement; S) dissolution pore. (Scale=0.1 mm.)

contributed to the porosity of the reservoir sandstones. Large isolated vugs are common in samples that contained early poikilotopic siderite cement (Figs. 84 and 85). These large voids are interpreted to have formed from feldspar dissolution. Considering the size of the pores relative to the grain-size, it is unlikely that the pores are the result of only carbonate dissolution. The size of the pores indicates that a framework grain probably existed within it prior to dissolution. This belief is supported by remnants of dissolved feldspars encountered in some oversized pores (Fig. 86).

Partial dissolution of argillaceous rock fragments was noted in several of the samples. Dissolution of these grains did not appreciably add to the porosity of the sandstones. These partially dissolved shale clasts commonly show high residual oil saturations and thick authigenic clay coats (Fig. 87). Woody (1983) observed dissolution of sedimentary rock fragments elsewhere in the Cherokee Basin.

The final stage of diagenesis in the KB Field reservoir was the precipitation of kaolinite filling pores and replacing feldspar. It is believed that kaolinite followed feldspar dissolution, but this relationship is not entirely clear. Kaolinite commonly fills large, oversized pores that once contained

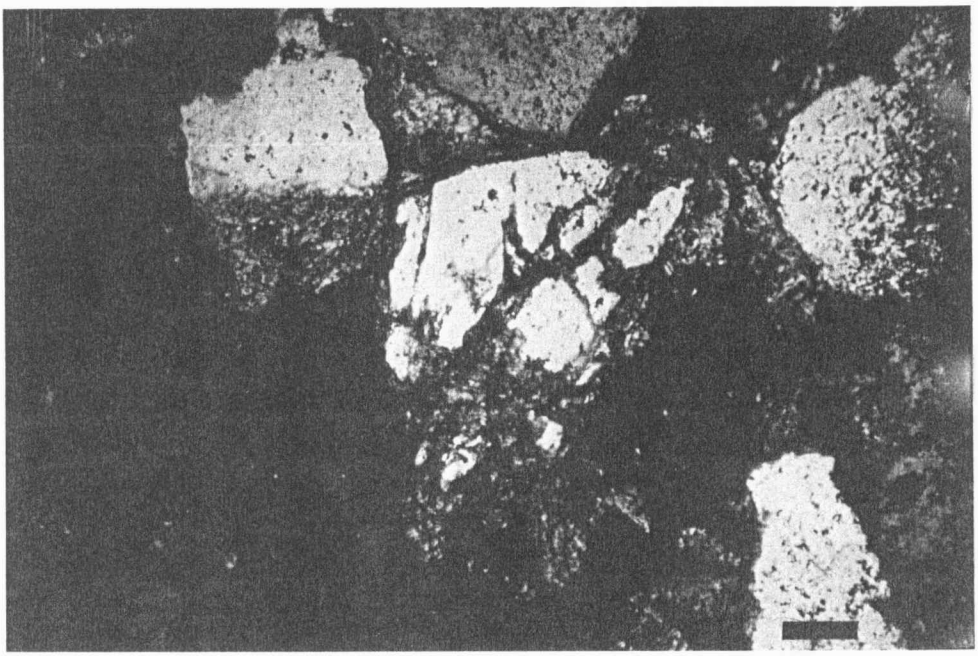

Figure 80. Colt 28A Smith, 762 ft. (X-nicols, 100X) Photomicrograph exhibits Ca-Mg-Fe carbonate cement replacing quartz framework grain. (Scale=0.1 mm.)

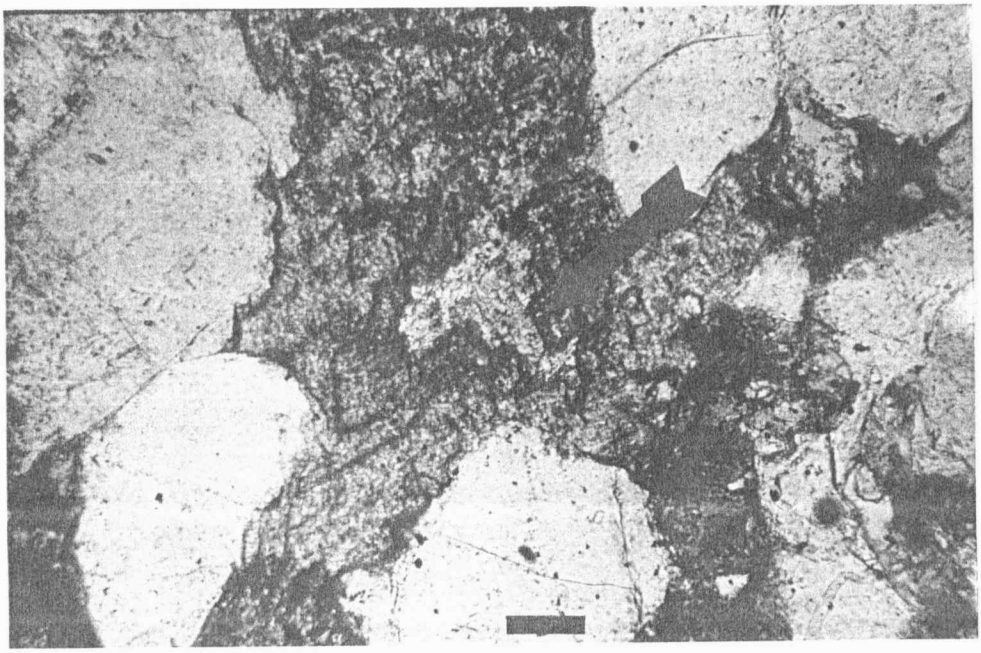

Figure 81. Colt 28A Smith, 752 ft. (Pl-light, 100X) Sample shows Ca-Mg-Fe carbonate partially replacing feldspar (arrow). Scale=0.1 mm.)

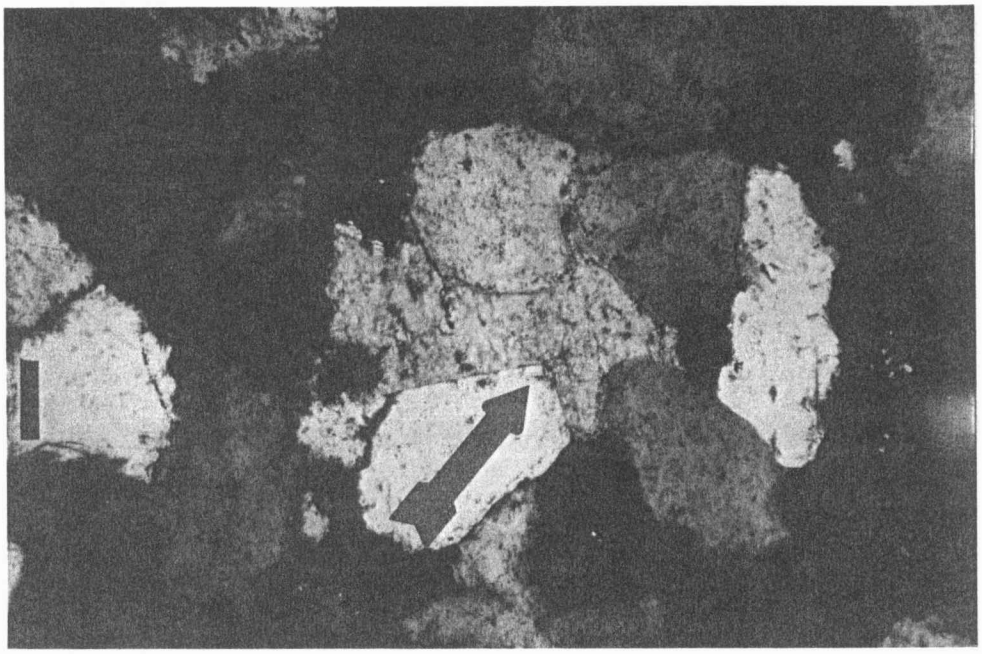

Figure 82. Colt 28A Smith, 759.5 ft. (X-nicols, 100X) Sample demonstrates that precipitation of Ca-Mg-Fe carbonate post-dates the development of silica overgrowths. Note euhedral overgrowth in contact with carbonate (arrow). (Scale=0.1 mm.)

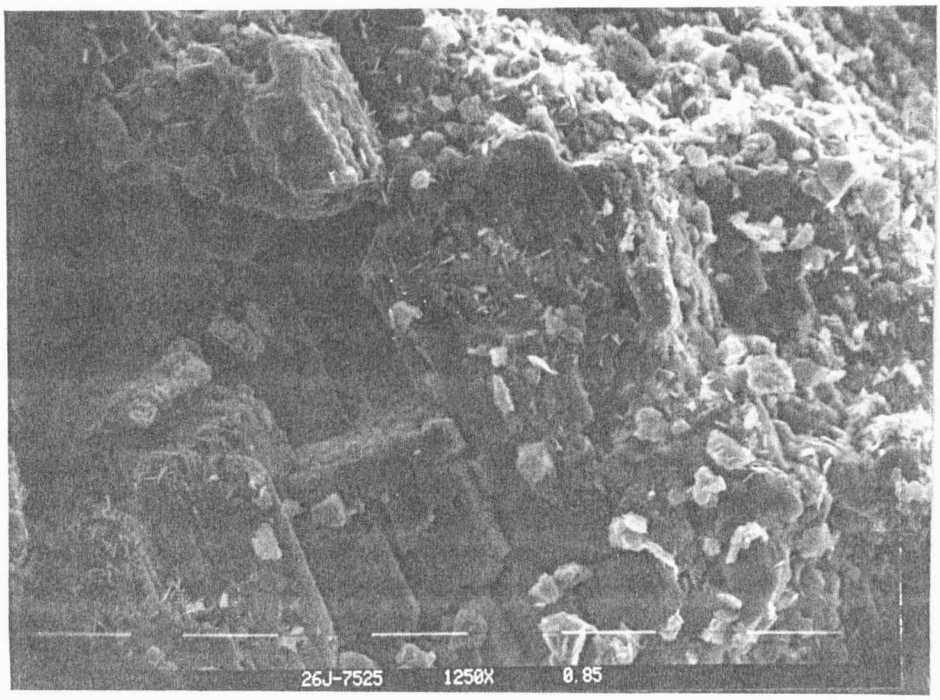

Figure 83. Colt 26AO Johnson, 752.5 ft. (1250X) S.E.M. photomicrograph of partially dissolved feldspar. Note dissolution occurs along cleavage faces. (Scale divisions=0.01 mm.)

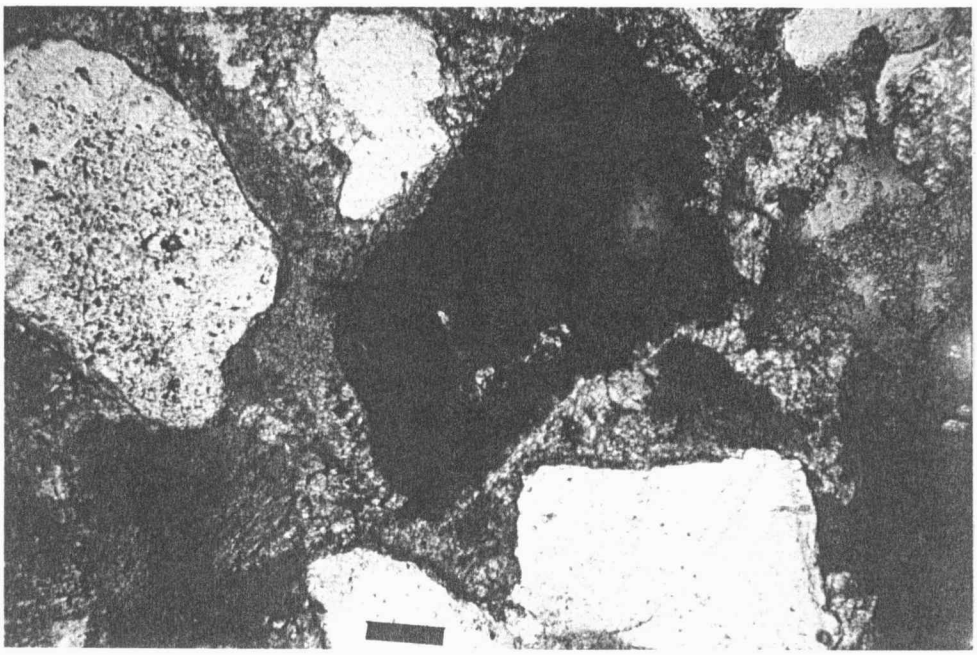

Figure 84. Colt 5A Harvey, 769.5 ft. (Pl-light, 100X) Large dissolution vug in sample cemented with poikilotopic siderite. (Scale=0.1 mm.)

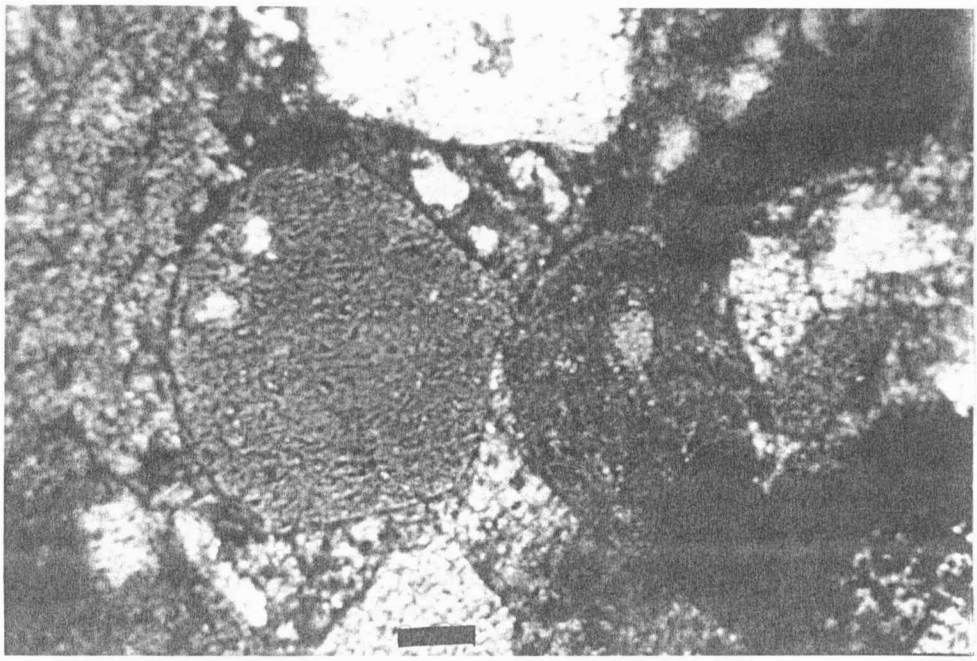

Figure 85. Colt 13AO Johnson, 742 ft. (Pl-light, 100X) Two large dissolution vugs resulting from the likely dissolution of feldspar or sedimentary rock fragments. (Scale=0.1 mm)

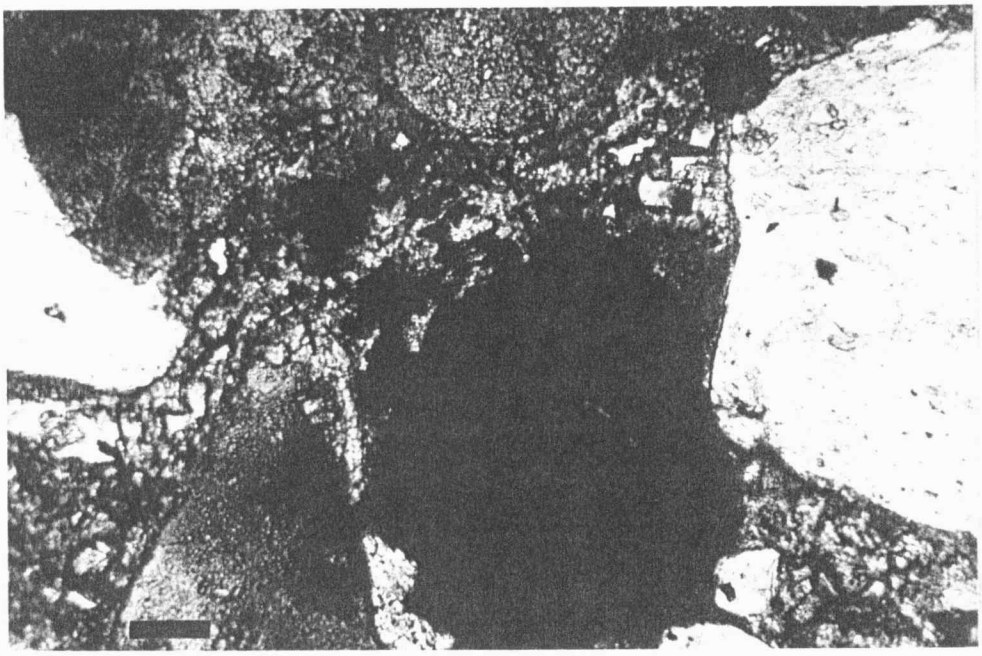

Figure 86. Colt 5A Harvey, 769.5 ft. (Pl-light, 100X) Remnants of partially dissolved feldspar observed in large dissolution vug (arrow). Note partial dissolution of siderite cement (S) in center of photo. (Scale=0.1 mm.)

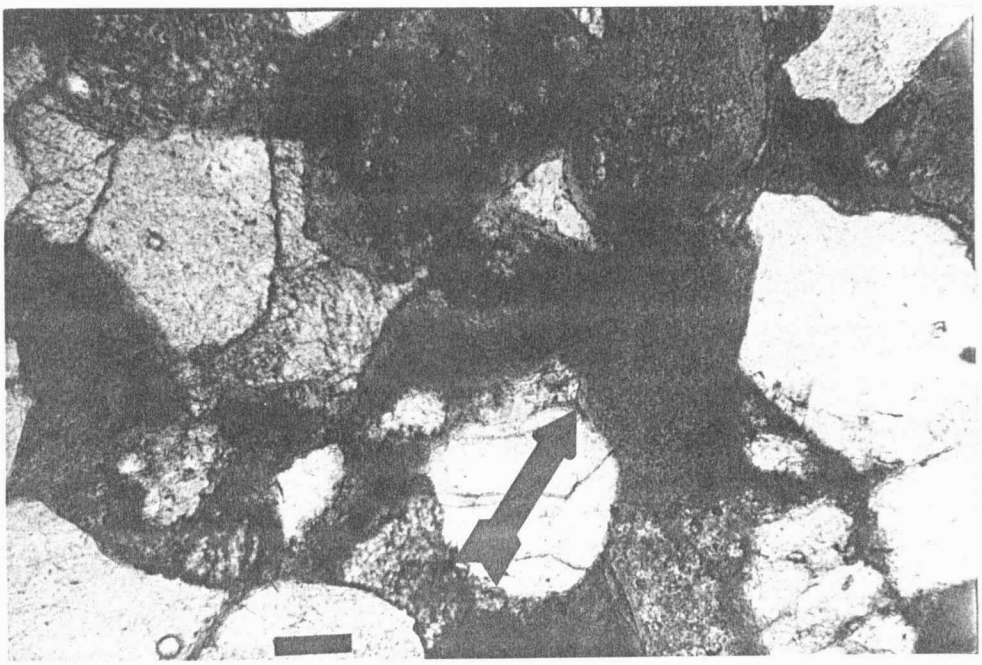

Figure 87. Colt 5A Harvey, 749.5 (Pl-light, 100X) Sample exhibits partially dissolved shale clasts with thick, isopachous clay cement (arrow). (Scale=0.1 mm)

feldspars (Fig. 65). It is unknown whether kaolinite filled an empty dissolution pore or completely replaced the feldspar.

PETROPHYSICAL PROPERTIES

INTRODUCTION

Two petrophysical properties, effective liquid porosity and liquid permeability, were measured in the laboratory on 44 samples from the KB Field (Table 1a-1h). The samples were distributed throughout the reservoir to measure the porosity and permeability from not only different lithofacies and grain-sizes, but each of the four sand bodies as well. The salinity of the brine used in both the porosity and permeability measurements was 45 grams/litre (parts/1000) sodium chloride. This salinity is similar to the concentrations measured from brine samples extracted from the KB Field (Data provided by the K.G.S.).

The measurements were conducted on cylindrical plugs that were cut parallel to bedding and oriented at right angles to the strike of the crossbed faces. The plugs were 1.85 cm (0.75 in.) in diameter and 2.5 cm (1 in.) in length. A detailed explanation of the procedures and calculations used to determine petrophysical properties is given by Woody (1983).

All porosity and permeability measurements were conducted prior to thin-section examination. This was done in an attempt to correlate the pore characteristics observed in thin-section with the

measured laboratory results. The pore characteristics that affected porosity and permeability were the amount and type of cement, the size and degree of occlusion of the pore throats, the degree of dissolution of cement and grains, and the pore lining mineralogy. Subsequent to the comparison of the thin-sections and the laboratory results, the remaining 78 thin-sections were studied. It was felt that an accurate estimate of the porosity and permeability could be made based on petrographic evidence. The thin sections for which the properties were estimated were directly compared to thin-sections from laboratory measured samples. Only thin-sections that showed similar sample characteristics, such as cement type and grain size, were compared. The results of these estimates are shown in Table 2a through 2h (pages 130 through 137).

POROSITY

Porosity is the proportion of total void space to the bulk volume of a sample. The effective porosity is the portion of the total void space that is interconnected and accessible through normal porosity measurement techniques. For example, large, apparently isolated dissolution pores in samples exhibiting poikilotopic carbonate cement are not likely to be included in the effective porosity (e.g. Fig. 42)

because they are not in communication with the rest of the sample.

Measured effective porosity from the Upper Bluejacket Sandstone ranged from 7 to 29 percent (Tables Xa-Xh and 2a-2h). The average porosity for the 44 samples was 21 percent (Table 2h).

PERMEABILITY

Permeability is a measure of the capacity of a porous medium to transmit fluids. The permeability of the samples from the KB Field were measured using a Ruska liquid permeameter (see Woody, 1983).

The permeability of the samples from the Upper Bluejacket Sandstone ranged from less than 1 millidarcy to 260 millidarcies (Tables 1a-1h and 2a-2h). The average permeability for all of the samples measured was 72 millidarcies (Table 2h). Some samples could not be measured because the maximum plug diameter was less than that required for the permeameter (ie. Colt 13AO Johnson, 734.5 ft.). Samples that could not be tested contained abundant authigenic clay coatings and were poorly indurated. These samples were partially damaged during the boring of the petrophysical plugs.

As previously mentioned, the permeability of the samples for which laboratory measurements were not conducted were estimated based on petrographic evidence

(Table 2a-2h). The permeability was estimated in 25 millidarcy increments ranging from 0 to 150 md. Permeabilities that were interpreted to be less than 25 md. were estimated in 5 md. increments. The estimation of permeability based solely on thin-section is difficult and these figures should not be regarded as absolute. It is believed that the estimates of permeability are accurate to within $\pm$ 25 millidarcies. This belief is based on the strong correlation between pore type and permeability presented in the next section. The estimated permeabilities will be useful in understanding the fluid migration patterns in the KB Field.

WELL NAME	M.C. COLT 28A SMITH							
	PORE TYPE (%)				GRAIN SIZE	ESTIMATED POROS/PERM		SUBFACIES # AND
DEPTH	I	K	M	D	(mm)	(%)	(md)	DESCRIPTION
752	30	9	4	57	.20	20	100	4 low_ tabular
754.5	25	22	4	49	.26	22	162	3 mod_ tabular
757	14	11	3	72	.21	21	100	4 low_ tabular
759.5	16	22	5	57	.21	22	125	3 mod_ tabular
762	20	32	1	47	.24	22	150	2 hi_ tabular
764.5	37	18	6	39	.24	22	145	2 hi_ tabular
765.5	44	16	37	3	.28	21	50	1 basal sand
AVG.	27	19	8	46	.23	21	97	AVG. SAND D
					CONTACT SAND D(^) AND SAND C			
767	72	14	4	10	.18	22	138	5 horizontal
770	50	11	17	22	.13	21	75	4 low_ tabular
772.5	74	15	3	8	.18	23	261	3 mod_ tabular
775.5	22	29	38	11	.19	18	13	1 basal sand
AVG.	54	17	16	13	.17	21	122	AVG. SAND C
					CONTACT SAND C(^) AND SAND B			
777.5	46	4	40	10	.11	10	10	6 ripples
780	65	15	4	16	.22	20	180	2 hi_ tabular
782.5	53	24	14	9	.27	10	0	1 basal sand
AVG.	55	14	19	12	.20	13	63	AVG. SAND B
					BASE SAND B			
AVG.	41	17	13	29	.21	20	97	AVG. FOR CORE

TABLE 2a. LIST OF PORE TYPES, AVERAGE GRAIN-SIZES, MEASURED OR ESTIMATED POROSITY AND PERMEABILITY, AND SUBFACIES FOR COLT 28A SMITH (I=intergranular, K=kaolinite {intercrystalline}, M=microporosity, D=dissolution; low_=low angle. Underlined porosities and permeabilities were measured in the lab).

WELL NAME			M.C. COLT 31A SMITH					
	PORE TYPE (%)				GRAIN SIZE	ESTIMATED POROS/PERM		SUBFACIES # AND
DEPTH	I	K	M	D	(mm)	(%)	(md)	DESCRIPTION
731.5	53	8	10	29	.15	20	100	5 horizontal
733.5	68	8	4	20	.16	21	158	5 horizontal
736	47	11	7	35	.16	20	150	4 low_ tabular
738.5	49	7	5	39	.17	23	151	5 horizontal
741	-	-	-	-	.18	20	150	5 horizontal
743.8	58	14	8	20	.18	20	159	5 horizontal
745.5	56	11	3	30	.20	20	100	3 mod_ tabular
AVG.	55	10	6	29	.17	21	138	AVG. SAND B
CONTACT SAND B(^) AND SAND A								
747.5	49	24	2	25	.20	18	75	3 mod_ tabular
751	56	22	7	15	.25	19	62	3 mod_ tabular
753.5	68	6	10	16	.16	18	170	3 mod_ tabular
AVG.	58	17	6	19	.20	18	102	AVG. SAND A
BASE SAND A								
AVG.	56	12	6	26	.18	20	128	AVG. FOR CORE

TABLE 2b. LIST OF PORE TYPES, AVERAGE GRAIN-SIZES, MEASURED OR ESTIMATED POROSITY AND PERMEABILITY, AND SUBFACIES FOR COLT 31A SMITH

(I=intergranular, K=kaolinite (intercrystalline), M=microporosity, D=dissolution; low_=low angle. Underlined porosities and permeabilities were measured in the lab).

WELL NAME	M.C. COLT 5A HARVEY							
	PORE TYPE (%)				GRAIN SIZE	ESTIMATED POROS/PERM		SUBFACIES # AND
DEPTH	I	K	M	D	(mm)	(%)	(md)	DESCRIPTION
740.5	-	-	-	-	-	0	0	7 linsen-beds
742	16	0	53	31	.14	7	<1	6 ripples
744.5	30	0	42	28	.21	25	0	2 hi_ tabular
747	44	0	44	12	.19	25	0	2 hi_ tabular
749.5	7	0	68	25	.24	26	3	2 hi_ tabular
752	14	0	56	30	.29	26	<1	2 hi_ tabular
AVG.	22	0	53	25	.21	18	<1	AVG. SAND D
CONTACT SAND D(^) AND SAND C								
754.5	32	0	36	32	.20	25	0	5 horizontal
757	-	-	-	-	.20	25	0	5 horizontal
759.5	25	1	64	10	.22	28	<1	2 hi_ tabular
762	28	0	62	10	.19	25	0	3 mod_ tabular
764.5	34	0	54	12	.19	25	0	3 mod_ tabular
767	11	0	53	36	.26	25	5	3 mod_ tabular
769.5	0	0	39	61	.29	25	50	3 mod_ tabular
AVG.	22	0	51	27	.22	25	8	AVG. SAND C
CONTACT SAND C(^) AND SAND B								
772	-	-	-	-	.14	0	0	3 mod_ tabular
774.5	-	-	-	-	.09	10	10	5 horizontal
775.5	10	8	58	24	.27	26	161	3 mod_ tabular
777.5	-	-	-	-	.11	10	10	6 ripples
779.5	52	16	16	16	.27	20	50	1 basal sand
AVG.	31	12	37	20	.18	13	46	AVG.SAND B
BASE SAND B								
AVG.	23	2	50	25	.21	20	16	AVG. FOR CORE

TABLE 2c. LIST OF PORE TYPES, AVERAGE GRAIN-SIZES, MEASURED OR ESTIMATED POROSITY AND PERMEABILITY, AND SUBFACIES FOR COLT 5A HARVEY (I=intergranular, K=kaolinite (intercrystalline), M=microporosity, D=dissolution; low_=low angle. Underlined porosities and permeabilities were measured in the lab).

WELL NAME	M.C. COLT 5A JOHNSON							
	PORE TYPE (%)				GRAIN SIZE	ESTIMATED POROS/PERM		SUBFACIES # AND
DEPTH	I	K	M	D	(mm)	(%)	(md)	DESCRIPTION
710.5	48	7	33	12	.05	14	8	6 ripples
713	22	38	10	30	.21	25	131	2 hi_ tabular
715.5	33	34	3	30	.19	24	125	2 hi_ tabular
718	35	33	12	20	.26	24	125	2 hi_ tabular
720.5	43	21	6	30	.24	24	125	2 hi_ tabular
721.5	38	31	7	24	.20	23	126	2 hi_ tabular
723	38	12	8	42	.20	22	125	2 hi_ tabular
725.5	43	20	10	27	.22	22	125	2 hi_ tabular
728	8	13	4	75	.22	22	131	2 hi_ tabular
AVG.	34	23	10	33	.20	22	115	AVG. SAND D
CONTACT SAND D(^) AND SAND C								
730.5	21	33	41	5	.19	21	52	2 hi_ tabular
733	26	20	7	47	.24	21	125	4 low_ tabular
735.5	46	12	8	34	.27	20	125	3 mod_ tabular
738	37	36	4	23	.20	19	114	4 low_ tabular
740.5	21	14	2	63	.16	24	116	4 low_ tabular
743	42	22	16	20	.20	20	75	2 hi_ tabular
745.9	38	19	32	11	.23	10	10	1 basal sand
AVG.	33	22	16	29	.21	19	88	AVG. SAND C
BASE SAND C								
AVG.	34	23	13	30	.21	21	103	AVG. FOR CORE

TABLE 2d. LIST OF PORE TYPES, AVERAGE GRAIN-SIZES, MEASURED OR ESTIMATED POROSITY AND PERMEABILITY, AND SUBFACIES FOR COLT 5A JOHNSON (I=intergranular, K=kaolinite (intercrystalline), M=microporosity, D=dissolution; low_=low angle. Underlined porosities and permeabilities were measured in the lab).

WELL NAME	M.C. COLT 13AO JOHNSON							
	PORE TYPE (%)				GRAIN SIZE	ESTIMATED POROS/PERM		SUBFACIES # AND
DEPTH	I	K	M	D	(mm)	(%)	(md)	DESCRIPTION
714.5	30	8	33	29	.26	24	32	5 horizontal
717	74	8	10	8	.21	10	10	5 horizontal
AVG.	52	8	21	19	.24	17	21	AVG. SAND D
					CONTACT SAND D(^) AND SAND C			
719.5	70	8	12	10	.17	10	25	4 low_ tabular
722	40	3	42	15	.21	25	10	5 horizontal
724.5	13	2	46	39	.22	24	<1	3 mod_ tabular
727	29	1	24	46	.25	28	153	3 mod_ tabular
729.5	39	0	34	27	.27	26	150	2 hi_ tabular
732	57	4	31	8	.21	24	50	2 hi_ tabular
734.5	15	0	40	45	.21	26	N/A	5 horizontal
737	54	4	34	8	.17	24	25	5 horizontal
739.5	52	7	33	8	.20	22	25	4 low_ tabular
742	8	0	5	87	.27	25	10	3 mod_ tabular
744.5	20	0	57	23	.17	29	60	4 low_ tabular
747	59	13	15	13	.22	24	125	2 hi_ tabular
749.5	12	2	8	78	.25	17	<1	2 hi_ tabular
752	64	11	11	14	.27	22	125	2 hi_ tabular
754.5	54	12	28	6	.27	20	100	2 hi_ tabular
757	-	-	-	-	.21	10	20	5 horizontal
759.5	68	6	16	10	.15	5	0	5 horizontal
AVG.	43	5	26	26	.22	21	55	AVG. SAND C
					BASE SAND C			
AVG.	42	5	27	26	.22	21	51	AVG. FOR CORE

TABLE 2e. LIST OF PORE TYPES, AVERAGE GRAIN-SIZES, MEASURED OR ESTIMATED POROSITY AND PERMEABILITY, AND SUBFACIES FOR COLT 13AO JOHNSON (I=intergranular, K=kaolinite (intercrystalline), M=microporosity, D=dissolution; low_=low angle. Underlined porosities and permeabilities were measured in the lab).

WELL NAME	M.C. COLT 14AO JOHNSON							
	PORE TYPE (%)				GRAIN SIZE	ESTIMATED POROS/PERM		SUBFACIES # AND
DEPTH	I	K	M	D	(mm)	(%)	(md)	DESCRIPTION
711.5	45	5	42	8	.16	23	100	2 hi_ tabular
714	56	2	34	8	.18	24	116	4 low_ tabular
716.5	66	6	18	10	.19	23	150	5 horizontal
717.5	68	0	30	2	.31	25	125	3 mod_ tabular
AVG.	59	3	31	7	.21	24	123	AVG. SAND D
					CONTACT SAND D(^) AND SAND C			
721	32	8	60	0	.21	24	50	4 low_ tabular
724	26	2	54	18	.24	26	<1	4 low_ tabular
726.5	50	0	39	11	.17	24	50	3 mod_ tabular
729	20	0	25	55	.27	25	10	2 hi_ tabular
731.5	17	2	27	54	.25	25	25	2 hi_ tabular
734	28	1	38	33	.25	24	25	2 hi_ tabular
736.5	38	12	24	26	.21	18	10	4 low_ tabular
739	48	6	42	4	.16	19	0	3 mod_ tabular
741.5	70	7	19	4	.22	25	125	5 horizontal
744	65	3	25	7	.23	26	140	4 low_ tabular
746.5	-	-	-	-	.18	24	100	2 hi_ tabular
749	68	5	22	5	.25	24	100	2 hi_ tabular
751.5	-	-	-	-	.05	23	N/A	4 low_ tabular
754	62	14	8	16	.14	10	0	1 basal sand
AVG.	44	5	32	19	.20	23	49	AVG. SAND C
					BASE SAND C			
AVG.	47	5	32	16	.20	23	66	AVG. FOR CORE

TABLE 2f. LIST OF PORE TYPES, AVERAGE GRAIN-SIZES, MEASURED OR ESTIMATED POROSITY AND PERMEABILITY, AND SUBFACIES FOR COLT 14AO JOHNSON

(I=intergranular, K=kaolinite (intercrystalline), M=microporosity, D=dissolution; low_=low angle. Underlined porosities and permeabilities were measured in the lab).

WELL NAME			M.C. COLT 26AO JOHNSON					
	PORE TYPE (%)				GRAIN SIZE	ESTIMATED POROS/PERM		SUBFACIES # AND
DEPTH	I	K	M	D	(mm)	(%)	(md)	DESCRIPTION
725	18	22	49	11	.18	24	10	3 mod_ tabular
727.5	52	8	40	0	.21	22	10	4 low_ tabular
730	-	-	-	-	.24	24	10	5 horizontal
732.5	50	8	36	6	.20	22	25	5 horizontal
735	49	7	41	3	.22	24	18	3 mod_ tabular
737.5	40	16	26	18	.26	23	50	2 hi_ tabular
AVG.	42	12	38	8	.22	23	25	AVG. SAND D
CONTACT SAND D(^) AND SAND C								
740	53	16	17	14	.23	21	50	2 hi_ tabular
742	32	15	8	45	.24	22	100	3 mod_ tabular
743	47	8	14	31	.24	22	96	5 horizontal
745	55	13	2	30	.24	24	215	2 hi_ tabular
747.5	61	13	12	14	.20	22	100	2 hi_ tabular
750	64	14	12	10	.22	22	100	2 hi_ tabular
752.5	60	13	9	18	.22	20	95	2 hi_ tabular
755	36	2	58	4	.20	22	0	2 hi_ tabular
757.5	32	4	34	30	.27	20	16	4 low_ tabular
760	45	11	27	17	.21	20	25	4 low_ tabular
AVG.	49	11	19	21	.23	22	80	AVG. SAND C
BASE SAND C								
AVG.	46	11	26	17	.22	22	59	AVG. FOR CORE

TABLE 2g. LIST OF PORE TYPES, AVERAGE GRAIN-SIZES, MEASURED OR ESTIMATED POROSITY AND PERMEABILITY, AND SUBFACIES FOR COLT 26AO JOHNSON (I=intergranular, K=kaolinite (intercrystalline), M=microporosity, D=dissolution; low_=low angle. Underlined porosities and permeabilities were measured in the lab).

WELL NAME	M.C. COLT 50AO JOHNSON							
	PORE TYPE (%)				GRAIN SIZE	ESTIMATED POROS/PERM		SUBFACIES # AND
DEPTH	I	K	M	D	(mm)	(%)	(md)	DESCRIPTION
752	46	26	8	20	.20	20	117	4 low_ tabular
754.5	33	35	4	28	.24	20	100	2 hi_ tabular
757	40	22	10	28	.24	19	44	5 horizontal
759.5	-	-	-	-	.27	24	17	4 low_ tabular
762	52	26	10	12	.18	21	150	3 mod_ tabular
764	53	9	7	31	.20	22	211	2 hi_ tabular
767	44	26	12	18	.21	21	150	2 hi_ tabular
769.5	36	25	12	27	.19	22	125	2 hi_ tabular
770	29	30	10	31	.22	20	75	2 hi_ tabular
AVG.	42	25	9	24	.22	21	108	AVG. SAND C
CONTACT SAND C(^) AND SAND B								
772	64	16	9	11	.16	20	75	5 horizontal
774.5	68	16	14	2	.11	10	10	5 horizontal
777	58	18	17	7	.22	20	75	2 hi_ tabular
780	41	9	36	14	.24	17	46	5 horizontal
AVG.	57	15	19	9	.18	17	52	AVG. SAND B
BASE OF SAND B								
AVG.	47	22	12	19	.21	20	91	AVG. FOR CORE
TOTAL AVERAGE ALL SAMPLES								
AVG.	42	12	23	23	.21	21	72	AVG. SAMPLES

TABLE 2h. LIST OF PORE TYPES, AVERAGE GRAIN-SIZES, MEASURED OR ESTIMATED POROSITY AND PERMEABILITY, AND SUBFACIES FOR COLT 50AO JOHNSON (I=intergranular, K=kaolinite {intercrystalline}, M=microporosity, D=dissolution; low_=low angle. Underlined porosities and permeabilities were measured in the lab).

RELATIONSHIP BETWEEN PORE TYPE AND PERMEABILITY IN THE UPPER BLUEJACKET SANDSTONE RESERVOIR

PORE TYPE

Four different pore types were identified in the sandstones from the KB Field: 1) intergranular pores; 2) intercrystalline kaolinite pores; 3) micropores; and 4) dissolution pores. Pore type determinations were based on 100-point counts of the pores in each thin-section. The results of the pore type point-counts are given in Table 2a-2h. The pores were recognized by the presence of blue epoxy, which was injected before thin section were cut. The pore types were identified based on the pore characteristics described by Schmidt and MacDonald (1979) and Pittman (1979).

Primary intergranular pores range from 0 to 74 percent of the pores in the samples and average 42 percent for all the samples examined. Primary pores have remained unfilled since the time of deposition. Primary porosity is gradually reduced through time by precipitation of cement, compaction of the grains and deformation of soft rock fragments. Pores between grains that were interpreted to be the result of dissolution of cement were counted as dissolution pores. This determination was based on evidence of

definite cement dissolution, such as cox-comb carbonate.

The second pore type identified and quantified was intercrystalline pores among kaolinite crystals (Fig. 65). The pore space between kaolinite crystals is, in the strictest definition, intergranular porosity. These small voids have remained as pore space between framework grains since the sands were deposited. As noted earlier, several large dissolution pores were completely filled with kaolinite. These pores were also counted as intercrystalline kaolinite pores instead of dissolution pores. Intercrystalline kaolinite pores were counted separately from intergranular and dissolution pores because of the small size of the pore throats. Reservoir fluids flow more easily through unoccluded pores than those partially or completely blocked with kaolinite. It was felt that a greater understanding of the factors controlling permeability in the reservoir could be gained through differentiating these pore types.

Intercrystalline kaolinite pores ranged from 0 to 38 percent of the pores counted in the samples. On average, intercrystalline kaolinite pores accounted for 12 percent of the porosity in the samples from the KB Field.

Micropores were the third pore type recognized (Table 2a-2h). Micropores are defined as pores with a radius less than 0.5 micrometers (Pittman, 1979). Abundant micropores occur between clay minerals in sedimentary rock fragments and authigenic clay cements. Micropores are too small to be observed with normal optical microscopy but were assumed to be associated with argillaceous material. During point-counting, all argillaceous rock fragments, syndepositional clay matrix and grain-coating authigenic clay cements were counted as micropores (Fig. 44). Several argillaceous rock fragments exhibited a faint blue tint from epoxy that was injected into the micropores (Fig. 44). Abundant micropores associated with authigenic chlorite were observed with the scanning electron microscope (Fig. 67). The amount of microporosity ranged from 1 to 68 percent of the pores counted and averaged 23 percent.

Siderite and feldspar dissolution were the two main types of dissolution pores noted (Figs. 45 and 39, Table 2a-2h). Pores adjacent to siderite cement showing cox-comb structures were interpreted to be results of dissolution. Large vugs that were the same size or larger than framework grains were also interpreted as dissolution pores. All of the samples examined showed evidence of partial dissolution. The

amount of dissolution porosity ranged from 1 to 78 percent of the pores counted. The average dissolution porosity was 23 percent.

EFFECTS OF PORE TYPE ON PERMEABILITY

The pore type of the sandstones was determined to gain an understanding of the relationship between pore characteristics and permeability. Pore character has a direct effect on the capacity of the sandstone to transmit fluids (Pittman, 1979). Permeability is a function of not only pore size, but the size of the pore throats, the pore-lining mineralogy and the degree of pore interconnectedness. The determinations of the pore type help delineate the pore characteristics that affect permeability.

The pore types were plotted on a ternary diagram to establish the relationships that govern permeability (Fig. 88; Table 3). The pole located at the apex of the triangle is intergranular and intercrystalline kaolinite pores combined. The ratio of intergranular to intercrystalline kaolinite pores is provided with the permeabilities on Table 3. These two pore types were combined because kaolinite generally completely or partially occludes the intergranular pores. These two pore types behave more similarly to each other with respect to fluid transmissibility than to other pore-types.

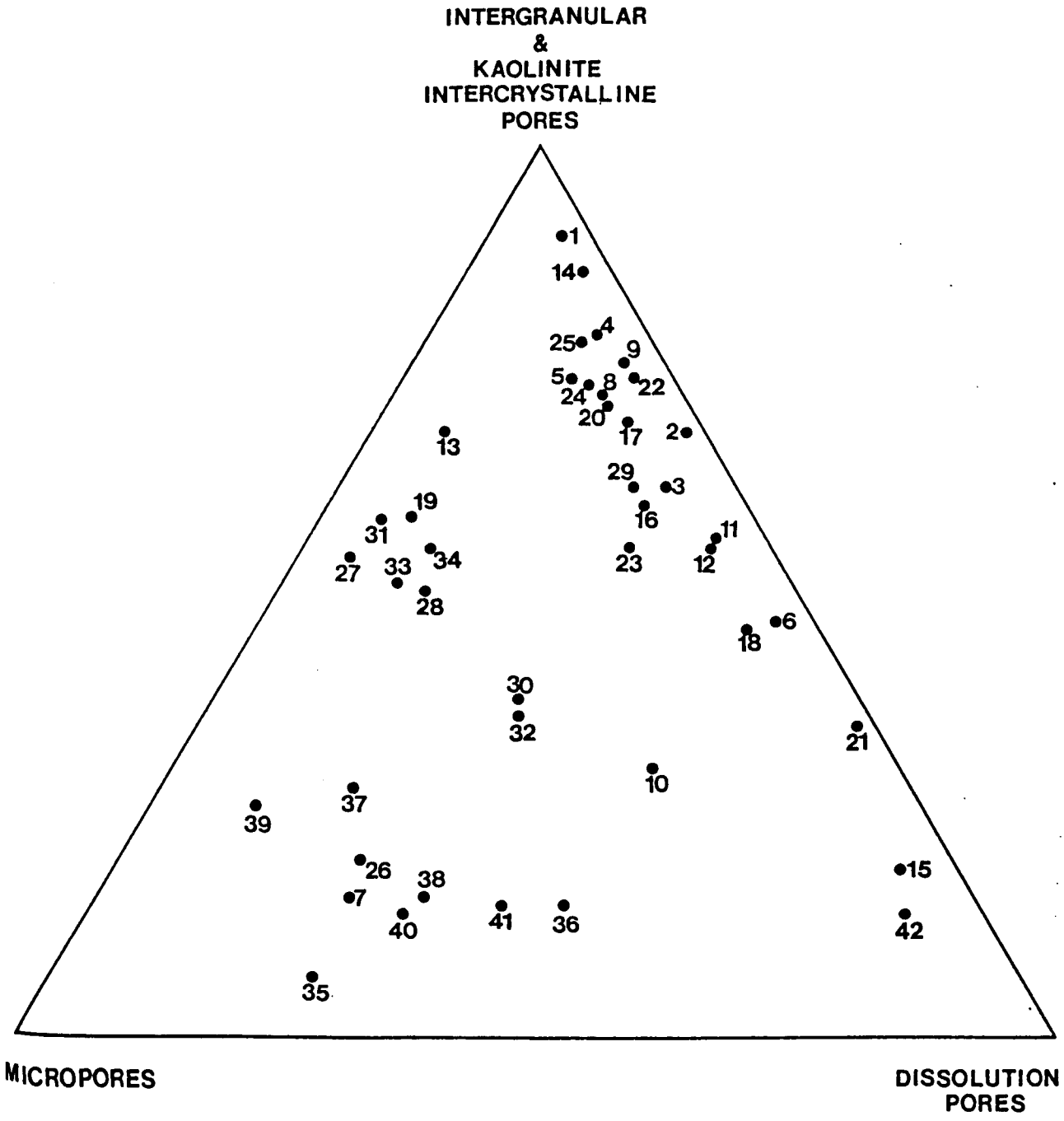

Figure 88. Ternary plot of pore types. Samples are ranked by permeability (See Table 3).

TABLE 3. PERMEABILITY, INTERGRANULAR/KAOLINITE PORE RATIO AND SAMPLES USED IN FIGURE 88 RANKED BY PERMEABILITY.

RANK	PERM(md)	INTERGRANULAR/ KAOLINITE INTERCRYSTALLINE PORE RATIO	RANK	PERM(md)	INTERGRANULAR/ KAOLINITE INTERCRYSTALLINE PORE RATIO
1	261	5:1	22	114	1:1
2	215	4:1	23	96	6:1
3	211	6:1	24	95	5:1
4	180	4:1	25	62	3:1
5	170	11:1	26	59	---
6	162	1:1	27	52	1:2
7	160	1:1	28	46	5:1
8	159	4:1	29	44	2:1
9	158	8:1	30	32	4:1
10	153	29:1	31	19	7:1
11	151	7:1	32	16	8:1
12	145	2:1	33	13	1:1
13	140	20:1	34	8	7:1
14	138	5:1	35	3	---
15	131	1:2	36	<1	---
16	131	1:2	37	<1	13:1
17	126	1:1	38	<1	16:1
18	125	---	39	<1	25:1
19	116	28:1	40	<1	---
20	116	2:1	41	<1	---
21	116	2:1	42	<1	6:1

The ternary diagram demonstrates that microporosity or an abundance of argillaceous material greatly reduces the permeability because nearly all the samples with low numbers (denoting high permeability) lie along the right side of the trianglar plot. The samples with high numbers (denoting low permeability) plot near the micropore pole. The sandstones with the highest permeabilities generally contain relatively minor amounts of microporosity. With minor exceptions, samples containing less than 25 percent microporosity showed permeabilities in excess of 95 millidarcies (See also Fig. 89). Samples that plotted along the line that joins the intergranular and dissolution poles (<10% microporosity) exhibited an average permeability of 145 millidarcies. The small-diameter pore throats and abundant surface area associated with clay-rich sediments tend to inhibit the flow of interstitial fluids.

As noted above, intergranular and intercrystalline kaolinite pores were plotted in combination on Figure 88. The ratio of intergranular to intercrystalline pores was determined to demonstrate the relative effects of these two pore types (Table 3). Samples that exhibited permeabilities in excess of 150 millidarcies usually contain greater than 50 percent intergranular and intercrystalline kaolinite pores

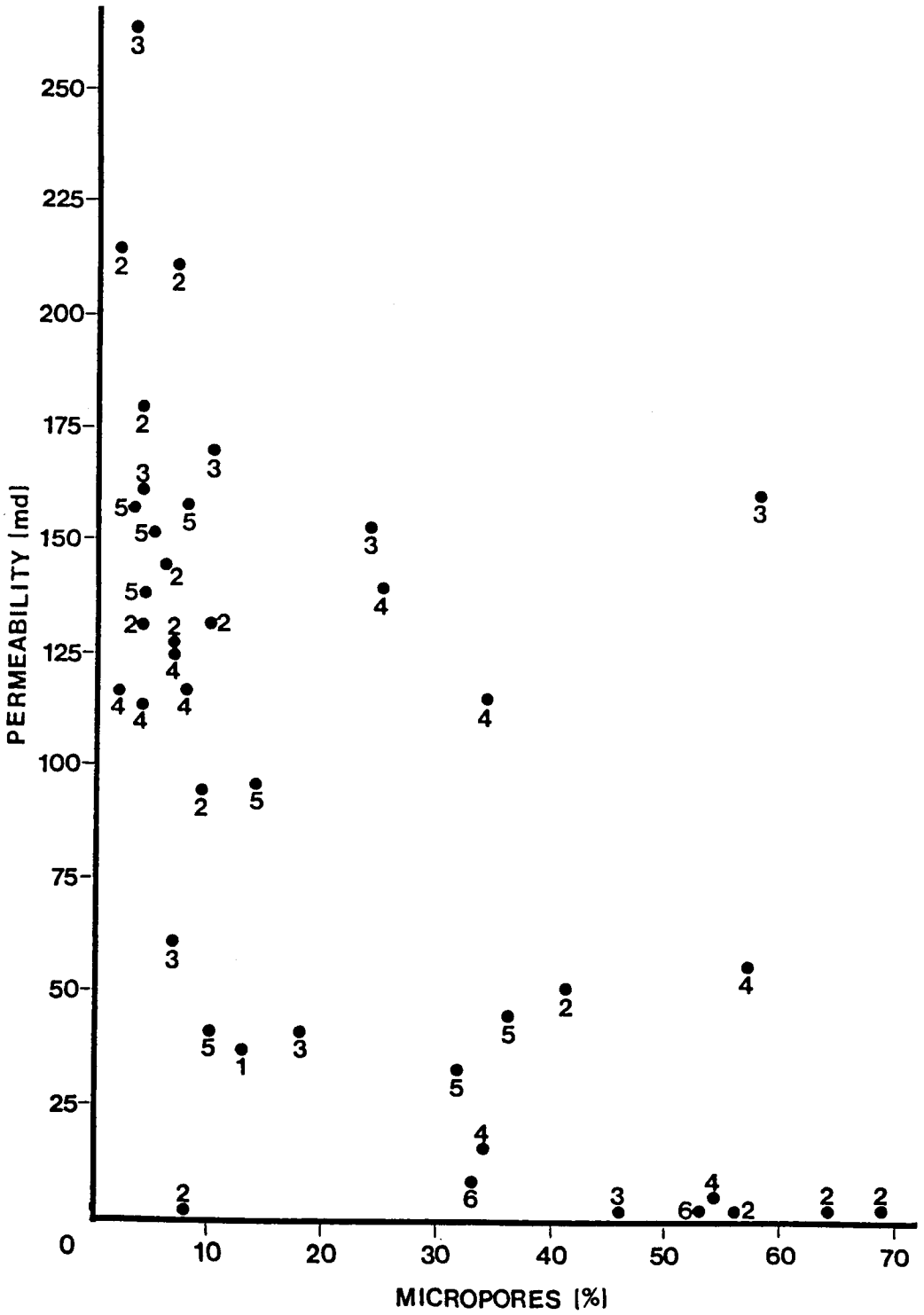

Figure 89. Plot of permeability versus micropores (%). Numbers denote subfacies type (1-Basal sand, 2-High angle crossbeds, 3-moderate angle crossbeds, 4-low angle crossbeds, 5-horizontal bedding, 6-ripple bedding, 7-linsen bedding).

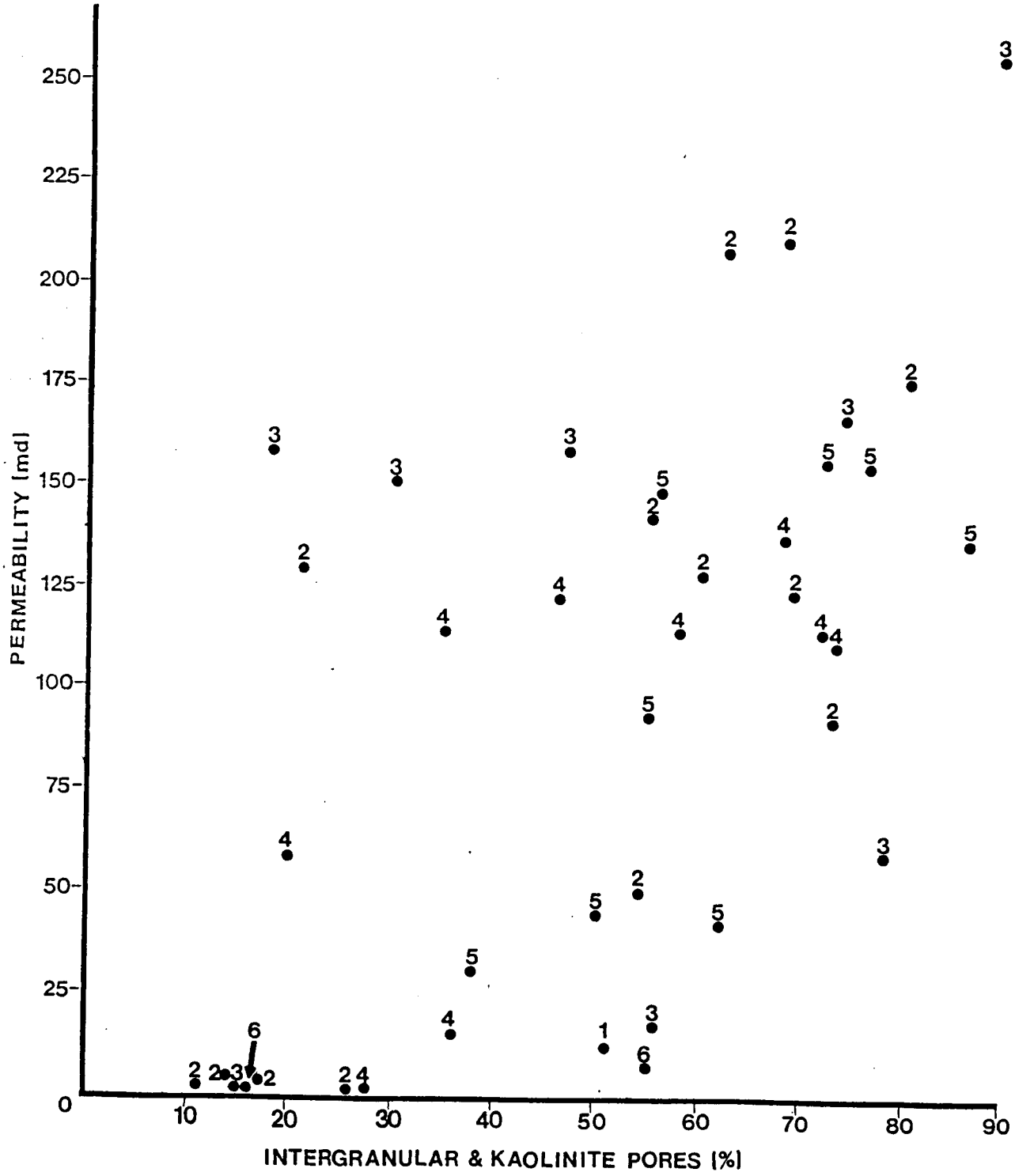

Figure 90. Plot of permeability versus intergranular and kaolinite intercrystalline pores, combined (percent). Numbers denote subfacies type (1-basal sand, 2-high angle crossbeds, 3-moderate angle crossbeds, 4-low angle crossbeds, 5-horizontal bedding, 6-ripple bedding, 7-linsen bedding).

(Fig. 90), with four or more intergranular pores for each intercrystalline kaolinite pore. Fluids flow more easily through large, unoccluded intergranular pores than the abundant small pores associated with kaolinite. It is strongly emphasized that the kaolinite pores are small relative to intergranular pores but many times larger than micropores. Abundant kaolinite tends to reduce the permeability of the sandstones, but not to the extent that authigenic and allogenic clay do.

Dissolution pores are also associated with the development of high permeability. The dissolution of feldspar grains and siderite cement tends to create numerous, unplugged pores. These large pores can greatly increase the permeability, but this depends upon the degree of interconnection. One sample (Colt 13AO Johnson, 749.5 ft.) contained 78 percent dissolution pores with less than 1 millidarcy permeability. In thin-section, this sample showed abundant siderite cement with numerous feldspar dissolution pores. The large dissolution pores are believed to be completely isolated and, therefore, the sample is nearly impermeable.

SUMMARY

From the analysis of the pore type, the factors controlling permeability can be delineated. The

highest permeability sandstones (>150 md.) in the KB Field contained minor microporosity (<10%), abundant intergranular porosity (>50%), and moderate dissolution porosity (<40%). These highly permeable sands also contain at least four volumes of intergranular pore space for each intercrystalline kaolinite-filled pore space. Samples that contain various combinations of intergranular, dissolution and kaolinite pores generally show permeabilities in excess of 100 millidarcies. The effect of the dissolution pores on the permeability is a function of the pore interconnectedness. Samples that contained 30 percent or more micropores commonly showed permeabilities less than 50 millidarcies.

OTHER GEOLOGICAL PROPERTIES CONTROLLING PERMEABILITY

Other studies of Cherokee Group sandstones have attempted to define the relationships between average grain-size, the scale of the sedimentary structures, and permeability (Woody, 1983; Hulse, 1978). Hulse noted that sandstones exhibiting large-scale sedimentary structures were more permeable than those with small scale structures. He attributed the higher permeabilities to the increased grain-size and the lack of fine-grained material in large scale cross-stratified sands. Woody (1983) outlined a

similar increase in permeability with structural scale but noted that 80 percent of the large-scale crossbedded sands in his study were below the minimum permeability (10 md.) predicted by Hulse (1978). Both of these studies demonstrated that permeability tended to increase with increasing mean grain-size in the sandstones. The coarse sandstones were interpreted to show higher permeability because of large pore-throats and a high degree of pore interconnectedness.

Figure 91 was constructed to demonstrate the relationship between the grain-size and the scale of the sedimentary structures. This graph shows a general trend of decreasing grain-size with decreasing structural scale. The high and moderate angle cross-stratified sands show greater average grain-size than the low angle, horizontal and ripple stratified sands. This relationship is not surprising considering the upward decreasing grain-size and scale of the structures associated with fluvial sands.

Figures 92 and 93 show permeability plotted against average grain-size and lithofacies, respectively. Other studies have reported that coarse-grained sandstones are usually more permeable than fine-grained sandstones (Bouquet, 1984; Woody, 1983). The relationship between grain-size and permeability is not obvious in the KB Field because of the paucity of the fine-grained samples (Subfacies 6;

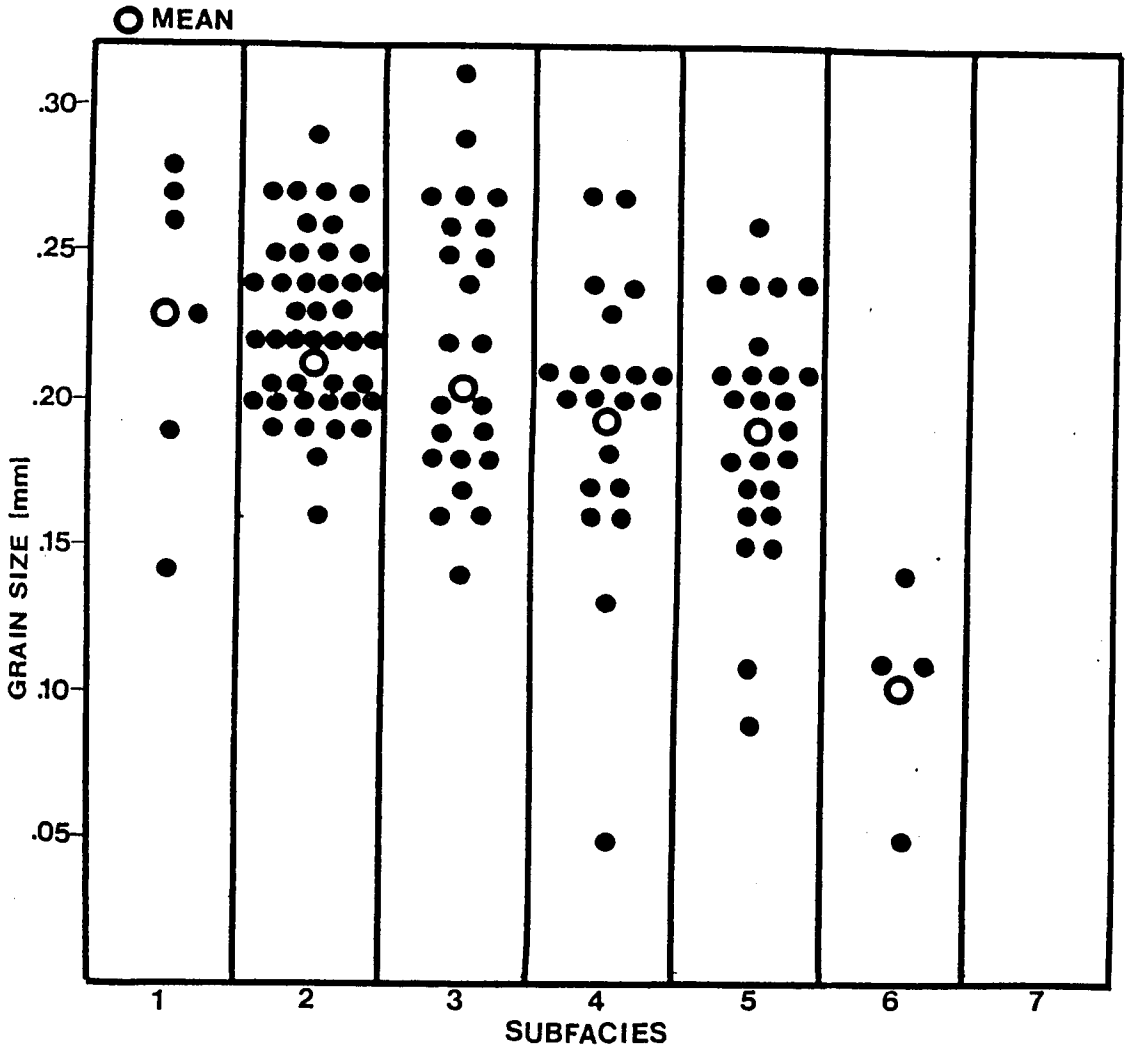

Figure 91. Plot of grain size versus subfacies (1-basal sand, 2-high angle crossbeds, 3-moderate angle crossbeds, 4-low angle crossbeds, 5-horizontal bedding, 6-ripple bedding, 7-linsen bedding).

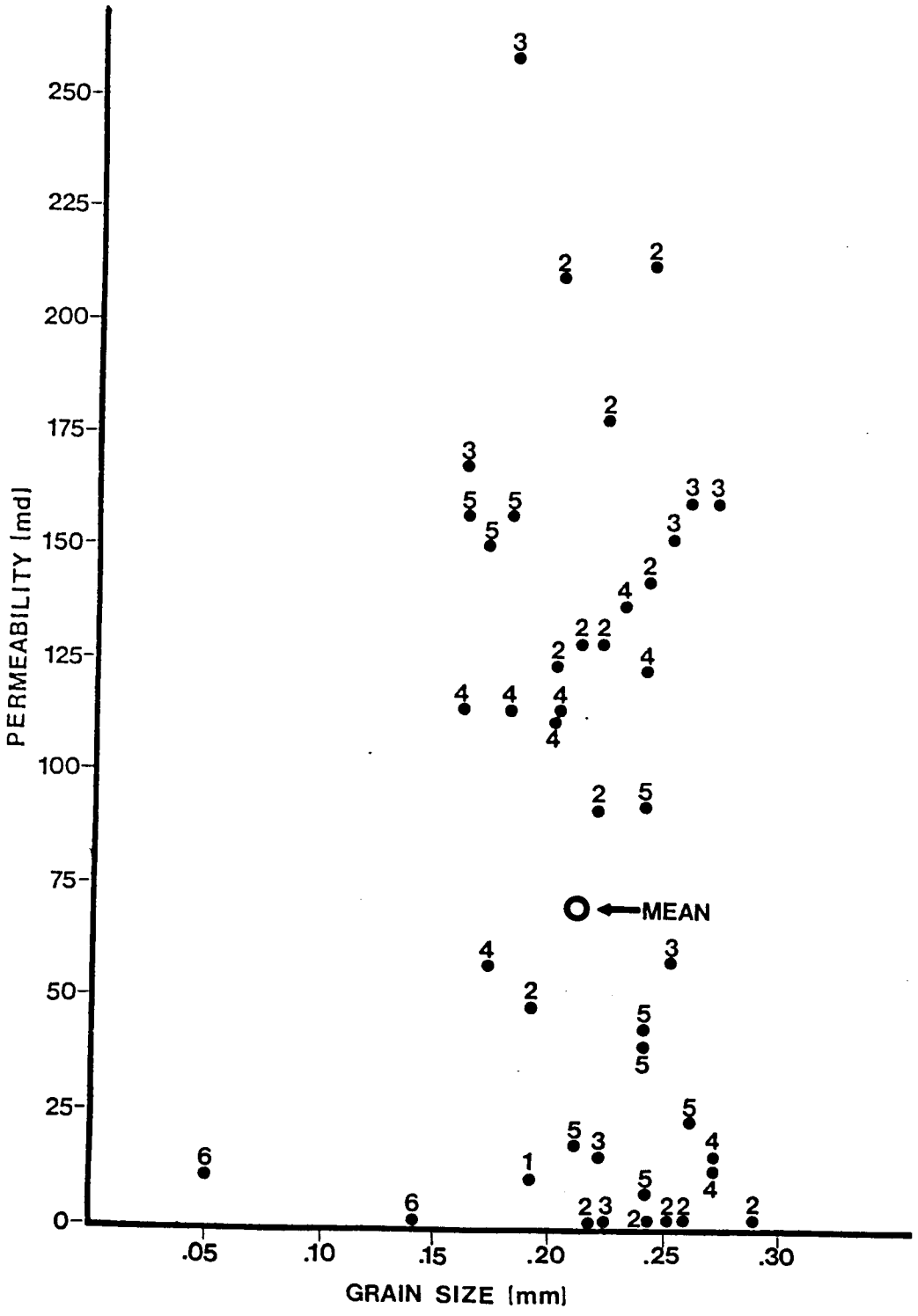

Figure 92. Plot of grain size versus permeability. Numbers denote subfacies type (1-basal sand, 2-high angle crossbeds, 3-moderate angle crossbeds, 4-low angle crossbeds, 5-horizontal bedding, 6-ripple bedding, 7-linsen bedding).

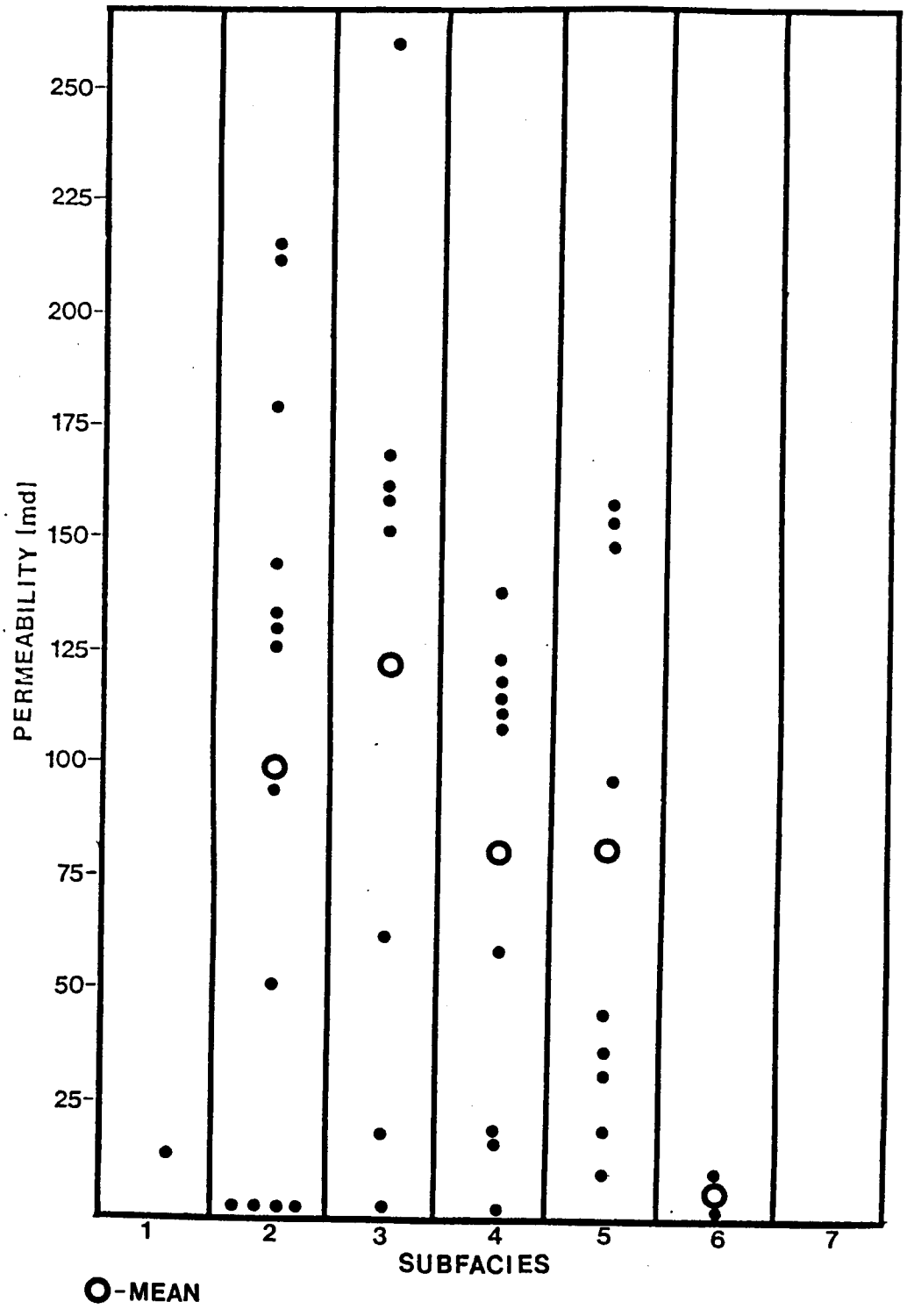

Figure 93. Plot of permeability versus subfacies (1-basal sand, 2-high angle crossbeds, 3-moderate angle crossbeds, 4-low angle crossbeds, 5-horizontal bedding, 6-ripple bedding, 7-linsen bedding).

Fig. 92). As stated earlier, Subfacies 6 represents only 3% of all the sand observed in the cores. The graph of permeability versus subfacies (Fig. 93) does demonstrate that the samples from Subfacies 6 are low permeability. It is significant that most of the subfacies show a wide range of permeabilities that are fairly evenly distributed.

Figures 91, 92 and 93 demonstrate that diagenesis has had a great effect on the permeability of the sandstones in the KB Field. As expected, there exists a direct relationship between grain-size and the scale of the sedimentary structures (Fig. 91). This relationship is a function of the energy of the depositional medium, but grain size only partially influences the permeability after diagenesis. The fine grained sandstones (Subfacies 6) do exhibit low permeability. Prior to extensive diagenesis, the coarse grained sandstones (Subfacies 1-5) likely showed similar permeabilities. The complex history of cementation and dissolution has markedly changed the capacity of the sandstones to transmit fluids since the time of deposition (Figs. 92 and 93). The subsequent diagenetic changes exert a great influence on the petrophysics. It is obvious that the pore characteristics are the most significant geological factor controlling petrophysical properties in sandstones showing similar grain-size (Fig. 88).

IMPLICATIONS FOR ENHANCED RECOVERY IN THE KB FIELD

INTRODUCTION

This study has demonstrated several characteristics of the Upper Bluejacket Sandstone in the KB Field that should be considered when evaluating enhanced oil recovery techniques. For example, chemical reactions can result from the interaction of reservoir rock constituents and fluids injected into the reservoir for enhanced recovery. If the chemistry of the reservoir is substantially changed, authigenic minerals, such as kaolinite, iron-rich carbonates, pyrite and chlorite, can unfavorably alter reservoir properties. This is particularly important in the KB Field because all pores are lined with authigenic minerals. Migration of authigenic clays, especially kaolinite, can also result from these reactions.

The sand-body geometry can be used to delineate fluid migration pathways in the reservoir. High permeability conduits in the reservoir usually follow the long axis of the sand body. The geometry of the reservoir is important in the design of an array of injection and production wells. This array should prevent the bypassing of portions of the reservoir with high residual oil saturations.

POTENTIAL ROCK/FLUID INTERACTIONS

The introduction of oxidizing fluids into the reservoir can mobilize reduced iron by partially dissolving siderite and Ca-Mg-Fe carbonate. Chlorite and pyrite, though less abundant, are also potential sources of reduced iron. The mobilization of iron can result in reduction of the permeability due to the precipitation of iron-oxides. The presence of iron can also reduce the desired high viscosity of polymers injected into the reservoir by destroying the long molecular chains.

Surface area and mobility of clay minerals are important reservoir characteristics to consider when choosing an enhanced recovery program. The large surface areas of kaolinite, chlorite and argillaceous rock fragments can be detrimental to enhanced recovery. Absorption of expensive fluids by these reservoir constituents can affect the economic feasibility of certain enhanced recovery techniques. Kaolinite mobility can also cause a problem in enhanced recovery operations. Individual kaolinite crystals or 'booklets' can migrate with passing fluids, accumulate and occlude pore throats. The blockage of pore throats can greatly reduce the permeability. Hulse (1978) presented an excellent discussion of the effects of reservoir geology on enhanced recovery.

RFSERVOIR GEOMETRY

The geometry of fluvially deposited sandstone reservoirs commonly delineate the preferred direction of fluid flow. The migration pathways of the reservoir usually are parallel to the long axis of the sand body. The array of injection and production wells should be designed to maximize sweep of the reservoir and maximize contact with zones of high residual oil saturation.

The multistory and multilateral reservoir geometry of KB Field can be used to predict fluid migration patterns during enhanced recovery. Each of the four sand bodies will likely behave as an individual reservoir with high permeability trends parallel to the long axis of the sand body. Cross flow between sand bodies is unlikely because the sands located just above the basal scour surfaces are relatively impermeable. These sands (Subfacies 1) commonly contain abundant argillaceous rock fragments and authigenic chlorite. As stated earlier, sands containing these constituents show low permeability because of the abundance of micropores. The basal low permeability zones that separate sand bodies are believed to be continuous across the reservoir and, therefore, partition the KB Field. This is substantiated by the multiple gas/oil and oil/water contacts observed in the KB Field (M. C. Colt, pers. comm., 1982).

RESERVOIR MODELS

Woody (1983) proposed an idealized model for Cherokee Group sandstones based on the distribution of geological and petrophysical properties (Fig. 94). He noted an upward vertical increase in the amount of argillaceous rock fragments and silica cement, and a decrease in authigenic chlorite. He also noted a vertical reduction in the grain size, porosity, permeability and effective pore radius. Woody proposed that chloritic grain coatings inhibit the precipitation of silica cement and, therefore, preserve primary porosity (Fig. 94). The preservation of primary porosity in these sandstones results in relatively high permeabilities.

The results of the KB Field study are difficult to directly compare to Woody's (1983) model. The Upper Bluejacket Sandstone in the KB Field does not contain the abundant rippled fine sands that were observed by Woody (Lithofacies D, Fig. 94). As noted earlier, Subfacies 6 composes only 3% of the total sand measured in the cores. The sandstone reservoir in this study is composed of mostly crossbedded coarse sandstone (Subfacies 2, 3, 4 and 5; Woody's Lithofacies C, Fig. 94). Therefore, the results for this study can only be compared to the lower section of Woody's (1983) model (Lithofacies A_1 and C, Fig. 94).

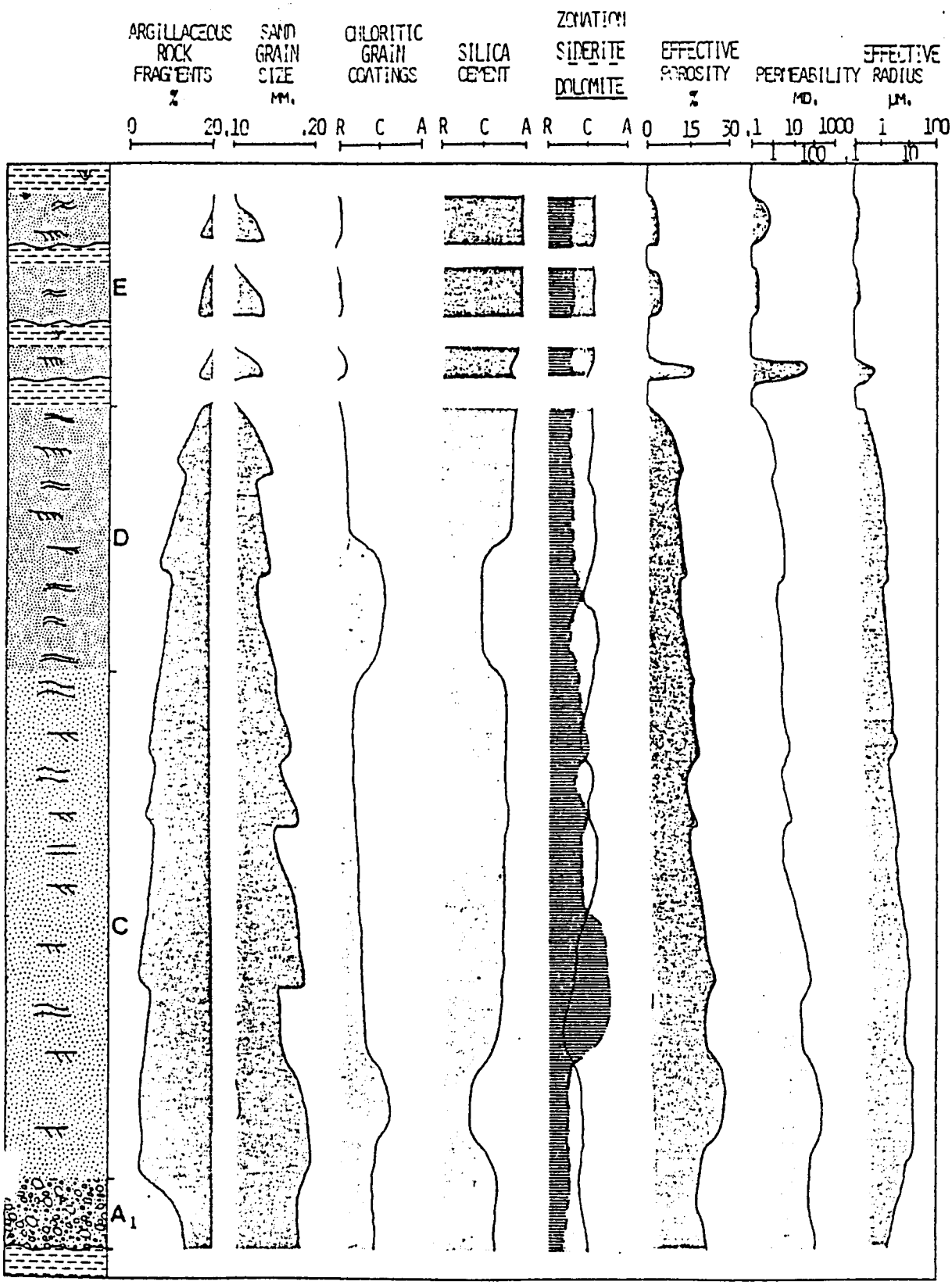

Figure 94. Idealized reservoir model for Cherokee Group sandstones proposed by Woody (1983). Lithofacies A_1 - thin basal conglomerate; C - crossbedded coarse sandstones; D - rippled fine sandstone; E - interbedded sandstones, shales and siltstones.

The study of the KB Field has produced few conclusions that favorably compare with Lithofacies A_1 and C of Woody's (1983) model (Fig. 94). In the KB Field, the reservoir sandstone does not show a gradual increase in the percent of argillaceous rock fragments. As stated previously, the rock fragments are commonly associated with the erosional surfaces. Sandstone samples that contained rock fragments commonly showed abundant authigenic chlorite. These samples commonly exhibited very low permeability, not high permeability as Woody predicts. The sandstones in the KB Field also do not show a vertical reduction in permeability. The permeability in the KB Field is more strongly influenced by pore type than grain size (Figs. 88 and 92).

REFERENCES

Allen, J.R.L., 1963, Depositional features of the Dittonian rocks: Precambrian compared with the Welsh borderland: Geol. Mag., v. 100, p. 385-400.

Allen, J.R.L., 1964, Studies in fluviatile sedimentation: Six cyclothems from the Lower Old Red Sandstone, Anglo-Welsh Basin: Sedimentology, v. 3, p. 163-198.

Allen, J.R.L., 1965, Sedimentation and paleogeography of the Old Red Sandstone of Anglesey, North Wales: Proc. Yorks. Geol. Soc., v. 35, p. 139-185.

Allen, J.R.L., 1970, Studies in fluviatile sedimentation: a comparison of fining-upwards cyclothems, with special reference to coarse-member composition and interpretation: Jour. Sed. Petrology, v. 40, p. 298-323.

Allen, J.R.L., 1978, Studies in fluviatile sedimentation: An exploratory quantitative model for the architecture of avulsion-controlled alluvial suites: Sed. Geol., v. 21, p. 129-147.

Baker, D.R., 1962, Organic geochemistry of the Cherokee Group in southeastern Kansas and northeastern Oklahoma: Am. Assoc. Petrol. Geol. Bull., v. 46, p. 1621-1642.

Bass, N.W., 1934, Origin of Bartlesville shoestring sands, Greenwood and Butler Counties, Kansas: Am. Assoc. Petrol. Geol. Bull., v. 18, p. 1313-1345.

Bass, N.W., 1936, Origin of the shoestring sands of Greenwood and Butler Counties, Kansas: Kansas Geol. Survey Bull. 23, 135 p.

Bass, N.W., Leatherock, C., Dillard, W.R., and Kennedy, L.E., 1937, Origin and distribution of the Bartlesville and Burbank shoestring oil sands in parts of Oklahoma and Kansas: Am. Assoc. Petrol. Geol. Bull., v. 21, p. 30-66.

Berner, R. A., 1980, Early Diagenesis, A Theoretical Approach, Princeton Univ. Press, Princeton, N.J. 241 p.

Blatt, H., 1979, Diagenetic processes in sandstone: p. 141-157, in Aspects of Diagenesis (P.A. Scholle and P.R. Schluger, eds.), Soc. Econ. Paleon. Miner., Spec. Pub. 26, 443 p.

Boles, J.R., 1978, Active ankerite cementation in the subsurface Eocene of southwest Texas: Contr. Min. and Petr., v. 68, p. 13-22.

Bouquet, D.J., 1984, Depositional Environment, Diagenesis, Reservoir Quality, and Enhanced Oil-Recovery Potential of a Reservoir in the Skinner Sandstone (Desmoinesian), Crawford, Labette and Neosho Counties, Kansas: unpub. M.S. Thesis, Univ. of Kansas, Lawrence.

Bridge, J.S., and Leeder, M.R., 1979, A simulation model of alluvial stratigraphy: Sedimentology, v. 26, p. 617-644.

Brown, J.C., and Dey, A.K., 1975, The mineral and nuclear fuels of the Indian Subcontinent and Burma: A guide to the study of the coal, oil, natural gas, uranium and thorium resources of the area: Oxford University Press, 517 p.

Busch, D.A., 1959, Prospecting for stratigraphic traps: Am. Assoc. Petrol. Geol. Bull., v. 43, p. 2829-2843.

Cheyney, A.E., 1929, Madison shoestring pool, Greenwood County, Kansas: in Structure of Typical American Oilfields, Am. Assoc. Petrol. Geol., v. 2, p. 150-159.

Cole, J.G., 1969, Cherokee Group east flank of the Nemaha Ridge: Shale Shaker, v. 19, no. 8, p. 134-146, no. 9, p. 150-160.

Collinson, J.D., 1978, Alluvial Sediments, p. 15-60, in Sedimentary Environments and Facies (H.D. Reading, ed.), Elsevier, New York, 557 p.

Dickinson, W.R., (ed.), 1975, Current concepts of depositional systems with applications for petroleum geology: San Joaquin Geol. Society, Bakersfield, California.

Ebanks, W.J., Jr., 1975, Kansas oil For enhanced recovery, a resource appraisal: Tertiary Oil Recovery Project Contribution 1, 31 p.

Ebanks, W.J., Jr., 1979, Correlation of Cherokee (Desmoinesian) sandstones of the Missouri-Kansas-Oklahoma tri-state Area, p. 295-312: in Hyne, N.J. (ed.), Pennsylvanian Sandstones of the Midcontinent, Tulsa Geol. Soc. Spec. Pub. 1.

Ebanks, W.J., Jr., and James, G.W., 1974, Heavy-crude oil bearing sandstone of the Cherokee Group (Desmoinesian) in southeastern Kansas: in Canadian Soc. Petrol. Geol., Memoir 3, Oil Sands, Fuel of the Future, p. 19-34.

Elliott, T., 1978, Deltas, p. 97-142, in Sedimentary Environments and Facies (H.D. Reading, ed.), Elsevier, New York, 557 p.

Garrels, R.M., and Christ, C.L., 1965, Solutions, Minerals and Equilibria: Harper and Row, New York, 450 p.

Harms, J.C., MacKenzie, D.B., and McCubbin, D.G., 1963, Stratification in modern sands of the Red River, Louisiana: Jour. Geol., v. 71, p. 566-580.

Harms, J.C., Southard, J.B., and Walker, R.G., 1982, Structures and Sequences in Clastic Rocks, Soc. Econ. Paleon. Miner. Short Course Notes, no. 9, 249 p.

Harris, J.W., 1985, Stratigraphy and Depositional Environments of the Krebs Formation - Lower Cherokee Group (Middle Pennsylvanian) in Southeatern Kansas: unpub. M.S. thesis, Kansas Univ.

Howe, W.B., 1956, Stratigraphy of pre-Marmaton Desmoinesian (Cherokee) rocks in southeastern Kansas: Kansas Geol. Survey Bull. 123, 132 p.

Hudson, A.S., 1969, Depositional environment of the Red Fork and equivalent sandstones east of the Nemaha Ridge, Kansas and Oklahoma: M.S. Thesis, Tulsa Univ., 80 p.

Hulse, W.J., 1978, A geologic study of the Sallyards Field area Greenwood County, Kansas: unpub. M.S. thesis, Kansas Univ., 152 p.

Jackson, R.G., II, 1975, Velocity-Bedforms-Texture patterns of meander bends in the lower Wabash River of Illinois and Indiana: Geol. Soc. Amer. Bull., v. 86, p. 1511-1522.

Jackson, R.G., II, 1976b, Depositional model of point bars in the lower Wabash River: Jour. Sed. Petrology, v. 46. p. 579-594.

Jackson, R.G., II, 1978, Preliminary evaluation of lithofacies models for meandering alluvial streams: in Miall, A. D., ed., Fluvial sedimentology: Canadian Soc. Petrol. Geol. Memoir 5, p. 543-576.

Johnson, H.D., 1978, Shallow Siliciclastic Seas, p. 207-258, in Sedimentary Environments and Facies (H.D. Reading, ed.), Elsevier, New York, 557 p.

Jordan, L., 1957, Subsurface stratigraphic names of Oklahoma: Okla. Geol. Surv. Guidebook VI.

Land, L. S., and Dutton, S. P., 1978, Cementation of a Pennsylvanian deltaic sandstone: isotopic data: Jour. Sed. Pet., v. 48, p. 1167-1176.

Leatherock, C., 1937, Physical Characteristics of Bartlesville and Burbank sands in northeastern Oklahoma and southeastern Kansas: Am. Assoc. Petrol. Geol. Bull., v. 21, p. 246-258.

MacKenzie, D.B., 1972, Primary stratigraphic traps in sandstones, in Stratigraphic Oil and Gas Fields, Classification, Exploration, Methods and Case Histories: Soc. Econ. Geol. Spec. Pub., no. 10, p. 47-63.

Milliken, K.L., Land, L.S., and Loucks, R.G., 1981, History of burial diagenesis determined from isotopic geochemistry, Frio Formation, Brazoria County, Texas: Am. Assoc. Petrol. Geol. Bull., v. 65, p. 1397-1413.

Moore, R.C., Frye, J.C., Lee, W., and O'Connor, H.G., 1951, The Kansas Rock Column: Kansas Geol. Survey Bull. 89, 132 p.

Phares, R.S., 1969, Depositional Framework of the Bartlesville Sandstone in northeastern Oklahoma: unpub. M.S. thesis, Tulsa Univ., 59 p.

Pittman, E.D., and Lumsden, D.N., 1968, Relationships between chlorite coatings on quartz grains and porosity, Spiro Sand, Oklahoma: Jour. Sed. Petrol., V. 38, p. 668-670.

Pittman, E.D., 1979, Porosity, diagenesis and productive capability of sandstone reservoirs: p. 159-173, in Aspects of Diagenesis (P.A. Scholle and P.R. Schluger, eds.), Soc. Econ. Paleon. Miner., Spec. Pub. 26, 443 p.

Reineck, H.E., and Singh, I.B., 1980, Depositional Sedimentary Environments: Springer-Verlag, 450 p.

Schlumberger, 1972, Log Interpretation, Volume 1-Principles, 113 p.

Schmidt, V., and MacDonald, D.A., 1979, Secondary reservoir porosity in the course of sandstone diagenesis: Am. Assoc. Petrol. Geol. Continuing Education Course Note Series 12, 125 p.

Schumacher, M., 1976, Depositional Environment of the Bartlesville Sandstone, La Harpe Field, Allen County, Kansas: unpub. M.S. thesis, Texas A&M Univ., 82 p.

Visher, G.S., 1965a, Fluvial processes as interpreted from ancient and recent fluvial deposits: in Primary Sedimentary Structures; Soc. Econ. Paleon, Miner., Spec. Pub. 12, p. 116-132.

Visher, G.S., Saitta, B.S., and Phares, R.S., 1971, Pennsylvanian delta patterns and petroleum occurrences in eastern Oklahoma: Am. Assoc. Petrol. Geol. Bull., v. 55, p. 1206-1230.

Visher, G.S., 1972, Physical characteristics of fluvial deposits: in Recognition of ancient sedimentary environments, Soc. Econ. Paleon. Miner., Spec. Pub no. 16, p. 84-98.

Weirich, T.E., 1953, Shelf principle of oil origin, migration and accumulation: Am. Assoc. Petrol. Geol. Bull., v. 37, p. 2027-2045.

Weirich, T.E., 1968, Guidebook to the Geology of the Bluejacket-Bartlesville Sandstone, Oklahoma: Okla. City Geol. Soc., p. 69-72.

Woody, M.D., 1983, Sedimentology, Diagenesis and Petrophysics of Selected Cherokee Group (Desmoinesian) Sandstones in Southeastern Kansas: Shale Shaker, v. 34, p. 91-122.

Zeller, D.E. (ed.), 1968, The stratigraphic succession in Kansas: Kansas Geological Survey Bulletin 189, 81 p.

APPENDIX A

CORE DESCRIPTIONS OF THE

UPPER BLUEJACKET SANDSTONE

IN THE KB FIELD

LIST OF CORES

1) M.C. Colt 28A Smith
2) M.C. Colt 31A Smith
3) M.C. Colt 3AO Harvey
4) M.C. Colt 5A Harvey
5) M.C. Colt 5A Johnson
6) M.C. Colt 13AO Johnson
7) M.C. Colt 14AO Johnson
8) M.C. Colt 26AO Johnson
9) M.C. Colt 50 AO Johnson

EXPLANATION OF SYMBOLS

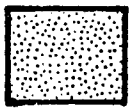

SANDSTONE

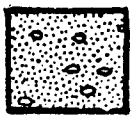

SANDSTONE WITH COAL AND SHALE CLASTS

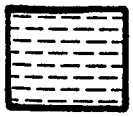

SHALE

INTERBEDDED V. FINE SAND AND SHALE

COAL

HIGH ANGLE PLANAR-TABULAR CROSSBEDS

MODERATE ANGLE PLANAR-TABULAR CROSSBEDS

LOW ANGLE PLANAR-TABULAR CROSSBEDS

HORIZONTAL BEDDING

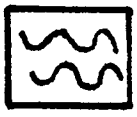

CURRENT RIPPLES

MACK C. COLT 28A SMITH
33-24S-21E
SAND D 750-766 FT., SAND C 776-766 FT., SAND B 776-783 FT.

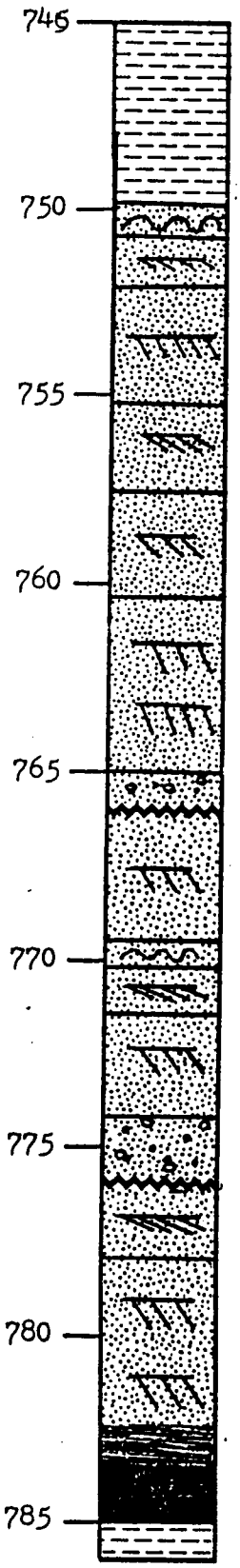

SUBFACIES #	
	745-749.7 FT.....DARK GRAY SHALE WITH ABUNDANT SIDERITE.
6	749.7-751 FT.....CURRENT-RIPPLE BEDDED VERY FINE SANDSTONE
4	751-752.3 FT.....HIGHLY SIDERITIC LOW ANGLE PLANAR-TABULAR CROSSBEDDED FINE SANDSTONE.
2	752.3-755.1 FT....HIGH ANGLE PLANAR-TABULAR CROSS-STRATIFIED MEDIUM TO FINE SANDSTONE.
4	755.1-757.5 FT....LOW ANGLE PLANAR-TABULAR CROSSBEDDED FINE SANDSTONE.
3	757.5-760.5 FT....MODERATE ANGLE PLANAR-TABULAR CROSSBEDDED FINE TO MEDIUM SANDSTONE.
2	760.5-765 FT.....HIGH ANGLE PLANAR-TABULAR CROSS-STRATIFIED FINE TO MEDIUM SANDSTONE.
1	765-766 FT.....STRUCTURLESS MEDIUM SANDSTONE WITH COAL CLASTS. EROSIONAL BASAL CONTACT.
3	766-769.4 FT.....MODERATE ANGLE CROSSBEDDED FINE SANDSTONE.
6	769.4-770.1 FT....RIPPLED FINE SANDSTONE WITH SHALE LAMINAE.
4	770.1-771.5 FT....LOW ANGLE CROSSBEDDED FINE SANDSTONE.
3	771.5-774 FT.....MODERATE ANGLE PLANAR-TABULAR CROSSBEDDED FINE SANDSTONE.
1	774-776 FT.....STRUCTURLESS MEDIUM TO FINE SANDSTONE WITH ABUNDANT COAL CLASTS AND EROSIONAL BASE.
4	776-778 FT.....LOW ANGLE CROSSBEDDED V. FINE TO FINE SAND.
2	778-782.5 FT.....HIGH ANGLE PLANAR-TABULAR CROSS-STRATIFIED MEDIUM SANDSTONE WITH MINOR SHALE CLASTS.
7	782.5-783.2 FT....INTERBEDDED V. FINE SAND, SILT, AND SHALE.
	783.2-785 FT.....BLUEJACKET B COAL
	785-785.6 FT.....DARK GRAY SHALE.

MACK C. COLT 31A SMITH
33-24S-21S
SAND B 731-746 FT., SAND A 748-754 FT.

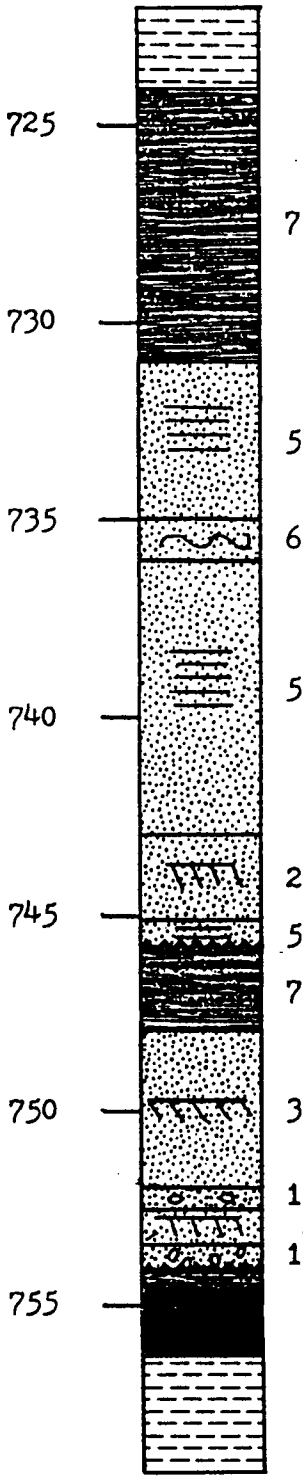

722-724 FT.....GRAY SHALE

724-731 FT.....INTERBEDDED OR LINSEN-BEDDED VERY FINE SANDSTONE, SILTSTONE AND BLACK SHALE.

731-735 FT.....HORIZONTALLY LAMINATED FINE SANDSTONE.

735-736 FT.....CURRENT-RIPPLE BEDDED FINE SANDSTONE.

736-743 FT.....HORIZONTALLY BEDDED FINE SANDSTONE

743-745 FT.....HIGH ANGLE PLANAR-TABULAR CROSSBEDDED FINE SANDSTONE.

745-746 FT.....HORIZONTALLY BEDDED FINE SANDSTONE WITH EROSIONAL (?) BASE.

746-748 FT.....INTERBEDDED V. FINE SANDSTONE AND SHALE.

748-752 FT.....MODERATE ANGLE PLANAR-TABULAR CROSSBEDDED FINE SANDSTONE.

752-752.7 FT.....STRUCTURELESS FINE SAND WITH SHALE CLASTS.

752.7-753.2 FT....HIGH ANGLE CROSSBEDDED MEDIUM SAND.

753.2-754.2 FT....STRUCTURELESS MEDIUM TO FINE SANDSTONE WITH SHALE CLASTS AND EROSIONAL BASE.

754.2-754.5 FT....LINSEN-BEDDED V.FINE SANDSTONE AND SHALE.

754.5-756.2 FT....BLUEJACKET B COAL

756.2-759 FT.....DARK GRAY SHALE.

MACK C. COLT 3A0 HARVEY
33-24S-21E

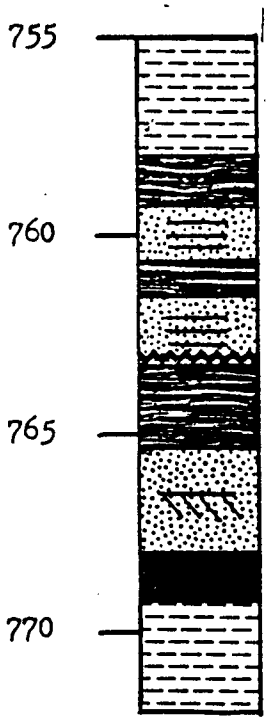

SUBFACIES #

755-758 FT.....GRAY SHALE

7 758-759.3 FT.....LINSEN-BEDDED VERY FINE SANDSTONE AND SHALE

5 759.3-760.5 FT....HORIZONTALLY LAMINATED, MODERATELY SORTED, FINE-GRAINED SANDSTONE.

7 760.5-761.5 FT....LINSEN-BEDDED VERY FINE SANDSTONE AND SHALE.

5 761.5-763 FT.....HORIZONTALLY LAMINATED, MODERATELY-SORTED, FINE-GRAINED SANDSTONE.

7 763 FT.....EROSIONAL SURFACE

763-765.5.....INTERBEDDED VERY-FINE-SANDSTONE AND SHALE.

3 765.5-768 FT.....MODERATELY SORTED, MODERATE ANGLE (20°), PLANAR-TABULAR CROSS-STRATIFIED SANDSTONE.

768-769.2 FT.....BLUEJACKET A COAL

769.2-772 FT.....GRAY SHALE WITH PLANT FRAGMENTS.

MACK C. COLT 5A HARVEY
33-24S-21E

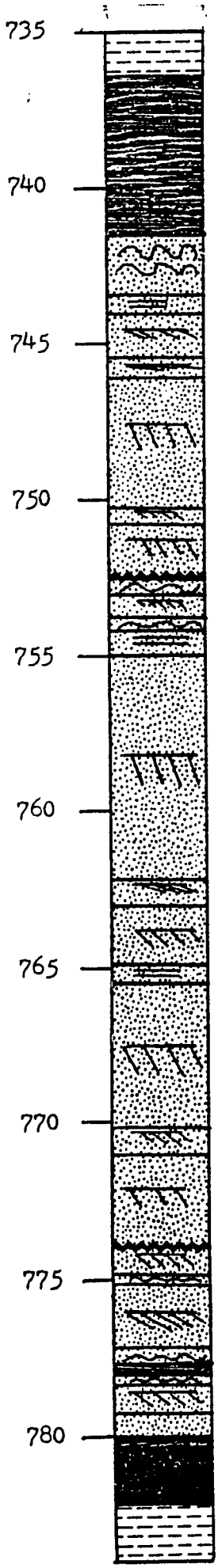

SUBFACIES — SAND D 753-741 FT. SAND C 774-753 FT.

#	
	735-736.5 FT.....DARK GRAY SHALE
	736.5-741.5 FT....HIGHLY SIDERITIC INTERBEDDED VERY FINE SANDSTONE, SILTSTONE AND SHALE. MINOR BURROWING.
6	741.5-743.5 FT....CURRENT-RIPPLE BEDDED VERY FINE SANDSTONE.
5	743.5-744 FT.....HORIZONTALLY BEDDED VERY FINE SANDSTONE.
2	744-745.5 FT.....SIDERITIC HIGH ANGLE PLANAR-TABULAR CROSS-BEDDED FINE SANDSTONE.
4	745.5-746 FT.....LOW ANGLE PLANAR-TABULAR CROSS-BEDDED FINE SANDSTONE.
2	746-750.2 FT.....HIGH ANGLE PLANAR-TABULAR CROSS-BEDDED FINE SANDSTONE.
4	750.2-750.5 FT....LOW ANGLE CROSS-BEDDED FINE SANDSTONE.
2	750.5-752.5 FT....HIGH ANGLE PLANAR-TABULAR CROSS-STRATIFIED MEDIUM SANDSTONE.
6	752.5 FT.....EROSIONAL SURFACE
3 6 5	752.5-753 FT.....CURRENT RIPPLE BEDDED VERY FINE TO FINE SANDSTONE. MINOR SHALE LAMINAE.
	753-754 FT.....MODERATE ANGLE CROSS-BEDDED FINE SANDSTONE.
	754-754.5 FT.....CURRENT RIPPLE BEDDED V. FINE SANDSTONE.
	754.5-755 FT.....HORIZONTALLY LAMINATED FINE SANDSTONE.
2	755-762 FT.....HIGH ANGLE CROSS-STRATIFIED FINE SANDSTONE.
4	762-763 FT.....LOW ANGLE CROSS-STATIFIED FINE SANDSTONE.
3	763-764.9 FT.....MODERATE ANGLE CROSS-BEDDED FINE SANDSTONE.
5	764.9-765.5 FT....HORIZONTALLY LAMINATED FINE SANDSTONE.
3	765.5-770.3 FT....MODERATE ANGLE PLANAR-TABULAR CROSS-STRATIFIED MEDIUM TO FINE SANDSTONE.
4	770.3-771 FT.....LOW ANGLE PLANAR-TABULAR CROSSBEDDED FINE SANDSTONE.
3	771-774 FT.....MODERATE ANGLE CROSSBEDDED MEDIUM TO FINE SANDSTONE.
4	774 FT.....EROSIONAL SURFACE
6	774-775 FT.....LOW ANGLE CROSSBEDDED FINE SANDSTONE.
4	775-775.3 FT.....RIPPLE BEDDED V. FINE TO FINE SANDSTONE.
	775.3-777 FT.....LOW ANGLE CROSSBEDDED FINE SANDSTONE.
6 7	777-778.2 FT.....RIPPLE BEDDED V. FINE SAND AND INTERBEDDED SANDSTONE AND SHALE.
6 4	
1 7	778.2-780.....LOW ANGLE FINE SANDSTONE WITH MINOR SHALE CLASTS.
	780-782.....BLUEJACKET B COAL
	782-784 FT.....DARK GRAY MUDSTONE.

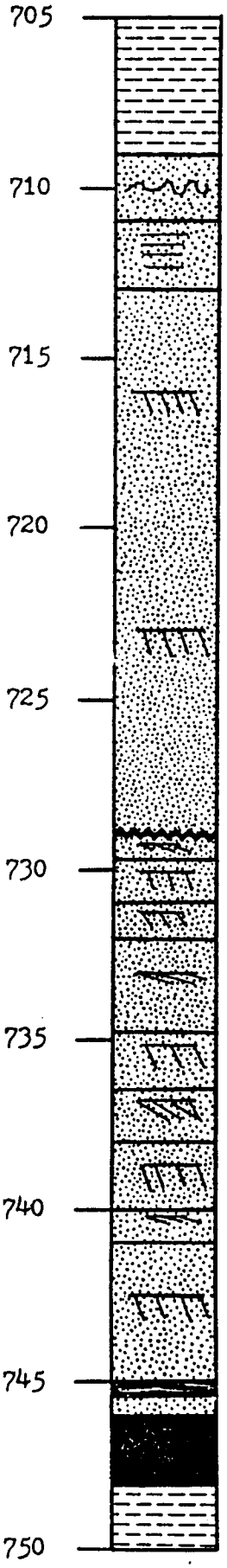

MACK C. COLT 5A JOHNSON
33-24S-21E
SAND D 709-729 FT., SAND C 729-746 FT.

SUBFACIES

705-709 FT.....GRAY SHALE.

6 709-711 FT.....CURRENT RIPPLE BEDDED V. FINE SANDSTONE.

5 711-713 FT.....HIGHLY SIDERITIC HORIZONTALLY LAMINATED FINE SANDSTONE.

2 713-729 FT.....HIGH ANGLE PLANAR-TABULAR CROSS-STRATIFIED MEDIUM TO FINE SANDSTONE. COMMON SIDERITE. EROSIONAL (?) SURFACE AT BASE ON UNIT.

4
2 729-729.8 FT.....LOW ANGLE CROSSBEDDED FINE SANDSTONE.
3 729.8-731 FT.....HIGH ANGLE CROSSBEDDED FINE SANDSTONE.
731-732.2 FT.....MODERATE ANGLE CROSSBEDDED FINE SANDSTONE.

4 732.2-734.8 FT....LOW ANGLE CROSSBEDDED FINE TO MEDIUM SAND.

2 734.8-736.5 FT....HIGH ANGLE CROSSBEDDED FINE TO MEDIUM SAND.

4 736.5-738 FT.....LOW ANGLE CROSSBEDDED FINE SANDSTONE.

2
4 738-740 FT.....HIGH ANGLE CROSSBEDDED MEDIUM SANDSTONE.
740-741 FT.....LOW ANGLE TABULAR CROSSBEDDED MEDIUM SAND.

2 741-745 FT.....HIGH ANGLE PLANAR-TABULAR CROSS-STRATIFIED MEDIUM SANDSTONE.

7
1 745-745.3 FT.....LINSEN-BEDDED V. FINE SAND AND BLACK SHALE.
745.3-746 FT.....STRUCTURELESS FINE SANDSTONE.
746-748 FT.....BLUEJACKET B COAL

748-750 FT.....DARK GRAY SHALE.

MACK C. COLT 13A0 JOHNSON
33-24S-21E
SAND D 714-718 FT., SAND C 719-760 FT.

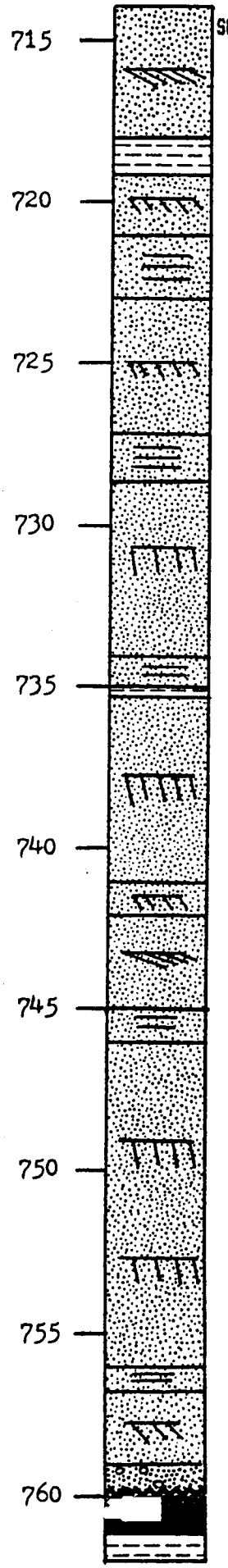

SUBFACIES #	
4	714-718 FT.....LOW ANGLE CROSSBEDDED FINE SANDSTONE.
	718-719 FT.....HIGHLY SIDERTIIC SILTSTONE AND SHALE.
3	719-721 FT.....MODERATE ANGLE CROSSBEDDED FINE SANDSTONE.
5	721-723 FT.....HORIZONTALLY BEDDED V. FINE TO FINE SAND.
3	723-727 FT.....MODERATE ANGLE PLANAR-TABULAR CROSS-STRATIFIED FINE SANDSTONE.
5	727-728.5 FT.....HORIZONTALLY BEDDED FINE SANDSTONE.
2	728.5-734 FT.....HIGH ANGLE PLANAR-TABULAR CROSS-STRATIFIED MEDIUM TO FINE SANDSTONE.
	734-735 FT.....HORIZONTALLY LAMINATED FINE SANDSTONE.
5	735-735.1 FT.....HIGHLY SIDERITIC THIN SHALE BED.
2	735.1-741 FT.....HIGH ANGLE PLANAR-TABULAR CROSS-STRATIFIED MEDIUM TO FINE SANDSTONE.
3	741-742 FT.....MODERATE ANGLE CROSSBEDDED MEDIUM TO FINE SANDSTONE.
4	742-745 FT.....LOW ANGLE PLANAR-TABULAR CROSS-STRATIFIED MEDIUM TO FINE SANDSTONE.
5	745-746 FT.....HORIZONTALLY LAMINATED FINE TO MEDIUM SAND.
2	746-756 FT.....HIGH ANGLE PLANAR-TABULAR CROSS-STRATIFIED MEDIUM-GRAINED SANDSTONE. SIDERITE NODULES.
5	756-757 FT.....HORIZONTALLY LAMINATED MEDIUM SANDSTONE.
3	757-759 FT.....MODERATE ANGLE CROSSBEDDED MEDIUM SAND.
1	759-760 FT.....STRUCTURELESS MEDIUM SAND WITH SHALE CLASTS
	760-761.2 FT.....BLUEJACKET B COAL
	761.2-762 FT.....GRAY SHALE WITH PLANT FRAGMENTS.

MACK C. COLT 14AO JOHNSON
33-24S-21E
SAND D 710-717 FT., SAND C 717-754 FT.

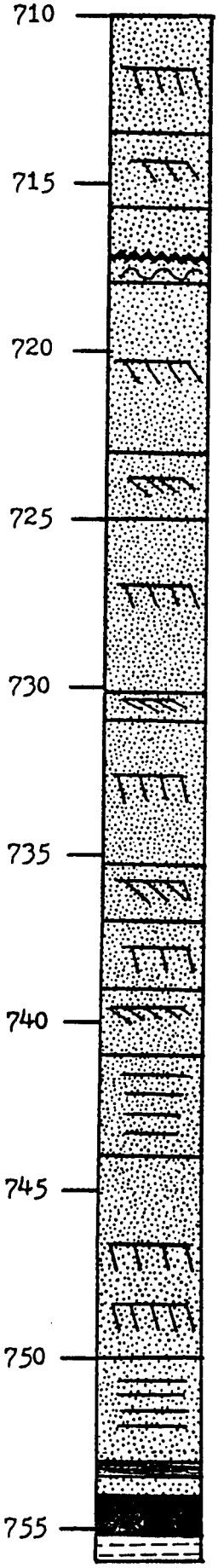

SUBFACIES

#	
2	710-713 FT.....HIGH ANGLE PLANAR-TABULAR CROSSBEDDED FINE SANDSTONE.
	713-715.5 FT.....MODERATE ANGLE CROSSBEDDED FINE SANDSTONE.
3	715.5-717 FT.....MASSIVE FINE SANDSTONE WITH EROSIONAL(?) BASE.
1	717-717.5 FT.....CURRENT RIPPLE BEDDED V. FINE TO FINE SAND.
6	
3	717.5-723 FT.....MODERATE ANGLE PLANAR-TABULAR CROSS-STRATIFIED FINE SAND WITH MINOR SHALE PARTINGS.
	723-725 FT.....LOW ANGLE CROSSBEDDED FINE SAND WITH RARE SHALE CLASTS.
4	
2	725-730.1 FT.....HIGH ANGLE PLANAR-TABULAR CROSSBEDDED FINE SANDSTONE.
	730.1-731 FT.....LOW ANGLE TABULAR CROSSBEDDED FINE SAND.
4	
2	731-735.2 FT.....HIGH ANGLE PLANAR-TABULAR CROSS-STRATIFIED MEDIUM TO FINE SANDSTONE.
	735.2-737 FT.....LOW ANGLE CROSSBEDDED MEDIUM TO FINE SAND.
4	737-739 FT.....HIGH ANGLE CROSSBEDDED MEDIUM SANDSTONE.
2	739-741 FT.....LOW ANGLE TABULAR X-BEDDED FINE SANDSTONE.
4	
5	741-744 FT.....HORIZONTALLY BEDDED FINE SANDSTONE.
2	744-750 FT.....HIGH ANGLE PLANAR-TABULAR CROSS-STRATIFIED FINE SANDSTONE. COMMON SHALE CLASTS.
5	750-753 FT.....HORIZONTALLY BEDDED MEDIUM-GRAINED SAND.
7	753-753.5 FT.....LINSEN-BEDDED V. FINE SAND, SILT AND SHALE.
5	753.5-754 FT.....STRUCTURELESS FINE SANDSTONE.
	754-755.2 FT.....BLUEJACKET B COAL
	755.2-756 FT.....DARK GRAY SHALE.

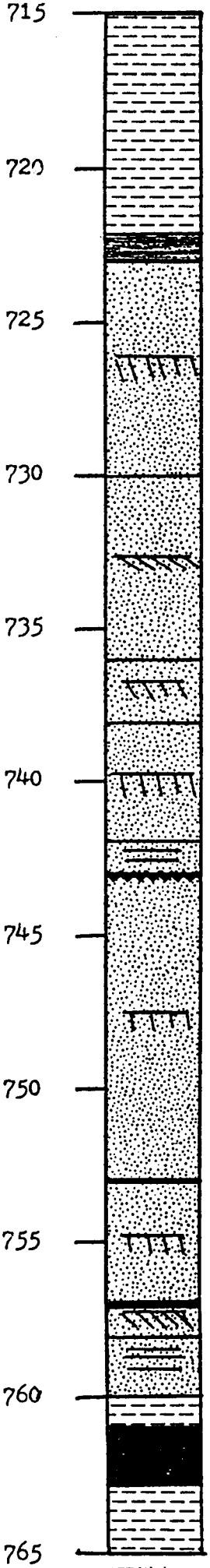

MACK C. COLT 26AQ JOHNSON
33-24S-21E
SAND D 723-743 FT., SAND C 743-760 FT.

SUBFACIES

715-722 FT.....SIDERITIC MUDSTONE AND RIPPLED SILTSTONE. COMMON SIDERITE NODULES AND FRACTURE FILLS.

7 722-723 FT.....LINSEN-BEDDED V. FINE SAND AND SHALE.

3 723-730 FT.....MODERATE ANGLE PLANAR-TABULAR CROSS-STRATIFIED FINE SAND.

4 730-736 FT.....LOW ANGLE PLANAR-TABULAR CROSS-STRATIFIED FINE SANDSTONE. SELECTIVE CEMENTATION ALONG CROSSBED FACES.

3 736-738 FT.....MODERATE ANGLE CROSSBEDDED FINE SANDSTONE.

2 738-742 FT.....HIGH ANGLE PLANAR-TABULAR CROSSBEDDED MEDIUM TO FINE SANDSTONE.

5 742-743 FT.....HORIZONTALLY BEDDED MEDIUM SANDSTONE. BASAL EROSIONAL SURFACE.

2 743-753 FT.....HIGH ANGLE PLANAR-TABULAR CROSS-STRATIFIED V. FINE TO FINE SANDSTONE. MEAN GRAIN-SIZE DECREASES VERTICALLY.

2 753-757 FT.....HIGH ANGLE CROSSBEDDED MEDIUM TO FINE SANDSTONE.

4 757-758 FT.....LOW ANGLE CROSSBEDDED MEDIUM TO FINE SAND.

5 758-760 FT.....HORIZONTALLY BEDDED MEDIUM SANDSTONE.

760-761 FT.....GRAY SHALE

761-762.8 FT.....BLUEJACKET B COAL

762.8-765 FT.....GRAY SHALE WITH COMMON PLANT FRAGMENTS.

MACK C. COLT 50A0 JOHNSON
33-24S-21E
SAND C 749.5-770 FT., SAND B 770-779.2 FT.

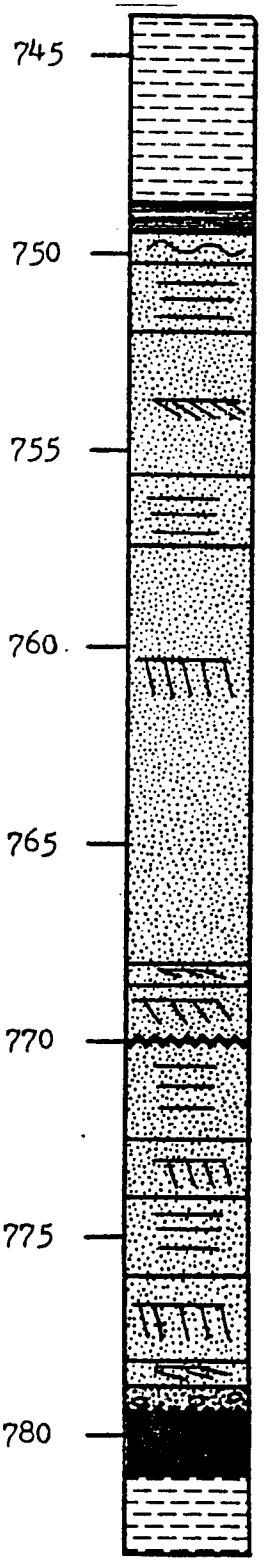

SUBFACIES #

744-748.5 FT.....GRAY SHALE

7 748.5-749.5 FT....INTERBEDDED V. FINE SANDSTONE AND SHALE.
6 749.5-750.2 FT....CURRENT RIPPLED BEDDED V. FINE SANDSTONE.
5 750.2-752 FT.....HORIZONTALLY BEDDED FINE SANDSTONE.
4 752-755.5 FT.....LOW ANGLE PLANAR-TABULAR CROSSBEDDED FINE SANDSTONE.
5 755.5-757.5 FT....HORIZONTALLY LAMINATED FINE SANDSTONE.
2 757.5-768 FT.....HIGH ANGLE PLANAR-TABULAR CROSS-STRATIFIED FINE SANDSTONE.
4 768-768.5 FT.....LOW ANGLE CROSSBEDDED FINE SANDSTONE.
2 768.5-770 FT.....HIGH ANGLE TABULAR CROSSBEDDED MEDIUM TO FINE SANDSTONE WITH EROSIONAL BASE.
5 770-772.5 FT.....HORIZONTALLY BEDDED V. FINE SANDSTONE.
2 772.5-774 FT.....HIGH ANGLE CROSSBEDDED FINE SANDSTONE.
5 774-776 FT.....HORIZONTALLY LAMINATED V. FINE TO FINE SANDSTONE.
2 776-778 FT.....HIGH ANGLE CROSSBEDDED FINE SANDSTONE.
4 778-778.8 FT.....LOW ANGLE CROSSBEDDED FINE SANDSTONE.
1 778.8-779.2 FT....STRUCTURELESS (OR HORIZONTALLY BEDDED) MEDIUM TO FINE SANDSTONE WITH COAL OR SHALE CLASTS.
779.2-781 FT.....BLUEJACKET B COAL
781-783 FT.....GRAY SHALE

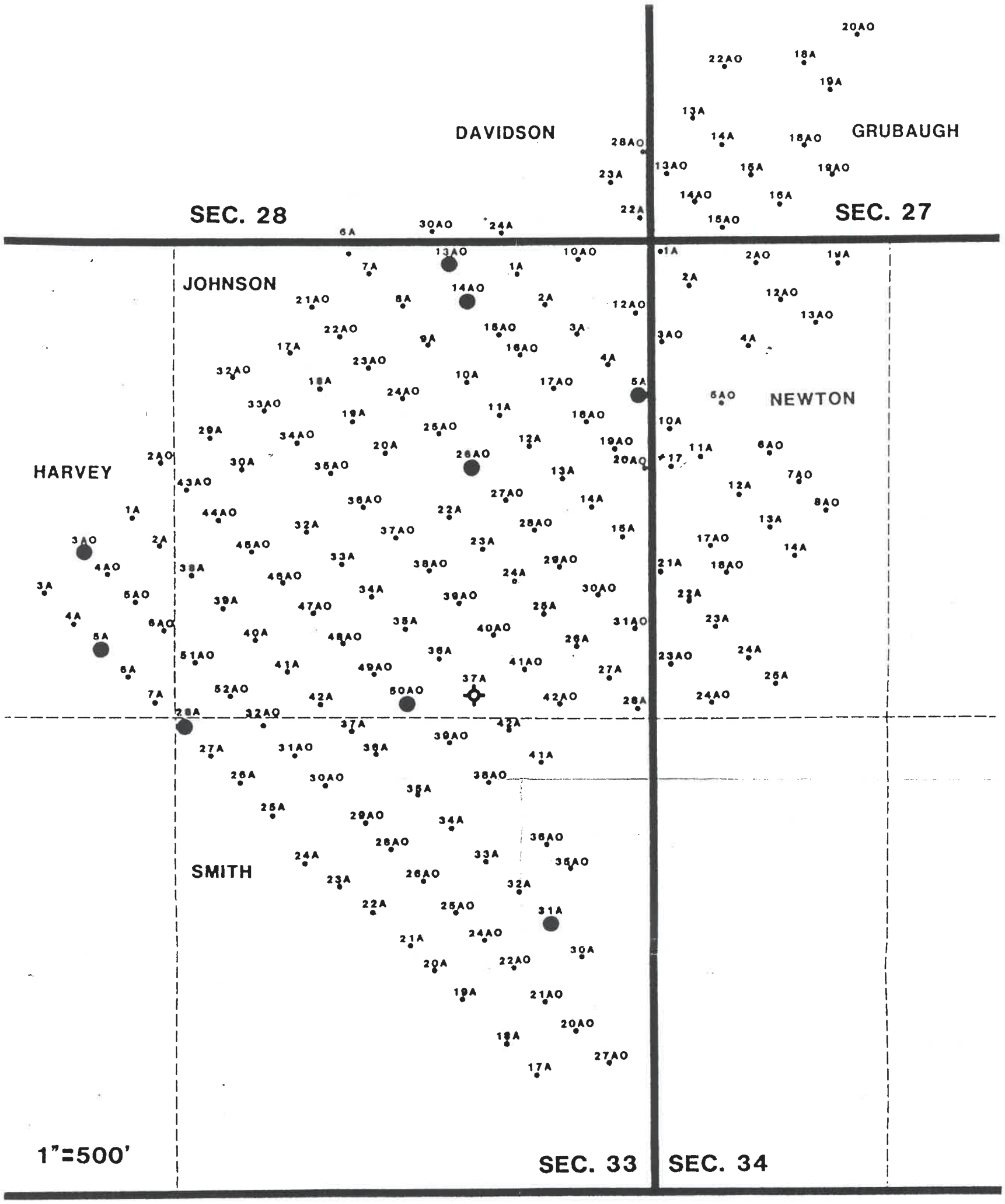

PLATE 1

WELL LOCATION MAP OF KB FIELD

Kansas Geological Survey
Open-file Report 86-23
plate 1

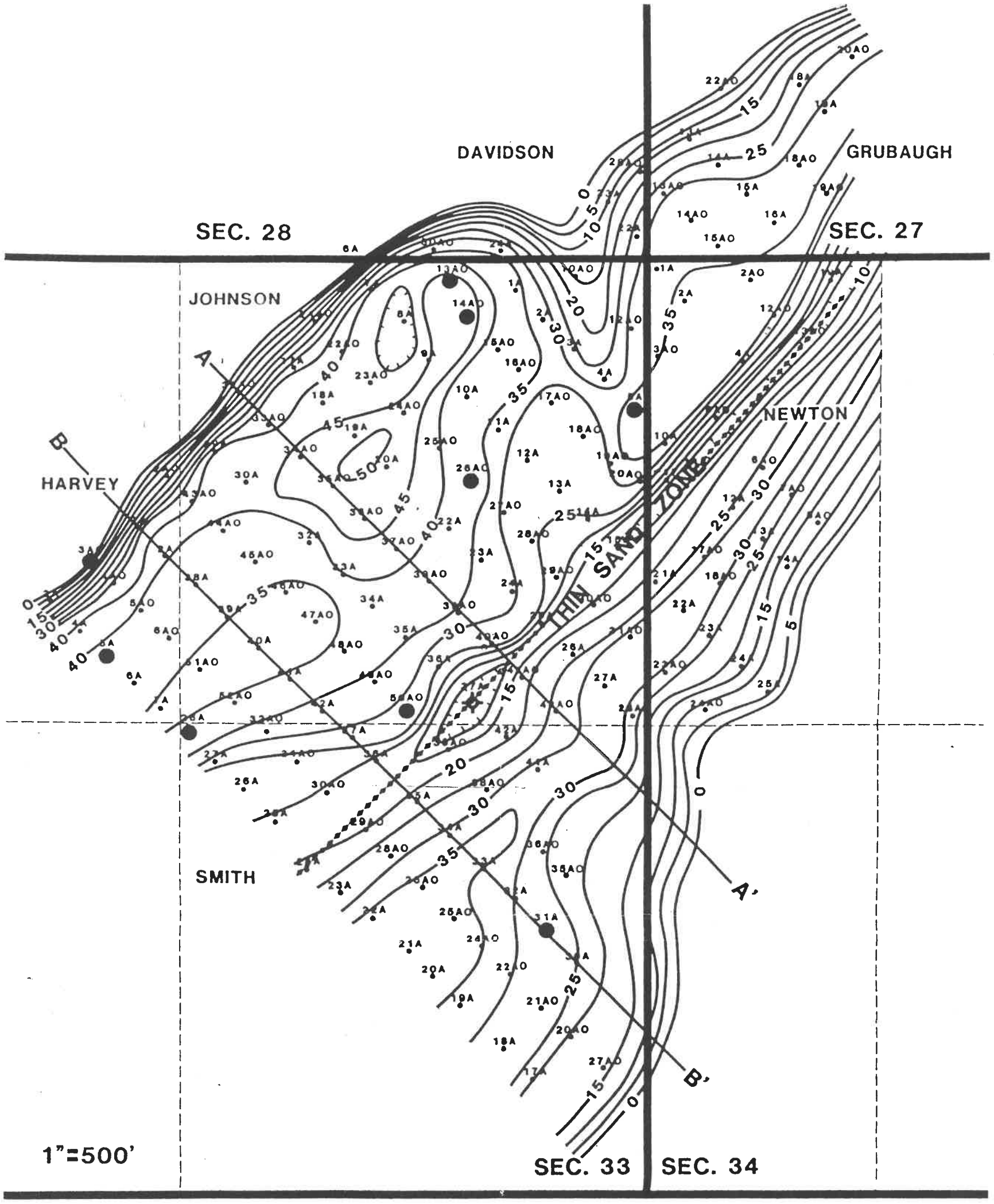

●Wells with cores used in this study • Well Location ⊕Dry Hole

Contour Interval – 5'

See PLATE 6 for cross-sections.

PLATE 2

NET SAND ISOLITH MAP OF UPPER BLUEJACKET SANDSTONE

sis
6
29
2
nce

Kansas Geological Survey
Open-file Report 86-23
plate 2

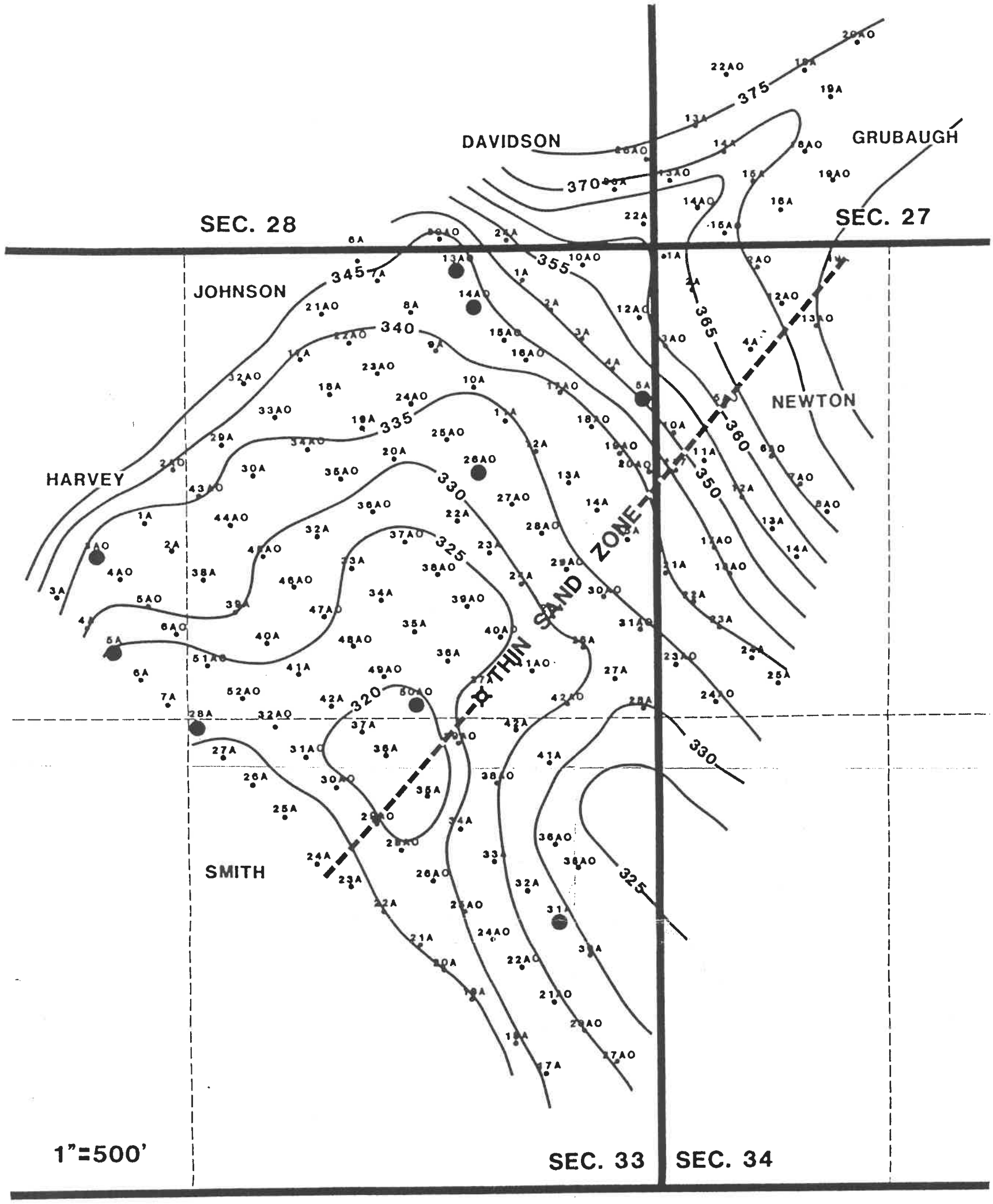

● Wells with cores used in this study • Well Location ⊹ Dry Hole

Contour Interval - 5'

PLATE 3

STRUCTURE MAP
TOP OF BLUEJACKET B COAL

DATUM = SEA LEVEL

Kansas Geological Survey
Open-file Report 86-23
plate 3

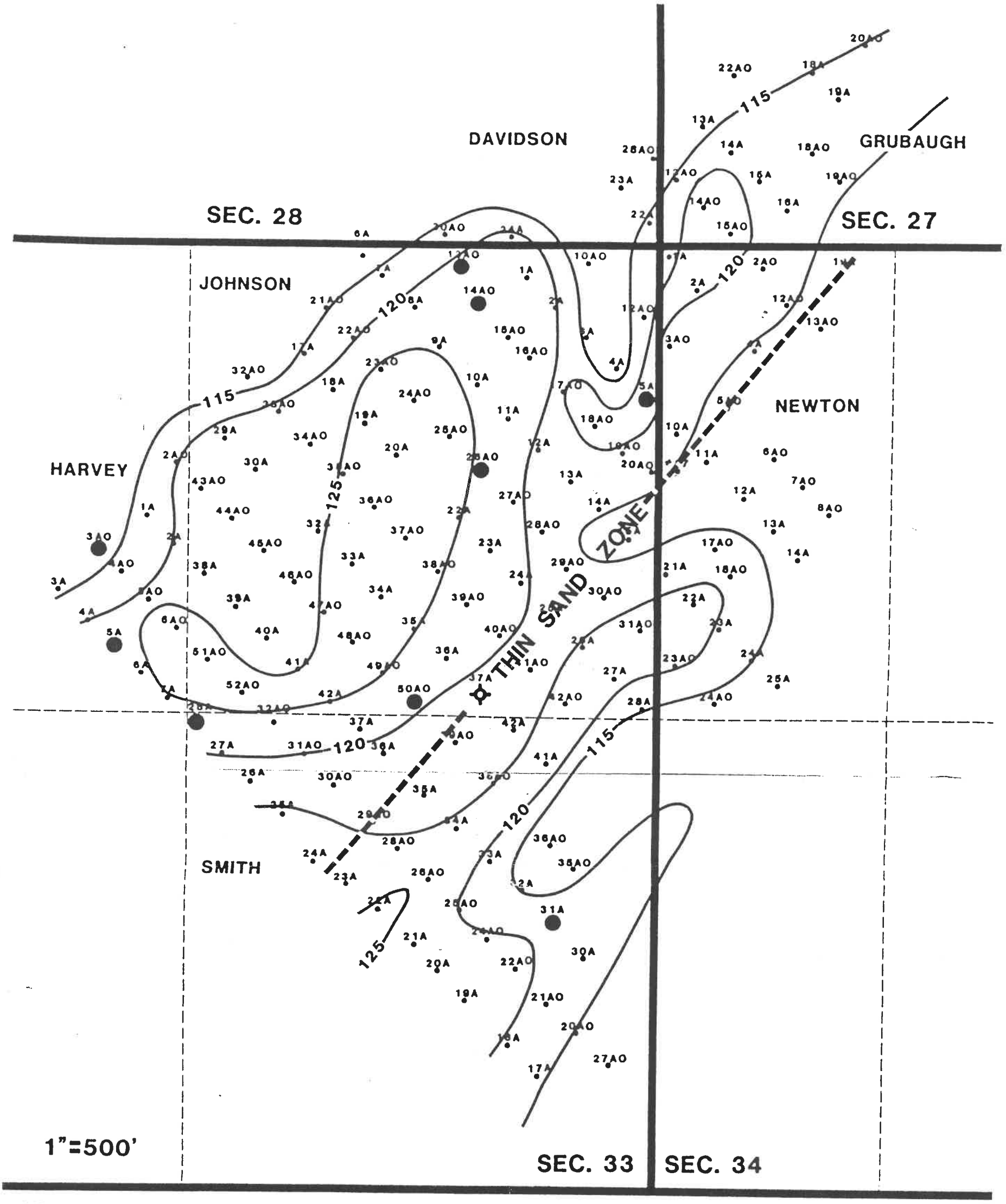

●Wells with cores used in this study • Well Location ⊹Dry Hole

Contour Interval – 5'

PLATE 4

ISOPACH MAP OF STRATIGRAPHIC INTERVAL BETWEEN BLACK SHALE – 1 (V-SHALE) AND TOP OF BLUEJACKET B COAL

Kansas Geological Survey
Open-file Report 86-23
plate 4

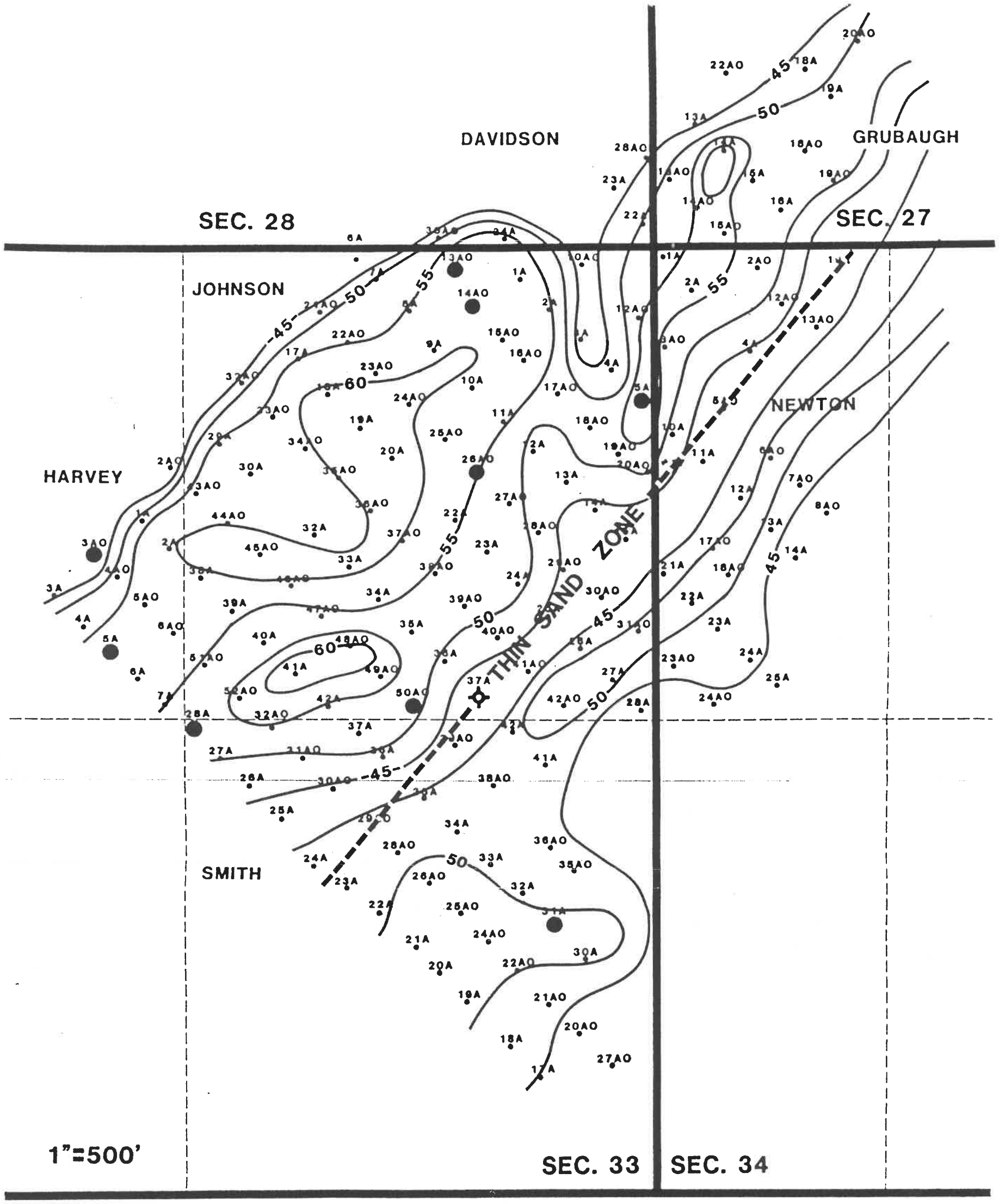

● Wells with cores used in this study • Well Location ⊕ Dry Hole

Contour Interval - 5'

PLATE 5

ISOPACH MAP OF STRATIGRAPHIC INTERVAL BETWEEN BLACK SHALE-2 (ASSOCIATED WITH TEBO COAL)

Kansas Geological Survey
Open-file Report 86-23
plate 5

PLATE 6

CROSS-SECTIONS FROM THE KB FIELD

PLATE 6A

DIAGRAMMATIC CROSS-SECTION SHOWING RELATIONSHIP BETWEEN THE UPPER BLUEJACKET SANDSTONE AND LATERAL FACIES (SEE FIG. 2)

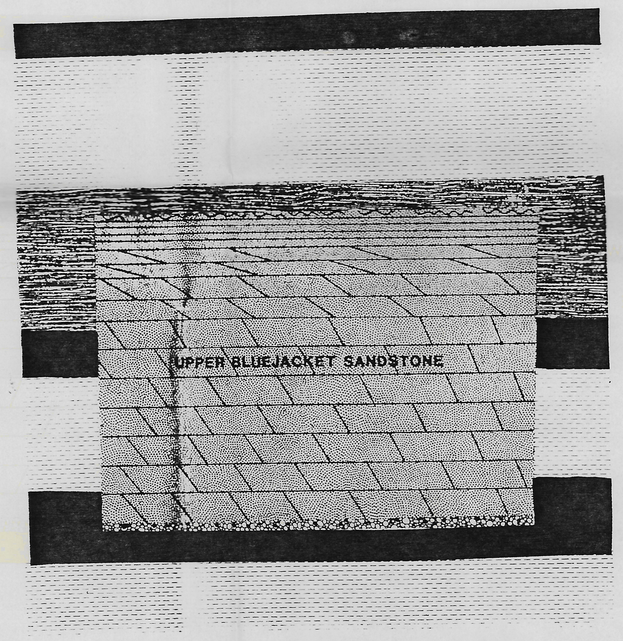

WEIR-PITTSBURG COAL

SHALE

LINSEN-BEDDED SS SH

BLUEJACKET A COAL

SHALE

BLUEJACKET B COAL

SHALE

VERTICAL SCALE: 1" - 5 ft

HORIZONTAL SCALE: 1" - 660 FT

NOTE: COAL THICKNESSES ARE EXAGGERATED TO COMPENSATE FOR POST-DEPOSITIONAL COMPACTION

PLATE 6B

SCHEMATIC CROSS-SECTION SHOWING RESERVOIR GEOMETRY (SEE PLATE2)

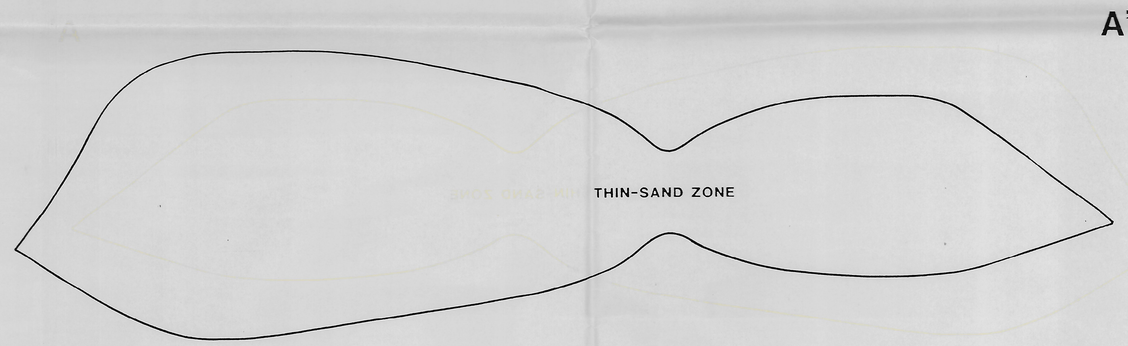

VERTICAL SCALE: 1" - 12.5 ft

HORIZONTAL SCALE: 1" - 500 ft

PLATE 6C

CORRELATION OF GAMMA-RAY LOG DEFLECTIONS ACROSS KB FIELD (SEE PLATE 2)

VERTICAL SCALE: 1" - 30 Ft

NO HORIZONTAL SCALE

DATUM - BLACK SHALE-2 (ASSOCIATED WITH TEBO COAL; SEE FIG. 23)

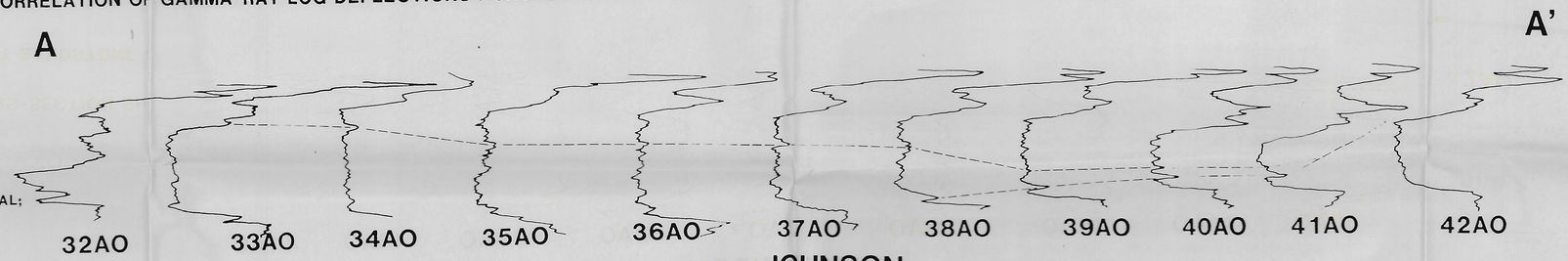

PLATE 6D

INTERPRETIVE CROSS-SECTION SHOWING CONTACTS BETWEEN DIFFERENT SAND BODIES (SEE PLATE 2)

VERTICAL SCALE: 1" - 30 Ft

NO HORIZONTAL SCALE

DATUM - BLACK SHALE-2

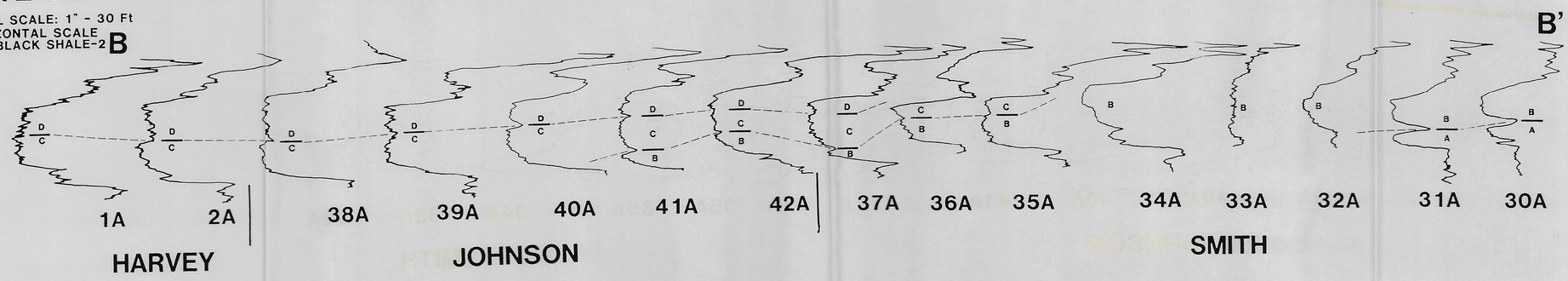

PLATE 7

INTERPRETED GAMMA RAY LOGS FROM THE KB FIELD
ALLEN COUNTY, KANSAS

LOG SCALE: 1" - 40'

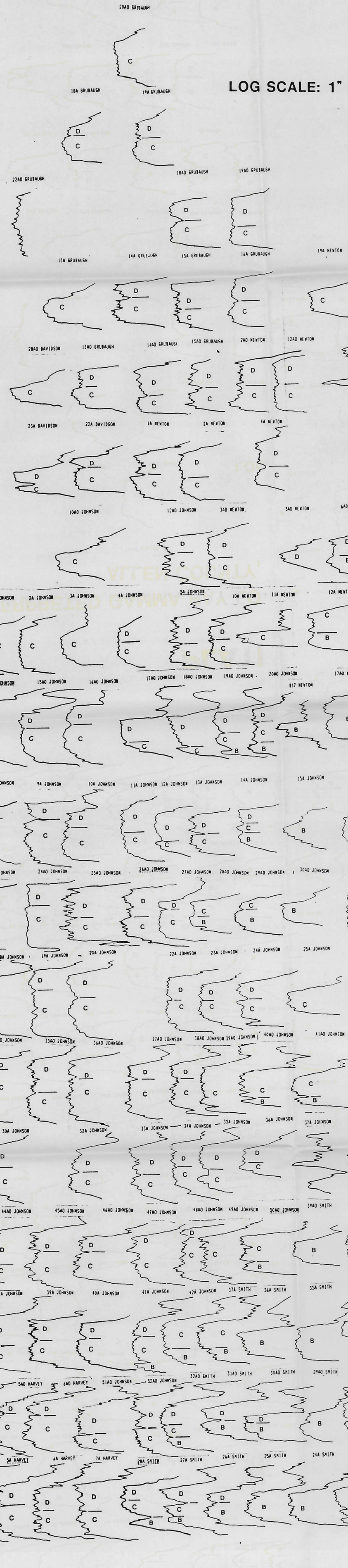

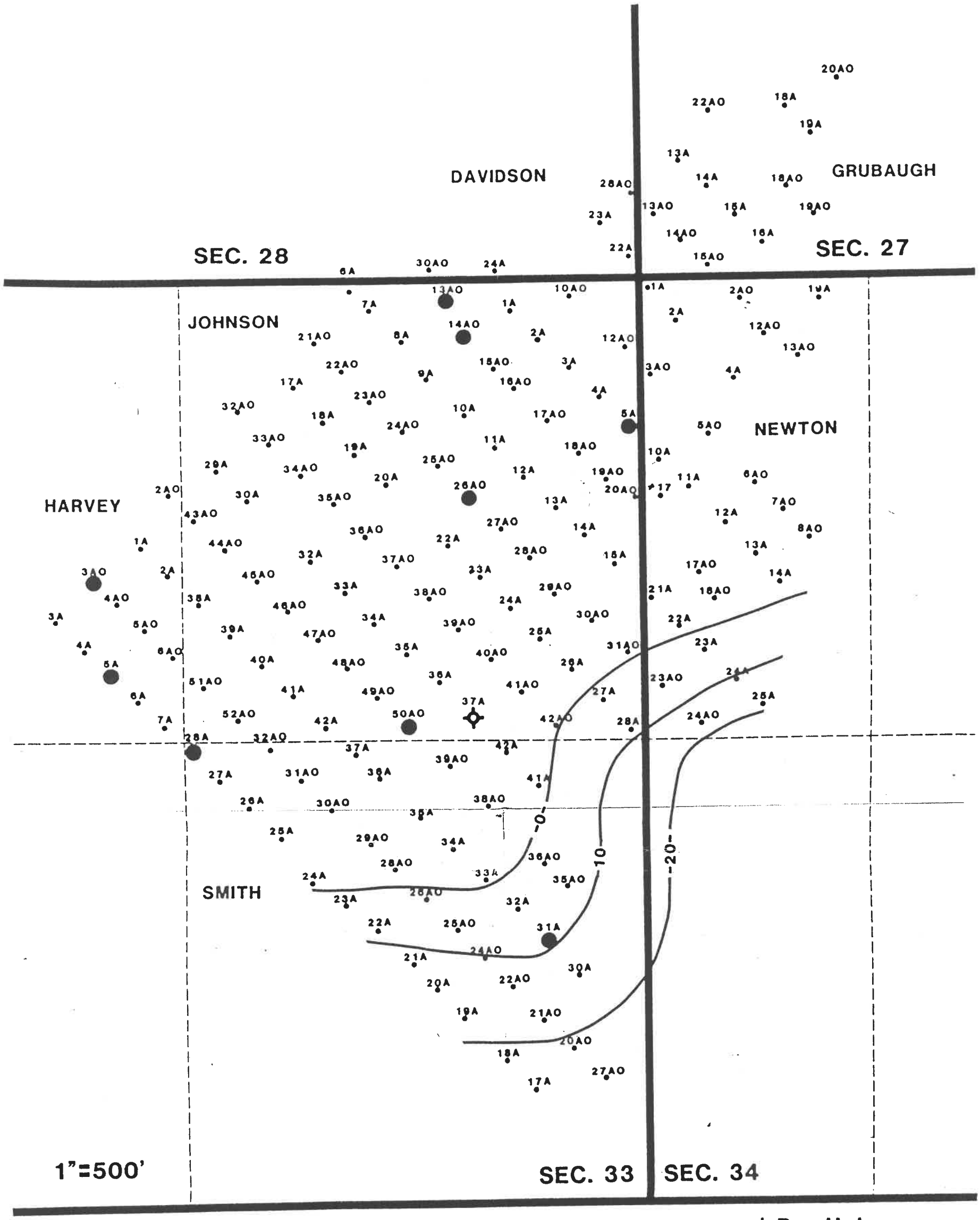

1"=500'

● Wells with cores used in this study • Well Location ⊕ Dry Hole

Contour Interval - 10'

PLATE 8

ISOPACH MAP OF SAND A

Kansas Geological Survey
Open-file Report 86-23
plate 8

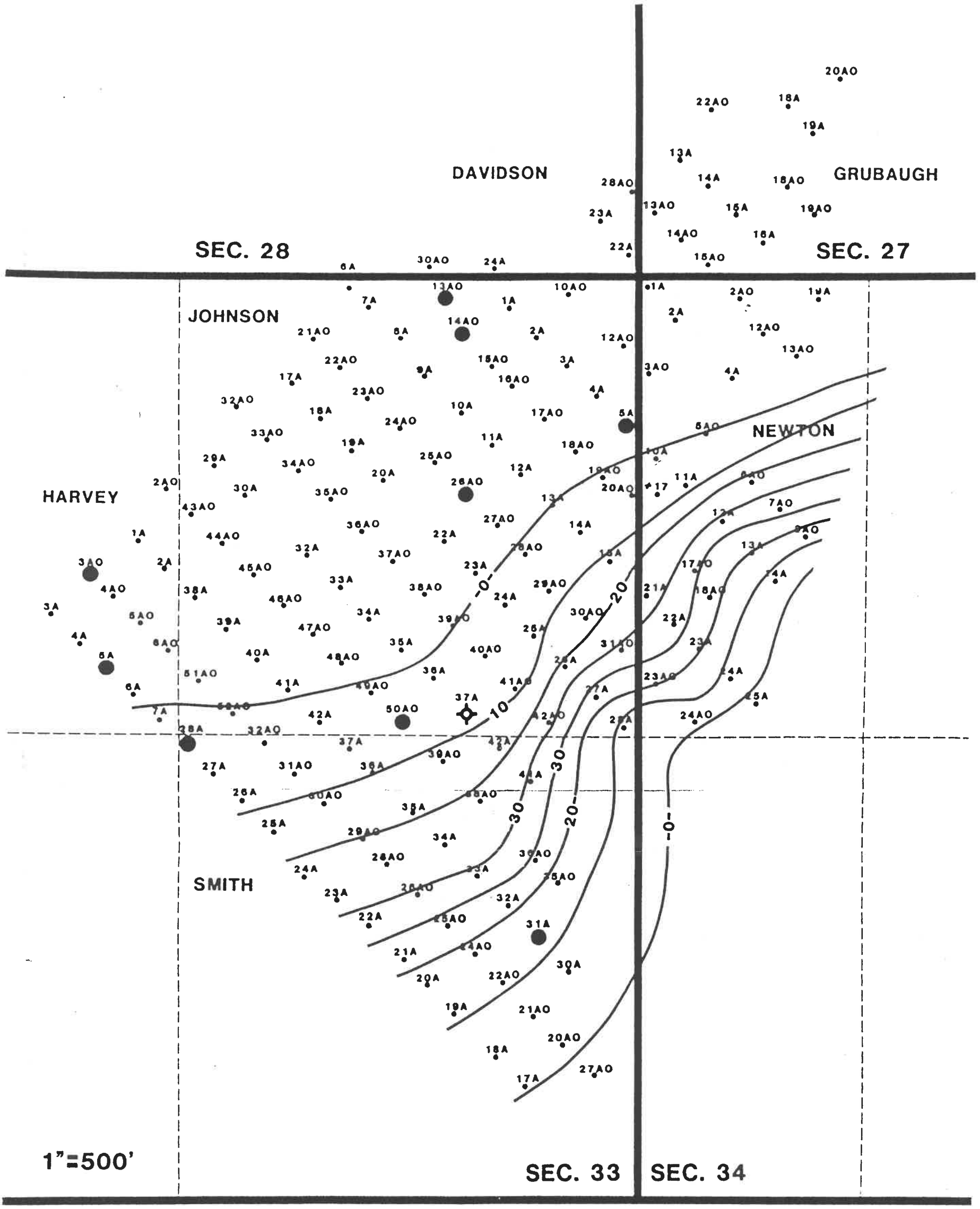

● Wells with cores used in this study • Well Location ⊕ Dry Hole

Contour Interval = 10'

PLATE 9

ISOPACH MAP OF SAND B

Kansas Geological Survey
Open-file Report 86-23
plate 9

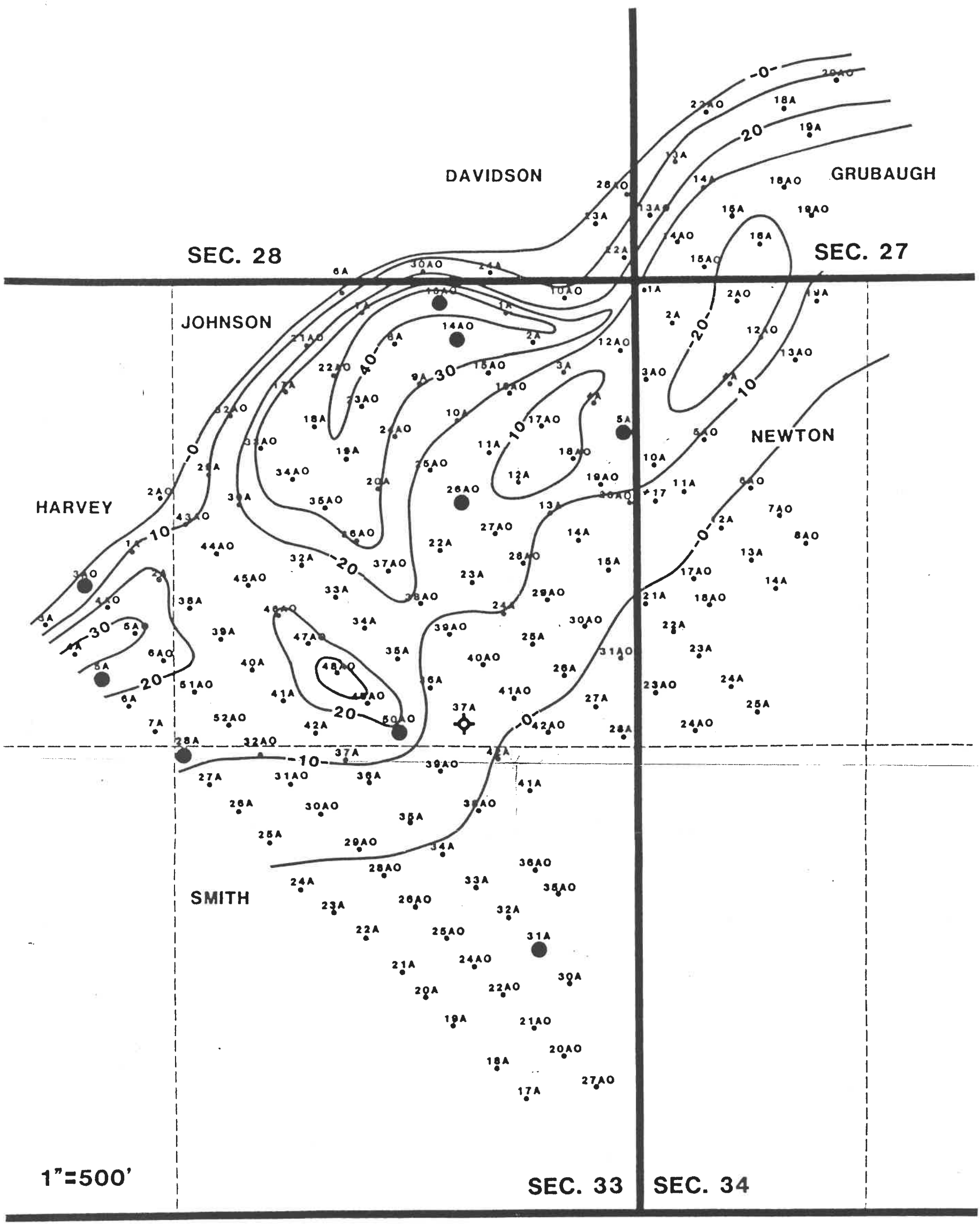

● Wells with cores used in this study • Well Location ⊕ Dry Hole

Contour Interval - 10'

PLATE 10

ISOPACH MAP OF SAND C

Kansas Geological Survey
Open-file Report 86-23
plate 10

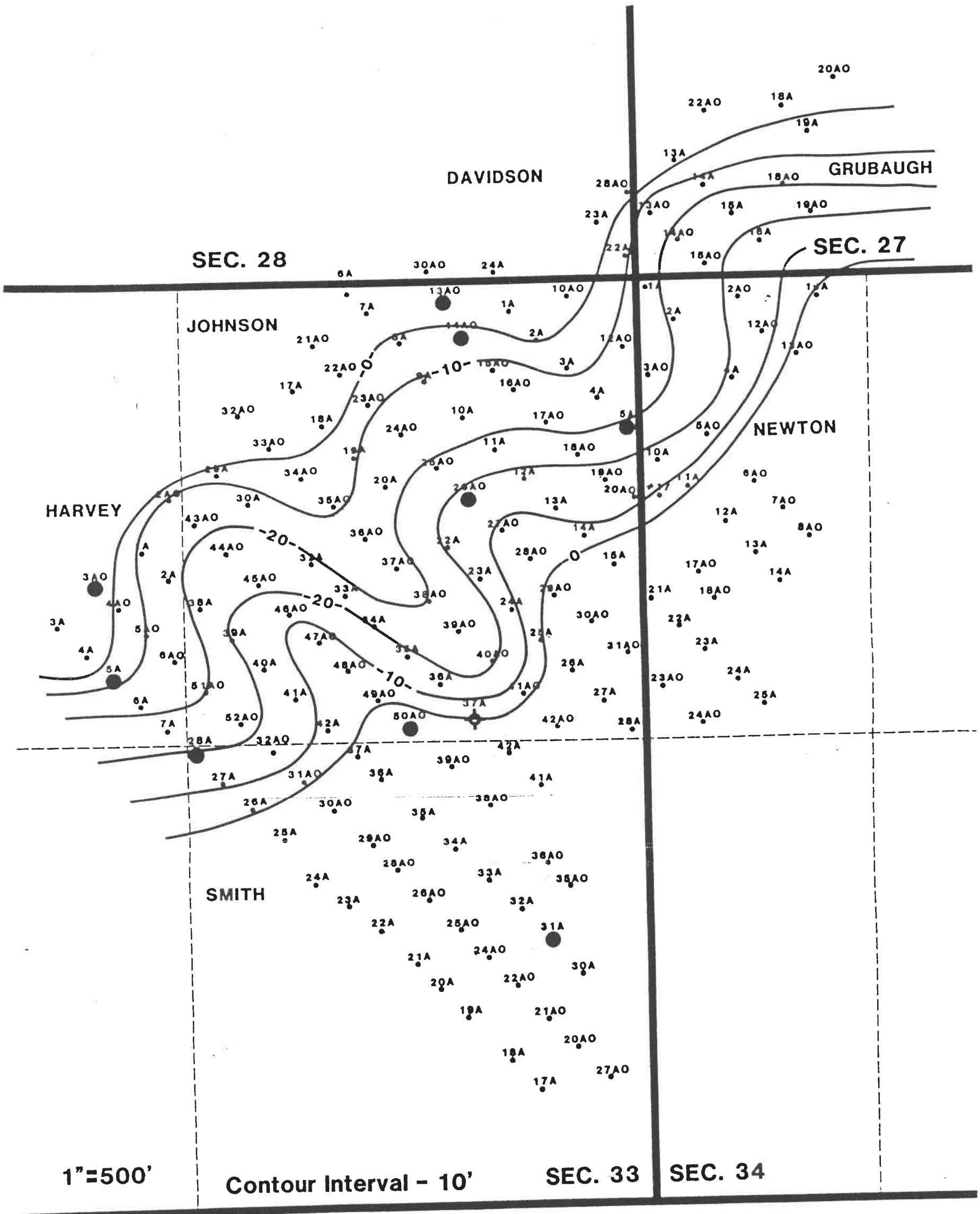

1"=500' | Contour Interval - 10'

●Wells with cores used in this study • Well Location ⊹Dry Hole

PLATE 11

ISOPACH MAP OF SAND D

Kansas Geological Survey
Open-file Report 86-23
plate 11

Kansas Geological Survey
Open-file Report 86-23
plate 12

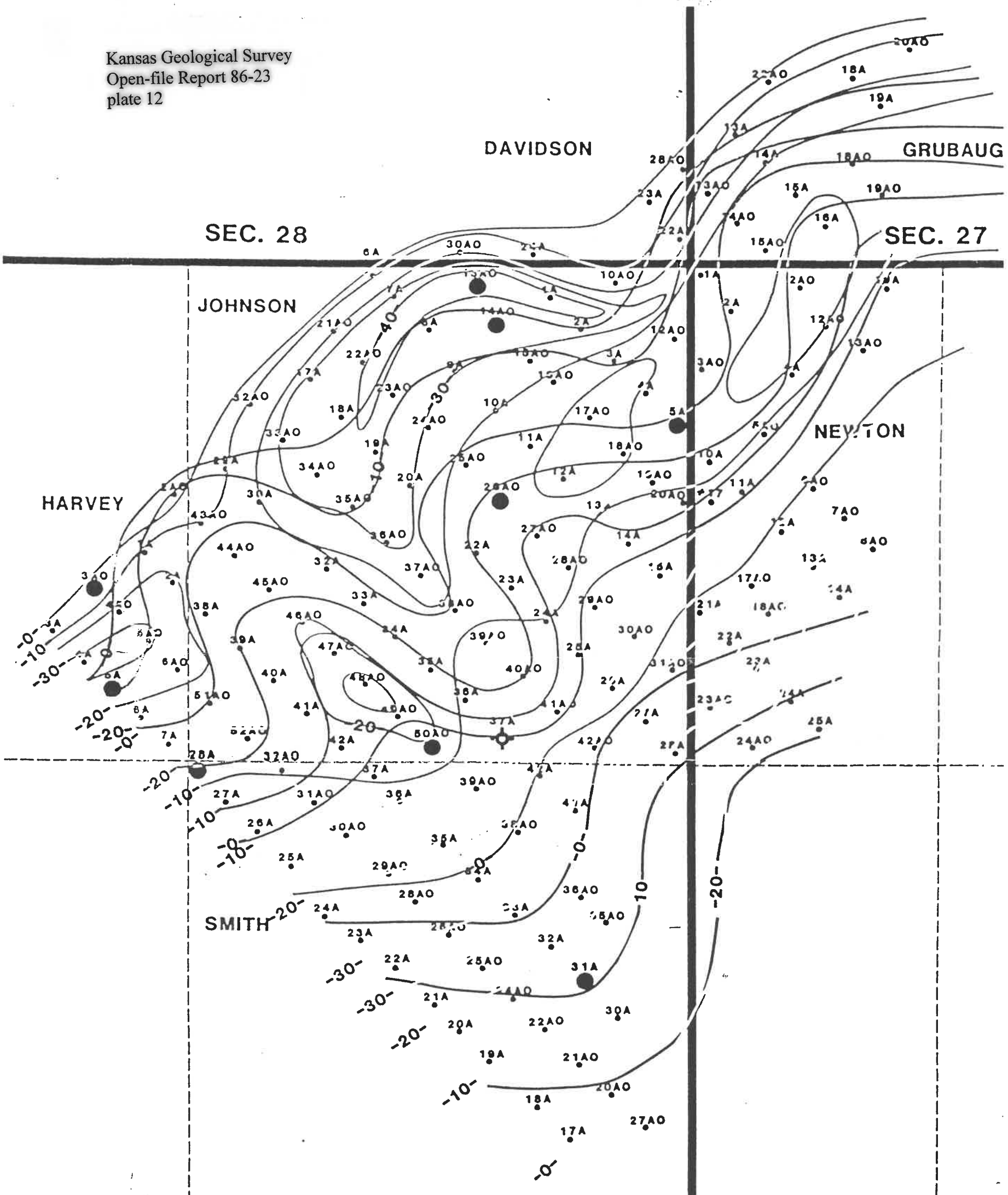

● Wells with cores used in this study • Well Location ✣ Dry Hole

SAND D

SAND C

SAND B

SAND A

PLATE 12

MULTILAYERED ISOPACH MAP

SANDS A, B, C, AND D